FINITE ELEMENT ANALYSES OF
GRAVITY EARTH RETAINING STRUCTURES FOUNDED ON SOIL

by

Levi R. Regalado

Dissertation submitted to the Faculty of the
Virginia Polytechnic Institute and State University
in partial fulfillment of the requirements
for the degree

of

DOCTOR OF PHILOSOPHY

in

Civil Engineering

APPROVED :

J. M. Duncan, Co-Chairman

G. W. Clough, Co-Chairman

T. Kuppusamy

S. M. Holzer

E. G. Henneke

February, 1992
Blacksburg, VA

Finite Element Analyses of

Gravity Earth Retaining Structures Founded on Soil

by

Levi R. Regalado

J. M. Duncan and G. W. Clough, co-chairmen

Civil Engineering

(ABSTRACT)

The safety of gravity earth retaining structures is usually evaluated with regard to : (1) overturning about the toe, (2) sliding along the base and (3) bearing failure of the foundation. Conventional equilibrium methods are utilized in these analyses, which are performed using assumed earth loads based on simplified earth pressure theories. Recent finite element studies performed on gravity retaining walls founded on rock revealed that the use of conventional methods may lead to overly conservative results. The effects of soil-structure interaction result in a greater degree of wall stability than conventional approaches would indicate.

This research examines the behavior of gravity earth retaining structures founded on soil. Two methods of analyses were used in these studies : (1) the Following Load method, which does not account for soil-structure interaction effects, and (2) the Backfill Placement method, which does account for soil-structure interaction effects. A procedure called the "Alpha Method" for 2D soil elements was developed for the purpose of improving the post-failure stress-strain behavior of the backfill and foundation soils and incorporated in the finite element program (SOILSTRUCT) utilized in the analyses.

A series of analyses demonstrated the effectiveness of the Alpha Method in controlling overshoot and providing good estimates of collapse loads on wall-foundation systems. Following Load analyses indicated that walls on soil become unstable by bearing capacity rather than

overturning or sliding. These results also provided the basis for modifications to Vesic's bearing capacity theory, which extended the applicability of the theory to the conditions encountered in retaining wall problems. The Backfill Placement analyses showed that there are significant differences in behavior between walls founded on rock and walls founded on soil. These analyses also led to new insight into the factors that affect the shear forces within the backfill and which contributes to the stability of the wall.

ACKNOWLEDGMENTS

I am deeply grateful to my advisers, Prof. James Michael Duncan and Prof. Gerald Wayne Clough for patiently and thoroughly reviewing the manuscript, for sharing from their wealth of engineering experience, for giving me the opportunity and privilege to pursue graduate studies at VPI, and for their support and friendship.

My gratitude also to Professors Edmund Henneke, Siegfried Holzer and Thangavelu Kuppusamy for their willingness to be involved in my research. Their contributions are greatly appreciated.

Funding for this research was provided by the US Army Corps of Engineers. Dr. Bob Ebeling's help during the initial phase of this work is invaluable. Dr. Reed Mosher's continuing interest in the project kept it going.

The support from countless people in the Blacksburg Christian Fellowship has been a constant source of spiritual strength for me. I am particularly thankful for the likes of the Craigs, Dodsons, Houghtons, Huffs and Thompsons.

Many thanks to the Filipino community in VPI for making me forget time and again that I am actually in another country. Mr. Greg Foliente's life so enriched my own.

All my love to my wife Carmen who, in sharing life's journeys and burdens with me, is ever so loving, patient and understanding.

Lastly, thanks to the Almighty Creator God who has blessed my life so abundantly and granted me the strength to finish my studies.

LEVI REGALADO

TABLE OF CONTENTS

LIST OF FIGURES

LIST OF TABLES

LIST OF SYMBOLS

B	Width of footing or wall
B'	Length of the toe projection for cantilever walls
B_e	Width of footing or wall in contact with the foundation
B_{mod}	Bulk modulus of soil
B_t	Width of the crest of a gravity wall
c	Soil cohesion
D	Top width of a soil backfill wedge
E	Young's modulus
E_c	Modulus of elasticity of concrete
E_f	Failure modulus of soil
E_{pl}	Primary loading modulus of soil
E_{ur}	Unload-reload modulus of soil
EPI	Earth pressure index
F_h	Normal force acting on a vertical plane within the backfill
F_v	Shear force acting on a vertical plane within the backfill
$FS_{bearing}$	Factor of safety against bearing capacity failure
$FS_{sliding}$	Factor of safety against sliding along the wall base
G	Shear modulus
h	Height of the soil backfill
h_t	Height of the toe fill
H	Height of the retaining wall/soil backfill wedge
I_r	Soil rigidity index
I_{rc}	Critical value of soil rigidity index
K	Modulus number
K_b	Bulk modulus number
K_h	Lateral earth pressure coefficient
K_a	Rankine active earth pressure coefficient
K_n	Normal stiffness of an interface element
K_s	Shear stiffness of an interface element
K_o	At-rest lateral earth pressure coefficient
K_p	Rankine passive earth pressure coefficient

K_v	Vertical shear force coefficient
K_2	Unloading parameter used to estimate the minimum value of B_{mod}
L	Length of footing or wall
m	Bulk modulus exponent
n	Modulus exponent
n_s	Number of "steps" on a stepped-face wall
N	Vertical component of the force acting on the base of a footing or wall
N_γ	Bearing capacity factor
N_q	Bearing capacity factor
q_{max}	Maximum bearing pressure on the base of a footing or wall
q_{ult}	Ultimate bearing capacity of a foundation soil
P or $\{P\}$	Load vector
P_{atm}	Atmospheric pressure
P_a	Theoretical value of the minimum Rankine active force
P_o	At-rest lateral earth force
P_p	Theoretical value of the maximum Rankine passive force
q_c	Characteristic pressure used for rigidity index calculations
q_s	Surcharge on the ground surface
R	Resultant force exerted by a backfill on a wall
RC	Relative compaction
R_f	Failure ratio
s_{SL}	Standard deviation of soil element stress levels
SL	Stress level
SL_{crit}	Critical stress level
SS	Stress state parameter
$SS_{max\ past}$	Maximum value of the stress state parameter in soil element's history
t_b	Thickness of the base slab for cantilever walls
t_w	Thickness of the wall stem for cantilever walls
T	Horizontal component of the force acting on the base of a footing or wall
U_x	X (horizontal) nodal displacement
U_y	Y (vertical) nodal displacement
w	Water content of soil
$\overline{x}_{SL}$	Mean value of soil element stress levels

α	Load reduction factor used in the Alpha Method
γ_b	Unit weight of the soil backfill
γ_c	Unit weight of concrete
γ_s	Unit weight of the foundation soil
δ	Angle of friction between a wall-soil interface
δ_{mob}	Mobilized angle of friction along a wall-soil interface
Δ	Horizontal displacement of the top of the retaining wall
ΔP	Horizontal load applied on wall in Rankine analyses
ΔP_{fa}	Theoretical magnitude of load on wall for active Rankine conditions to occur
ΔP_{fp}	Theoretical magnitude of load on wall for passive Rankine conditions to occur
$\Delta\sigma_x$	Change in σ_x during a load step
$\Delta\sigma_y$	Change in σ_y during a load step
$\Delta\tau_{xy}$	Change in $\Delta\tau_{xy}$ during a load step
ϵ	Axial strain
ν_c	Poisson's ratio of concrete
ν_s	Poisson's ratio of soil
ξ_{qi}	Inclination factor
ξ_{qr}	Compressibility factor
$\xi_{\gamma i}$	Inclination factor
$\xi_{\gamma r}$	Compressibility factor
λ	Reduction factor for soil strength parameters
σ_x	Normal stress in the X-direction
σ_y	Normal stress in the Y-direction
σ_v	Soil overburden pressure
σ_1	Major principal stress in a soil element
σ_3	Minor principal stress (confining pressure) in a soil element
σ_{3crit}	Critical confining pressure
$\tau_{xy}(=\tau_{yx})$	Shear stress on the X (or Y) plane
Φ	Angle of internal friction
$\Phi_{backfill}$	Angle of internal friction of a backfill soil
$\Phi_{foundation}$	Angle of internal friction of a foundation soil

CHAPTER 1

INTRODUCTION

Procedures for designing gravity earth retaining structures have changed little since the 1940s and are considered by many engineers to be well established. However, recent studies have provided better insight into the behavior of gravity earth retaining structures, and have shown that conventional methods can lead to designs that are exceedingly conservative for gravity walls that have free-draining backfill and are founded on rock.

As illustrated in the free body diagram in Figure 1.1, once the magnitudes of the forces exerted on a wall by the backfill have been specified, the equations of equilibrium may be utilized to determine the magnitudes of the shear and normal forces that act on the base of the wall. Possible failure modes (i.e., sliding, overturning and bearing failure) can then be investigated. Conventional methods usually assume that the horizontal and vertical planes within the backfill are principal planes. Consequently, there is no shear force on the vertical plane through the heel of the wall and the only vertical component of the force exerted by the backfill on the wall is the weight of any backfill that is above the wall. The magnitude of the horizontal earth pressure force, H_{AA}, depends on the value of the lateral earth pressure coefficient, K_h, used for the design. Depending on the magnitudes of the expected wall movements, either an active earth pressure coefficient (K_a), or an at-rest earth pressure coefficient (K_o) is used for design.

In an recent study, Ebeling, et al. (1988) conducted finite element analyses of gravity retaining walls founded on rock using the finite element program SOILSTRUCT. A significant step in that study was the development of a procedure called the "Alpha Method" which

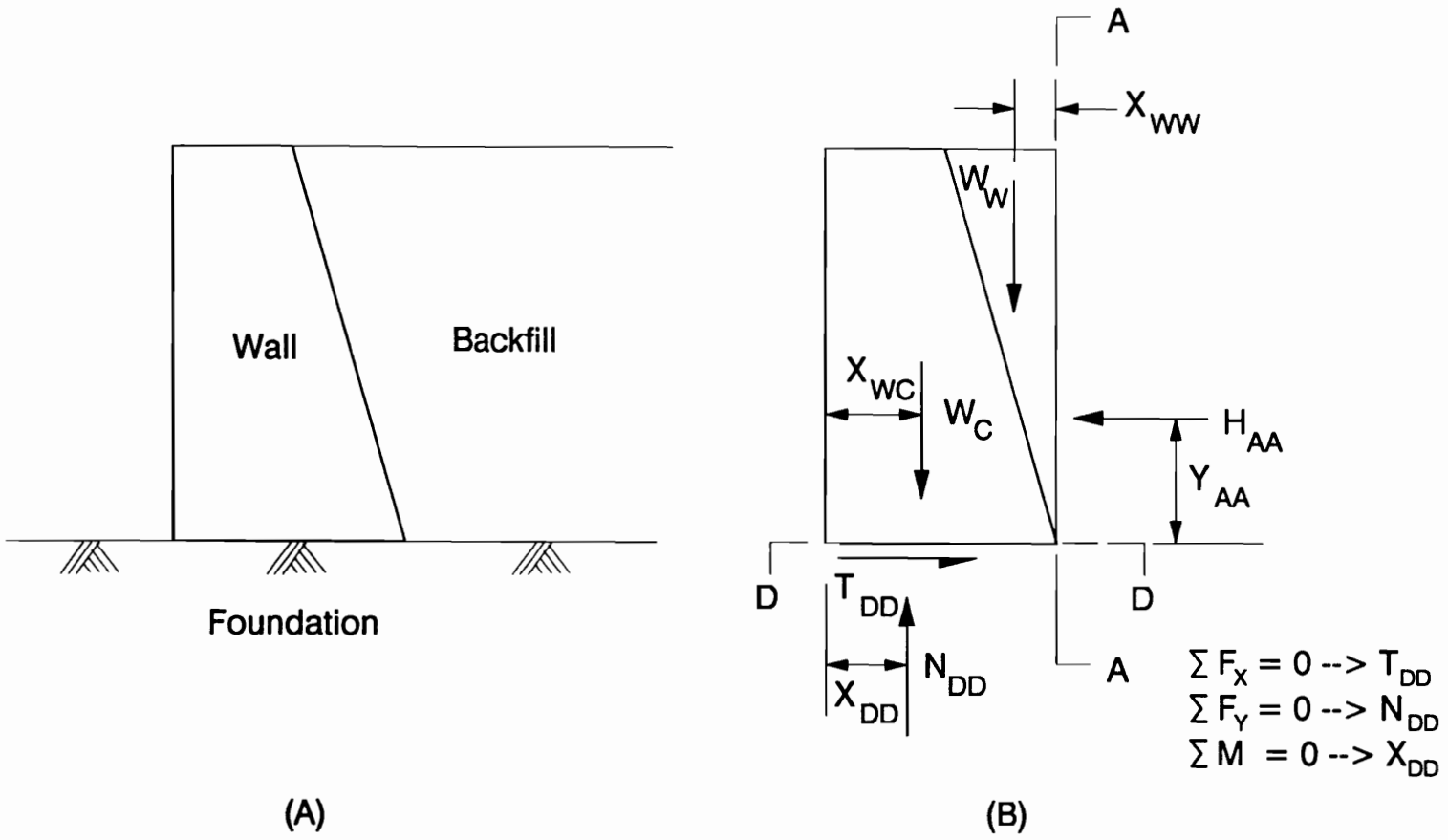

Figure 1.1 - Components of a Retaining Wall System and the Forces assumed in Conventional Design Procedures

enabled SOILSTRUCT to model accurately the process of progressive separation of the wall base from the rock foundation. This is especially important for studying the behavior of heavily loaded walls that do not have full contact with the underlying rock foundation. Another important aspect of the studies performed by Ebeling, et al. (1988) was to show that there is a downward shear force on the vertical plane through the heel of the wall as a consequence of the tendency for the backfill to settle more than the wall. These forces, which tend to stabilize the wall, are neglected in conventional equilibrium analyses. The existence of these shear forces provides an explanation for the fact that a number of gravity retaining Corps of Engineers walls showed no signs of instability, although analyses of these walls using conventional equilibrium methods indicate that they should be unstable.

The studies described in this report were performed to investigate the behavior of gravity retaining walls founded on soil. The soil was modeled as a nonlinear medium, and analyses were performed utilizing the computer program SOILSTRUCT, which was modified for this study.

A major difference between the behavior of walls on rock and walls on soil is that settlements are larger for walls founded on soil, and they have a significant effect on the behavior of the wall. Clough and Duncan (1971) performed an analysis of a retaining wall founded on medium dense sand, with a loose sand backfill. They found that the settlement of the foundation during placement of the backfill affected the movement of the wall. This in turn affected the forces exerted by the backfill on the wall.

This report on these studies is divided into eight chapters. Chapter 2 describes the modifications made on the computer program (SOILSTRUCT) to extend the Alpha Method for application to two-dimensional elements. This modification reduces overshoot of stresses and numerical innacuracies in the analyses.

Chapter 3 contains a review of a modern bearing capacity theory and discusses its use for evaluating the stability of retaining walls on soil.

Chapter 4 contains the results of finite element analyses using the following load method for walls founded on soil.

Chapter 5 contains the results of finite element analyses of gravity retaining walls on soil using the backfill placement method.

Chapter 6 discusses the results of finite element analyses performed on cantilever and stepped-face walls on soil.

Chapter 7 compares the results of finite element analyses with those obtained utilizing conventional design procedures.

Finally, Chapter 8 contains a summary of the study and conclusions.

CHAPTER 2

ANALYSES OF GRAVITY RETAINING WALLS FOUNDED ON SOIL USING THE FOLLOWING LOAD METHOD

INTRODUCTION

The objective of the study described in this chapter is to determine how foundation properties and wall geometry affect wall movement and wall stability. For this purpose, the "following load analysis" method described by Ebeling et al. (1988) was used. In this method, the soil backfill is represented by nodal forces applied on the surface of the foundation soil and the back of the wall rather than by soil elements. The applied loads are not affected by the movements of the wall, and thus do not reflect the effects of soil-structure interaction. Since they remain the same no matter what movements take place, the loads are said to "follow" the movements of the wall, and are thus described as "following loads." The advantage of the following load approach is that the reduced number of variables influencing the response of the wall-foundation system makes it easier to isolate the effects of a change in a single parameter.

HYPOTHETICAL STRUCTURES AND LOADING CONDITIONS USED IN THE FOLLOWING LOAD ANALYSIS

The first series of analyses performed used the version of SOILSTRUCT as it existed in the Fall of 1988. The program had the capability of modeling separation of the wall base from

the foundation and had been used by Ebeling et al. (1988) to study the behavior of gravity retaining walls on rock. The first analyses were done for the purpose of determining if the analytical techniques used by Ebeling for walls on rock were applicable also to analysis of walls on soil foundations.

The hypothetical wall-foundation system is shown in Fig. 2.1. The ranges of values for each of the parameters that describe the geometry and the properties are given in Table 2.1.

Run FOL1A is referred to as the "Base Case." The wall geometry for this Base Case is shown by the finite element mesh in Fig. 2.2. It contains 18 interface elements, 343 two-dimensional elements and 394 nodes.

The initial stresses in the foundation soil, before construction of the wall or placement of backfill, correspond to at-rest conditions.

The first phase of the analysis involved simulating construction of the gravity retaining wall itself. Construction of the wall was modeled using the following procedure, as shown in Fig. 2.3 :

(1) With the elements in the wall having been assigned the properties of air, pressure was applied to the interface elements along the base of the wall to simulate the weight of the wall.

(2) After the loads simulating the weight of the wall had been applied, the properties assigned to the elements in the wall were changed from the properties of air to the properties of hardened concrete.

Because the behavior of the soil elements in the foundation was stress dependent, the loads simulating the weight of the wall were applied in small increments to model the nonlinear behavior as closely as possible, and to avoid abrupt changes in soil modulus from one load increment to the next. Five increments of load were used to simulate construction of the wall.

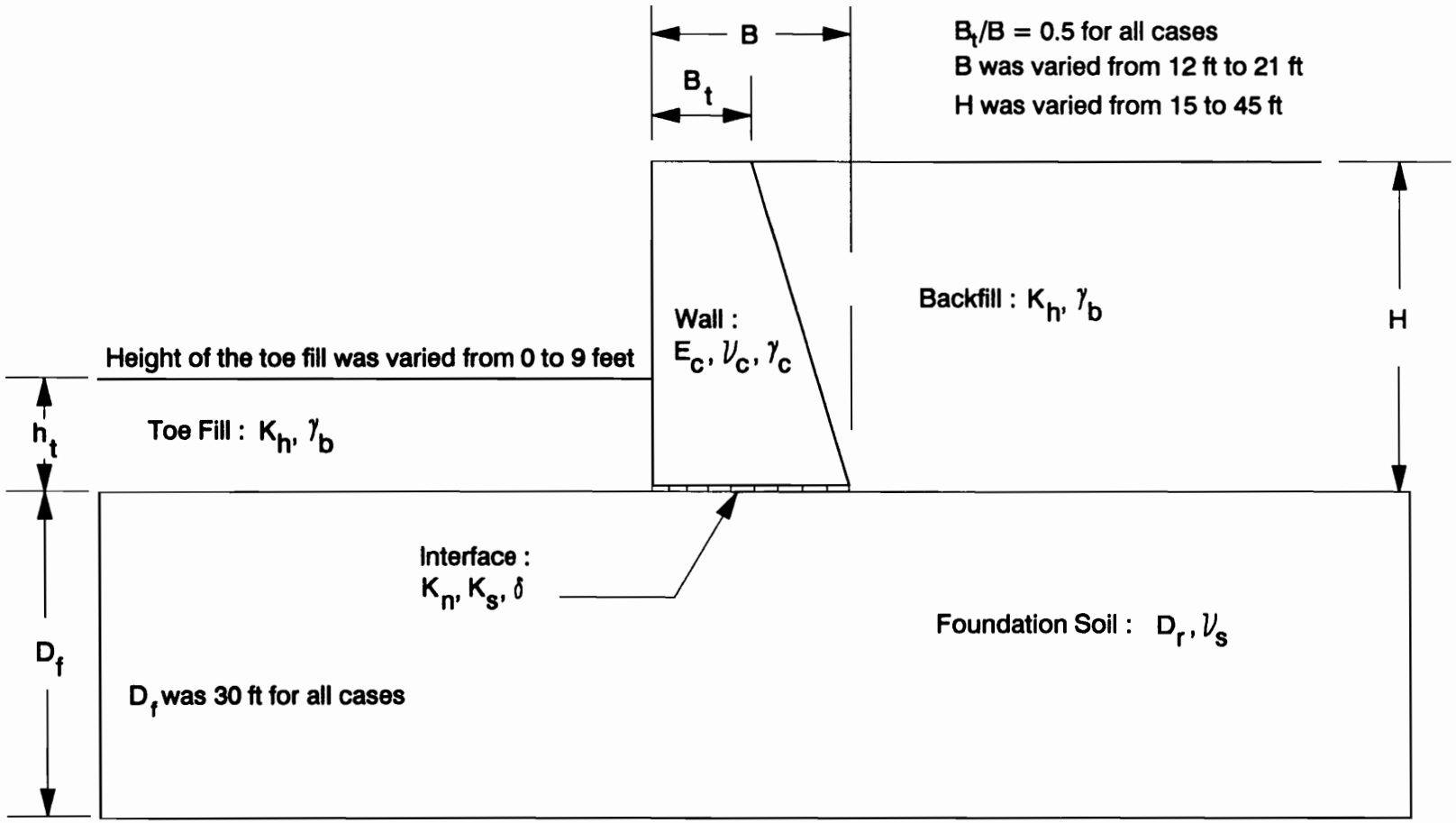

Figure 2.1 - Hypothetical Wall-Foundation System used for Following Load Analyses Showing Parameters

Table 2.1 - Parameter Values used in the Following Load Analyses

Constant Parameters

Geometric

- B_t/B = Ratio of width of top of wall to width of base of wall = 0.5

Material

- γ_b = Unit weight of backfill/toe fill = 135 pcf
- K_n = Normal stiffness of wall-base interface elements = 5.18×10^9 pcf
- δ = Friction angle of wall-base interface elements = 35 degrees
- γ_c = Unit weight of concrete = 150 pcf
- E_c = Modulus of elasticity of concrete = 4.3×10^8 pcf
- ν_c = Poisson's ratio of concrete = 0.20

Variable Parameters

Geometric

- D_f = Depth of foundation soil
- H = Height of wall
- B = Base width of wall
- h_t = Height of toe fill

Material

- K_s = Shear stiffness of wall-base interface elements
- ν_s = Poisson's Ratio of foundation soil
- D_r = Relative density of foundation soil

Others

- K_h = Earth pressure coefficient for horizontal loads on wall

Run No.	K_s (pcf)	ν_s	K_h	D_f (ft)	H (ft)	B (ft)	D_r *	h_t (ft)	Comments
FOL1A	2.1×10^5	0.35	0.37	30	30	18	75	0	Base Case
FOL1B	(2.9×10^4)	0.35	0.37	30	30	18	75	0	Low K_s
FOL1C	(3.9×10^5)	0.35	0.37	30	30	18	75	0	High K_s
FOL2A	2.1×10^5	0.35	(0.30)	30	30	18	75	0	Low K_h
FOL2B	2.1×10^5	0.35	(0.50)	30	30	18	75	0	High K_h
FOL3A	2.1×10^5	(0.32)	0.37	30	30	18	75	0	Low ν_s
FOL3B	2.1×10^5	(0.40)	0.37	30	30	18	75	0	High ν_s
FOL4A	2.1×10^5	0.35	0.37	30	30	18	(50)	0	Loose Sand
FOL4B	2.1×10^5	0.35	0.37	30	30	18	(25)	0	Medium Dense Sand
FOL4C	2.1×10^5	0.35	0.37	30	30	18	(100)	0	Very Dense Sand
FOL5A	2.1×10^5	0.35	0.37	(15)	30	18	75	0	Thin Foundation
FOL5B	2.1×10^5	0.35	0.37	(60)	30	18	75	0	Thick Foundation
FOL6A	2.1×10^5	0.35	0.37	30	(15)	18	75	0	B/H = 1.2
FOL6B	2.1×10^5	0.35	0.37	30	(36)	18	75	0	B/H = 0.5
FOL6C	2.1×10^5	0.35	0.37	30	(45)	18	75	0	B/H = 0.4
FOL7A	2.1×10^5	0.35	0.37	30	30	(12)	75	0	B/H = 0.4
FOL7B	2.1×10^5	0.35	0.37	30	30	(15)	75	0	B/H = 0.5
FOL7C	2.1×10^5	0.35	0.37	30	30	(21)	75	0	B/H = 0.7
FOL8A	2.1×10^5	0.35	0.37	30	30	18	75	(9)	With Toe Fill
FOL9A	2.1×10^5	0.35	0.37	30	30	18	75	0	Actual placement of conc FE

Note : Values in ( ) indicate a parameter value other than the base case value

* D_r = Relative Density - See table below for properties used

Hyperbolic parameters (from Duncan,Mabry, Wong & Byrne report)

Relative Density (%)	K	n	ϕ	K_o	γ_s (pcf)	R_f
100	600	0.4	42°	0.33	140	0.7
75	450	0.4	39°	0.37	135	0.7
50	300	0.4	36°	0.41	130	0.7
25	200	0.4	33°	0.46	125	0.7

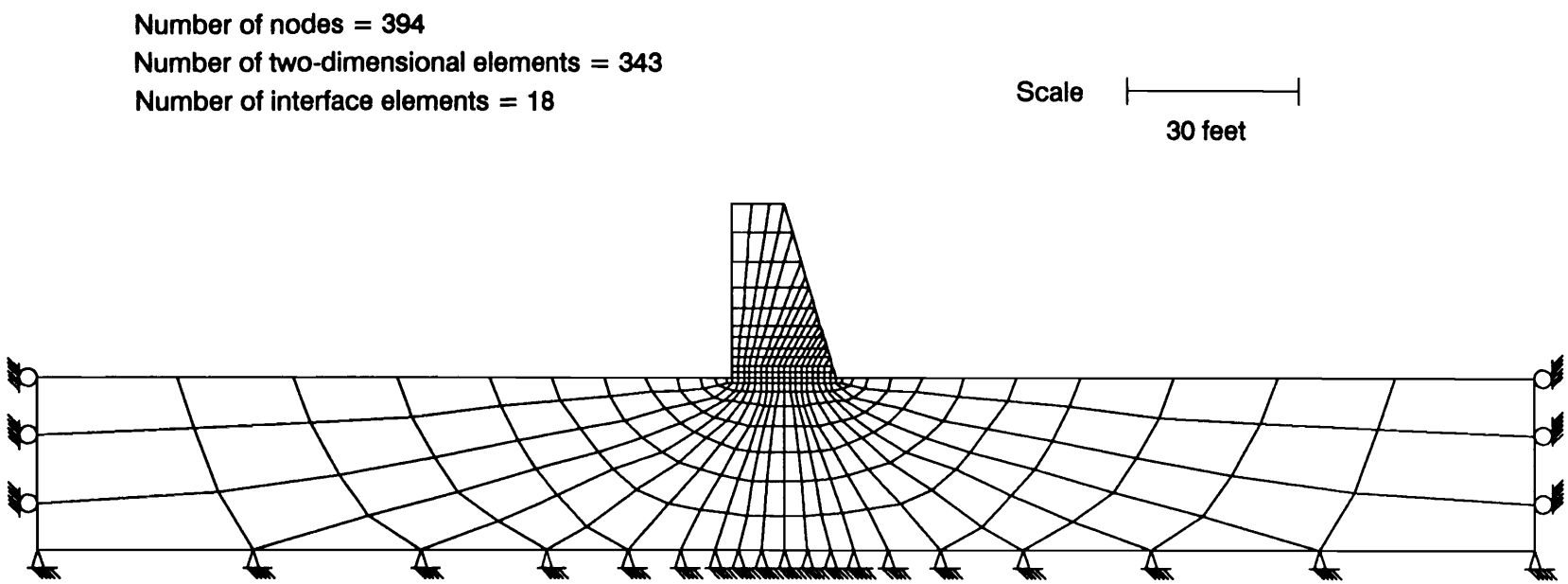

Figure 2.2 - Finite Element Mesh for the Base Case Wall-Foundation System

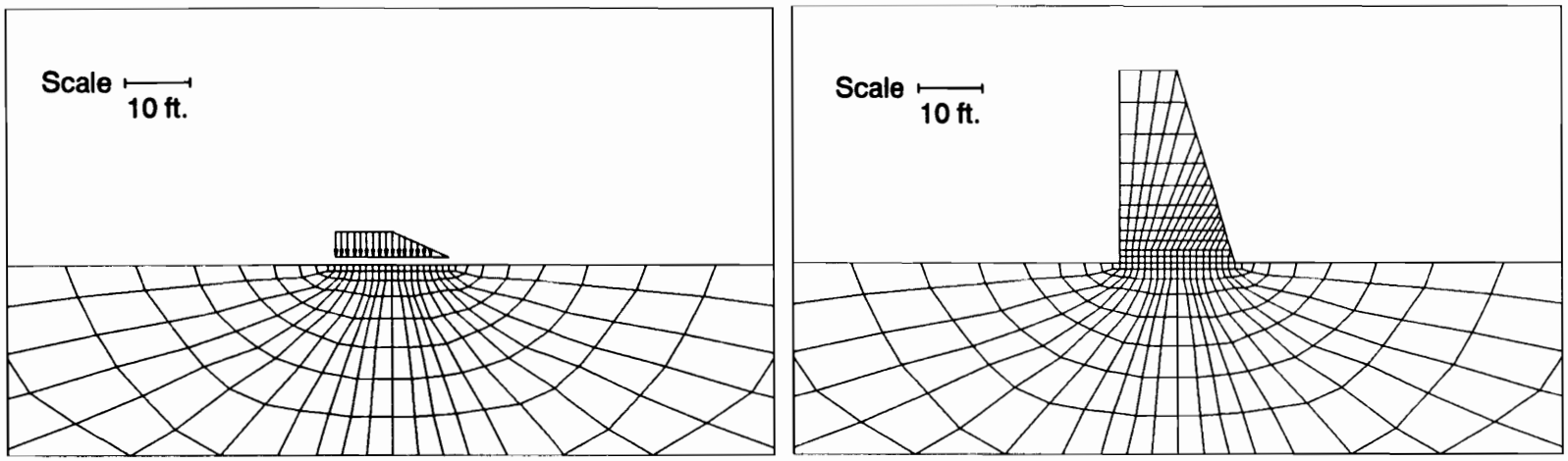

Step 1.) : With wall elements (not shown) having properties of air, specify pressure on foundation due to wall weight

Step 2.) : Specify a material type change : transform wall elements into concrete

Figure 2.3 - Buildup Simulation of Wall by specifying Base Pressure

The increments correspond to $\frac{1}{16}$, $\frac{1}{16}$, $\frac{1}{8}$, $\frac{1}{4}$ and $\frac{1}{2}$ of the total weight of the wall.

To model placement of backfill behind the wall, nodal forces were applied to the back of the wall and the surface of the soil behind the wall, as shown in Fig. 2.4. Each successive layer of backfill was represented by applying another set of forces to the back of the wall and the surface of the soil.

PROBLEMS WITH SOIL ELEMENT FAILURE AND RECOVERY

Nonlinear finite element analyses of the type described in this report are performed in stages. During each stage of these analyses, each element in the finite element mesh is assigned stress-strain properties consistent with the stresses in the element. Elements that fail are assigned small values of modulus consistent with their inability to carry more load.

Overshoot

One of the basic considerations in nonlinear finite element analyses of stresses and movements in earth masses is that the calculated stresses should not exceed the strengths of the materials. Although this can be viewed as a fundamental requirement, it is not always satisfied. Sometimes the changes in stress during a step of an analysis result in stresses that exceed the strength, as illustrated in Fig. 2.5. This is called "overshoot." In some cases the calculated stresses exceed the strength by a wide margin, and the results in such cases are unrealistic.

The strength of a cohesionless soil element depends mainly on the angle of internal friction of the material, Φ, and on the confining pressure it is subjected to, σ_3. For a constant value of Φ, the strength increases with confining pressure. When the confining pressure is extremely low or takes on a tensile value, the element has practically no strength. This makes the element of little significance in terms of affecting the overall behavior of the system.

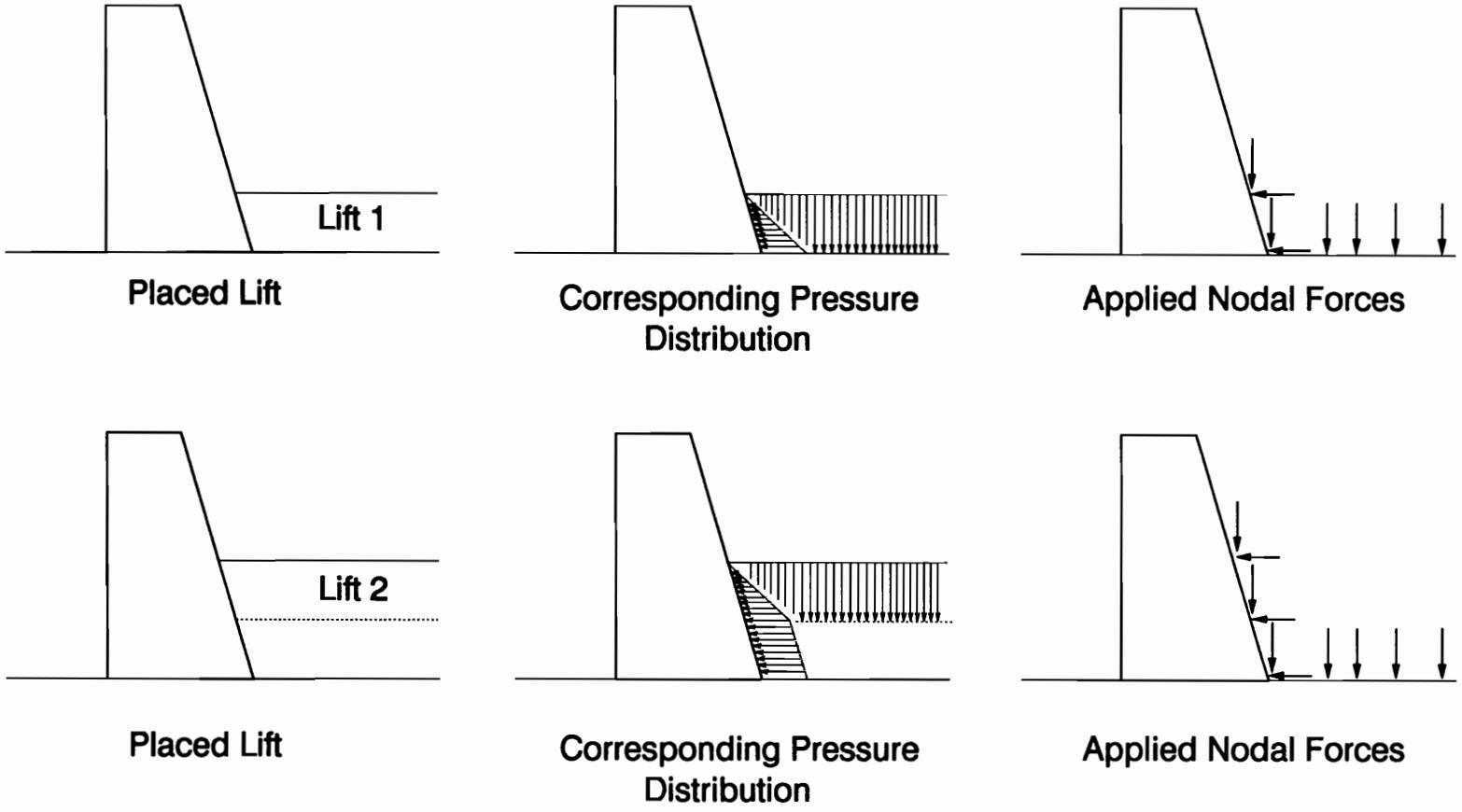

Figure 2.4 - Simulation of Lift Placement by Application of Nodal Forces - First Two Lifts

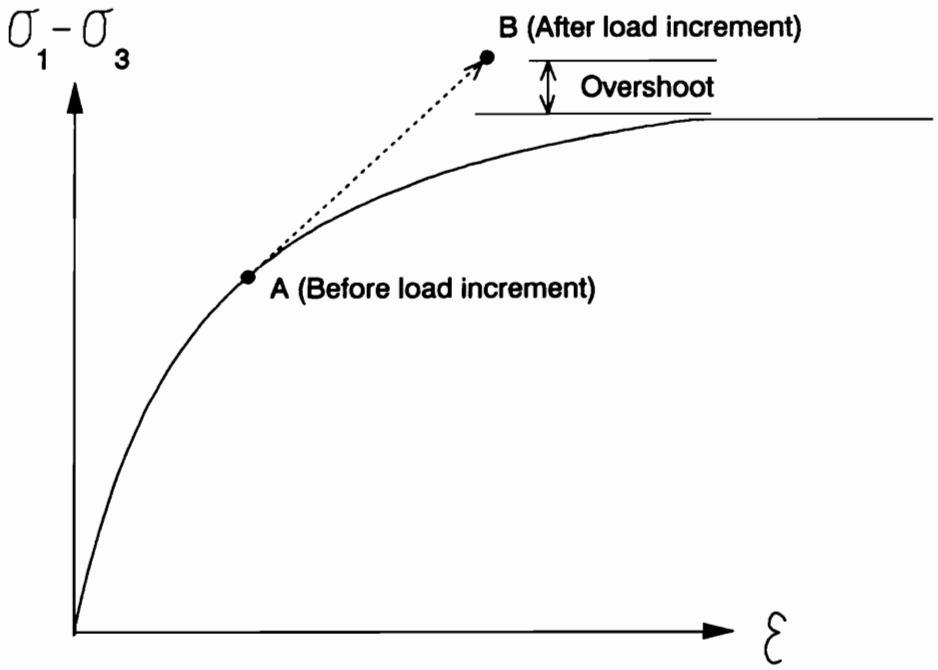

Figure 2.5 - Occurrence of Overshoot as seen on a Hyperbolic Stress-strain Curve

A distinction was made between overshoot that occurred in soil elements that had little or no strength and overshoot that occurred in soil elements that had significant values of strength. In the former case, overshoot may result even if the magnitudes of the stresses that act on an element are relatively small. In such cases, the occurrence of the overshoot has little or no bearing on the outcome of the analysis. In contrast, overshoot in elements with high strengths is more important, because these elements have the ability to carry a large amount of load. The occurrence of overshoot in these elements can thus be very significant.

For the purpose of making a distinction between "strong" elements and "weak" elements, a critical value of confining pressure , σ_{3crit}, was defined as follows :

$$\sigma_{3crit} = 0.8K_o\sigma_v \tag{2.1}$$

where K_o is the at-rest lateral pressure coefficient and σ_v is the vertical effective stress corresponding to the element by itself, with no overlying elements or external loads : σ_v is the overburden pressure corresponding to a depth of soil equal to half the vertical dimension of the element, and σ_{3crit} is typically less than 40 percent of this value. If the confining pressure for an element is greater than its critical confining pressure, the soil element will be referred to as "strong". Otherwise, it will be referred to as a "weak" element. In quantifying the amount of overshoot in an analysis, only the "strong" elements were considered.

The Alpha Method

In the analyses of walls on rock performed by Ebeling, et al. (1988), problems were encountered with overshoot in the interface elements between the base of the wall and the underlying rock. Ebeling, et al. (1988) developed a procedure called the "alpha method" to minimize the overshoot in the interface elements. The method worked well, and was capable of limiting the amount of overshoot to no more than a few percent in most cases.

In the case of walls founded on soil, failure and overshoot can occur in the soil beneath the wall as well as in the interface between the wall and the underlying soil. Examples are shown in Fig. 2.6. The mesh in Fig. 2.6(a) show the failure regions in the soil after the buildup of the wall was simulated. The zones in which the stresses exceed the strength have been darkened. The amounts of overshoot in these elements, all of which have sufficient strength, range from 1 percent to 45 percent.

During subsequent steps of the analysis, which involved application of forces to simulate placement of backfill, some of the failed elements recovered while others failed. The failure regions at the end of backfilling are shown shaded in the mesh in Fig. 2.6(b). At this stage, a total of sixteen strong elements failed, and the magnitude of the overshoot for these elements ranged from 0.3 percent to 480 percent. A total of four weak elements failed. Of these four, three failed in tension.

After this first analysis of a wall on soil had been performed, it became clear that the problems of large overshoot in soil elements would have to be addressed in order to achieve reasonably accurate and meaningful results. Accordingly, a study was undertaken to develop a procedure for applying the alpha-method to two-dimensional elements as well as interface elements, for which it had been originally developed by Ebeling, et al. (1988).

At the same time, revisions were made to the computer program to address the behavior of elements that "recover" from a failure state to a non-failure state.

Recovery from Failure

When the stresses in an element change so that it is no longer in a state of failure, it is assigned a higher modulus value consistent with its renewed ability to carry more load. This transition from low to high modulus is illustrated in Fig. 2.7. At stage A, the stresses in the element exceed its strength. This is shown in Fig. 2.7 by the fact that the "stress level" (SL), which is the stress divided by the strength, exceeds unity. Because SL exceeds unity, the

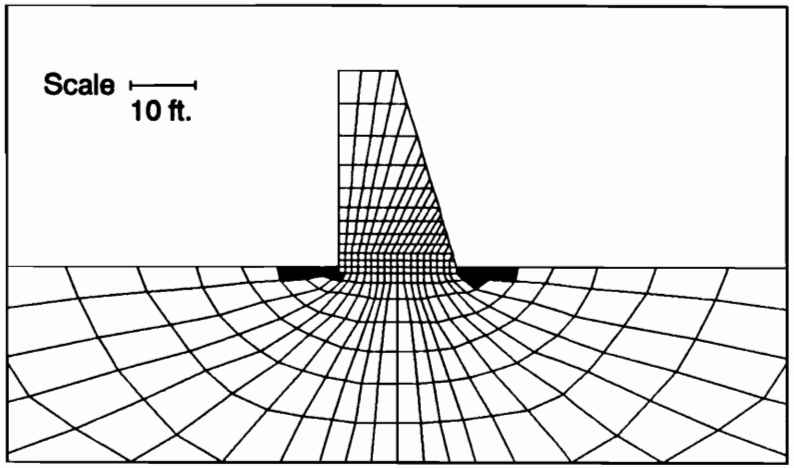

(a) Failure Regions after Wall Placement

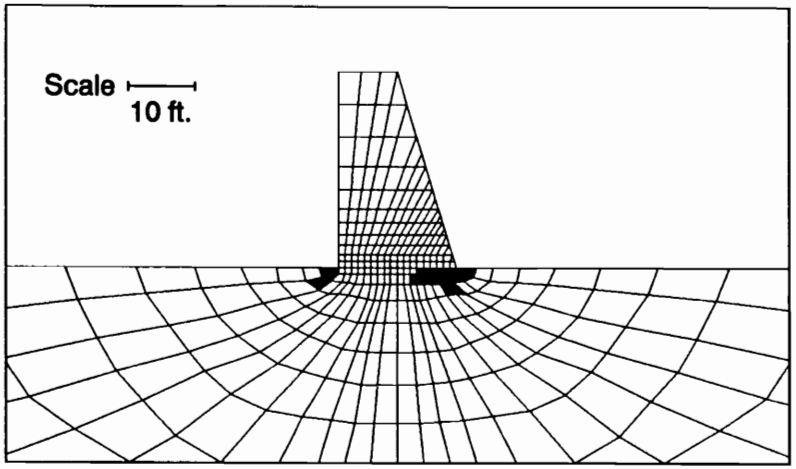

(b) Failure Regions after Backfill Placement

Figure 2.6 - Failure Regions for Base Case Problem Analyzed using "off the shelf" version of SOILSTRUCT

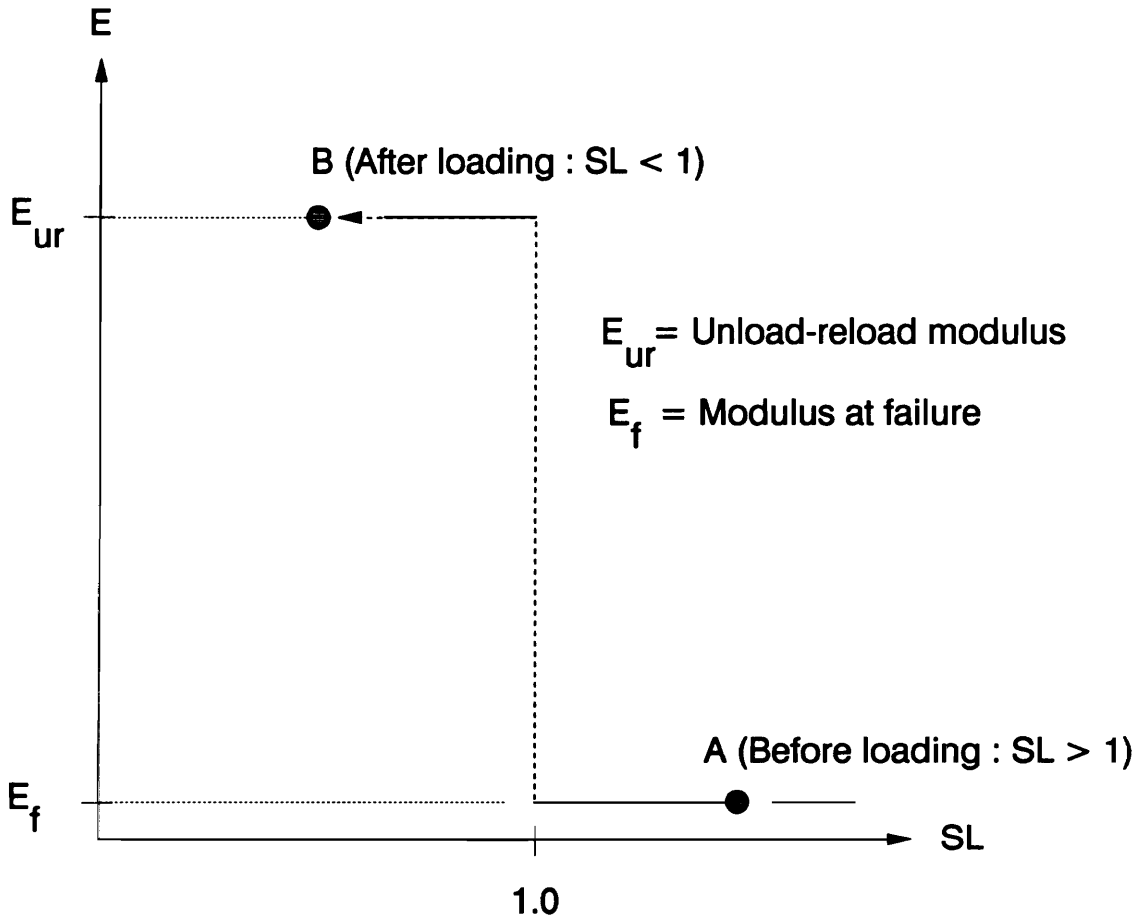

Figure 2.7 - Modeling a Soil Element's transition fron a Failure to a Non-failure State in unrevised SOILSTRUCT Program

element has a small modulus value. At stage B, the stresses have changed such that the stress level has dropped below unity, and the element would therefore be assigned a higher modulus value.

If the change in modulus from one step to another is very large, problems develop in the analyses. Elements with high modulus values tend to experience large changes in stress during subsequent steps of the analysis, particularly when neighboring elements have relatively small modulus values. In the worst case, a condition can develop in which an element snaps back and forth between failure and non-failure states in successive steps, as it is assigned alternately high and low modulus values. This problem, which is related to too-abrupt changes in modulus value, was addressed by Seed and Duncan (1983). They devised a procedure for changing modulus values gradually as the stresses in elements change. Their procedure was designed primarily to improve the behavior of soil elements during unload-reload. This model was incorporated in the program SOILSTRUCT. In addition, a procedure based on this model was developed to improve the behavior of soil elements that recover from failure during analysis. The changes made in SOILSTRUCT to achieve these aims are described in the following sections.

THE ALPHA METHOD FOR CONTROLLING OVERSHOOT IN TWO-DIMENSIONAL ELEMENTS

The finite element program used in this study (SOILSTRUCT) employs hyperbolic relationships to model the nonlinear stress-strain behavior of soils. As discussed previously, nonlinear behavior was approximated by performing the analyses in a series of increments, or "steps". Within each step of the analysis the materials were treated as if their behavior were linear. The modulus values assigned to each element were adjusted in accordance with their

stresses to simulate nonlinear behavior.

The way the stresses in an element might change during one step of an analysis is shown in Fig. 2.8. Fig. 2.8(a) shows the state of stress at the center of an element and the corresponding Mohr's circle at the beginning of a load step. Fig. 2.8(b) shows the state of stress and the Mohr's circle for the same element after a load step that brought about the changes in stress $\Delta\sigma_x$, $\Delta\sigma_y$ and $\Delta\tau_{xy}$. Fig. 2.8(b) illustrates that after the addition of the stress increments, the resulting combination of stresses may result in an unacceptable state of stress. A Mohr's circle of stress above the failure envelope is indicative of overshoot, as discussed previously in this chapter.

The ideal situation would be that the load applied during a load step was just large enough to bring the most severely stressed element to failure. This situation would correspond to a Mohr's circle which was tangent to the failure envelope. As discussed previously, the purpose of the alpha method is to achieve results closer to the ideal situation, where no element is overstressed. The basic idea behind the method is to reduce the magnitudes of the loads applied in any step of the analysis so that no soil element incurs a stress level greater than unity.

Fig. 2.9(a) illustrates the same situation shown in Fig. 2.8(b), in which the stress increments during a load step result in overshoot in a soil element. Fig. 2.9(b) shows a Mohr's circle which has been reduced in size so that it is tangent to the failure envelope. This reduction can be accomplished by multiplying the magnitudes of all the stress change components ($\Delta\sigma_x$, $\Delta\sigma_y$ and $\Delta\tau_{xy}$) by a factor α (hence the name "alpha" method). Reducing the stresses by this factor in all the elements in the mesh can be accomplished by reducing the load by the same factor, since the system behaves linearly during each step of the analysis.

A situation may arise where several elements fail, with each one requiring a different value of the reduction factor alpha. When this situation occurs, the most severely stressed

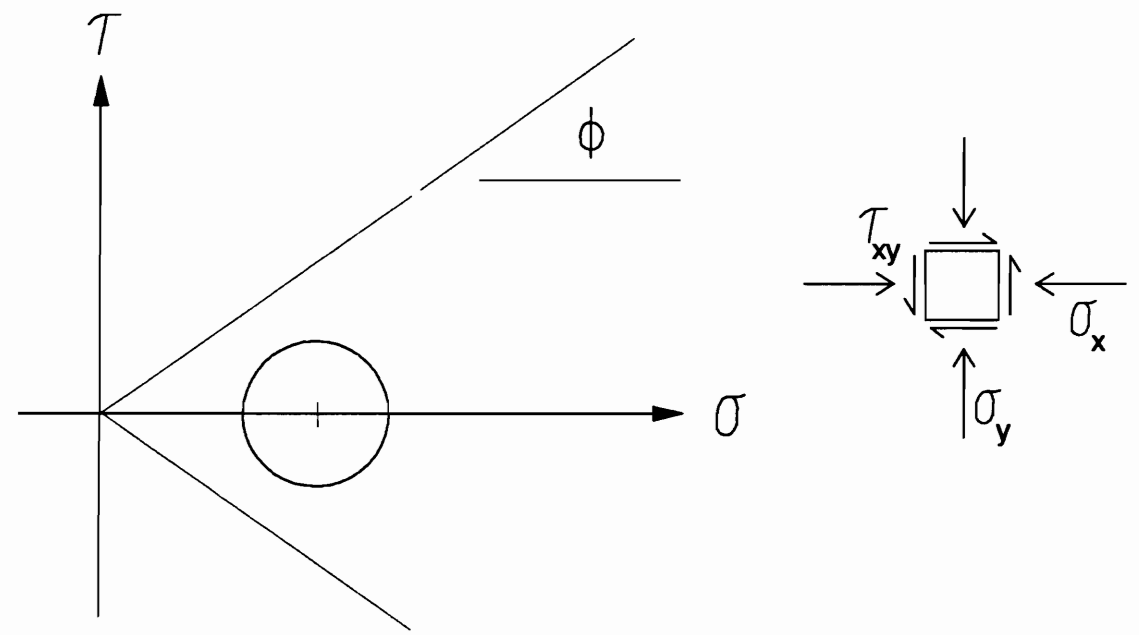

(a) Before Load Step

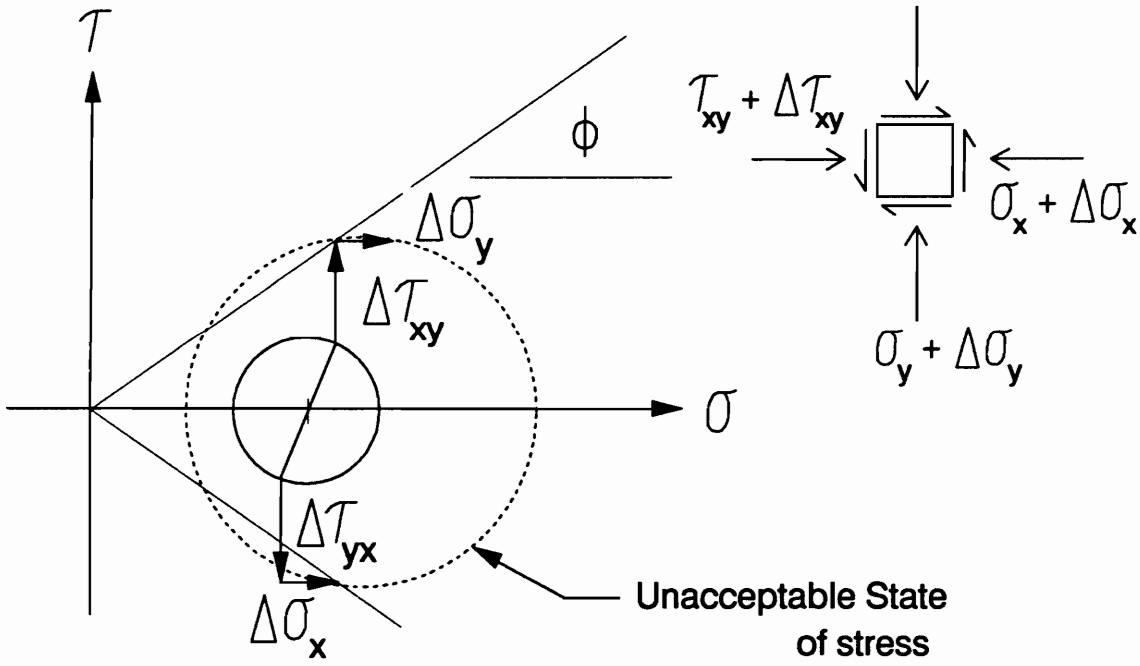

(b) After Load Step

Figure 2.8 - Stress Changes in a Soil Element during a Load Step and the Occurrence of Overshoot

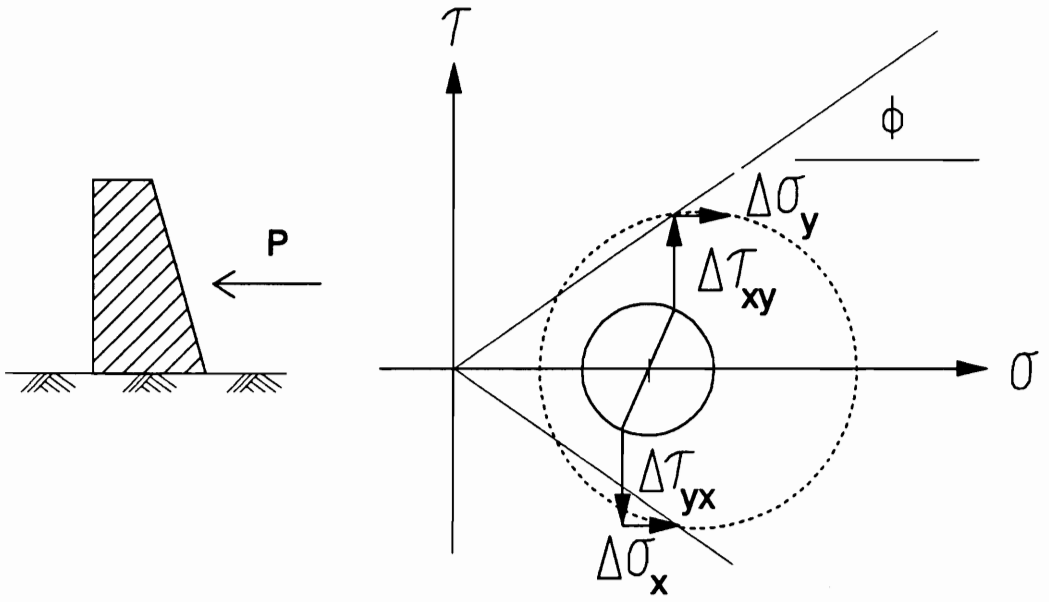

(a) Application of Full load and Corresponding Stress Component Increases in a Soil Element

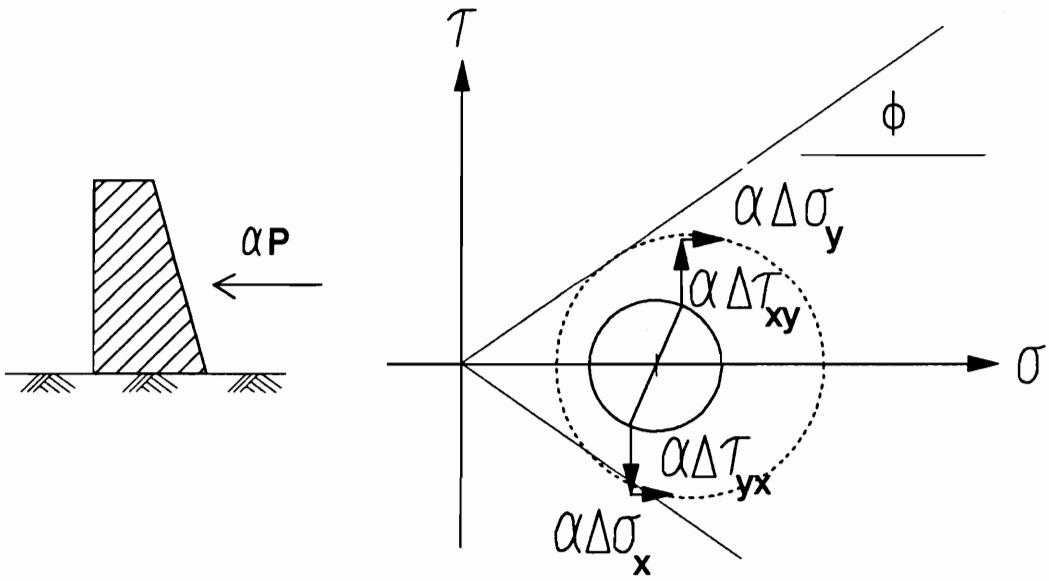

(b) Factored Load and Corresponding Stress Component Increases in a Soil Element

Figure 2.9 - Factoring the Load to Eliminate Overshoot

element will require the smallest value of alpha. Using this alpha value to reduce the load will ensure that failure takes place in the worst stressed element only and nowhere else in the mesh. This worst stressed element is then assigned properties that reduce its ability to carry more load. After this change in the properties of the most severely stressed element, the remaining portion of the load for this particular load step is applied. This process of reducing the load in order to allow only one element to fail at a time is repeated until the entire load for the load step has been applied.

In the process of assigning properties to a failed element, consideration is given to avoiding too abrupt changes in modulus value. When an element first incurs a stress level that indicates failure, its modulus is reduced to one-tenth its value before failure. This process of reducing the modulus is repeated in subsequent loadings for as long as the elements is in a state of failure. In order for the modulus value not to become unrealistically small, the program user can specify a lower limit for the modulus to be assigned to failed elements. When the process of continuous reduction of the value of modulus for a failed element results in a value smaller than the lower limit, its value is kept at the lower limit. It is also at this stage that the element is assigned a failure value of Poisson's ratio. The element retains these property values for as long as it does not recover from failure.

While this procedure allows a gradual transition to failure, it does not completely remove the load carrying capacity of a failed element. Consequently, failed elements are still able to carry some additional load, making it possible for them to exceed a stress level of unity by some amount, which is usually small.

In summary, the steps in the alpha method are as follows : 1.) If overshoot occurs in any soil element, reduce the stresses to eliminate overshoot in the most severely stressed element, 2.) Assign post-failure properties to this element, and 3.) Apply the remaining portion of the load and continue the analysis.

A ROUTINE FOR MODELING RECOVERY FROM A FAILURE STATE

Seed and Duncan (1983) formulated a routine that reduces computational instability associated with too-abrupt changes in modulus value during unloading and reloading. This routine was incorporated in the version of SOILSTRUCT used in this study. In the 1983 model devised by Seed and Duncan, a parameter called the "stress state" (SS) was defined as follows :

$$SS = SL\left(\frac{\sigma_3}{P_{atm}}\right)^{\frac{1}{4}} \tag{2.2}$$

where SL is the stress level defined previously. In the computation of the value os SS, SL cannot exceed unity.

During its loading history, each soil element experiences a maximum value of its stress state ($SS_{max\ past}$). This maximum value defines the element's "critical stress level" (SL_{crit}) through the following relationship :

$$SL_{crit} = \frac{SS_{max\ past}}{\left(\frac{\sigma_3}{P_{atm}}\right)^{\frac{1}{4}}} \tag{2.3}$$

This critical stress level determines whether an element is undergoing primary loading or unload-reload. Fig. 2.10 illustrates how the modulus (E) varies with stress level (SL) for this model. Consider an element that has a stress level indicated by point A on Fig. 2.10. For purposes of illustration, assume that no unloading took place in getting to this condition. The path taken would then be the primary loading curve, which is a second order curve. If and when the stress level decreases, the unload-reload behavior in the 1983 model would depend on

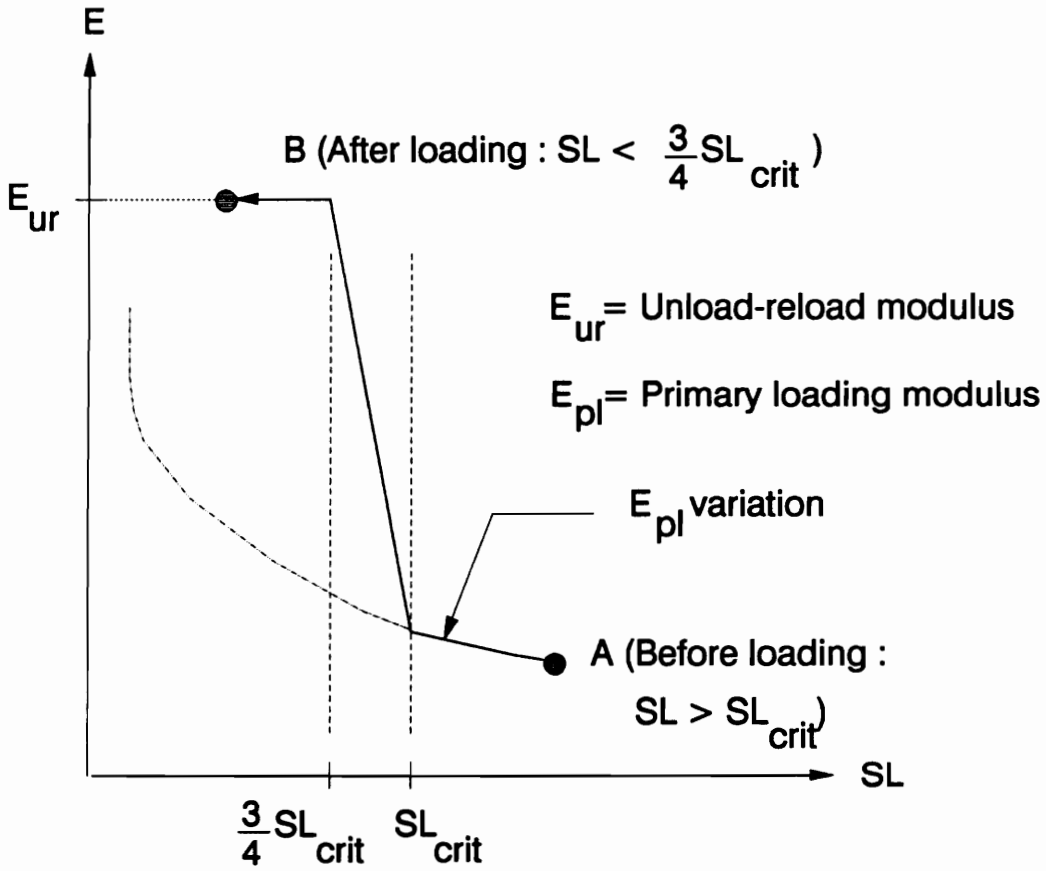

Figure 2.10 - Transition from Primary to Unload-reload Modulus in 1983 Hyperbolic Model

how the value of the current stress level compares with the value of SL_{crit}. As shown on Fig. 2.10, there is a linear variation in modulus between $SL = 0.75*SL_{crit}$ and $SL = SL_{crit}$ which provides a gradual transition in modulus value between primary loading and unloading-reloading states. The figure also illustrates how the E vs. SL behavior of an element may follow this linear path when the element is unloaded. In this example, the element's stress level is reduced to the state indicated by point B, which is a value of stress level less than SL_{crit}.

Another source of computational instability is the too-abrupt change in modulus associated with the transition of a soil element from a failure to a non-failure state. Seed and Duncan's model is able to provide a gradual transition of modulus in most, but not all cases that fit this category. An example of a situation for which this model does not suffice is illustrated in Fig. 2.11(a). Consider an element that has recovered from a failure state. This recovery would be indicated by a current value of SL less than unity. As previously explained, interpolation for the value of the modulus would be carried out if the value of SL is between $0.75*SL_{crit}$ and SL_{crit}. If the value of SL_{crit} for this particular element happens to be greater than unity, a wide range of possibilities exist. At best, SL_{crit} would be only slightly greater than unity, in which case $0.75*SL_{crit}$ would be only slightly greater than 0.75. At worst, SL_{crit} would be larger than to 1.33, in which case $0.75*SL_{crit}$ would be larger than unity. Interpolating for a modulus value using values of $0.75*SL_{crit}$ and SL_{crit} greater than unity is inconsistent with the fact that a maximum value of unity has been set for SL in the computation of the magnitude os the stress state (SS). Furthermore, the effect of interpolating to provide a gradual transition in modulus value would be less pronounced as the value of $0.75*SL_{crit}$ gets closer to unity. In the worst case, SL would not even be between $0.75*SL_{crit}$ and SL_{crit} and the interpolation process would not be carried out at all.

To ensure that the interpolation process would be carried out in such cases, a value of 0.999 is assigned to SL_{crit} whenever it attains a value greater than or equal to unity. As shown

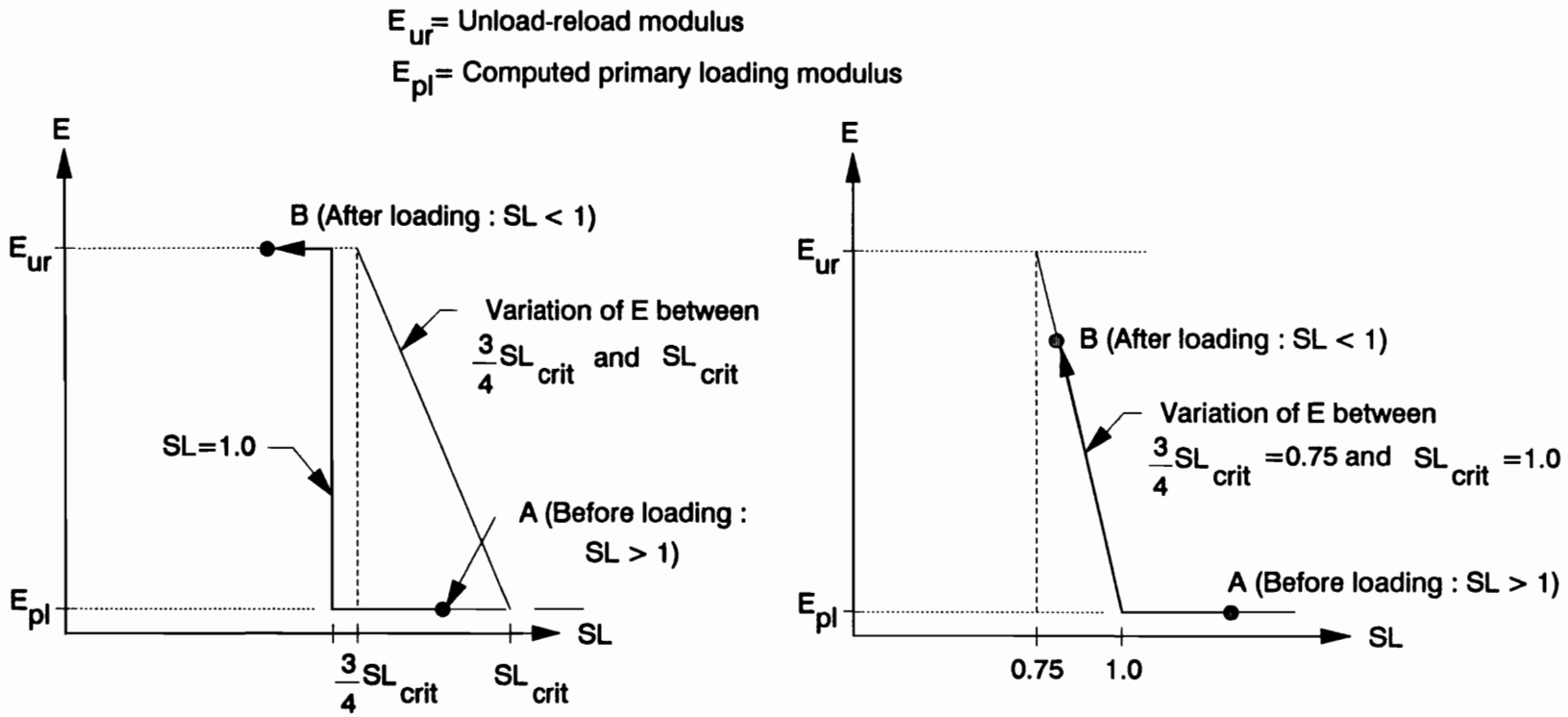

(A) Original 1983 model : possible non-interpolation of modulus value during recovery

(B) Modified 1983 model used whenever the critical stress level exceeds unity

Figure 2.11 - Additional Routine for use in Modeling Failure-to-recovery Behavior based on Seed and Duncan's 1983 Model

on Fig. 2.11(b), SL should be at least equal to 0.75 in order for the interpolation to be carried out.

This failure-to recovery model was incorporated in SOILSTRUCT in addition to the Seed and Duncan (1983) model for unload-reload. Analyses have shown, however, that situations wherein the critical stress level (SL_{crit}) of an element attains a value greater than unity are not very common.

ANALYSES OF CLASSICAL RANKINE EARTH PRESSURE PROBLEMS

Classical Rankine earth pressure problems were chosen to check the effectiveness of the revisions made to SOILSTRUCT. These problems were chosen as test cases primarily because the theoretical solutions are known. Runs were made using the original and the revised versions of the program, and the results were compared with the classical solutions.

The finite element mesh for the analyses, shown in Fig. 2.12, has provisions for a soil backfill, a concrete wall that can translate and rotate, and interface elements between the foundation soil and the elements at the bottom of the backfill. To insure that no shear was transmitted between the wall and soil, stiff bar elements were used to transfer the loads from the wall to the soil. The interface elements at the bottom of the backfill were assigned very low stiffness values to simulate a frictionless interface. The initial stresses in the soil were taken as those defined by the at-rest condition, with the at-rest lateral pressure coefficient equal to 0.37. The backfill soil was cohesionless, with a friction angle equal to 39 degrees.

Prior to the application of any load, the at-rest horizontal stresses in the soil mass have a resultant horizontal force P_o given by

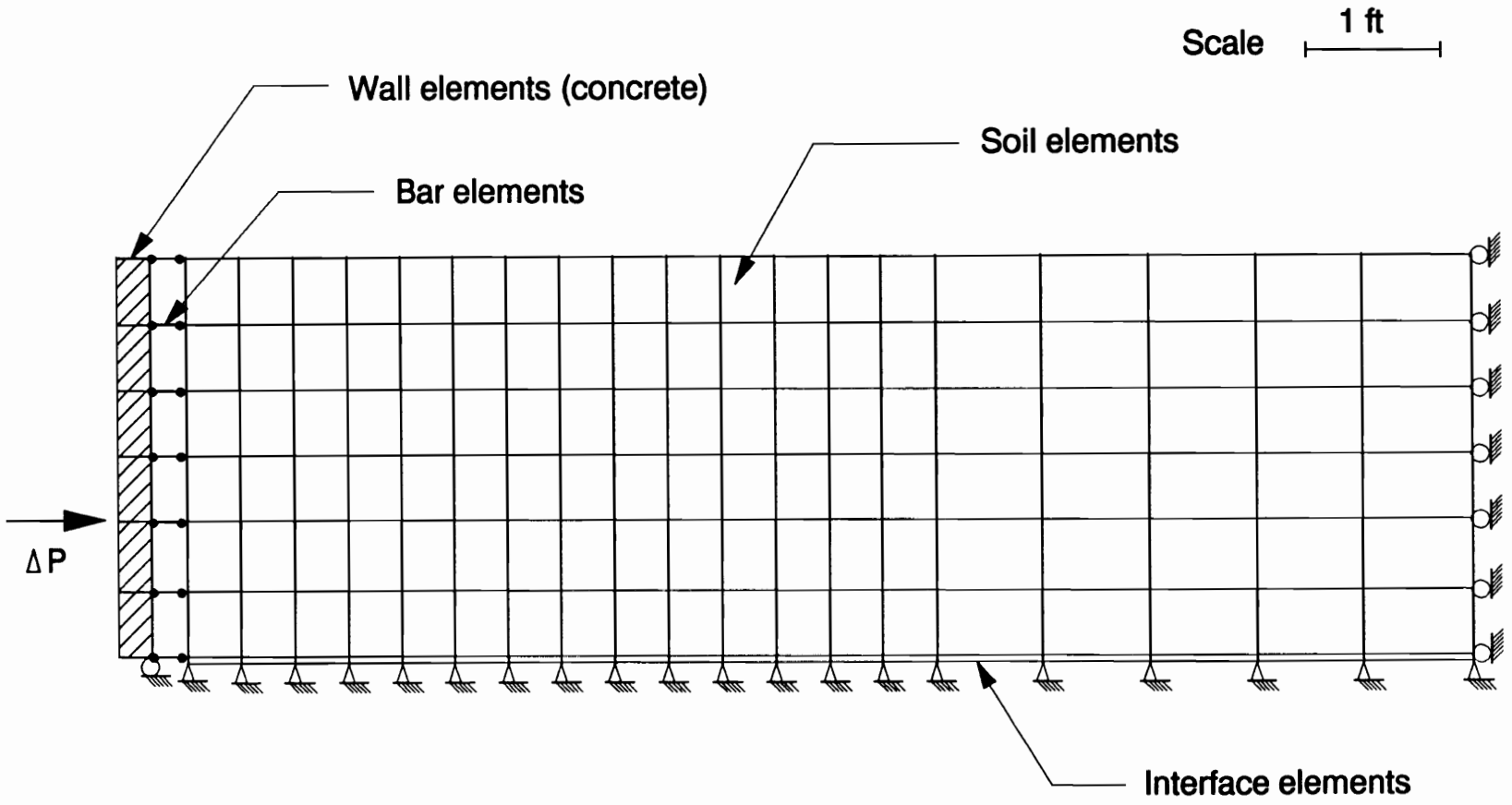

Figure 2.12 - FE Mesh for the Analyses of Rankine Active and Passive Earth Pressure Problems

$$P_o = \tfrac{1}{2}\,\gamma_b h^2 K_o \tag{2.4}$$

where γ_b is the backfill unit weight, h is the height of the backfill and K_o is the at-rest lateral earth pressure coefficient. The wall is then loaded by a horizontal force ΔP at its lower third point loading the wall to the left (the active case) or to the right (the passive case).

When ΔP is directed to the left, away from the backfill, the resultant of the horizontal at-rest stresses in the soil mass is reduced. A continuous reduction of these stresses will eventually bring the soil to the minimum active Rankine state. Letting ΔP_{fa} be the value of ΔP at which this active Rankine state is reached, and letting P_a be equal to the theoretical minimum active Rankine force for the soil mass, then

$$P_a = P_o - \Delta P_{fa} \tag{2.5}$$

Therefore, the theoretical value of the applied force at which active failure will occur is given by

$$\Delta P_{fa} = P_o - P_a \tag{2.6}$$

For the passive Rankine problem, the force ΔP is directed to the right, towards the backfill. As ΔP increases, the resultant of the at-rest stresses in the soil backfill increase. Eventually, the sum of ΔP and P_o will be equal to the theoretical maximum passive force in the soil mass. Letting ΔP_{fp} be the value of ΔP when this takes place, we have

$$P_p = \Delta P_{fp} - P_o \tag{2.7}$$

The theoretical value of the applied force ΔP at which passive failure will occur is thus given by

$$\Delta P_{fp} = P_p - P_o \tag{2.8}$$

RESULTS OF ANALYSES OF THE RANKINE ACTIVE EARTH PRESSURE PROBLEM

The first set of analyses of the active problem were made by loading the wall with a force equal to $\Delta P = 1.38\Delta P_{fa}$, applied in six load steps. Fig. 2.13 shows normalized load-displacement curves resulting from two analyses using the same load increments. One curve is the result of an analysis performed using the original program, and the other is from an analysis performed using the revised version of the program, with the alpha method. The lateral movements of the wall under each load increment were normalized by dividing by the wall height.

In the run performed utilizing the alpha method, very large displacements occurred when the applied load reached $1.03\Delta P_{fa}$, three percent in excess of the theoretical collapse load. A slight excess in the failure load occurs even with the alpha method. This occurs because some elements end up with stress levels slightly greater than 1.00 for the reasons previously explained. On the other hand, the run without the alpha method yielded small values of displacements, even when the full $\Delta P = 1.38\Delta P_{fa}$ had been applied, and thus resulted in a collapse load considerably greater than the theoretical (correct) value. Fig. 2.14 shows the failure regions calculated in the two analyses. The conditions in Fig. 2.14(a) resulted from the application of the full ΔP, while Fig. 2.14(b) shows the conditions just prior to the occurrence of large displacements, at a load less than ΔP. It can be seen that the use of the alpha method results in a failure region closer to that from the Rankine theory. The alpha method also results in considerably better control of overshoot, as indicated by the values of maximum and average

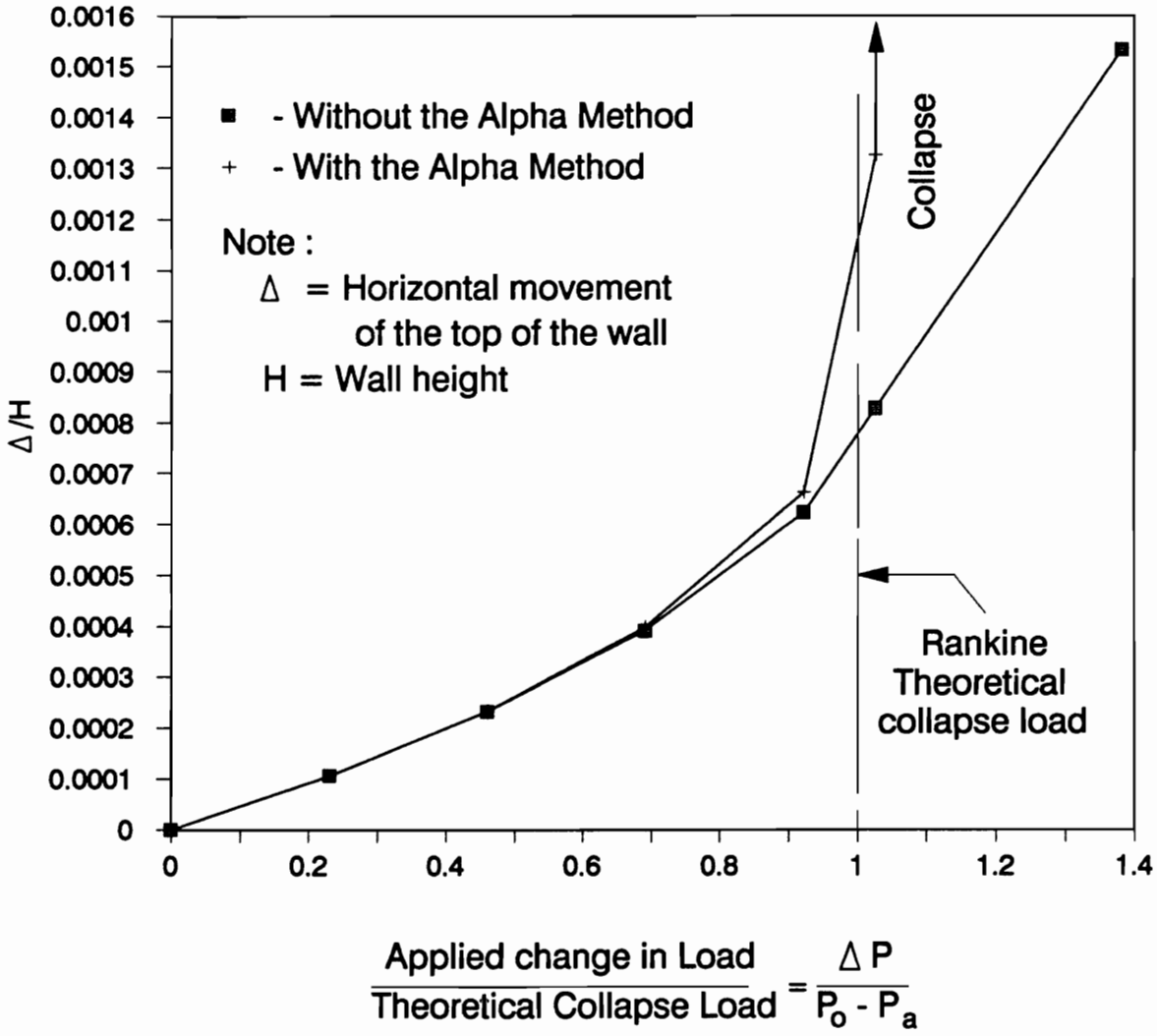

Figure 2.13 - Comparison of Normalized Load-displacement Curves from Analyses of the Rankine Active Pressure Problem with and without the Alpha Method

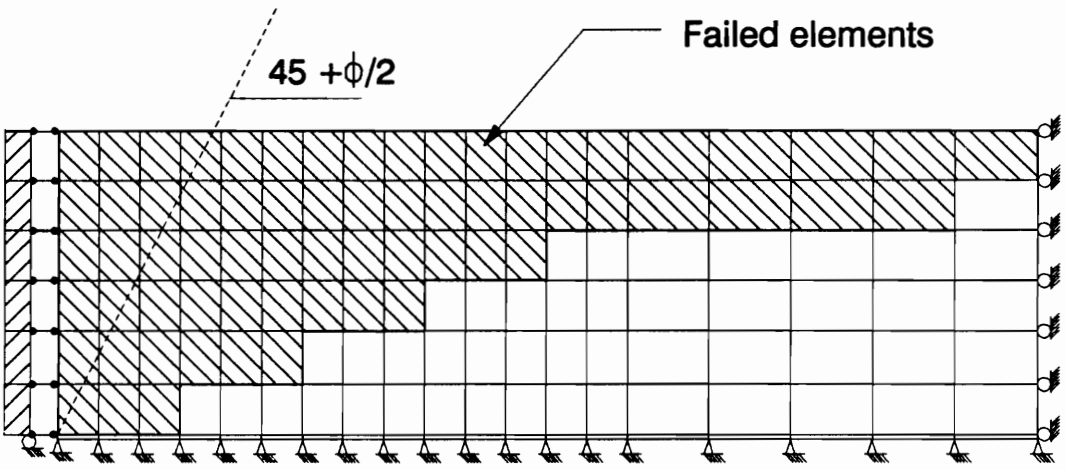

(a) Without the alpha method

Maximum stress level = 1.955
Average stress level = 1.178

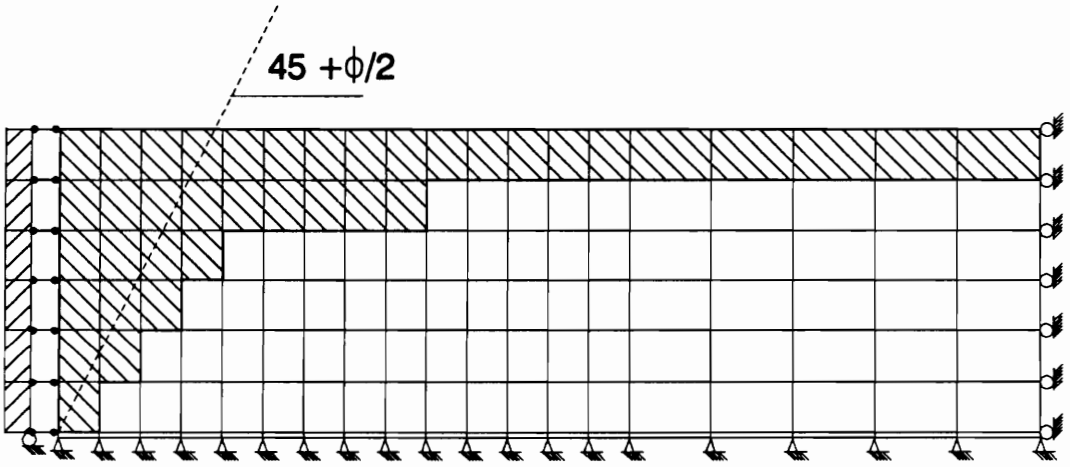

(b) With the alpha method

Maximum stress level = 1.021
Average stress level = 1.001

Figure 2.14 - Failure Regions for the Rankine Active Pressure Problem

stress levels of the failed elements that are shown in Fig. 2.14.

It may be noted that several soil elements located beyond the theoretical failure plane have failed, most notably at or near the surface of the soil. The reason for this occurrence is that there is a difference in the variation of the soil modulus with depth and the variation with depth of the stress decrease brought about by the applied load ΔP. The applied load (ΔP) is statically equivalent to a triangular load distribution applied on the wall, whereas the soil modulus varies parabolically with depth, as shown in Fig. 2.15. This difference gives the elements near the surface greater stiffness-to-load ratios and, as a consequence, these elements carry more of the load until they fail and their load carrying capacities are reduced.

Another result of the difference between the way the load distribution and the stiffnesses vary with depth is the displacement of the wall, as shown in Fig. 2.16. If the stiffness varied linearly with depth, the load would be proportional to the stiffness and the wall would simply translate. The resulting displacements, however, show a combination of translational and rotational movement.

Two additional runs were made using the alpha method to investigate the effect of varying the number of load steps to reach the full load. In one analysis, the full load $\Delta P = 1.38\Delta P$ was applied in a single load step. In the second analysis, the same load was applied in ten load steps, using small load increments as the total load approached the value required to reach a minimum active state. Some results of these runs are given in Table 2.2 along with the run using the alpha method wherein the full load was applied in five load steps. In these runs, collapse occurred at a load within three percent of the theoretical collapse load. The normalized wall displacements prior to collapse were also very close in magnitude, the values being 0.0012 for the ten load step run, 0.0013 for the five load step run and 0.0017 for the one load step run.

The reason for this insensitivity of the results to the number of load steps is that with the alpha method, load increments are automatically reduced in size to the largest that can be

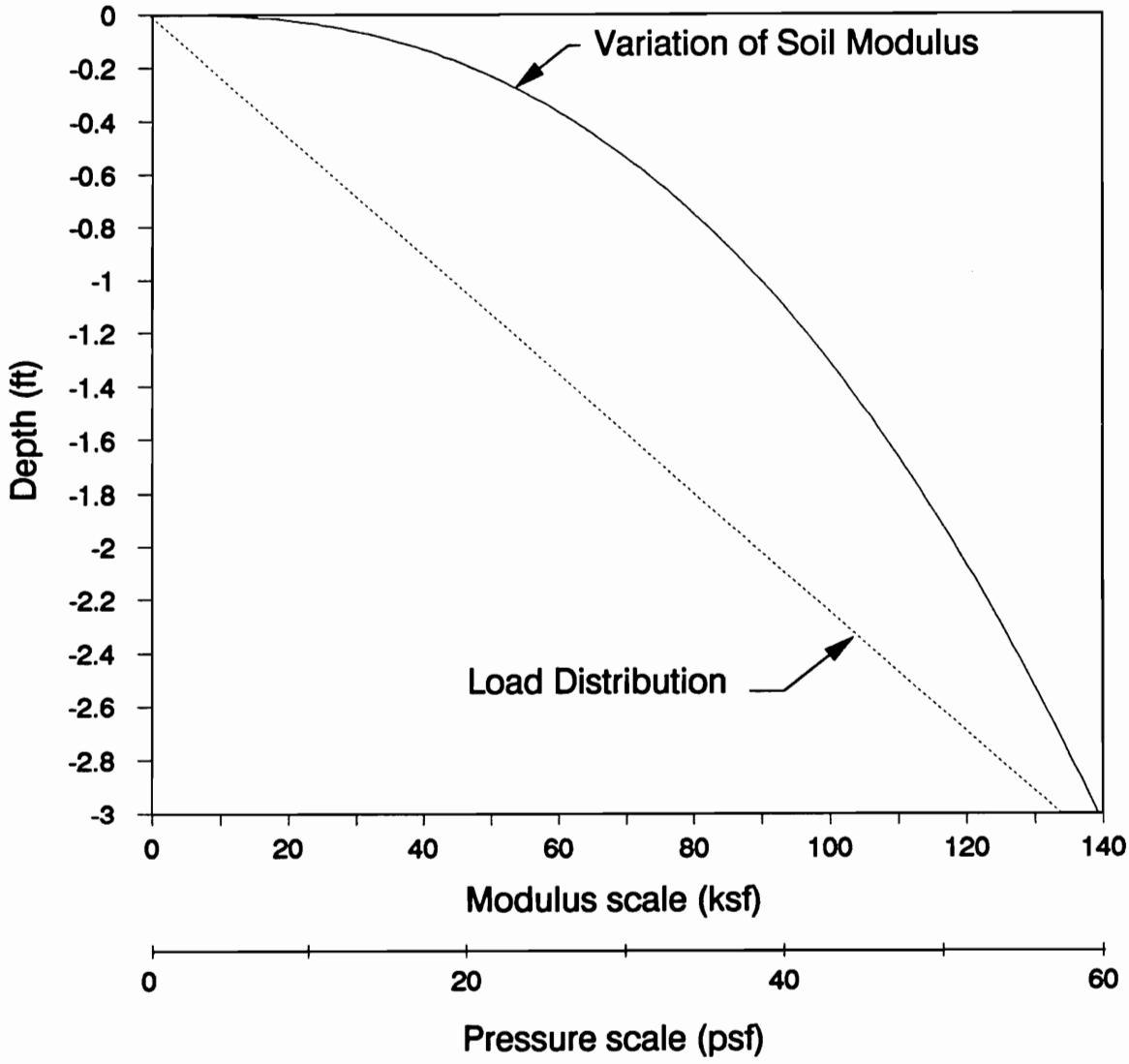

Figure 2.15 - A Comparison of the Variation of Load Distribution and Soil Modulus with Depth

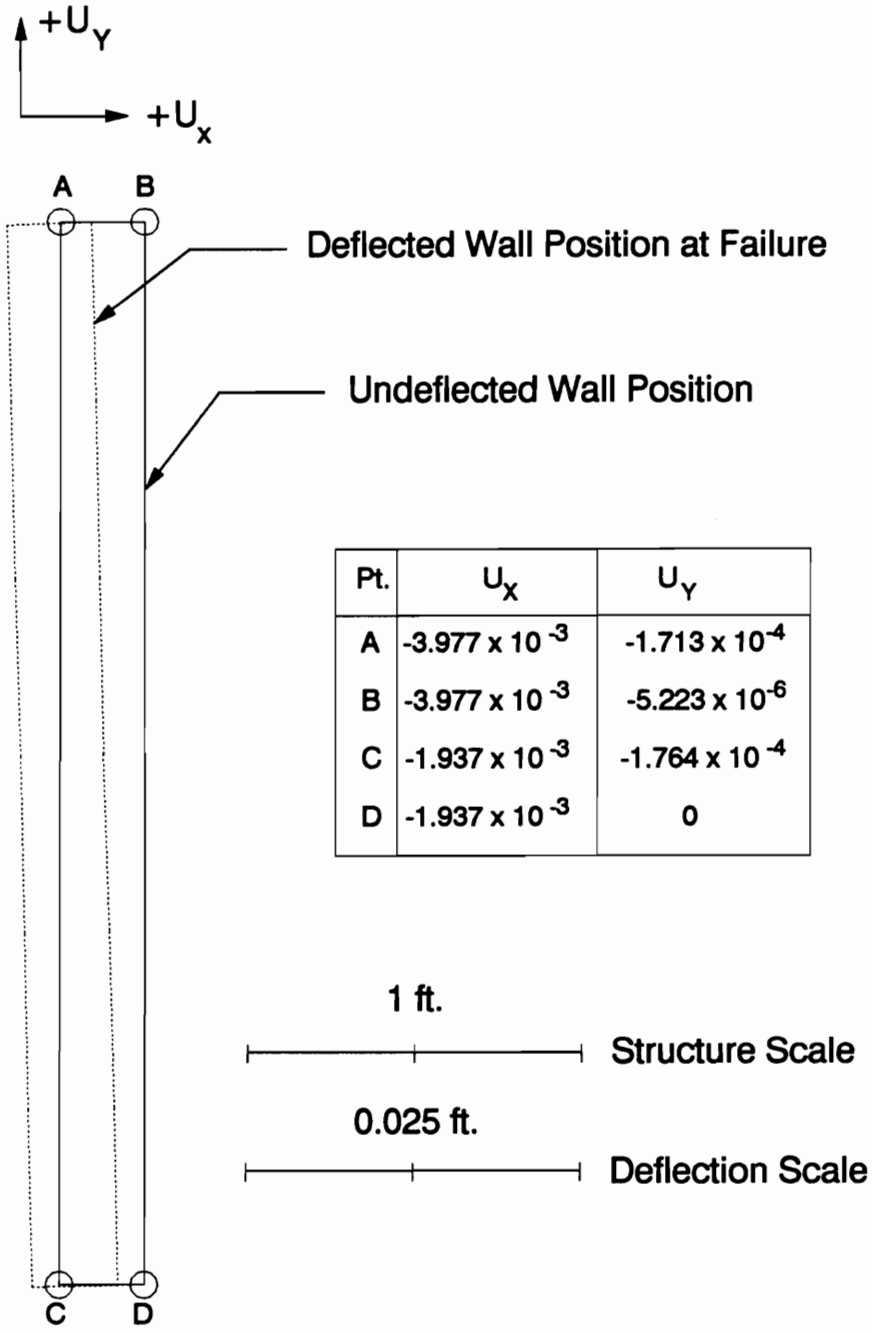

Pt.	U_X	U_Y
A	-3.977×10^{-3}	-1.713×10^{-4}
B	-3.977×10^{-3}	-5.223×10^{-6}
C	-1.937×10^{-3}	-1.764×10^{-4}
D	-1.937×10^{-3}	0

Figure 2.16 - Wall Deflection for the Rankine Active Pressure Problem

Table 2.2 - Results of Rankine Active Analyses with the Alpha Method using Different Load Steps

$\Delta P/\Delta P_{fa}$	No. of Load Steps	$(\Delta P/\Delta R_{fa})$ at Collapse	Δ/H at Collapse
1.38	10	1.03	0.0012
1.38	5	1.03	0.0013
1.38	1	1.03	0.0017

applied without overshoot. This automatic reduction of loads to allow only one element to fail at a time results in loading patterns for each run that bring about similar outcomes, manifested in the closeness of the calculated displacements as well as the calculated load at collapse.

The program SOILSTRUCT was written in such a way that displacements are output either at the at the end of a load step or when collapse occurs. Fig. 2.17 shows the load-displacement curves for the three runs utilizing the alpha method. Among the three runs, the run utilizing ten load steps described the load-displacement relationship best, particularly when the applied load approaches the value required for the minimum active condition.

Duncan, et al. (1990) compiled results of active earth pressure experiments conducted using different types of backfill. Table 2.3 lists the results of the experiments that made use of sand as a backfill. As indicated on the table, the researchers used two different definitions of an active state. The first one is the condition wherein the lateral earth pressure force on the wall is reduced to the minimum value. The experiments that fall under this category yielded values of Δ/H to reach the active state ranging from 0.0003 to 0.0020. The second definition of the active state is the condition whereby the distribution of the lateral earth pressure becomes triangular. Only two experiments fall under this category, and both resulted in Δ/H equal to 0.005 to reach this condition. Combining the results of all the experiments regardless of the definition of the active state yields Δ/H values at failure ranging from 0.0003 to 0.005. It can be seen that the results of the finite element analyses using the alpha method (Δ/H = 0.0012, 0.0013 and 0.0017) all fall within the range of values determined experimentally.

RESULTS OF ANALYSES OF THE RANKINE PASSIVE EARTH PRESSURE PROBLEM

Two analyses of the Rankine passive earth pressure problems were performed. In both

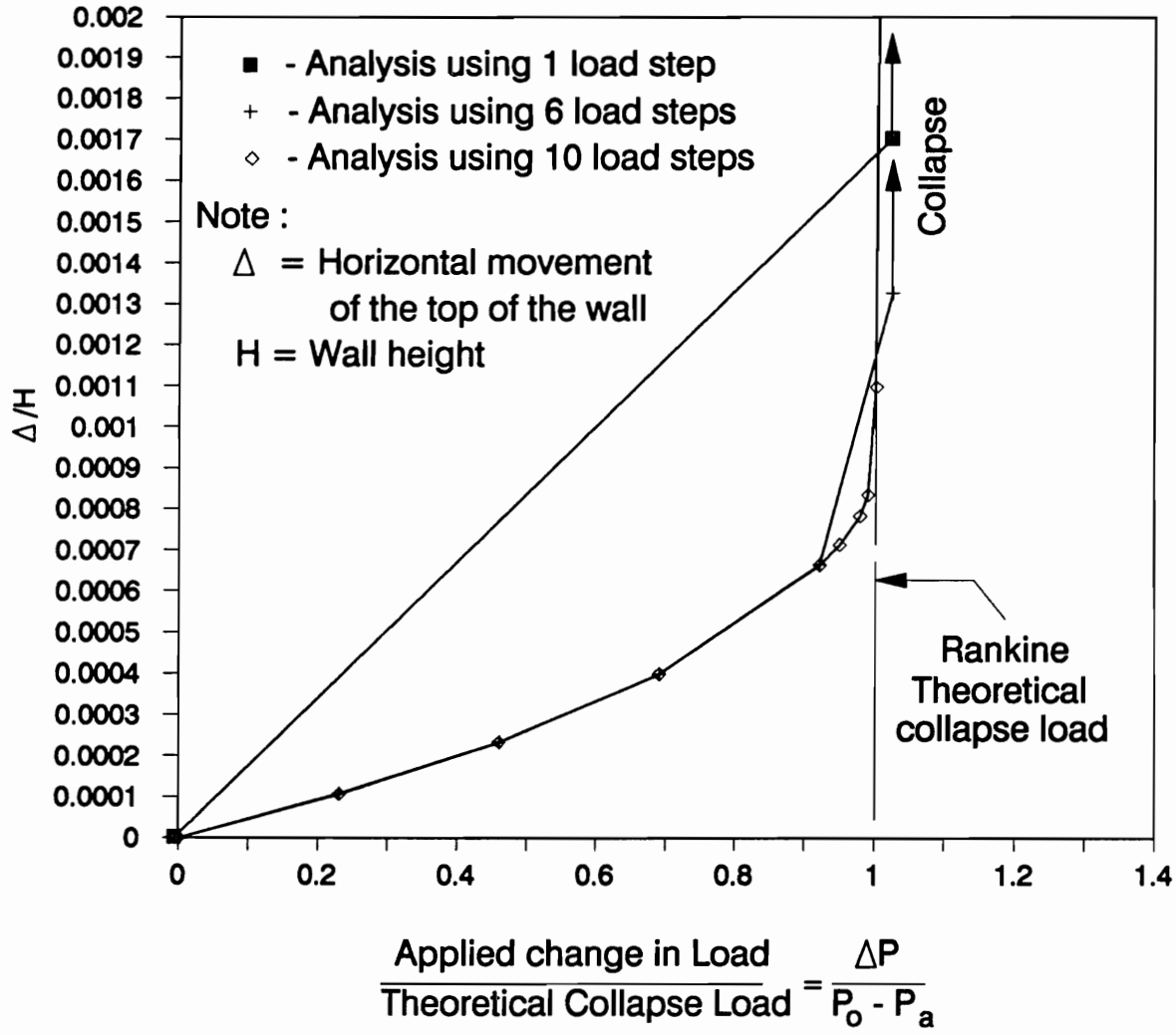

Figure 2.17 - Normalized Load-displacement Curves from Analyses of the Rankine Active Pressure Problem using the Alpha Method

Table 2.3 - Results of Active Earth Pressure Experiments (Adapted from Duncan, et al. (1990))

Investigators	Height (ft.)	Backfill	Compacted	Mode of Movement	Δ/H to Reach Active Failure
Broms & Ingleston (1971)	9.0	Sand	Yes	Rotate	0.0003(1)
Carder et. al. (1977)	6.6	Sand	Yes	Translate	0.0020(1)
Sherif et.al. (1984)	4.0	Sand	Yes	Rotate	0.0005(1)
Sherif et.al. (1984)	4.0	Sand	No	Rotate	0.0005(1)
Terzaghi (1934a)	4.9	Sand	Yes	Rotate	0.0011(1)
Terzaghi (1934a)	4.9	Sand	Yes	Translate	0.0011(1)
Terzaghi (1934a)	4.9	Sand	No	Rotate	0.0020(1)
Terzaghi (1936)	4.9	Sand	Yes	Rotate	0.002 (1)
Terzaghi (1936)	4.9	Sand	Yes	Rotate	0.005 (2)
Terzaghi (1936)	4.9	Sand	Yes	Translate	0.001 (1)
Terzaghi (1936)	4.9	Sand	Yes	Translate	0.005 (2)

(1) Movement to reach minimum total earth pressure force

(2) Movement to develop triangular pressure distribution, with resultant at lower third point

analyses, the wall was loaded with a force equal to $\Delta P = 1.34\Delta P_{fp}$, applied in ten load steps. The force was directed to the right, towards the backfill. One analysis was performed using the original program, and the other performed using the revised program, with the alpha method.

Fig. 2.18 shows normalized load-displacement curves resulting from the two analyses. These results lead to the same observations as those obtained from the analyses of the Rankine active pressure problem : 1) The run utilizing the alpha method yields large displacements when the applied load is very close to the theoretical value required for the maximum passive condition. In this case, $\Delta P = 1.04\Delta P_{fp}$ at collapse, the slight excess attributed to causes cited in the previous section. 2) The run without the alpha method yields small values of displacements even when the applied load is considerably greater than the theoretical (correct) value.

Fig. 2.19 shows the failure regions obtained from these analyses. The regions in Fig. 2.19(b) correspond to the condition just prior to collapse, at an applied load less than the full ΔP. Again, the use of the alpha method results in a failure region closer to that from the Rankine theory. Better control of overshoot also resulted from the use of the alpha method, as indicated by the maximum and average stress levels of the failed elements, as given in Fig. 2.19.

The effect of varying the number of load steps to reach the full load was also investigated. The analysis was carried out by applying $\Delta P = 1.34\Delta P_{fp}$ in just one load step. Table 2.4 lists results from this analysis, together with results from the analysis with the alpha method of the same load applied in ten load steps. Collapse in both analyses occurred at an applied load within four percent of the theoretical collapse load. The normalized wall displacements prior to collapse were 0.011 for the ten load step run and 0.017 for the one load step run.

These results again demonstrate how the use of the alpha method renders the end result insensitive to the number of load steps used. However, as discussed in the previous section, one

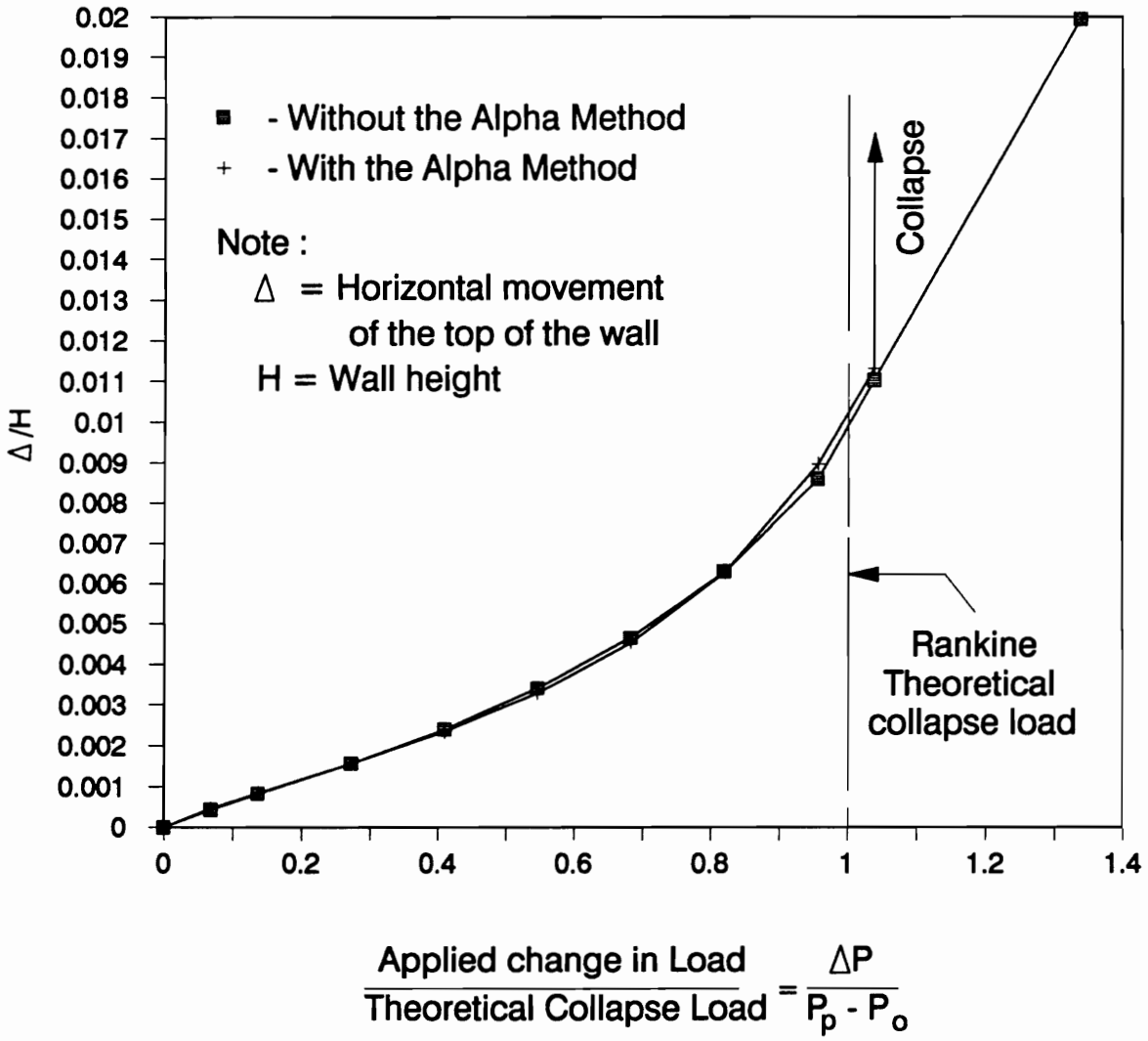

Figure 2.18 - Comparison of Normalized Load-Displacement Curves from Analyses of the Rankine Passive Pressure Problem with and without the Alpha Method

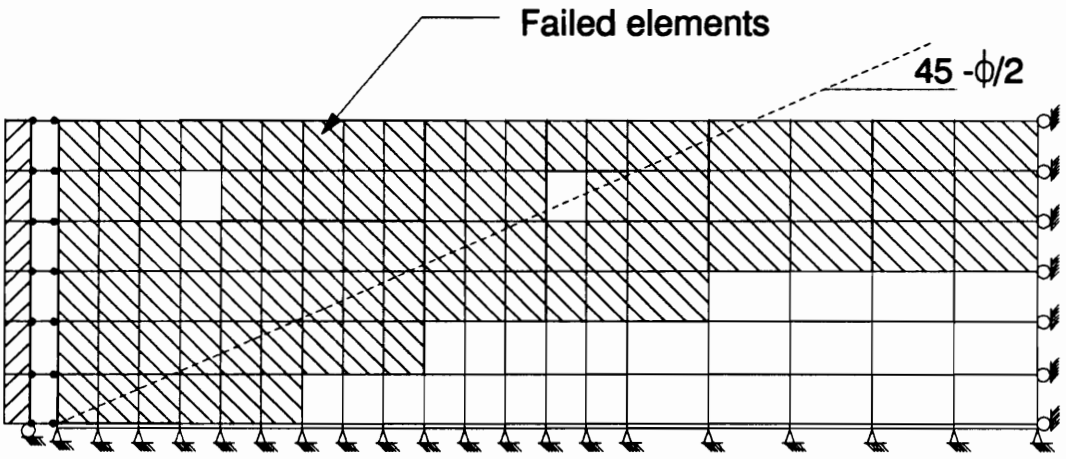

(a) Without the alpha method

Maximum stress level = 2.567
Average stress level = 1.246

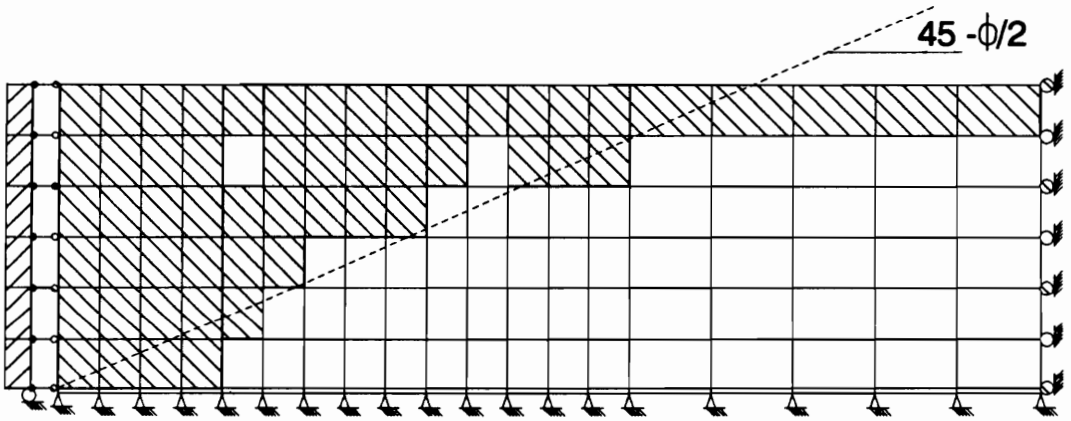

(b) With the alpha method

Maximum stress level = 1.141
Average stress level = 1.029

Figure 2.19 - Failure Regions for the Rankine Passive Pressure Problem

Table 2.4 - Results of Rankine Passive Analyses with the Alpha Method using Different Load Steps

$\Delta P/\Delta P_{fp}$	No. of Load Steps	$(\Delta P/\Delta P_{fp})$ at Collapse	Δ/H at Collapse
1.34	10	1.04	0.011
1.34	1	1.02	0.017

must use at least two load steps in order to obtain intermediate results.

The results of passive pressure experiments using sand as backfill were compiled by Duncan, et al. (1990), and given in Table 2.5. In these experiments, the normalized wall displacements, Δ/H required to reach passive conditions ranged from 0.001 to 0.06. The results from the finite element analyses using the alpha method (Δ/H = 0.011, 0.017) fall within the range of experimental values.

SUMMARY

The occurrence of large overshoot in two-dimensional soil elements is a problem in finite element analyses of soil masses that may lead to unrealistic results. The alpha method for two-dimensional elements was developed for the purpose of controlling overshoot in these elements. Analyses of Rankine active and passive earth pressure problems were performed using versions of the finite element program SOILSTRUCT with and without the alpha method, and the results were compared with the ideal theoretical results. It was found that analyses that utilized the alpha method resulted in excellent control of overshoot. The control of overshoot in individual elements was manifested in the behavior of the entire system, particularly when the system is in a near-failure condition. Fig. 2.20 combines results of four of the analyses and shows how the lateral pressure coefficient varied with normalized wall displacements for analyses performed with and without the alpha method. As shown in this figure, overshoot is apparent in the analyses performed without the alpha method, as the system experienced forces corresponding to values of lateral pressure coefficients much outside theoretical values defined by the $K_h = K_p$ and $K_h = K_a$ lines. On the other hand, the use of the alpha method resulted in behavior much closer to theory.

Table 2.5 - Results of Passive Earth Pressure Experiments (Adapted from Duncan, et al. (1990))

Investigators	Height (ft.)	Backfill	Compacted	Mode of Movement	Δ/H to Reach Passive Failure
Broms & Ingleston (1971)	9.0	Sand	Yes	Rotate	0.005
Carder et. al. (1977)	3.3	Sand	Yes	Translate	0.025
Tcheng & Isux (1972)	9.8	Sand	Yes	Rotate	0.02 to 0.06
Terzaghi (1934a)	4.9	Sand	Yes	Rotate	0.001

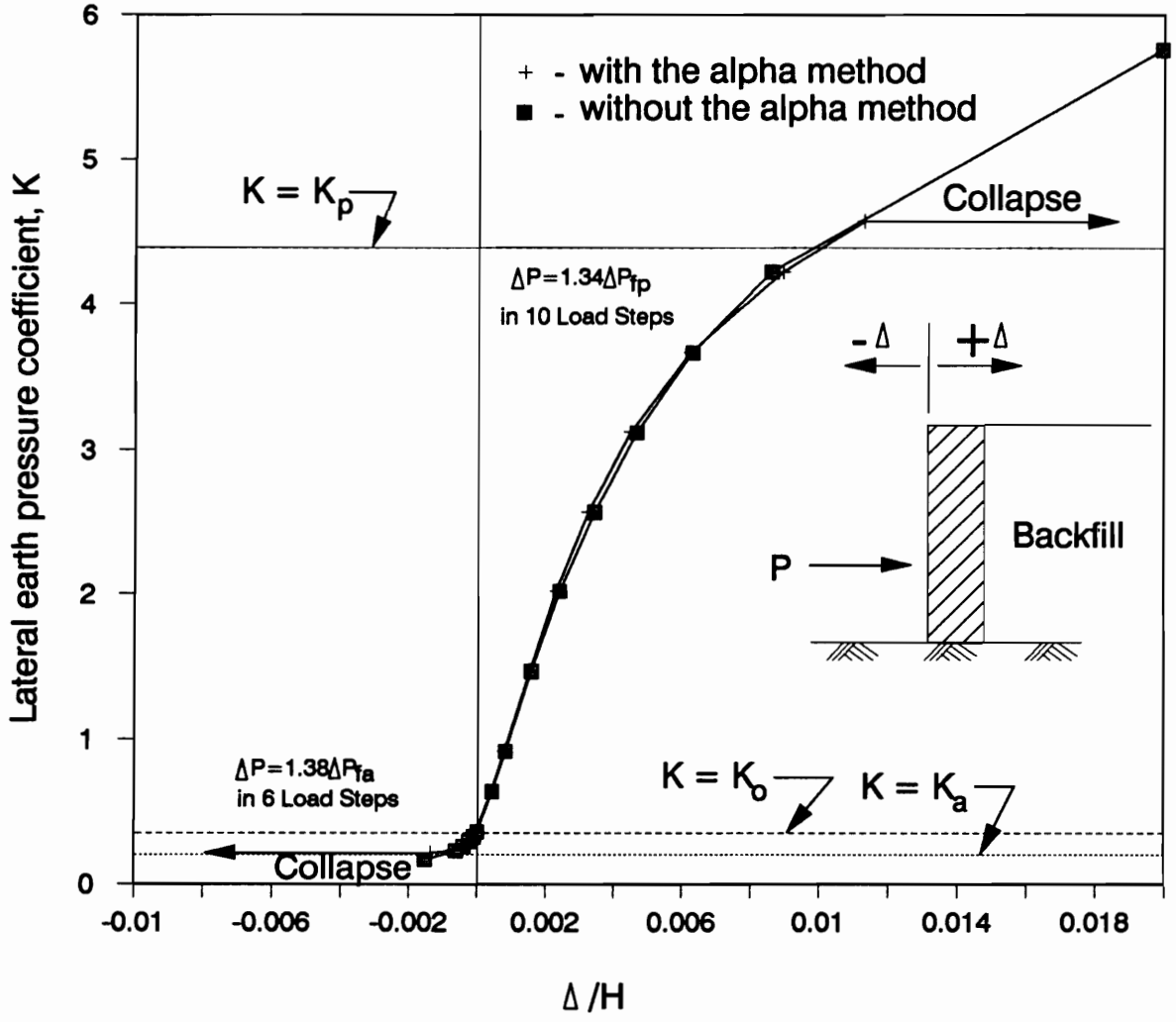

Figure 2.20 - Lateral Earth Pressure Coefficient vs. Normalized Wall Displacements - Rankine Analyses

CHAPTER 3

BEARING CAPACITY ANALYSES

INTRODUCTION

The results of the finite element analyses described in the next chapter show clearly the importance of the bearing capacity of the foundation soil under the eccentric and inclined loads imposed by the walls. In evaluating the results of the finite element analyses, it was found to be useful to compare the conditions causing failure to the results of bearing capacity calculations. The theory used for the comparison was the one developed by Vesic' (1973), which was judged to be the most accurate available. As presented by Kulhawy (1983), it accounts for load inclination, load eccentricity, and soil compressibility. The principal features of this theory are described in the following paragraphs.

MECHANISMS OF BEARING FAILURE

Bearing capacity failures can be divided into three types, depending on the compressibility of the soil. These three mechanisms are illustrated in Fig. 3.1. They are : (a) General shear failure, (b) Local shear failure, and (c) Punching shear failure.

General shear failure occurs when the compressibility of the foundation soil is so small that it is possible to mobilize the full strength of the soil mass with negligibly small displacements, a mode of behavior referred to in the theory of plasticity as a "rigid plastic" behavior. As shown in Fig. 3.1(a), the failure surface in this mode of failure is a well-defined

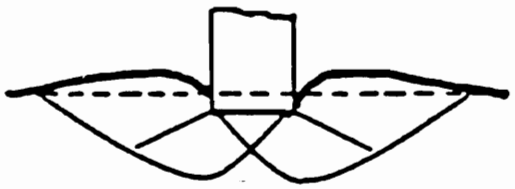

(a) General Shear

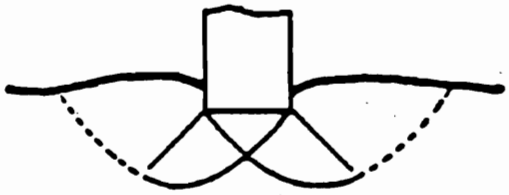

(b) Local Shear

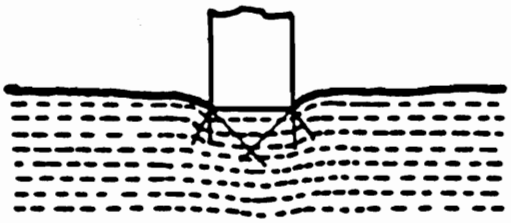

(c) Punching Shear

Figure 3.1 - Modes of Bearing Capacity Failure (Adapted from Vesic', 1973)

surface which forms a complete failure mechanism extending to the surface of the foundation soil adjacent to the footing.

As the compressibility of the foundation soil increases, the magnitudes of the displacements that occur when loads are applied to the footing increase. Because of these larger displacements, the shear failure in the soil is localized within an area beneath the footing. The resulting "local shear" failure is illustrated in Fig. 3.1(b). The failure surface does not extend to the top of the foundation soil, although bulging of the surface may occur. As loads are applied to the footing and displacements occur, the footing shifts to a new position before this failure surface develops fully. With the footing in a lower position, a second failure surface begins to develop within the soil. The development of this new failure surface is once again disrupted because of large displacements. As a result, no failure mechanism is ever developed fully, and the strength of the foundation soil is never fully mobilized.

Punching shear failure occurs when the foundation soil is extremely compressible. As illustrated in Fig. 3.1(c), the foundation punches through the soil in this mode of failure, without significant or extensive shear failure. The failure surface in this case is not well-defined. The failure mechanism is dominated by compression of the soil immediately beneath the footing.

VESIC'S (1973) BEARING CAPACITY THEORY

In general, bearing capacity decreases as the soil becomes more compressible, or less rigid. Vesic' (1973) suggested the use of a rigidity index, I_r, as a measure of how "rigid" a soil is. I_r is defined by the following equation :

$$I_r = \frac{G}{c + q_c \tan\Phi} \tag{3.1}$$

where q_c is a characteristic pressure equal to the overburden pressure at a depth of $B/2$ (B is the width of the foundation), G is the shear modulus at the same depth, and c and Φ are the soil strength parameters. For cohesionless soils, c is equal to 0, and I_r can be expressed as

$$I_r = \frac{G}{q_c \tan\Phi} \tag{3.2}$$

The shear modulus, G, can be expressed in terms of Young's modulus, E, and Poisson's ratio, ν_s, leading to the following expression for I_r for cohesionless soils :

$$I_r = \frac{E}{2\,(1+\nu_s)\,q_c \tan\Phi} \tag{3.3}$$

For the purpose of computing the value of E, the following equation based on a hyperbolic stress-strain model (Duncan, et al., 1973) was used :

$$E = K\,P_{atm}\left(\frac{\sigma_3}{P_{atm}}\right)^n (1 - R_f * SL)^2 \tag{3.4}$$

where K, n and R_f are the modulus number, modulus exponent and failure ratio. The value of the stress level SL used in the computation of the modulus E was based on at-rest stresses in the soil. The confining pressure σ_3 was computed using the following equation :

$$\sigma_3 = K_o q_c \tag{3.5}$$

where q_c is the characteristic pressure described previously.

To establish whether a soil mass should be considered "compressible" or "incompressible"

for the purpose of estimating its bearing capacity, the value of I_r is compared with a "critical rigidity index", I_{rc}, given by the following equation (Vesic', 1973) :

$$I_{rc} = \frac{1}{2} exp\ [(3.30 - 0.45 \frac{B}{L}) \cot (45^\circ - \frac{\Phi}{2})] \tag{3.6}$$

where B and L are the width and length of the foundation base, respectively. When $I_r > I_{rc}$, the soil mass is sufficiently rigid so that it may be considered to behave as a rigid-plastic material.

As discussed previously, the failure mode for a rigid-plastic material would be general shear failure. On the other hand, when $I_r < I_{rc}$, local or punching shear failure would be expected, and the bearing capacity is reduced accordingly.

Kulhawy (1983) presented a general bearing capacity equation based on the works of Hansen (1970) and Vesic' (1973). This equation contains several factors that take into account the effects of soil compressibility, foundation shape, load inclination, foundation base tilt, ground surface inclination and depth of foundation. Although lengthy in its complete form, the equation may be simplified when the conditions being analyzed do not involve all of the various complicating conditions considered by Kulhawy (1983).

BEARING CAPACITY ANALYSIS OF GRAVITY RETAINING WALLS

The following conditions were used to simplify the bearing capacity equation for use in the analyses of gravity retaining walls in this report :

(1) The wall footings were considered to be infinitely long strip footings,

(2) The foundation soil was considered to be cohesionless, with a horizontal ground surface,

(3) The base of the wall was considered to be at the ground surface,

(4) Backfill placed on the ground surface is weaker than the underlying soil, and so the failure surface will not extend into it,

(5) The wall was considered to be subjected to an inclined load resulting from the vertical and horizontal forces from the weight of the wall and the loads imposed by the backfill

These considerations simplify the general bearing capacity equation to the following form :

$$q_{ult} = \frac{1}{2}\,\gamma_s\, B_e N_\gamma \xi_{\gamma r} \xi_{\gamma i} + q_s N_q \xi_{qr} \xi_{qi} \tag{3.7}$$

where B_e is the width of the wall base in contact with the foundation soil and q_s is the magnitude of the surcharge on the ground surface. N_γ and N_q are bearing capacity factors whose values depend solely on Φ. $\xi_{\gamma i}$ and ξ_{qi} are factors that take into account the effects of load inclination, and $\xi_{\gamma r}$ and ξ_{qr} are factors that take into account the effects of soil rigidity.

For cohesionless foundation soil, the inclination factors are given by the following equations :

$$\xi_{\gamma i} = (1 - \frac{T}{N})^3 \tag{3.8}$$

$$\xi_{qi} = (1 - \frac{T}{N})^2 \tag{3.9}$$

where T and N are the resultant horizontal and vertical forces on the footing. In the case of a

retaining wall, these forces are due to the weight of the wall and the horizontal and vertical loads exerted on the wall by the backfill.

The compressibility factors $\xi_{\gamma r}$ and ξ_{qr} are both equal to unity if the soil behaves as a rigid plastic material ($I_r > I_{rc}$). Otherwise,they are computed using the following equation (Vesic', 1973) :

$$\xi_{\gamma r} = \exp \{ [(-4.4 + 0.6 \frac{B}{L}) \tan \Phi] + [(3.07 \sin \Phi) \log_{10}(2I_r) / (1 + \sin \Phi)] \} \quad (3.10)$$

$$\xi_{qr} = \xi_{\gamma r} \quad (3.11)$$

The second term in the right hand side of the bearing capacity equation (Equation 3.7) accounts for an increase in the ultimate bearing capacity due to the stabilizing effect of a surcharge on the ground surface. This term, however, was added on the assumption that a uniform surcharge, q_s, existed on both sides of the footing. This raises the question of whether or not this equation is applicable to retaining wall problems where q_s exists only on one side of the wall. If the surcharge existed only on one side, a direct application of Equation 3.7 would overestimate the ultimate bearing capacity, leading to unconservative results. Furthermore, the presence of a surcharge on one side would only increase the tendency of the wall to fail by bearing capacity in the direction of the side without the surcharge.

A conservative approach would be to neglect the surcharge term completely. The bearing capacity of the foundation would be solely due to the weight of the soil in the failure zone, and the bearing capacity equation would have the following form :

$$q_{ult} = \frac{1}{2}\gamma_s B_e N_\gamma \xi_{\gamma r} \xi_{\gamma i} \quad (3.12)$$

Even with this form of the bearing capacity equation, the effects of the presence of q_s on one side of the footing would still have to be accounted for, a problem which will be addressed in the paragraphs to follow.

Two formulations of the bearing capacity problem were tested for applicability to the retaining wall problem. In the first formulation, shown in Fig. 3.2(a), the retaining wall or footing is subjected to the inclined load R, which is the resultant of the horizontal and vertical forces exerted by the backfill. The surcharge is equal to zero on both sides of the wall, making the form of the bearing capacity equation given by Equation 3.12 applicable. The characteristic pressure, q_c, was computed as follows :

$$q_c = \gamma_s \frac{B}{2} \tag{3.13}$$

The second formulation, shown in Fig. 3.2(b), is the same as the one given in Fig. 3.2(a), with the exception of the vertical backfill pressure. In this formulation, the form of the bearing capacity equation given by Equation 3.12 was still used. However, the presence of the surcharge on one side of the wall was considered in the calculation of the characteristic pressure q_c as follows :

$$q_c = \gamma_s \frac{B}{2} + q_s \tag{3.14}$$

A first series of bearing capacity analyses of the retaining walls were performed using the formulation given in Fig. 3.2(a), ignoring completely the effects of the vertical backfill pressure and making use of Equation 3.12. Analyses were performed to determine the load on the wall and the corresponding height of backfill behind the wall, required to cause a bearing capacity failure in the soil beneath the wall. Where the backfill height that would be required to cause

Note : The modulus E and the characteristic pressure q_c are evaluated at point A

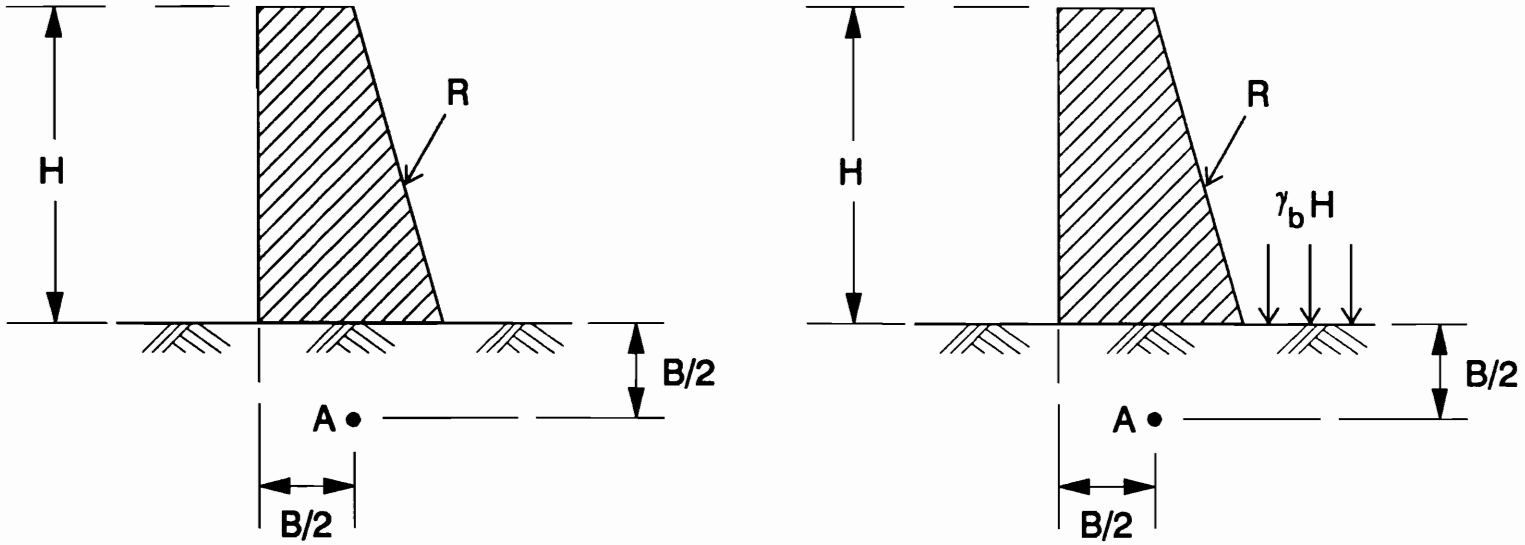

(a) Vertical backfill pressure neglected

(b) Vertical backfill pressure included

Figure 3.2 - Two ways of Formulating the Retaining Wall Problem as a Bearing Capacity Problem

failure was greater than the wall height, this was denoted as "no failure" (NF), because the maximum height of backfill did not cause failure. Backfill heights at failure for this set of analyses are given in the center column in Table 3.1, along with the backfill heights at failure obtained from finite element analyses. A comparison of the two sets of results show that the backfill heights at failure calculated using the formulation described above consistently yielded higher backfill heights at failure than those obtained using the finite element method. In four cases, (Runs FOL4B, FOL6B, FOL6C AND FOL7A), the differences between the two sets of backfill heights at failure ranged from 10 to 25 percent of the wall height. Only Run FOL7B yielded a close agreement between the two analyses, with the difference in the backfill height at failure equal to only one percent of the wall height. In one case (Run FOL2B), the first formulation indicated that the wall was stable whereas the finite element method indicated wall collapse. In general, this formulation (ignoring completely the effects of the vertical backfill pressure) yields unconservative results.

A second set of analyses of the bearing capacities of the retaining walls was performed, with the problem formulated in the manner illustrated in Fig. 3.2(b). For purposes of calculating values of the characteristic pressure, q_c, for these analyses, the backfill pressure ($\gamma_b H$) was added to q_c (Equation 3.14), as if the backfill actually existed on both sides of the wall. As pointed out earlier, although the backfill pressure was included in the expression for q_c, the surcharge was taken as zero for purposes of calculating the bearing capacity. This seems logical because there is no surcharge in front of the wall, and the failure mechanism can develop in that direction. The backfill heights at failure resulting from this second formulation and Vesic's method are given in the right-hand column of Table 3.1. Comparing these results with those from the finite element analyses, it can be seen that the two sets of results are in quite good agreement. Although the second formulation can give a backfill height at failure either higher or lower than what the finite element method would yield, the differences in the predicted

Table 3.1 Height of Backfill at Failure as obtained from Finite Element Analyses and Analyses of two Formulations of the Bearing Capacity Problem

Run	Finite Element Analyses	Bearing Capacity Analyses using First Formulation and Vesic' Method	Bearing Capacity Analyses using Modified Formulation and Vesic' Method
FOL1A	NF	NF	NF
FOL1B	NF	NF	NF
FOL1C	NF	NF	NF
FOL2A	NF	NF	NF
FOL2B	28.7	NF	26.9
FOL3A	NF	NF	NF
FOL3B	NF	NF	NF
FOL4A	NF	NF	28.3
FOL4B	21.6	28.7	23.6
FOL4C	NF	NF	NF
FOL5A	NF	NF	NF
FOL5B	NF	NF	NF
FOL6A	NF	NF	NF
FOL6B	31.0	34.8	31.3
FOL6C	31.2	35.4	30.4
FOL7A	20.9	24.0	21.2
FOL7B	28.9	29.2	26.5
FOL7C	NF	NF	NF
FOL8A	NF	NF	NF
FOL9A	NF	NF	NF

Note : All dimensions are in feet
NF = No Failure

backfill heights at failure between the two methods are small, never more than about 8 percent of the wall height.

SUMMARY

This study shows that if the bearing capacity problem is formulated so that the effects of the vertical backfill pressure are accounted for in an appropriate way, Vesic's theory provides an effective means of evaluating the loads required to cause bearing capacity failure in the soil beneath gravity retaining walls. The effects of the vertical backfill pressure are accounted for as follows :

(1) In evaluating the characteristic pressure, q_c, used to evaluate Young's Modulus and the compressibility index, I_r, the full depth of fill behind the wall is considered, as indicated by equation 3.14.

(2) In calculating the ultimate bearing capacity, the surcharge in front of the wall is considered. In these cases, with the walls founded on the ground surface, the surcharge was zero, and the ultimate bearing capacity was given by equation 3.12.

CHAPTER 4

RESULTS OF FOLLOWING LOAD ANALYSES OF GRAVITY RETAINING WALLS ON SOIL

INTRODUCTION

The results of following load analyses of gravity retaining walls founded on soil are discussed in this chapter. These analyses were performed using the revised version of the finite element program SOILSTRUCT described in Chapter 2. This version of SOILSTRUCT employs the Alpha Method for two-dimensional elements, and the Seed and Duncan (1983) model for unload-reload behavior of soil elements.

The values of parameters that characterize the wall-foundation system were varied systematically in the analyses. The parameters that were varied included :

(1) The shear stiffness value assigned to the interface elements between the wall and the foundation soil (K_s)

(2) The lateral earth pressure coefficient that governs the magnitude of the horizontal thrust on the wall (K_h)

(3) The value of Poisson's ratio assigned to the foundation soil (ν_s)

(4) The relative density of the foundation soil (D_r)

(5) The thickness of the foundation soil (D_f)

(6) The height of the wall (H)

(7) The width of the base of the wall (B)

(8) The presence or absence of a toe fill

(9) The method used to simulate construction of the retaining wall

Table 2.1 in Chapter 2 lists the range of values used for these parameters, and the values of the other parameters, which were kept constant in the analyses.

Using the results of the finite element analyses, the following aspects of the behavior of the retaining wall have been examined :

(1) The extent of the zones of failure within the foundation soil,

(2) The normal and shear stresses on the base of the walls, and the effective base contact areas, and

(3) The horizontal displacements at the top of the walls.

A RE-ANALYSIS OF THE BASE CASE PROBLEM

The base case problem described in Chapter 2, which was analyzed using the original version of SOILSTRUCT was re-analyzed using the revised version of the program that contains the Alpha Method (Chapter 2).

Fig. 4.1 shows the failure regions resulting from the analysis of the base case problem using the revised version of SOILSTRUCT. A comparison between the failure regions obtained using the original version and those using the Alpha Method can be made by comparing Fig. 4.1 and Fig. 2.6. It can be seen that there is no significant difference between the results of the two analyses for the stage immediately after the wall placement. After the backfilling operation, however, the results of the analysis using the Alpha Method showed more extensive failure, and considerable improvement in the control of overshoot. The overshoot in the analysis using the

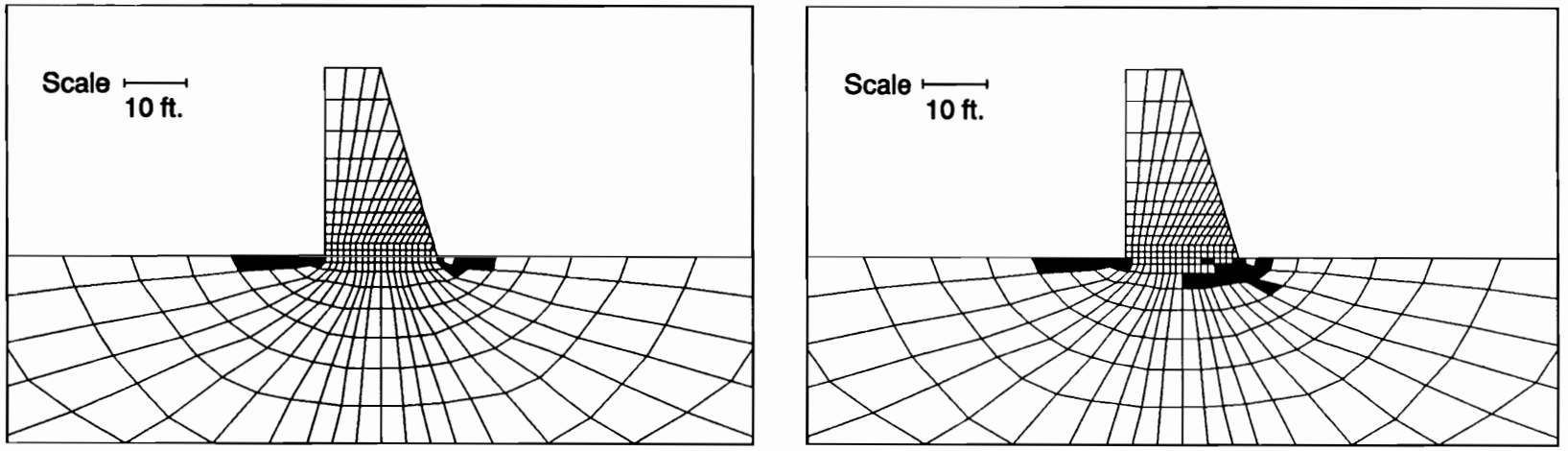

(a) Failure Regions after Wall Placement

(b) Failure Regions after Backfill Placement

Figure 4.1 - Failure Regions for Base Case Problem Analyzed using the Revised Version of SOILSTRUCT

Alpha Method ranged from 0.3 percent to 71 percent for 21 elements with significant strength, compared to 0.3 percent to 480 percent for 16 failed elements in the analysis using the original version of the program.

Fig. 4.2 shows the distribution of normal and shear stresses from the analyses of the base case using the original and the revised (the Alpha Method) version of SOILSTRUCT. For comparison, the normal stress distribution resulting from a conventional equilibrium analyses is plotted in Fig. 4.2(a) as well. Except for areas near the edges, the distribution of normal stress calculated in the finite element analyses is close to the one obtained using equilibrium analyses, which is based on the assumption that the normal stress varies linearly across the base. It may be noted that with the equilibrium analyses, the entire base width is in contact with the foundation soil, and the normal stress is zero at the heel. In both of the finite element analyses, the calculated width of the area in contact with the foundation was 93 percent of the base width of the wall.

The normal stress distribution calculated using the original version of SOILSTRUCT has its maximum value at the toe, whereas the maximum for the analysis using the Alpha Method version is at a distance of 3.3 feet (about 11% of the base width) from the toe. This is due to the fact that with the Alpha Method, more soil elements failed in the vicinity of the toe, leading to stress reductions in that area. The softening of the soil in the toe area resulted in redistribution of stresses, which shifted the maximum normal stress to the unfailed, stronger elements located to the right of the toe. The failure of additional elements in the toe area is viewed as an improvement in the results, in view of the fact that in the analysis using the original version of SOILSTRUCT, the magnitude of the overshoot in that area ranged from 14 percent to 460 percent. The failure of the soil in the area of the toe resulted in a similar distribution of shear stresses, as shown in Fig. 4.2(b).

The calculated values of Δ/H at the end of backfilling were 0.015 (positive values

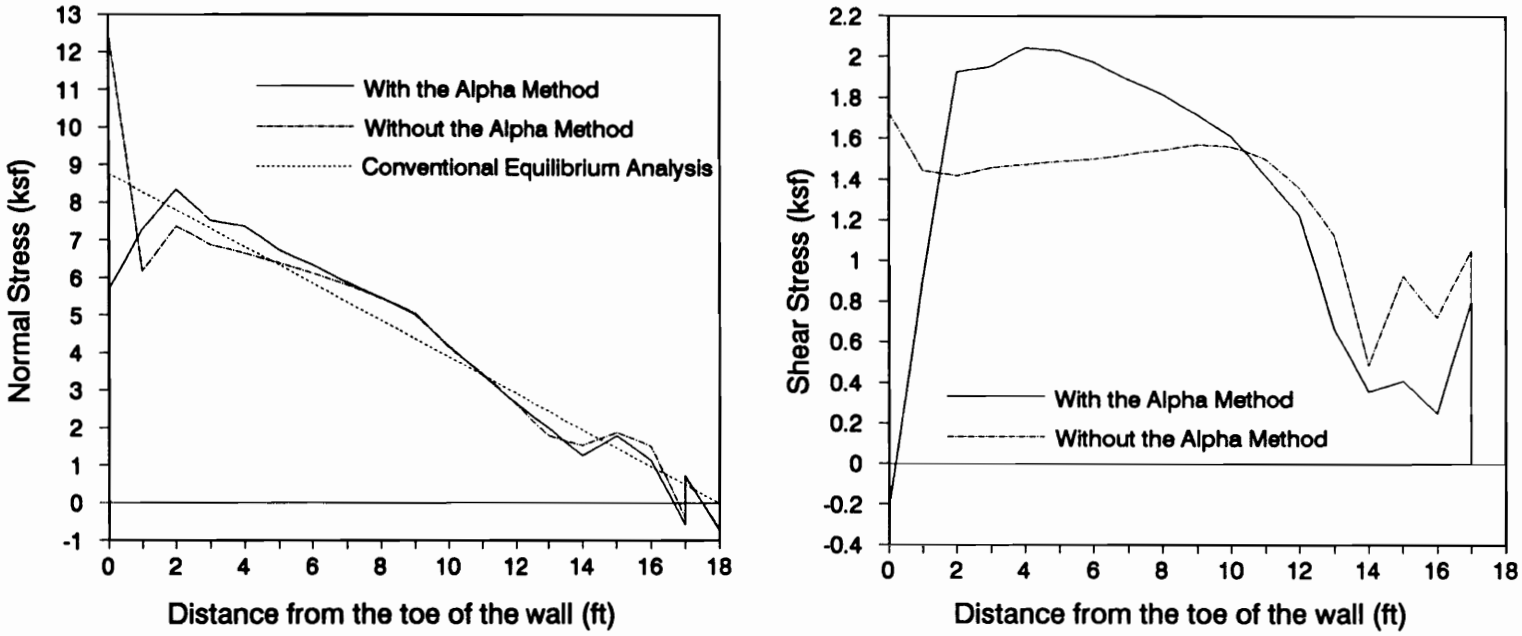

(a) (b)

Figure 4.2 - Base Stresses Resulting from Analyses of the Base Case Problem - With and Without the Alpha Method

indicate movement away from the backfill) for the original version of SOILSTRUCT and 0.016 for the Alpha Method version. As would be expected, the displacement for the analysis using the Alpha Method is somewhat larger, although the difference is quite small. The wall was stable at the end of backfilling in both analyses.

Fig. 4.3 shows the ground surface profile after backfilling, as obtained from the analysis using the revised program. The wall rotated away from the backfill, and the ground beneath the wall assumed a settlement profile consistent with the rotation of the wall. The settlement beneath the wall was greatest at the toe, and decreased towards the heel. It can be seen that the settlement of the ground directly beneath the base has a slight curvature. This curvature is the result of the application of a trapezoidal pressure distribution in simulating the construction of the wall (Fig. 2.3). As indicated in Fig. 4.3, the curved settlement profile may be approximated by a straight line, and the maximum error in this approximation is only approximately 0.05 feet (0.6 inches).

The failure of the elements surrounding some nodes in the heel area led to numerical inaccuracies that resulted in unrealistic values of displacements of those nodes. The points with unrealistic displacements were not plotted, which is responsible for the break in the plot of the ground surface profile. The settlement of the ground beneath the backfill increased very slightly with distance behind the wall, due to the vertical backfill loads in that area.

EFFECTS OF VARYING THE BASE INTERFACE SHEAR STIFFNESS

The stress-displacement behavior in shear of the base interface elements is shown graphically in Fig. 4.4. For values of Δ less than Δ_f, the interface behavior is linearly elastic, with a shear stiffness equal to K_s. For values of Δ greater than Δ_f, the element is assigned a

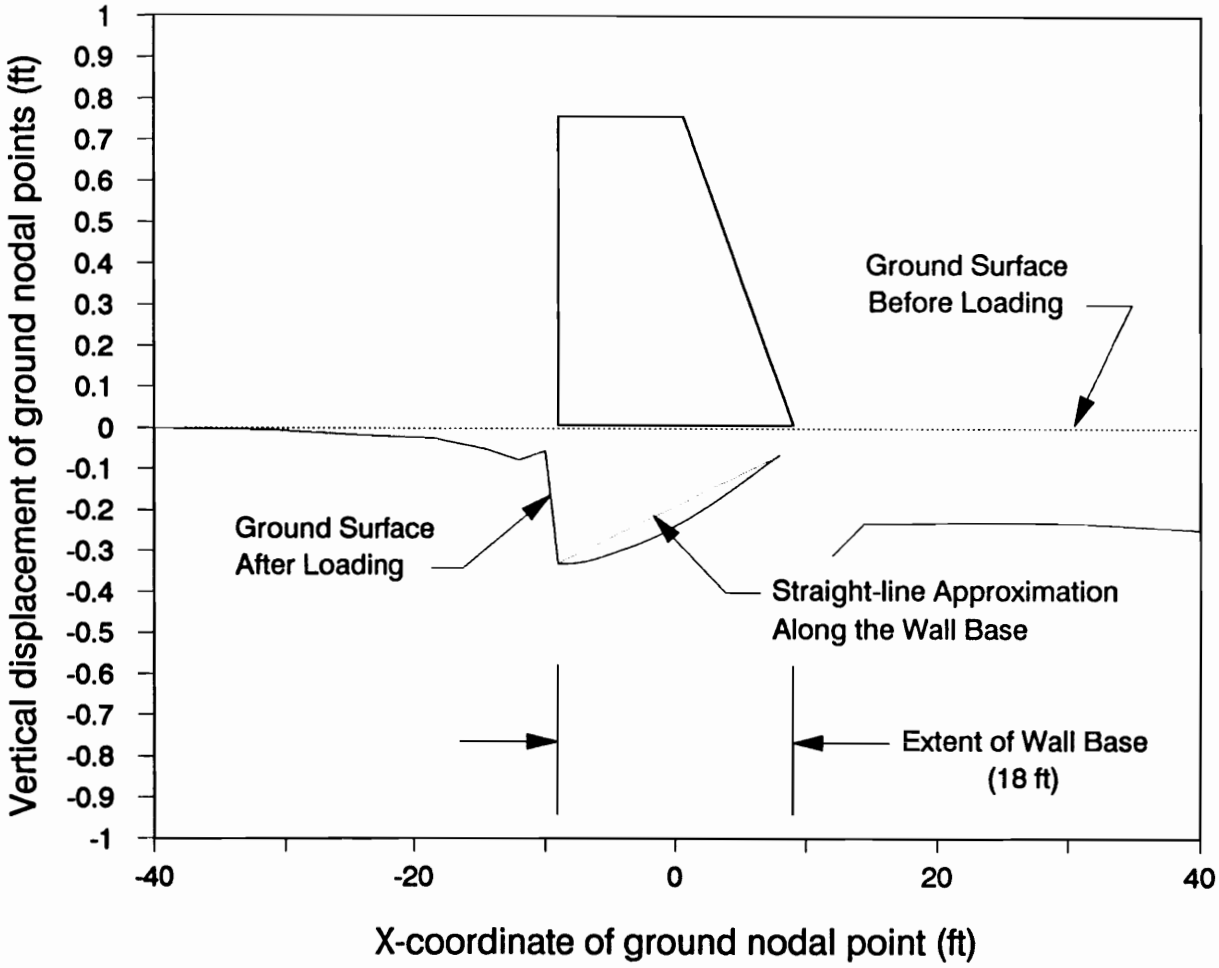

Figure 4.3 - Ground Surface Profile Resulting from a Finite Element Analysis of the Base Case using the Alpha Method

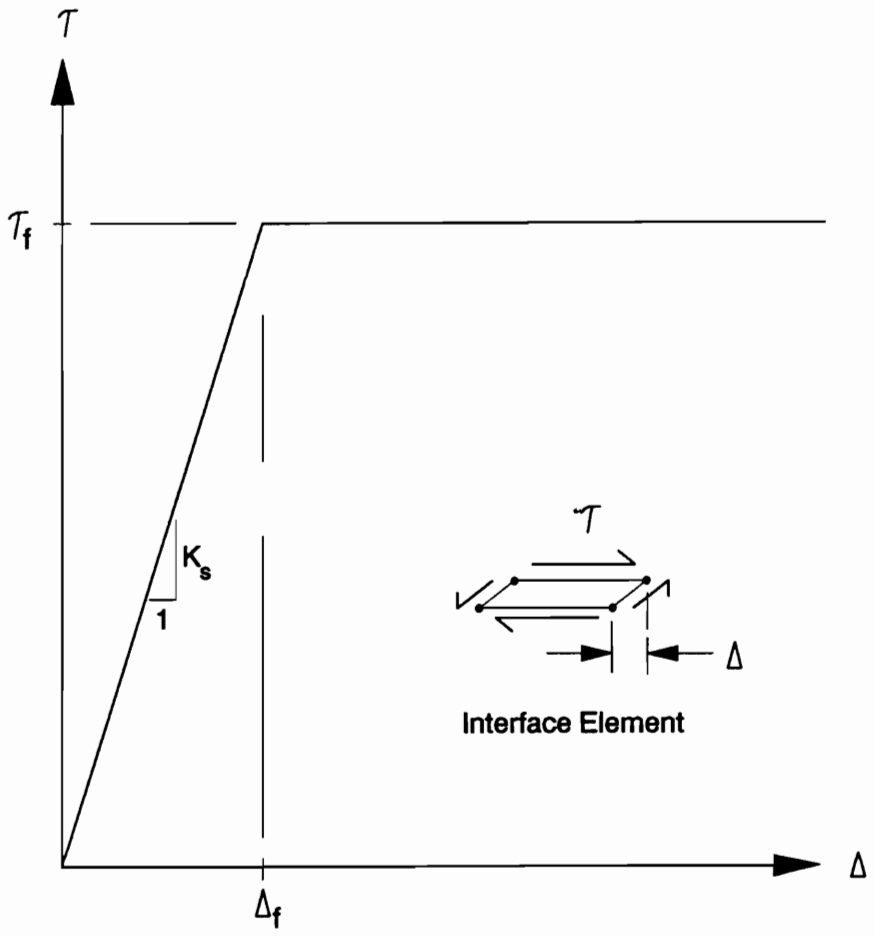

Figure 4.4 - Bilinear Stress-Strain Behavior of Interface Elements

very low value for the shear modulus, consistent with its failure state.

Three values of shear stiffness, K_s, were used in these analyses, modeling varying degrees of concrete-foundation interface roughness. These three values correspond to a rough concrete surface (the maximum value), a smooth concrete surface (the minimum value) and an intermediate condition (the base case value).

The failure regions for the three analyses are shown in Fig. 4.5. Although failure occurred in the same general areas (mainly the vicinity of the toe and the heel of the wall) for all three cases, it may be noted that fewer soil elements failed when the interface was stiff than when it was not so stiff.

The effective base contact areas (B_c/B) varied only slightly for the three runs. The values were : 94 percent for the maximum value of K_s, 93 percent for the base case, and 94 percent for the minimum value of K_s.

Fig. 4.6 shows the distributions of stresses at the base of the wall for the three analyses. It may be seen in Fig. 4.6(a) that the differences between the normal stresses were more pronounced in the toe area. The tendency was for the normal stress in the toe to decrease as K_s decreased. This trend is consistent with the fact that there was more extensive failure of the foundation soil when the value of K_s was lower. As explained previously, the redistribution of stresses caused by the softening of the toe area results in a shift of the location of the maximum normal stress toward the center of the wall base. Fig. 4.6(b) shows how the shear stress distribution was affected by the shear stiffness value. The distribution became flatter and more uniform as K_s decreased.

The wall displacements calculated for these three cases did not differ greatly. The values of Δ/H were 0.0202, 0.0161 and 0.0163 for the minimum, average and maximum shear stiffness values.

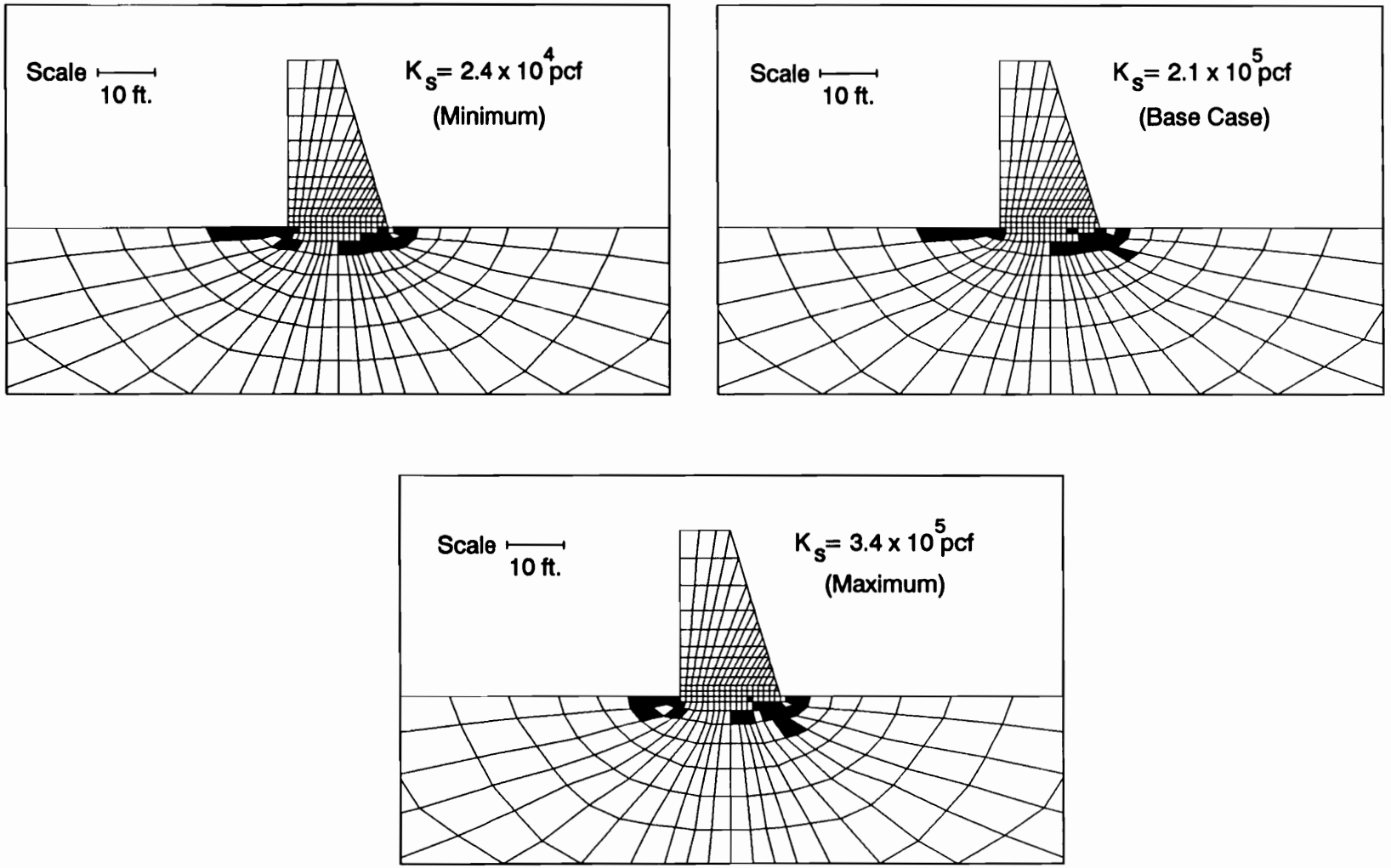

Figure 4.5 - Failure Regions After Backfilling for Different Base Interface Shear Stiffnesses

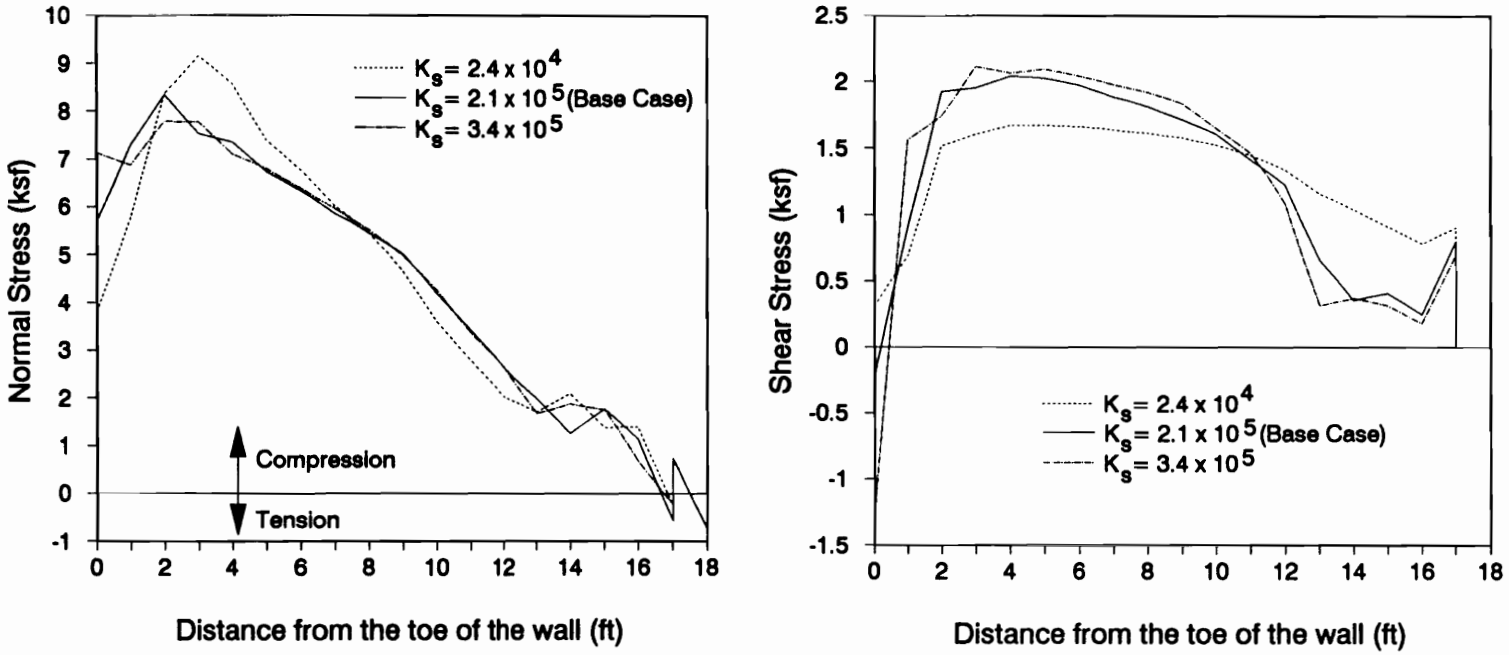

Figure 4.6 - Effect of Varying the Base Interface Shear Stiffness on Base Stresses

EFFECTS OF VARYING THE LATERAL EARTH PRESSURE COEFFICIENT OF THE BACKFILL

As mentioned in the previous chapter, the nodal forces used to represent the backfill load on the wall do not reflect soil-structure interaction effects. The forces that represent the horizontal thrust exerted by the backfill on the wall are statically equivalent to a triangular horizontal pressure distribution. The intensity of this horizontal pressure distribution is governed by the magnitude of the lateral earth pressure coefficient, K_h. Analyses were performed with values of K_h equal to 0.30, 0.37 (the base case value) and 0.50.

Fig. 4.7 shows the failure regions at the end of backfilling for the three cases. It can be seen that the failure regions became more extensive with increasing lateral thrust. In the case where K_h was equal to 0.50, a band of failed elements isolated the wall from the unfailed part of the foundation, a sufficient condition for wall instability.

For the purpose of summarizing the results of these and other analyses, it was found to be convenient to define a simple criterion of failure of the wall with regard to excessive movement. The criterion was set as follows : A wall was considered to have "failed" if, upon application of an increment of the backfill loads, the incremental horizontal displacement of the top of the wall exceeded 0.01 times the wall height. For a 30 ft. high wall this corresponds to an incremental displacement of 3.6 inches.

Fig. 4.8 shows the base normal and shear stress distributions for the three analyses with different values of K_h. Similar distributions of the normal and shear stresses along the base were obtained for K_h equal to 0.30 and for K_h equal to 0.37. For K_h equal to 0.50, the extensive failure of soil elements beneath the wall resulted in a jagged distribution of stresses along the base.

The values of effective base contact area (B_e/B) were 94 percent for K_h equal to 0.30, 93

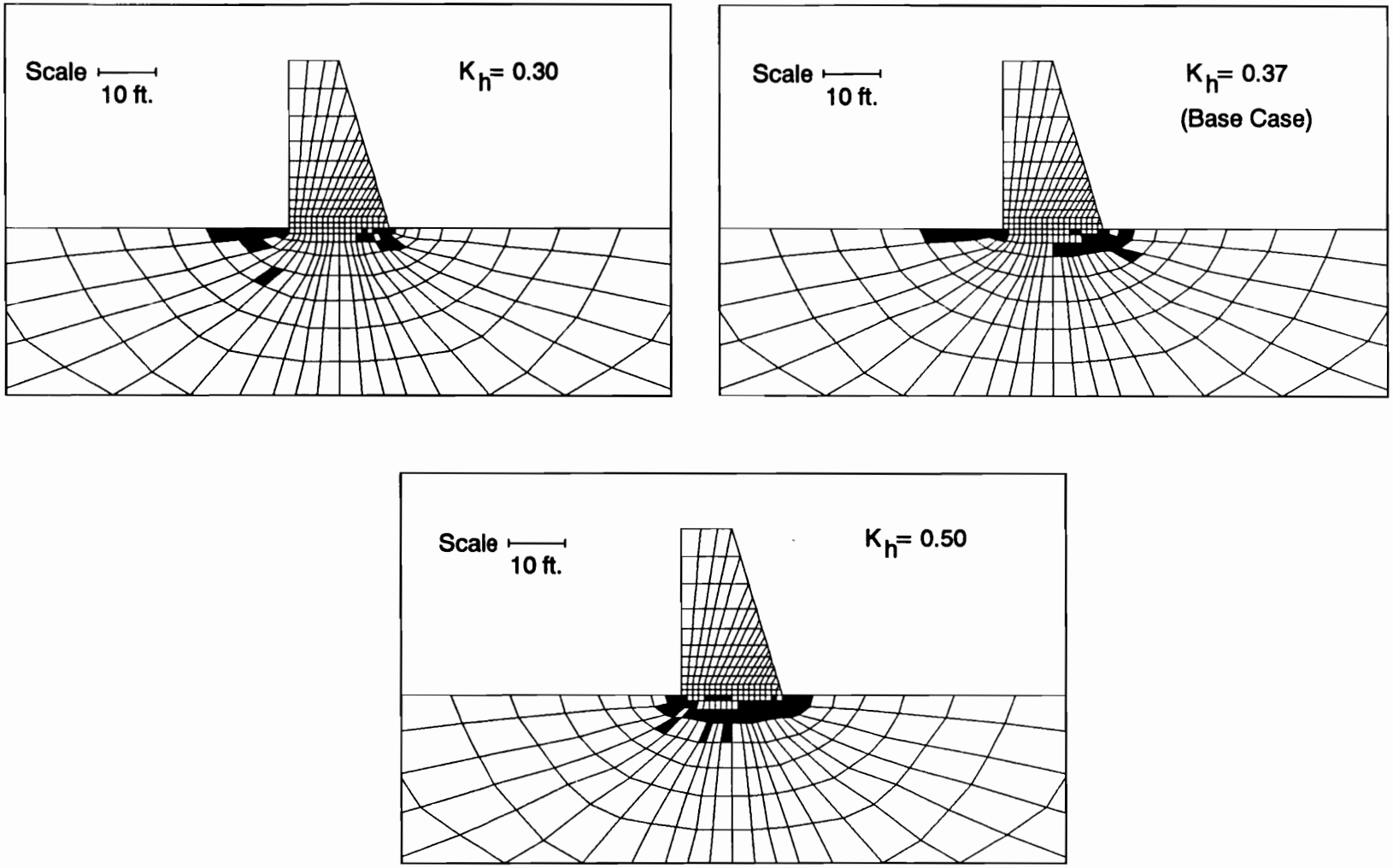

Figure 4.7 - Failure Regions After Backfilling for Different Lateral Earth Pressure Coefficients

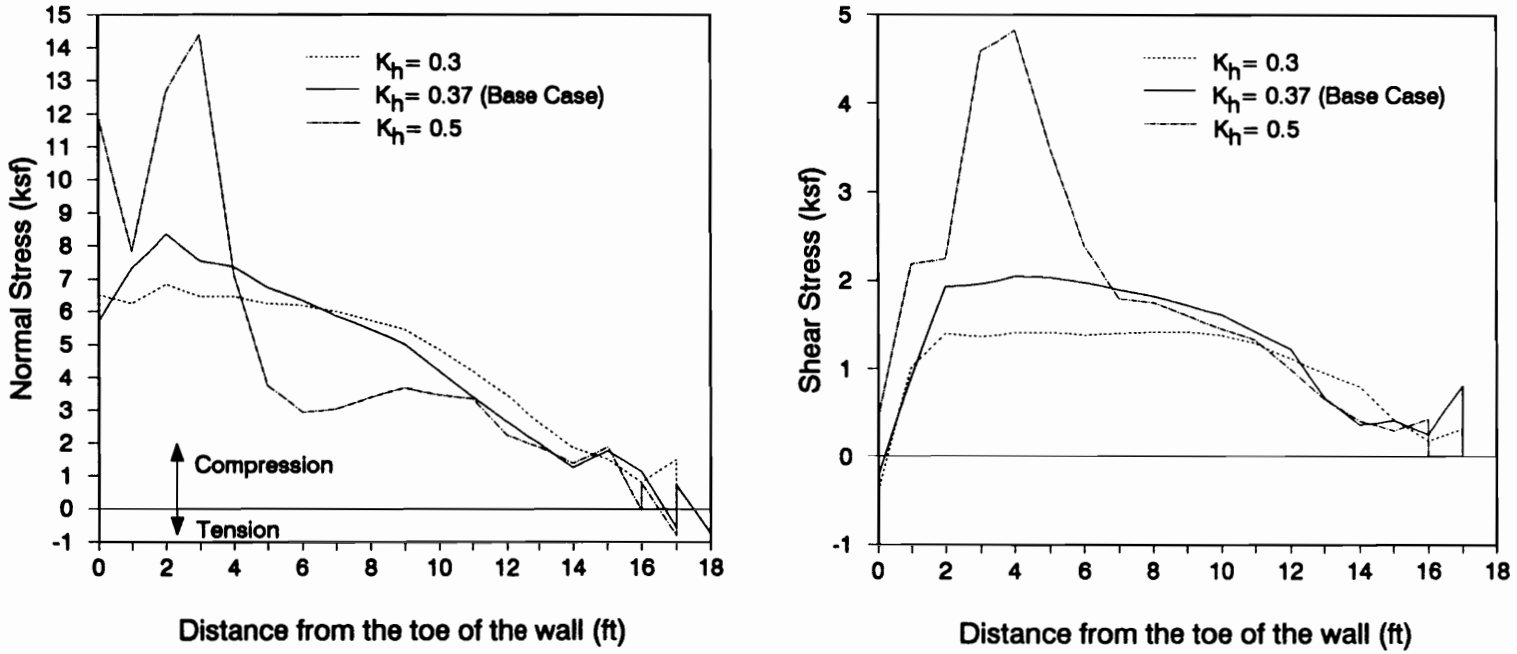

Figure 4.8 - Effect of Varying the Lateral Earth Pressure Coefficient on the Base Stresses

percent for K_h equal to 0.37, and 89 percent for K_h equal to 0.50. It is interesting to note that equilibrium analyses predict a 100 percent base contact area for K_h equal to 0.30 and 0.37. According to finite element results, six to seven percent of the base loses contact with the foundation under these magnitudes of lateral loading. This occurrence, as further results will show, is an artifact of the assumed pressure distribution that was applied to simulate wall construction. As shown in Fig. 2.3 in Chapter 2, the assumed initial bearing pressure was zero at the heel.

The values of Δ/H values at the end of backfilling were 0.0067 for K_h equal to 0.30 and 0.0161 for K_h equal to 0.37. For K_h equal to 0.50, collapse occurred prior to the full application of the load due to the last lift, and the calculated value of Δ/H was very large.

The validity of these finite element results was examined by comparing them with the results obtained independently using conventional equilibrium analyses and bearing capacity analyses. Fig. 4.9 shows how the normalized wall displacement, Δ/H, varied with the factor of safety against bearing capacity failure for the three values of K_h. The values of Δ/H were obtained from finite element analyses. The values of $FS_{bearing}$ from bearing capacity analyses were defined as follows :

$$FS_{bearing} = \frac{q_{ult}}{q_{max}} \tag{4.1}$$

where q_{ult} is the ultimate bearing capacity of the foundation obtained using Vesic' theory (described in Chapter 3), and q_{max} is the maximum normal stress at the toe calculated using equilibrium analysis. The variations of Δ/H with $FS_{bearing}$ for the three cases were very similar. Note that, initially, when the factor of safety against bearing capacity failure was very high, the movement of the wall was toward the backfill, as indicated by negative values of Δ/H. Movement away from the backfill commenced when the value of $FS_{bearing}$ fell below about

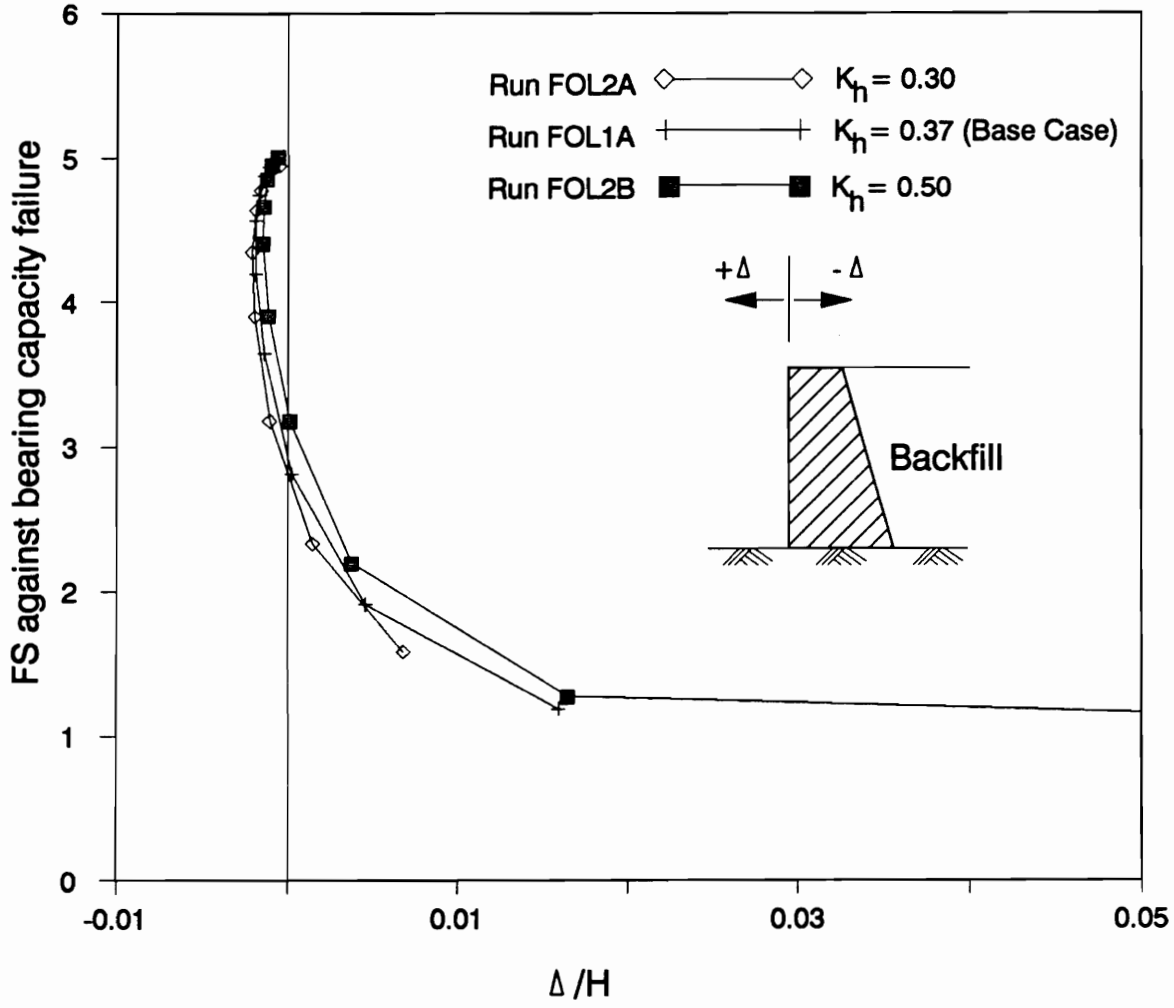

Figure 4.9 - Factor of Safety Against Bearing Capacity Failure vs. Normalized Wall Displacements for Different Lateral Earth Pressure Coefficients

three, a condition that was reached when the applied loads corresponded to a backfill height of about 18 feet in the base case, where K_h was equal to 0.37. For a value of $FS_{bearing}$ equal to 1.5, the value of Δ/H was equal to 0.012 to 0.014. The curve corresponding to K_h equal to 0.50 shows a sharp increase in the absolute value of Δ/H as the value of $FS_{bearing}$ approached unity.

Fig. 4.10 shows the variation of the value of $FS_{bearing}$ with the backfill height for the three values of K_h. The calculated values of $FS_{bearing}$ decrease as the backfill height increases for all three values of K_h. For the $K_h = 0.50$ case, the value of $FS_{bearing}$ is equal to 1.0 (indicating instability) for a backfill height of about 27 ft.

An approximate backfill height at failure can also be obtained from the finite element results. Of the three cases involving different values of K_h, only the analysis for K_h equal to 0.50 resulted in wall failure in the finite element analyses. In Fig. 4.10, a box was drawn on the Δ/H versus $FS_{bearing}$ line at the point corresponding to the value of backfill height at failure determined from the finite element analysis. It can be seen that the conventional equilibrium and bearing capacity analyses yield results in close agreement with finite element results.

EFFECTS OF VARYING THE POISSON'S RATIO OF THE FOUNDATION SOIL

According to elastic theory, the Poisson's ratio of a foundation soil, ν_s, is related to its at-rest earth pressure coefficient, K_o as follows :

$$K_o = \frac{1-\nu_s}{\nu_s} \tag{4.2}$$

Fig. 4.11 shows a plot of Equation 4.2. Because the value of K_o increases as the value of ν_s

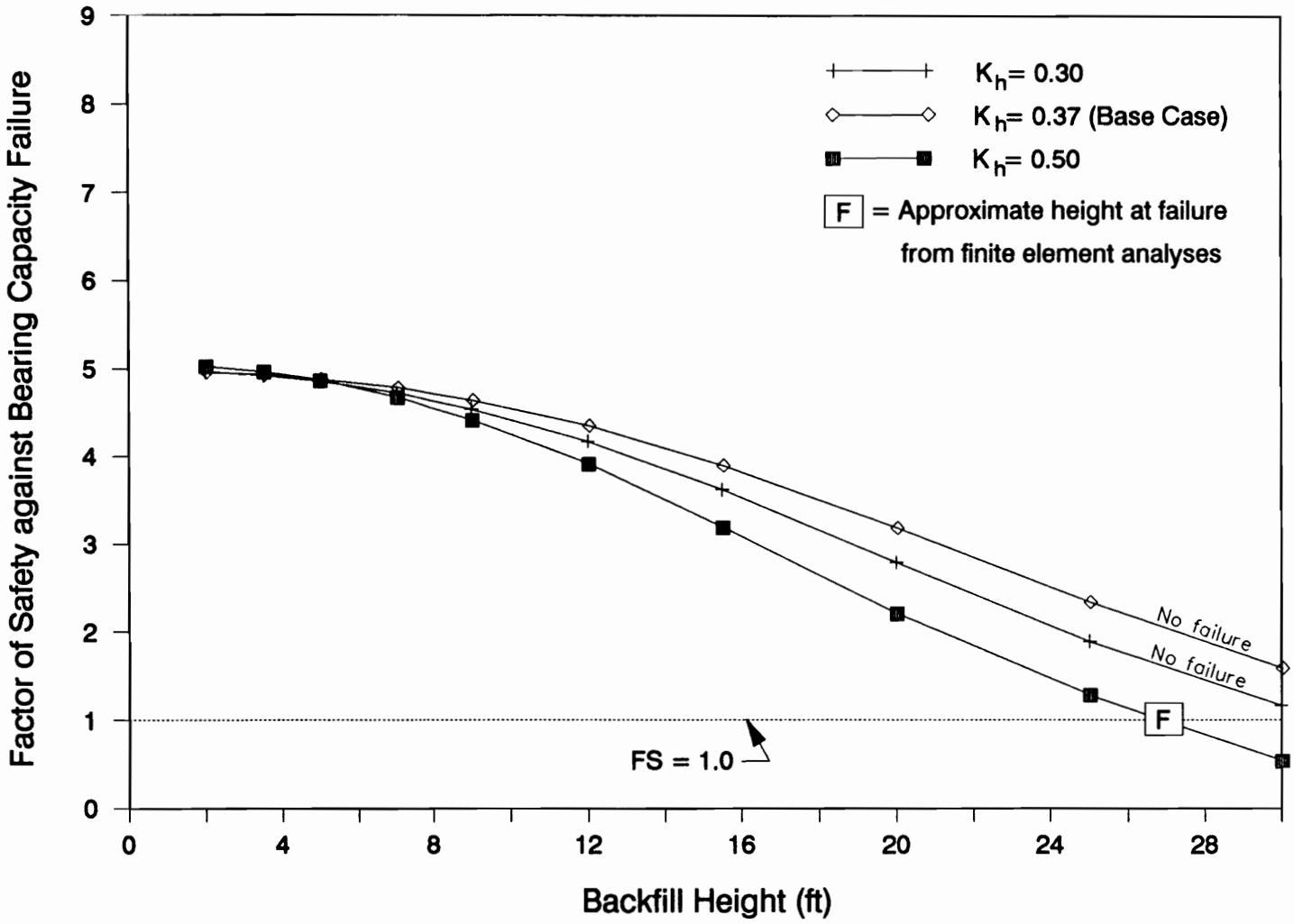

Figure 4.10 - Variation of Factor of Safety Against Bearing Capacity Failure with Backfill Height for Different Lateral Earth Pressure Coefficients

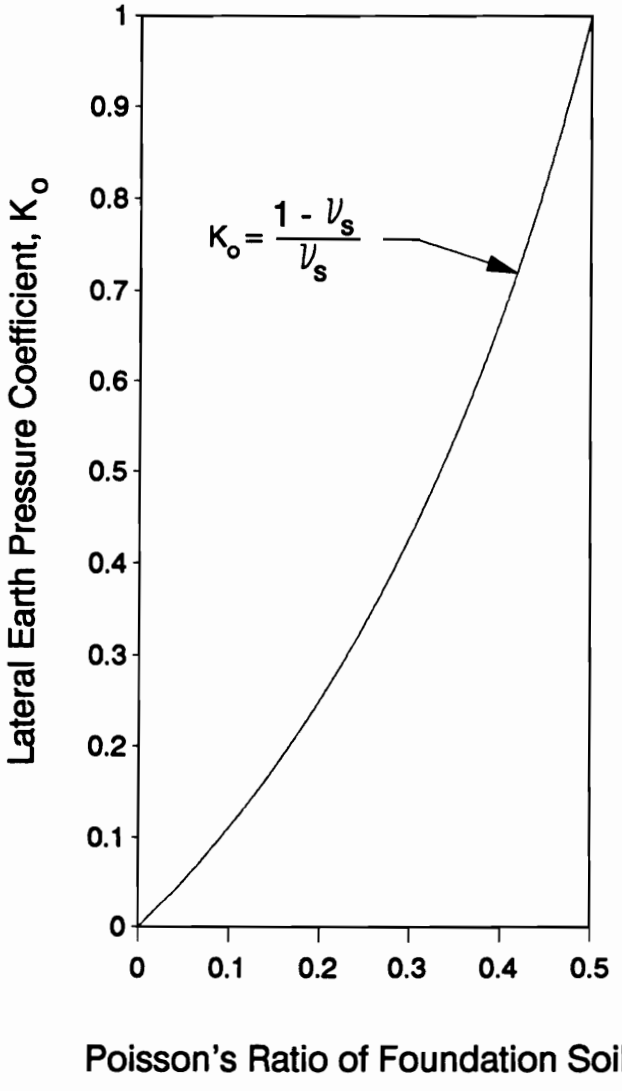

Figure 4.11 - Variation of the At-rest Earth Pressure Coefficient with the Poisson's Ratio of the Foundation Soil

increases, changes in the lateral stresses in the foundation induced by the application of vertical stresses are higher when the value of ν_s for the foundation soil are higher. Following load analyses were conducted using three values of ν_s for the foundation soil : 0.32, 0.35 and 0.40.

Fig. 4.12 shows the calculated failure regions at the end of backfilling obtained from these three cases. The failure regions were less extensive as the value of Poisson's ratio increased. This is a consequence of the increase in confining stresses brought about by the increase in ν_s. The wall did not become unstable in any of the three analyses.

The displacement of the top of the wall decreased with increasing values of Poisson's ratio. The values of Δ/H were 0.0238 for ν_s equal to 0.32, 0.0161 for ν_s equal to 0.35 and 0.0137 for ν_s equal to 0.40.

Fig. 4.13 shows the normal and shear stress distributions at the base for these three analyses. From a practical standpoint, the distributions do not differ significantly. It may be noted, however, that the previously observed tendency of the normal stress to be redistributed following the softening of some soil elements underneath the wall is also true of these analyses. This trend is most observable in the toe area, where the magnitude of the normal stress decreased as more soil elements in that area failed.

No significant change of the effective base contact area (B_e/B) occurred due to the changes in the values of ν_s. The calculated B_e/B values varied only slightly, from 93 to 94 percent, in the three cases.

EFFECTS OF VARYING THE RELATIVE DENSITY OF THE FOUNDATION SOIL

Duncan, et al. (1980) suggested values of the hyperbolic stress-strain parameters K, n and R_f for relative densities (D_r) equal to 25, 50, 75 and 100 percent. Analyses were performed

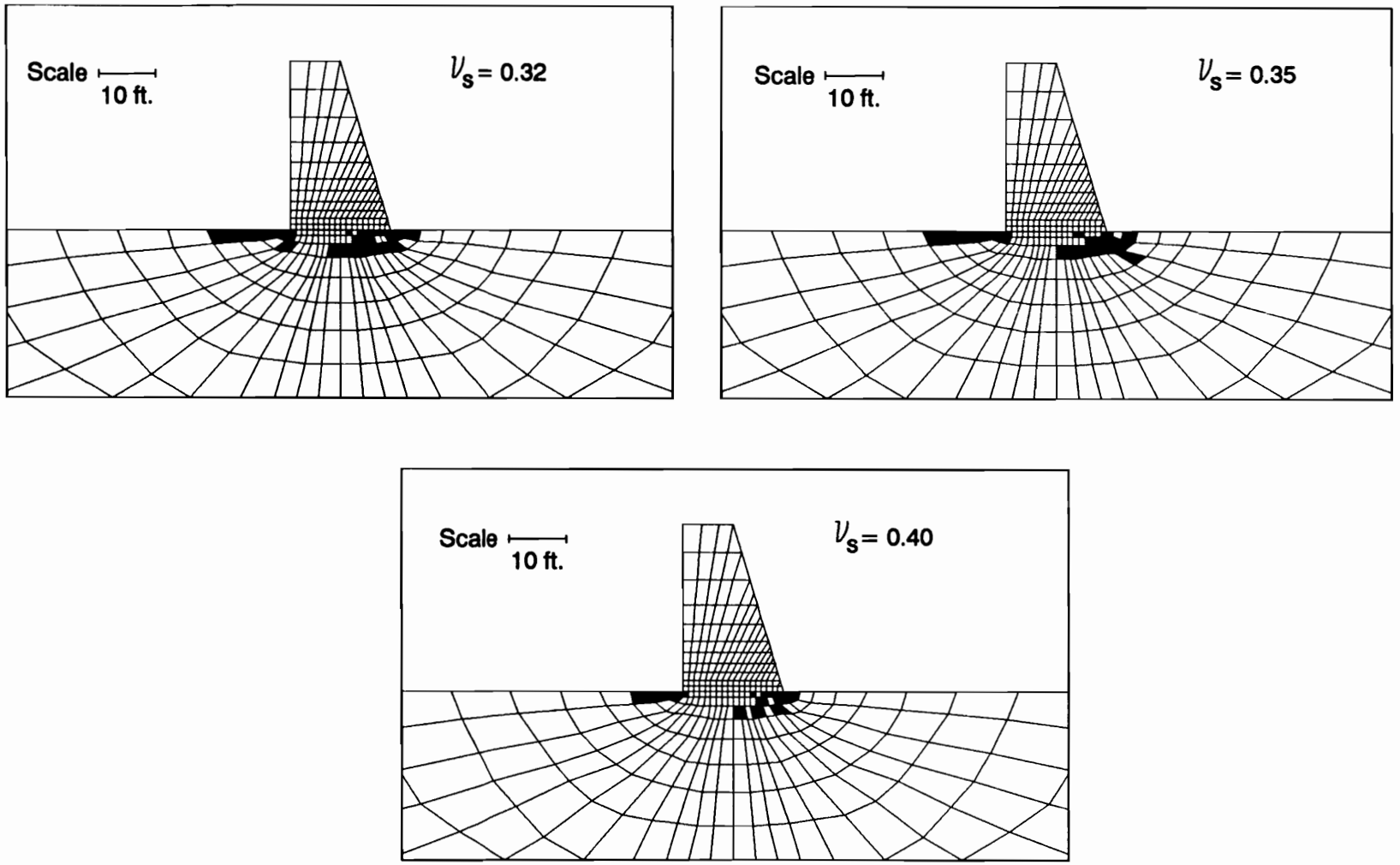

Figure 4.12 - Failure Regions After Backfilling for Different Poisson's Ratio of the Foundation Soil

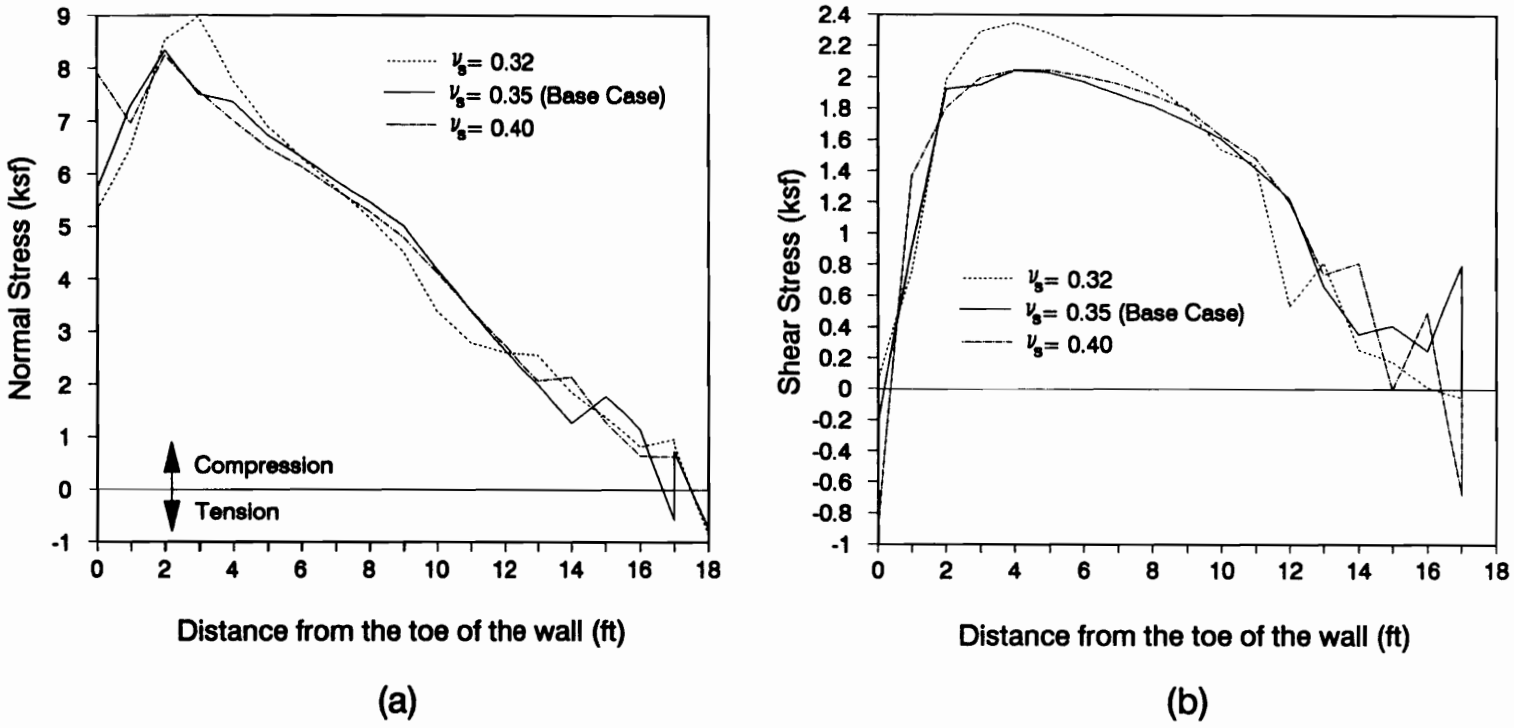

Figure 4.13 - Effect of Varying the Poisson's Ratio of the Foundation on the Base Stresses

utilizing these four values of relative density for the foundation soil, with the values of K, n and R_f suggested by Duncan, et al..

The initial stresses in the soil elements were computed using values of K_o obtained using the following equation (Jaky, 1948) :

$$K_o = 1 - \sin \Phi \tag{4.3}$$

where Φ is the angle of internal friction corresponding to the relative density of the foundation soil.

Fig. 4.14 shows the calculated failure regions after application of the full backfill loads for the four cases. It can be seen clearly that the extent of the failure region increases as the density of the foundation soil decreases.

The effective base contact area was only slightly affected by the change in relative density (B_e/B ranged from 93 percent to 94 percent for the four runs).

The base stress distributions for the four runs are shown in Fig. 4.15. Again, there is a tendency for the stresses to be redistributed along the base as local failure occurs. For the runs utilizing foundation relative densities equal to 50, 75 and 100 percent, this redistribution of stresses can be seen to be related to the extent of the failure regions in the foundation soil. The extensive failure associated with the foundation soil with a relative density equal to 25 percent resulted in jagged and erratic base stress distributions for this case.

After the full backfill loads had been applied, the maximum value of wall displacement (for the walls that did not fail) was : $\Delta/H = 0.0430$ for D_r equal to 50 percent, $\Delta/H = 0.0161$ for D_r equal to 75 percent, and $\Delta/H = 0.0104$ for D_r equal to 100 percent.

Fig. 4.16 shows the variations of the calculated values of Δ/H with the values of $FS_{bearing}$ for the four values of foundation relative density that were studied. At the start of

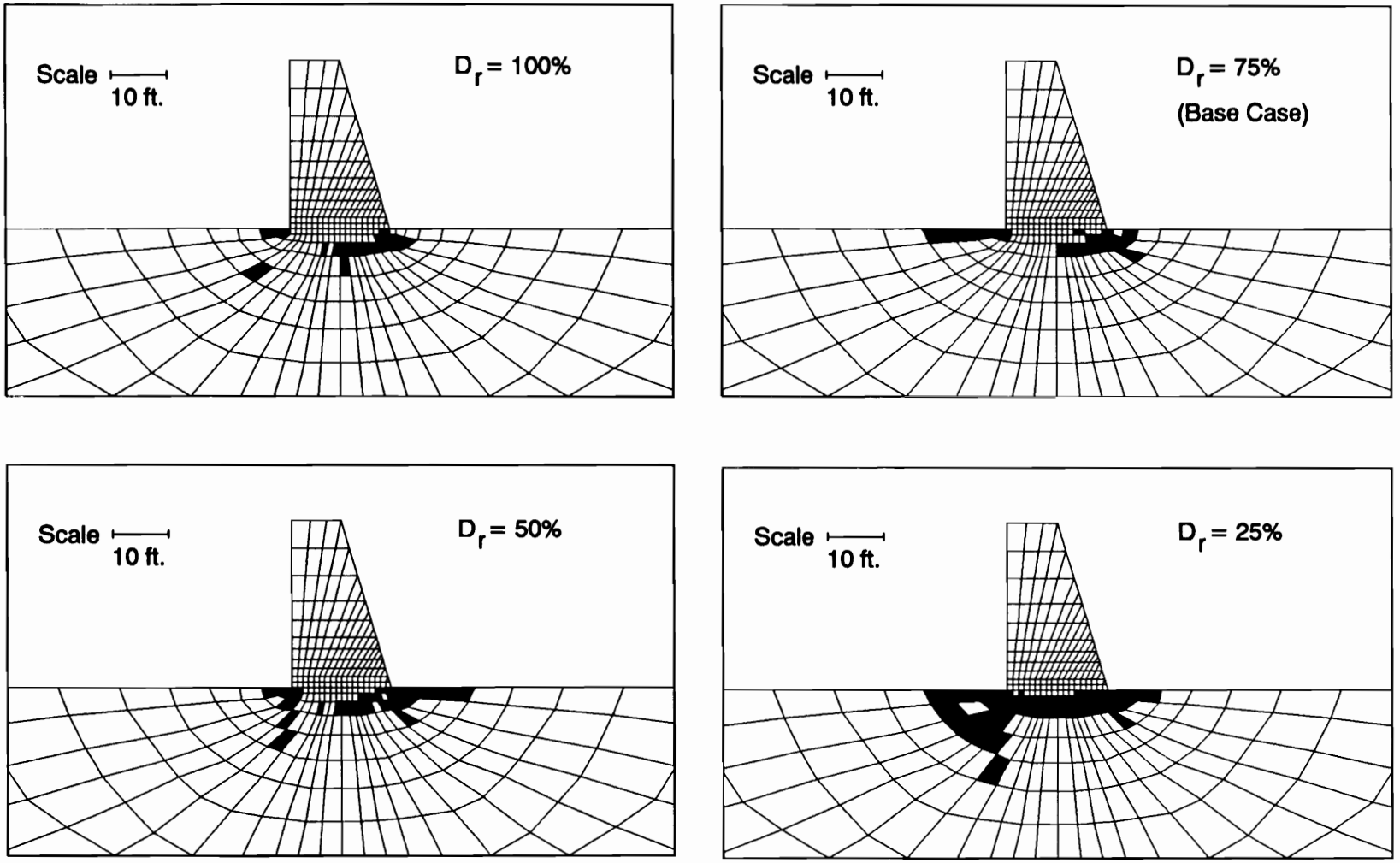

Figure 4.14 - Failure Regions After Backfilling for Different Relative Densities of the Foundation Soil

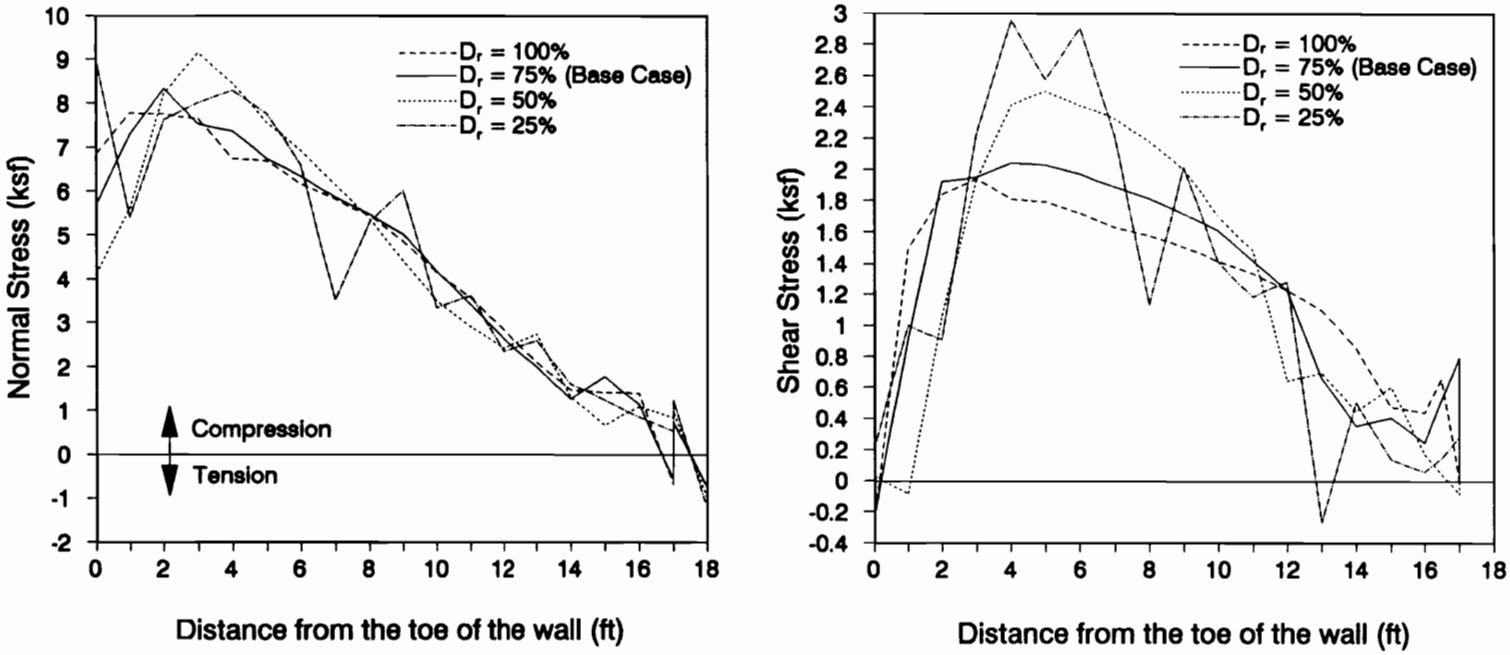

Figure 4.15 - Effect of Varying the Relative Density of the Foundation Soil on the Base Stresses

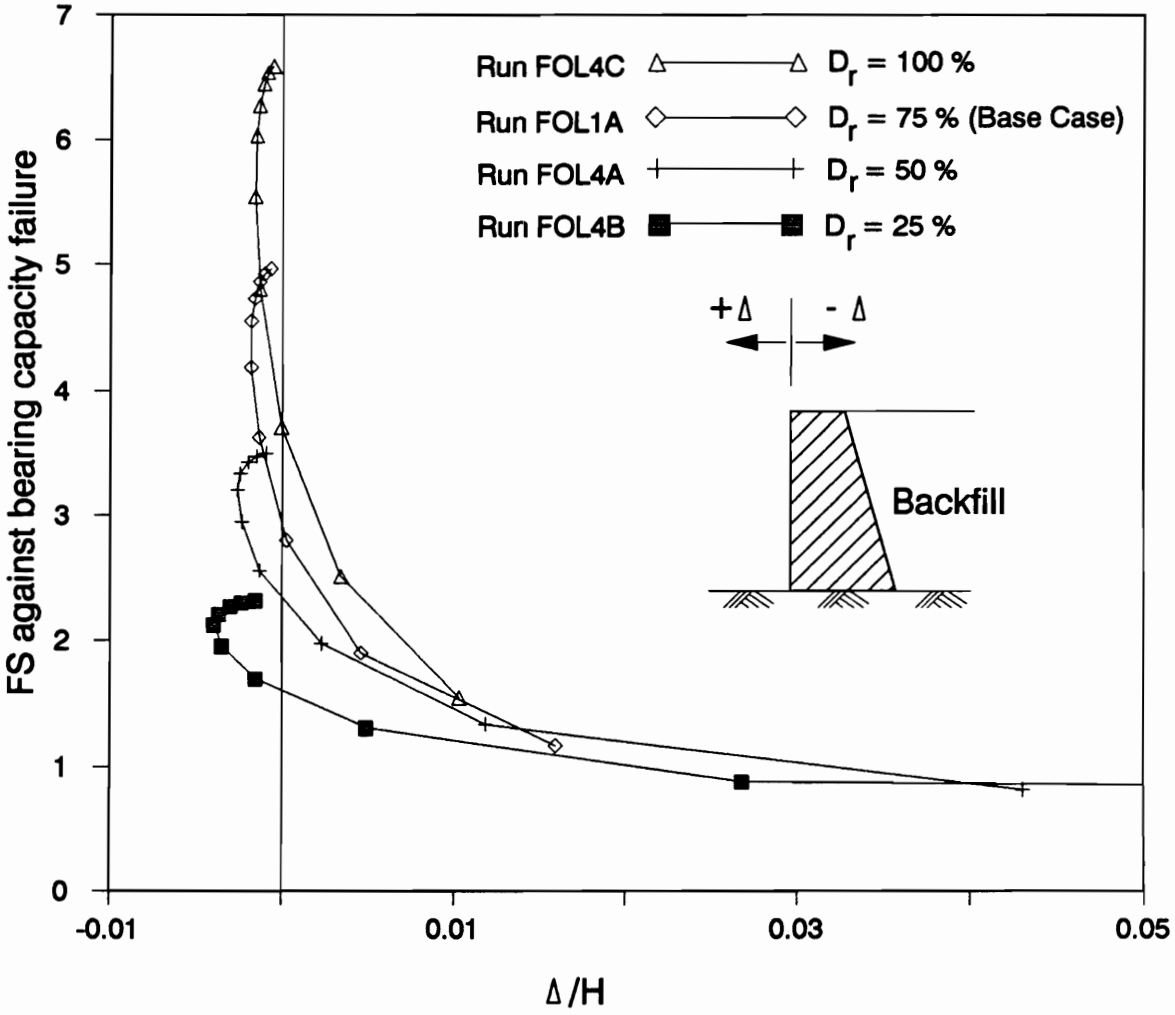

Figure 4.16 - Factor of Safety Against Bearing Capacity Failure vs. Normalized Wall Displacements for Different Foundation Soil Relative Densities

the backfilling operation, the factor of safety against bearing capacity failure ranged from 6.5 for D_r equal to 100 percent to 2.4 for D_r equal to 25 percent. The wall moved toward the backfill during the first seven loading stages, that is, until the backfill was 17 to 20 feet high (58 to 66 percent of the wall height). Beyond this backfill height, the wall moved away from the backfill. It may be noted that the movements during the first seven loading stages are practically the same for all four cases (values of Δ/H ranged from about -0.001 to -0.004), independent of the factor of safety. However, both the value of $FS_{bearing}$ and the relative density of the foundation soil influence the amount of wall movement once the wall starts to move away from the backfill. For lower values of relative density, the wall movement increases more rapidly as the factor of safety decreases.

In the analysis with D_r equal to 25 percent, large incremental displacements occurred in the late stages of backfilling. It should also be mentioned that large displacements occurred during construction of the wall in this case. A total of 360 alpha method computations were performed during the application of the base pressure to simulate the construction of the wall. A band of failed soil elements isolated the wall from the unfailed part of the mesh at some times during these computations, resulting in large incremental displacements. However, most of these elements recovered by the time the entire weight of the wall has been applied. The large incremental displacements prior to backfilling are not included in the value of the wall displacement shown in Fig. 4.16. The values of Δ shown in Fig. 4.16 is measured from the position of the wall after its construction.

Fig. 4.17 shows how the calculated values of factor of safety varied with the backfill height for these four analyses. Note that in the case where the relative density is equal to 25 percent, failure occurs when the simulated backfill height is about 24 feet. Failure occurred at about the same stage in the finite element analysis. The difference between the backfill heights at failure for the two methods was only two feet (refer to Table 3.1), or about six percent of the

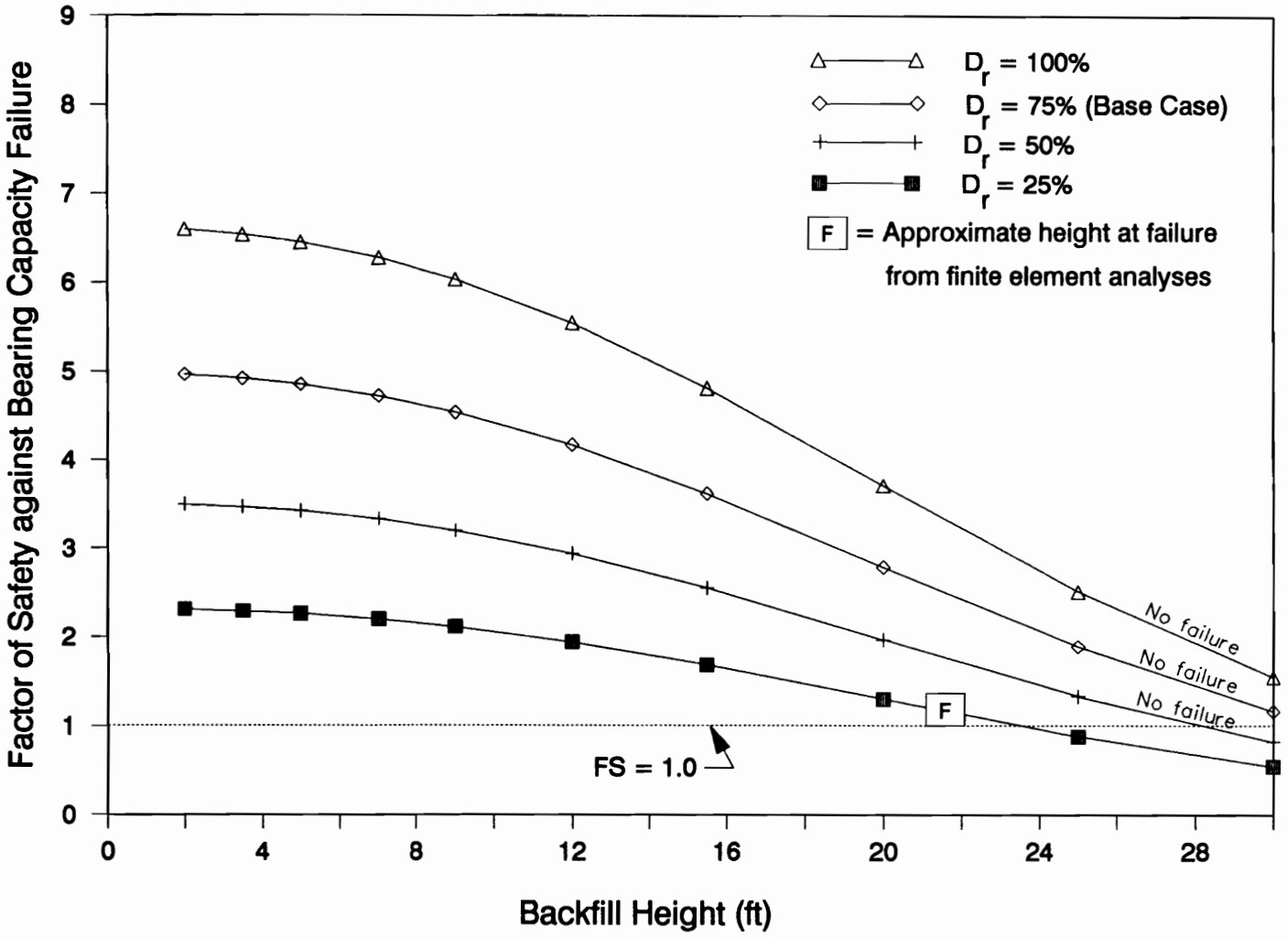

Figure 4.17 - Variation of Factor of Safety Against Bearing Capacity Failure with Backfill Height - Different Foundation Soil Relative Densities

wall height. In the case where the relative density was equal to 50 percent, the results from the bearing capacity analyses indicate that the wall should become unstable at a backfill height of 28.3 feet (94 percent of the maximum possible backfill height), whereas the finite element analysis of the same case indicate that it is possible to apply the full backfill load up to H equal to 30 ft. without reaching a condition of instability. Thus the difference in the predicted backfill height at failure for the two types of analysis is about six percent of the wall height in this case also.

EFFECTS OF VARYING THE THICKNESS OF THE FOUNDATION SOIL

Analysis were performed to determine the influence of the thickness of the foundation soil (D_f) on the behavior of retaining walls. Walls resting on medium dense sand layers 15, 30, and 60 feet thick were analyzed. For this purpose, two additional finite element meshes were constructed, one for the 15-foot thick foundation soil and another for the 60-foot thick foundation soil. A total of 184, 228 and 264 soil elements were used to represent the 15, 30 and 60 foot thick foundation soil. The number of elements that made up the retaining wall and wall base-foundation interface were the same for all three meshes.

Fig. 4.18 shows the failure regions at the end of backfilling calculated from analyses of these three cases. The number of failed soil elements totaled 36 for D_f equal to 15 feet, 29 for D_f equal to 30 feet and 40 for D_f equal to 60 feet. Although these results appear at first to be inconsistent, they are believed to be reasonable in view of the phenomena discussed in the following paragraphs.

To understand the reason for the increase in the number of failed soil elements with an increase in foundation thickness from 30 to 60 ft., consider Fig. 4.19, which shows the ground

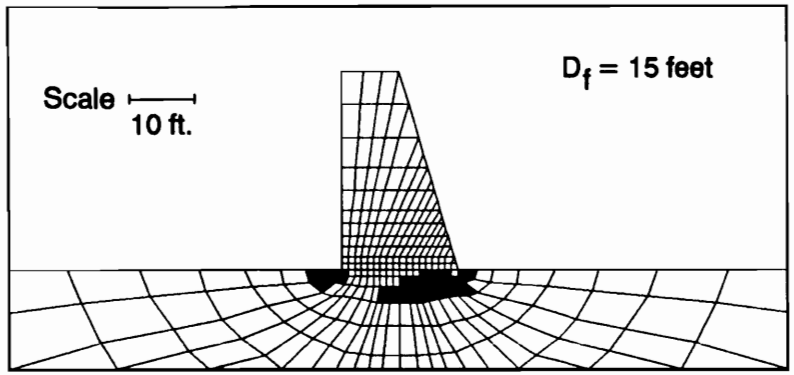

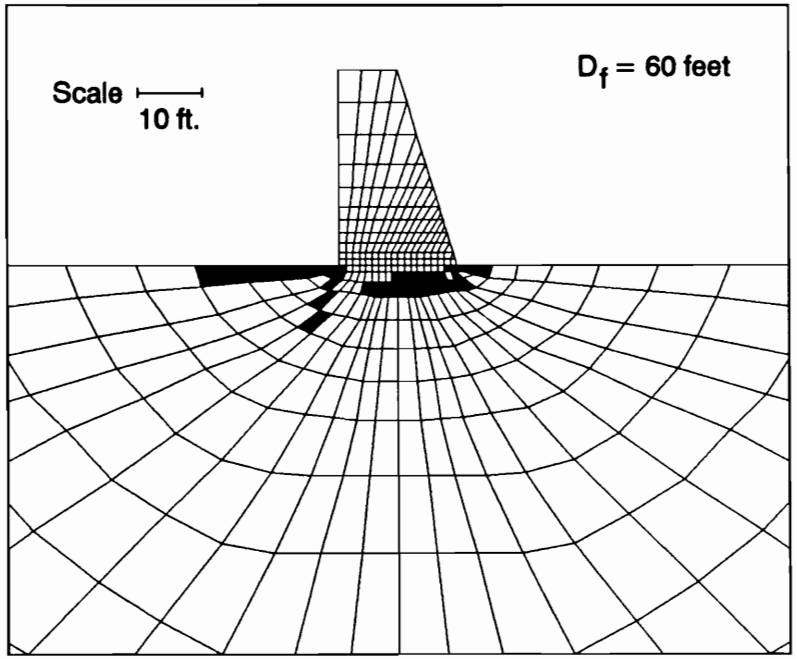

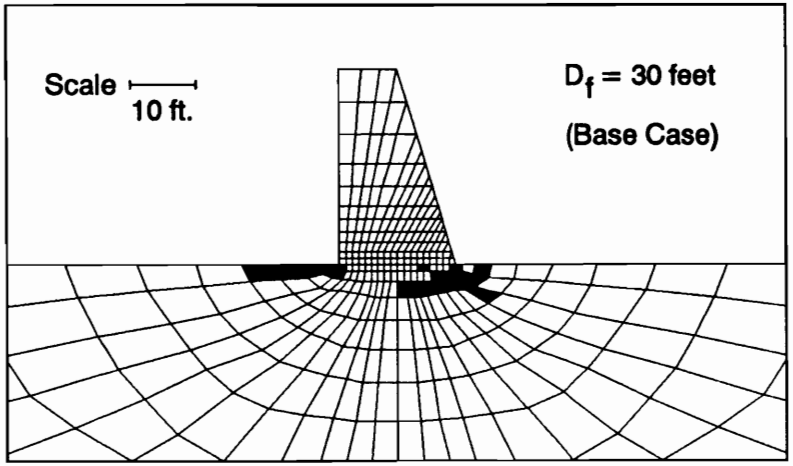

Figure 4.18- Failure Regions After Backfilling for Different Thicknesses of the Foundation Soil

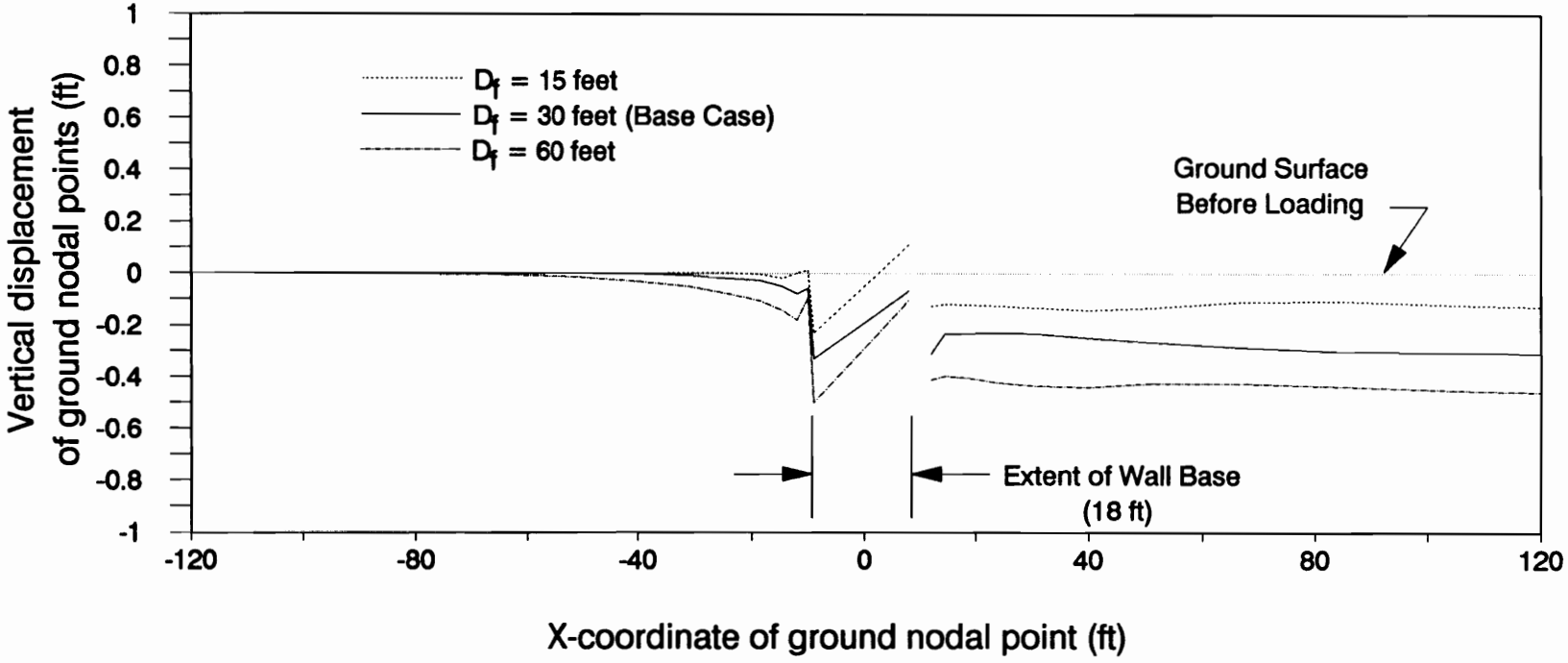

Figure 4.19 - Ground Surface Profiles After Backfilling for Three Different Foundation Thicknesses

surface profiles after backfilling for the three analyses. Note that as the foundation becomes thicker, the increased settlement of the wall results in a greater distortion of the foundation near the toe, due to the greater differential settlements. For this reason, more elements near the toe on the surface failed as the foundation thickness increased. This trend can be clearly seen in the failure regions in Fig. 4.18.

The global displacements of a portion of the foundation soil beneath the wall was isolated for the three analyses, and shown in Fig. 4.20. The displacement patterns of these same elements, with much of the components of the rigid body motion removed, are shown in Fig. 4.21. It may be seen that the shear distortions are more severe in this area for the thinner foundation than for the thicker foundation, explaining the greater number of failed elements in this area for the 15 ft. thick foundation case, as may be seen in Fig. 4.18.

Thus, when the foundation is thin, more elements fail beneath the center of the wall. When the foundation is thick, more elements fail beneath the toe. The combined effect is that the number of failed elements first decrease and then increase as the foundation is varied from 15 ft. to 60 ft.

The base normal stresses for the three analyses are given in the left hand side of Fig. 4.22. The distributions for the three cases are quite similar, with the difference between magnitudes of stresses no more than 1 ksf. All three analyses resulted in 93 percent of the wall base still in contact with the foundation. The same close agreement of results can be observed in the shear stress distributions given in the right hand side of Fig. 4.22, the values differing by no more than 0.5 ksf.

The maximum wall displacements at the end of backfilling were : Δ/H equal to 0.0251 for D_f equal to 15 feet, 0.0161 for D_f equal to 30 feet and 0.0251 for D_f equal to 60 feet. It may be noted that these values are consistent with extent of the failure regions that were calculated for each case.

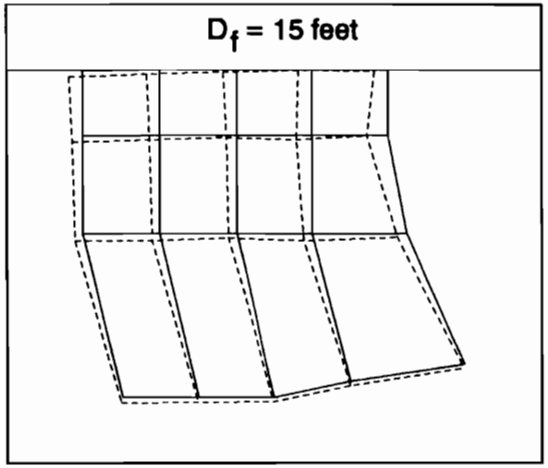

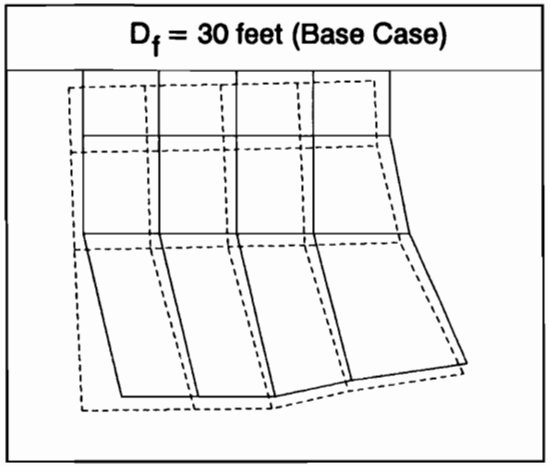

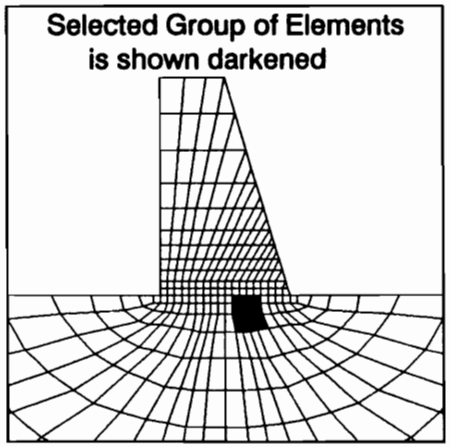

Legend :

Undeformed Mesh

Deformed Mesh

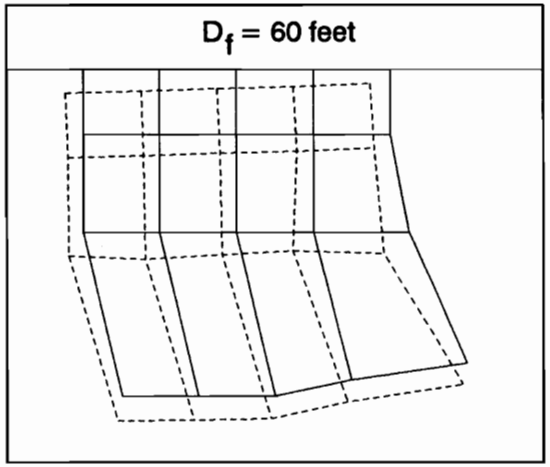

Figure 4.20 - Global Displacements of a Selected Group of Soil Elements After Backfilling

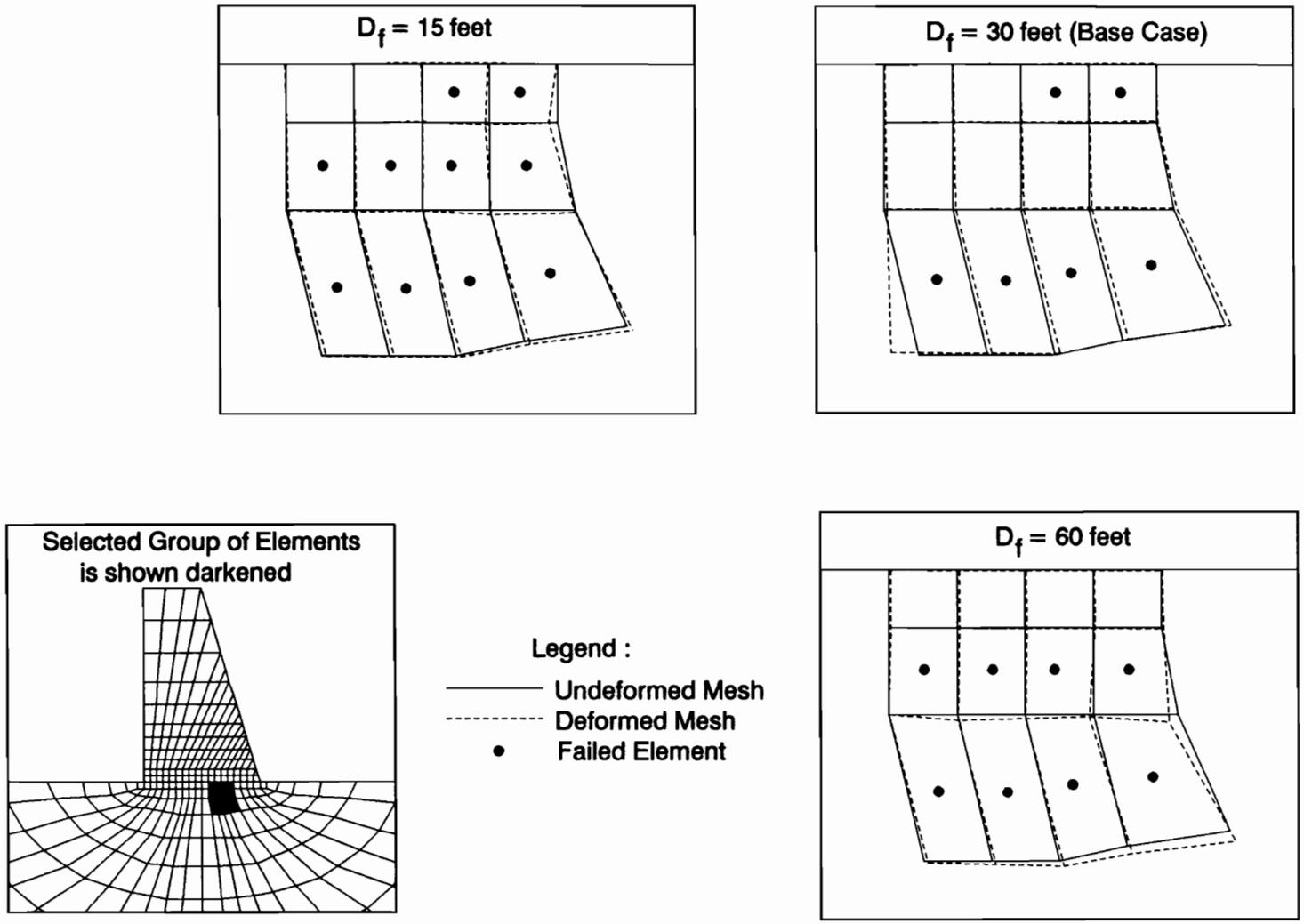

Figure 4.21 - Deformed Configuration of a Selected Group of Soil Elements upon removal of the Components of Rigid Body Motion

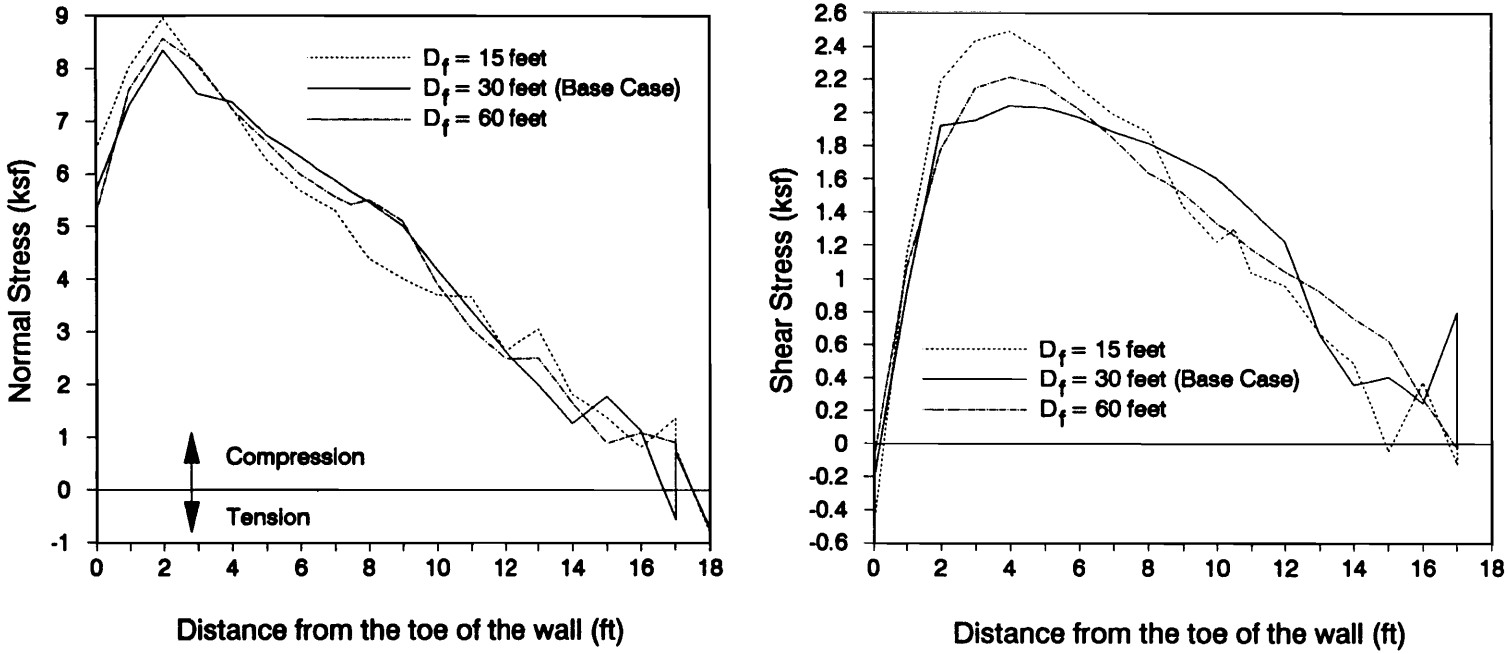

Figure 4.22 - Effect of Varying the Depth of the Foundation Soil on Base Stresses

EFFECTS OF VARYING THE HEIGHT OF THE RETAINING WALL

Finite element analyses were conducted to determine the effects of varying the retaining wall height (H), while keeping the base width (B) and the width of the top of the wall (B_t) constant. Four analyses were conducted using retaining wall heights equal to 45, 36, 30 (the Base Case) and 15 feet. For a base width B equal to 18 feet, these wall heights would correspond to B/H values of 0.4, 0.5, 0.6 and 1.2.

The meshes used for these analyses were obtained by multiplying the Y-coordinates of the nodal points above the ground level by scaling factors to increase or decrease the height of the wall.

The failure regions at the end of application of the full backfill loads for these four cases are given in Fig. 4.23. It can be clearly seen that the failure regions become more extensive as the height of the wall is increased (or, as B/H becomes smaller). It may also be noted that the failure regions calculated from the analyses of the two taller walls are sufficiently extensive to bring the wall to a "failure" state.

Fig. 4.24 shows the normal stress distributions for the same four cases, also at the end of backfilling. Two distributions were plotted together for each case. One distribution corresponds to the results calculated using the finite element method and the other distribution was obtained using conventional equilibrium analyses. For the most part, there is good agreement between the two sets of results, Note, however, that in the cases where failure occurred prior to the application of the full backfill load (B/H equal to 0.4 and B/H equal to 0.5) the normal stress distributions from finite element analyses were jagged and erratic, as was noted earlier.

The effective base widths (B_e/B) for both finite element and conventional equilibrium

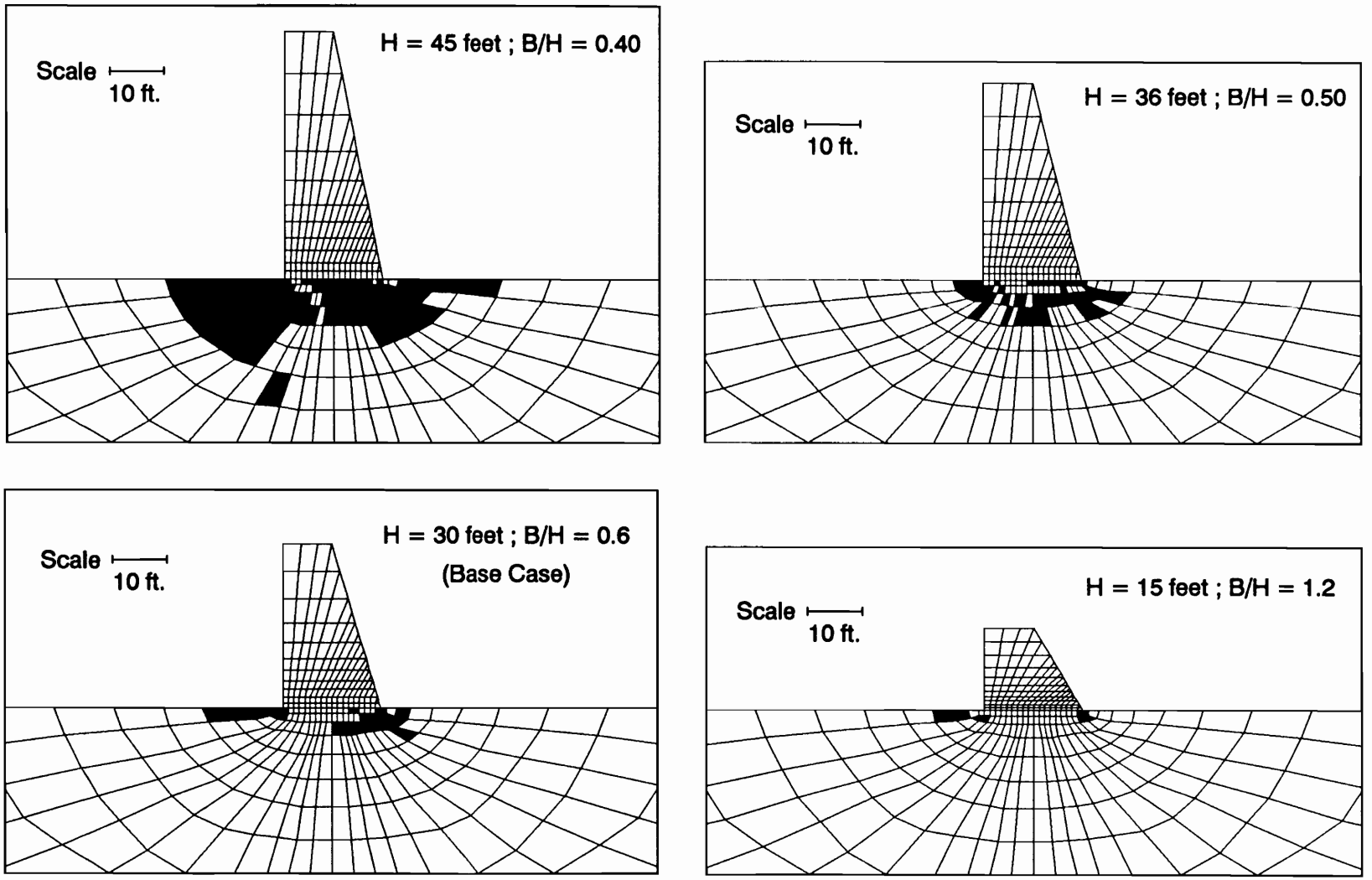

Figure 4.23 - Failure Regions After Backfilling for Different Retaining Wall Heights

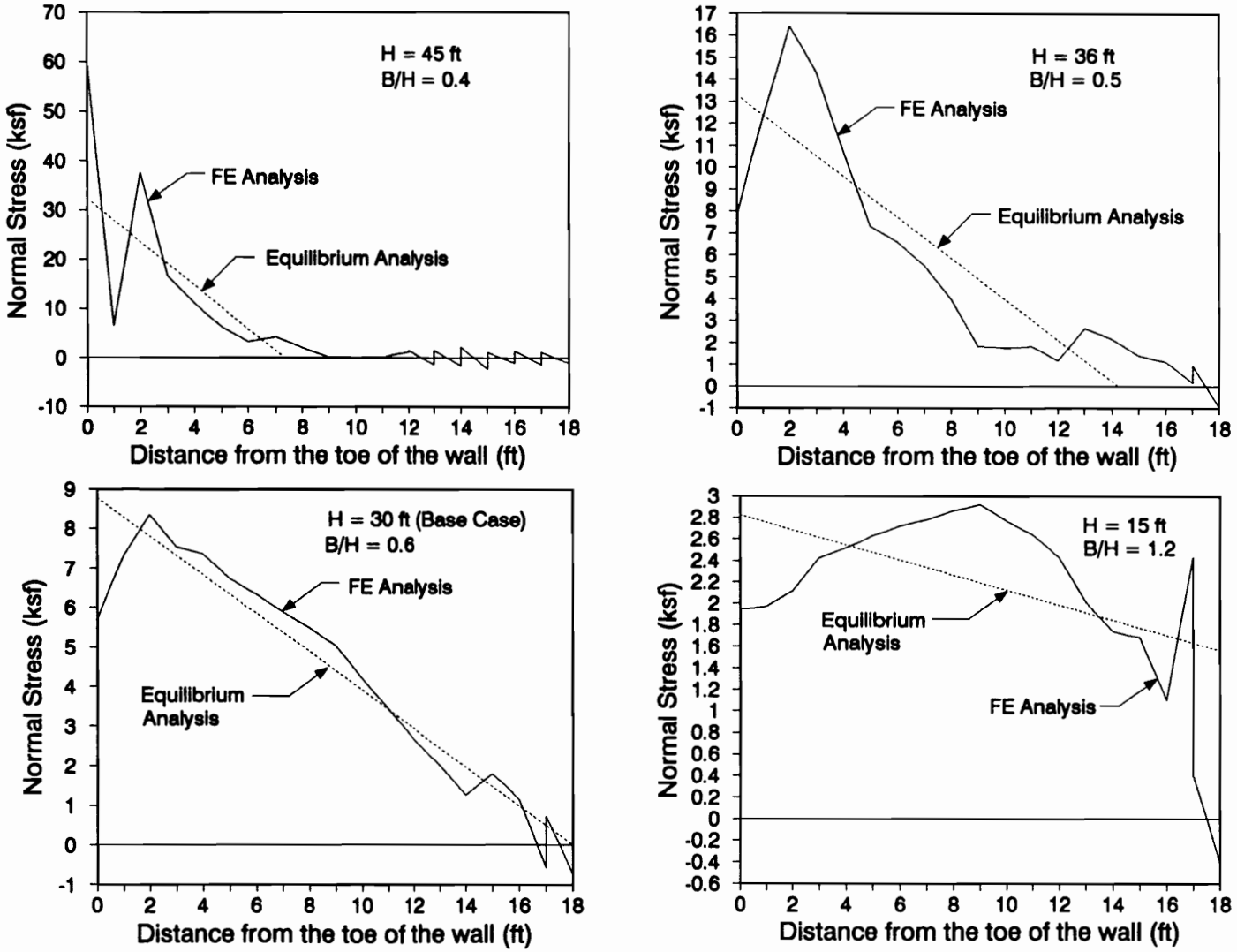

Figure 4.24 - Variation of Base Normal Stresses for different Wall Heights
- Finite Element and Conventional Equilibrium Analyses

analyses are given in Table 4.1. Note that conventional equilibrium analysis, which implicitly assumes a rigid foundation, yields smaller base contact areas than the finite element analyses in cases when conventional equilibrium analyses result in an effective base width less than 100 percent. It is interesting to note that even with a short, stocky wall as in the case of the fifteen-foot high wall, some parts of the base still lose contact with the foundation according to the results of the finite element analysis. It is the opinion of the writers that this loss of contact is merely an artifact of the assumed pressure distribution applied in order to simulate construction of the retaining wall. This assumed pressure distribution had a value of zero at the heel, a condition which greatly influenced the wall-foundation contact in that area during the application of the backfill loads.

The shear stress distributions from the finite element analyses, shown in Fig. 4.25, indicate a tendency of the distribution to "smooth out" and be more uniform as B/H increases. In three of the analyses (B/H equal to 0.4, 0.6 and 1.2), there is a concentration of shear stresses in the area where the wall base begins to separate from the foundation.

The maximum wall displacements during backfilling, Δ/H, were plotted against the factor of safety against bearing capacity failure, $FS_{bearing}$, for each of the four analyses in Fig. 4.26. As expected, the value of the factor of safety prior to backfilling is higher for the stockier walls, characterized by higher values of the aspect ratio B/H. However, even if each wall had a different initial value of the factor of safety, from the figure it seems that the Δ/H versus $FS_{bearing}$ curves converge once the wall begins to move away from the backfill. This convergence can be seen in the curves corresponding to runs FOL1A, FOL6B AND FOL6C. Values of Δ/H corresponding to certain values of $FS_{bearing}$ can be read from the converging portions of the curves. Δ/H is approximately 0.005 for $FS_{bearing}$ equal to 2.0 and increases to approximately 0.015 for $FS_{bearing}$ equal to 1.5 . Δ/H values increase very rapidly as $FS_{bearing}$ approaches unity.

Table 4.1 - Effective Base Widths After Backfilling Resulting from Finite Element and Conventional Equilibrium Analyses of Different Retaining Wall Heights

		B_e/B (%)	
H (ft)	B/H	FEA	CEA
45	0.4	65	41
36	0.5	94	79
30	0.6	93	100
15	1.2	93	100

Note : FEA - Finite Element Analyses
CEA - Conventional Equilibrium Analyses

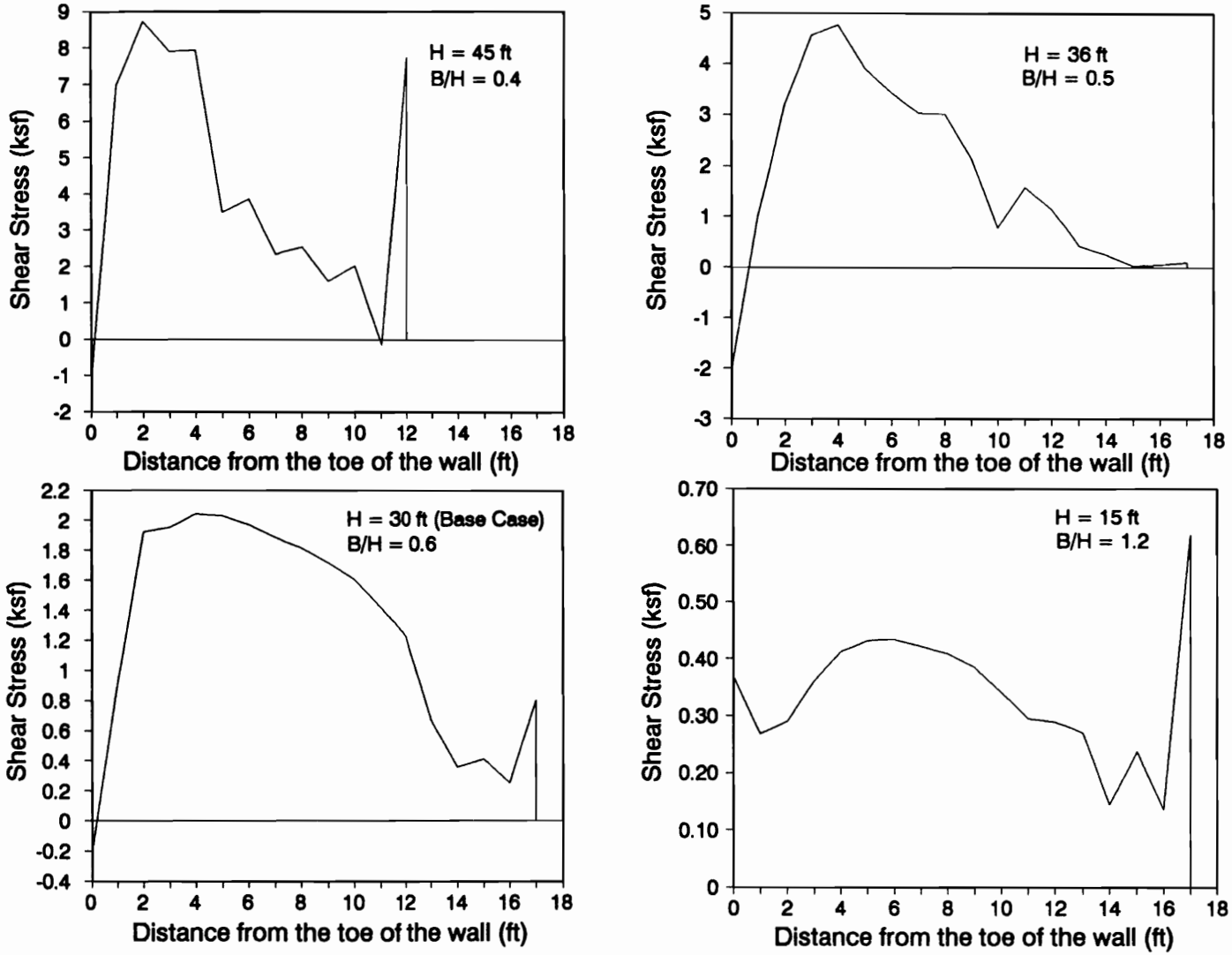

Figure 4.25 - Variation of Base Shear Stresses for Different Wall Heights - Finite Element Analyses

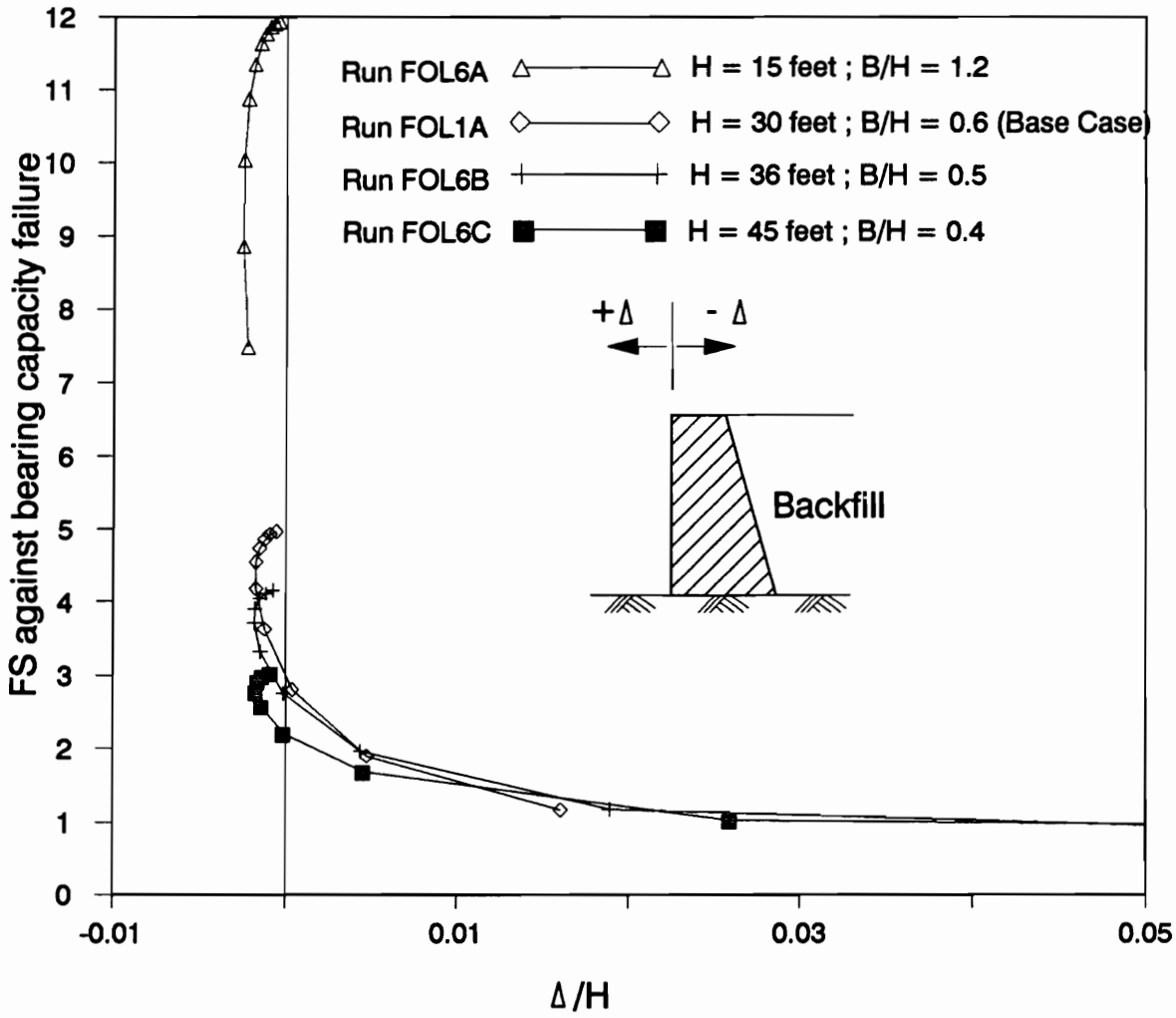

Figure 4.26 - Factor of Safety Against Bearing Capacity Failure vs. Normalized Wall Displacements for Different Retaining Walll Heights

Using bearing capacity theory and conventional equilibrium analyses, curves that show the relation between $FS_{bearing}$ and the backfill height for the four cases were constructed. These are shown in Fig. 4.27. Note that the curves for B/H equal to 0.4 and 0.5 crossed the horizontal failure line. As mentioned previously, analyses of these same two cases using the finite element method also indicated wall failure. Boxes were superimposed on the Δ/H versus backfill height curves to indicate the backfill height at failure calculated from finite element analyses. It may be noted that the box for B/H equal to 0.4 plotted very near the point where its corresponding Δ/H versus backfill height curve crossed the horizontal failure line, indicating that the results of the two methods of analysis used were very close. The same is true for B/H equal to 0.5.

EFFECTS OF THE VARYING THE WIDTH OF THE WALL BASE

In the analyses discussed in the previous section, the heights of the walls were varied while the base width remained constant. In the analyses discussed in this section, the wall height was kept constant and the width of the base was varied. Using a wall height equal to 30 feet, the four values of aspect ratio studied (0.4, 0.5, 0.6 and 0.7) correspond to walls with base widths equal to 12, 15, 18 (the Base Case value) and 21 feet. The ratio of the width of the top of the wall to the base width (B_t/B) was kept constant.

The finite element meshes used for the analyses were obtained by multiplying the X-coordinates of all the nodal points in the mesh used for the base case by an appropriate scaling factor.

In general, the trends observed when the wall height was varied were also true when the wall base width was varied. These observations include :

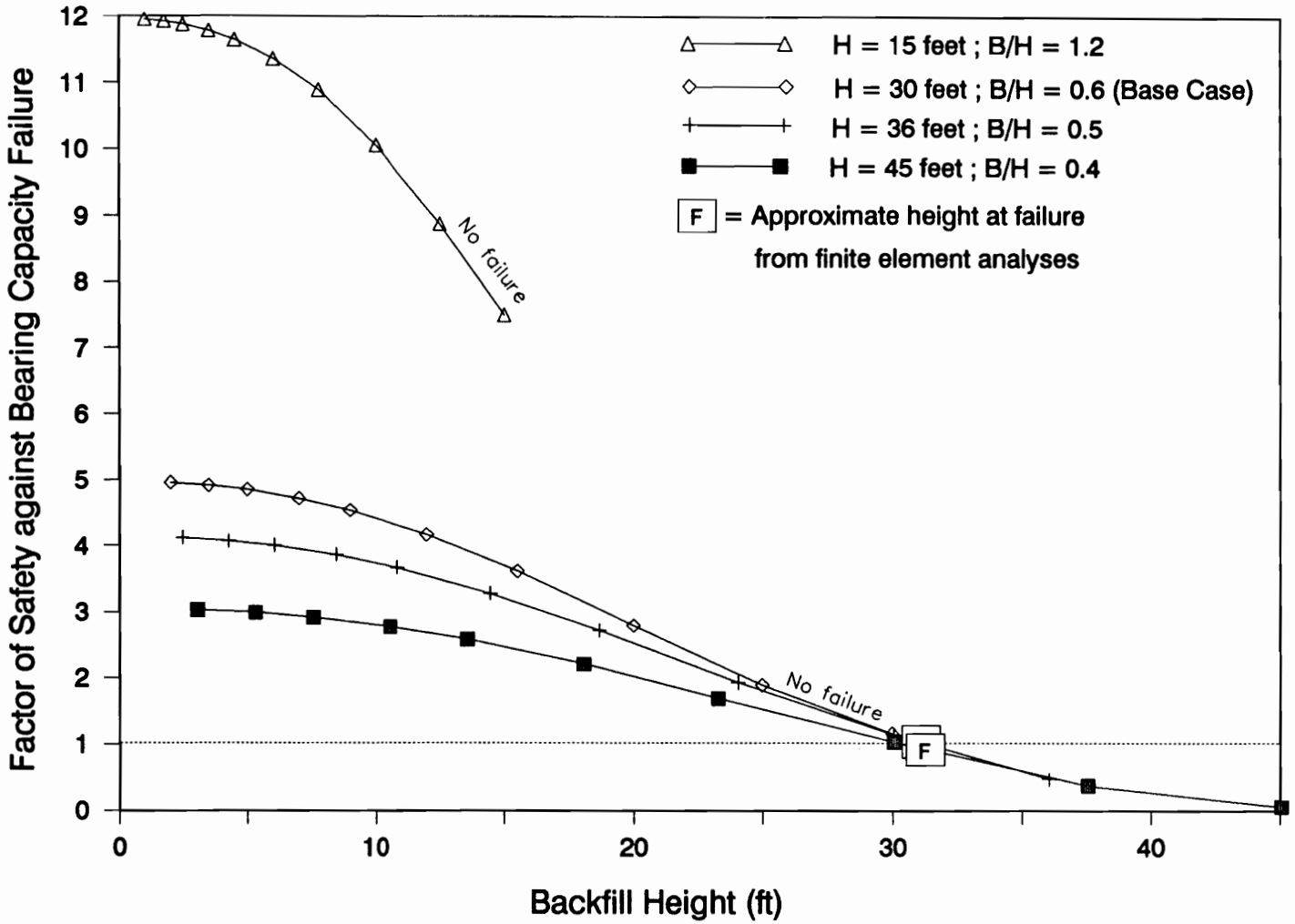

Figure 4.27 - Variation of Factor of Safety Against Bearing Capacity Failure with Backfill Height for Different Retaining Wall Heights

(1) More extensive failure regions as B/H became smaller. This trend is shown in Figure 4.28. In this case, B/H becomes smaller as the wall base width is decreased.

(2) Good agreement between normal stress distributions obtained from the finite element analyses and conventional equilibrium analyses. These stress distributions are shown in Fig. 4.29.

(3) The tendency of the shear stress distribution to "smooth out" as B/H is increased (Fig 4.30).

(4) The same tendency of the $FS_{bearing}$ versus Δ/H curves (Fig. 4.31) to converge as the wall moves away from the backfill. Note from Fig. 4.31 that Δ/H is approximately 0.005 for $FS_{bearing}$ equal to 2.0 and approximately 0.015 for $FS_{bearing}$ equal to 1.5.

(5) Good agreement between the estimates of backfill height at failure obtained using finite element analyses and those obtained using bearing capacity and conventional equilibrium analyses. Variations of factor of safety with backfill height are shown in Fig. 4.32.

(6) Conventional Equilibrium analyses yielded lower B_e/B values when compared to results calculated using Finite Element analyses in cases when Conventional Equilibrium analyses result in a B_e/B less than 100 percent. B_e/B values obtained from the two sets of analyses are listed in Table 4.2.

The walls with B/H values equal to 0.4 and 0.5 reached a state of failure prior to the application of the full backfill loads. The base stress distributions for these two cases at the end

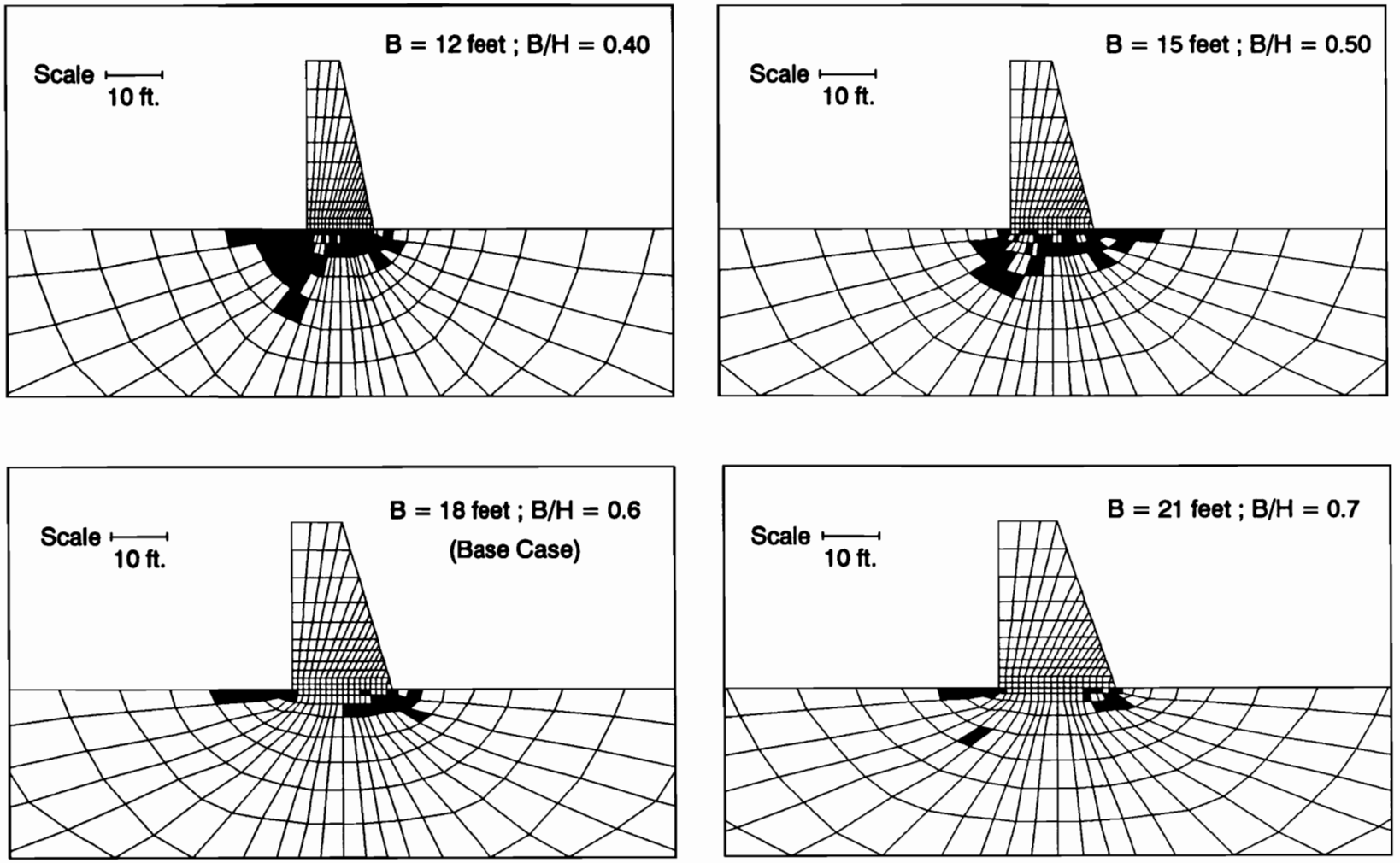

Figure 4.28 - Failure Regions After Backfilling for Different Wall Base Widths

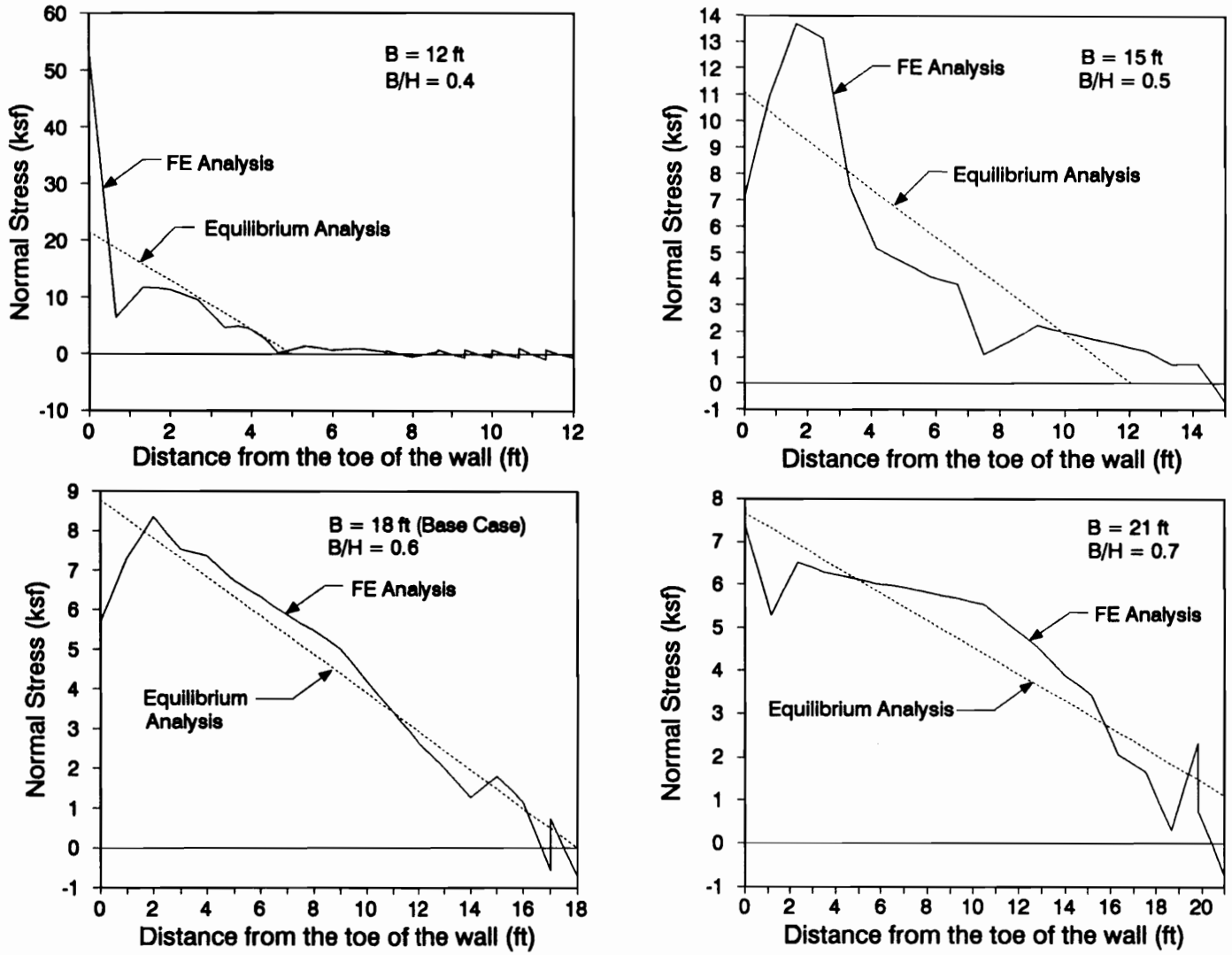

Figure 4.29 - Variation of Base Normal Stresses for Different Wall Base Widths - Finite Element and Conventional Equilibrium Analyses

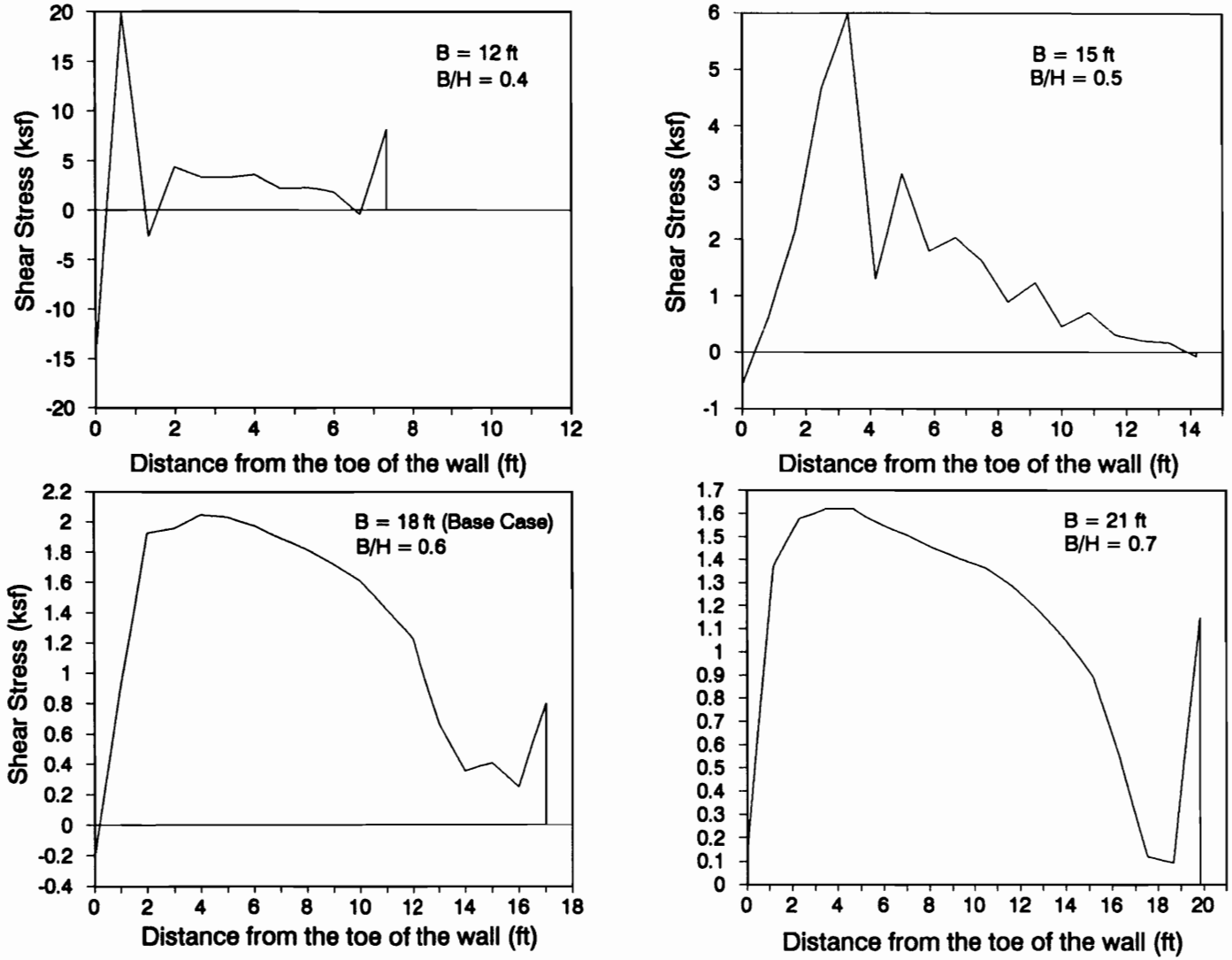

Figure 4.30 - Variation of Base Shear Stresses for Different Wall Base Widths - Finite Element Analyses

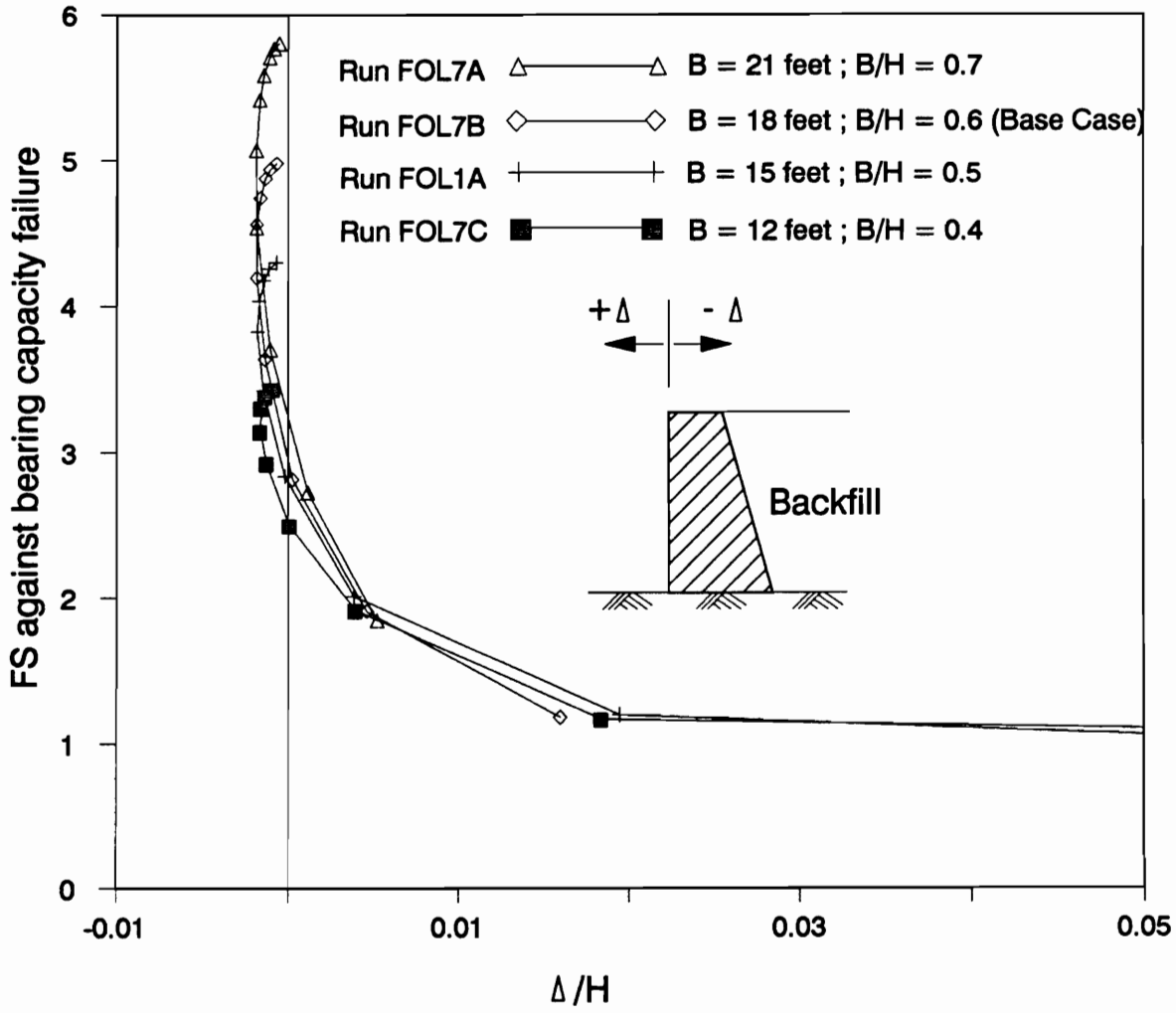

Figure 4.31 - Factor of Safety Against Bearing Capacity Failure vs. Normalized Wall Displacements for Different Retaining Wall Base Widths

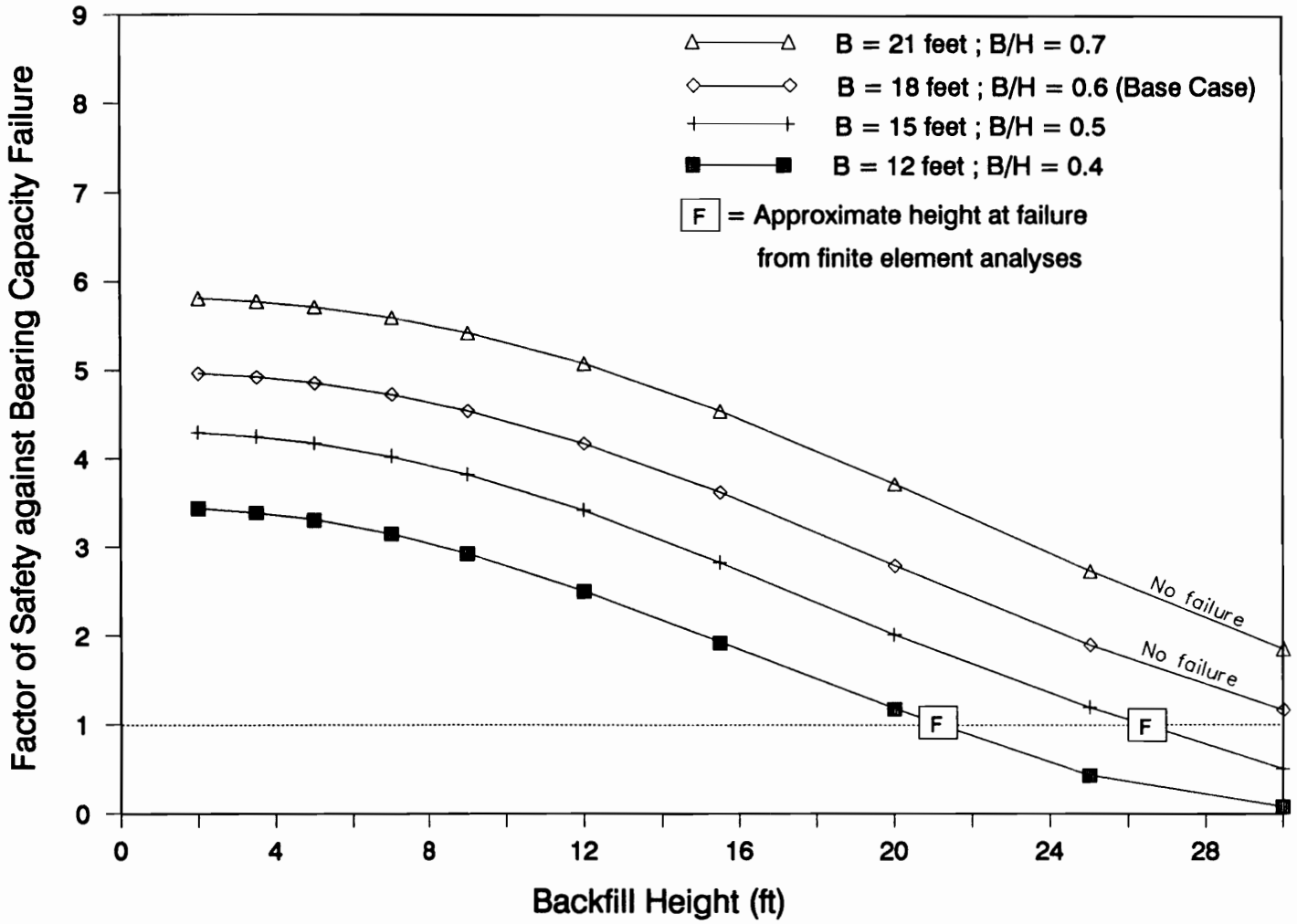

Figure 4.32 - Variation of Factor of Safety Against Bearing Capacity Failure with Backfill Height for Different Wall Base Widths

Table 4.2 - Effective Base Widths After Backfilling Resulting from Finite Element and Conventional Equilibrium Analyses of Different Retaining Wall Base Widths

		B_e/B (%)	
B (ft)	B/H	FEA	CEA
12	0.4	61	41
15	0.5	94	79
18	0.6	93	100
21	0.7	94	100

Note : FEA - Finite Element Analyses
CEA - Conventional Equilibrium Analyses

of backfilling were jagged and erratic, a condition that was previously observed in walls that failed.

It is also interesting to note that the results of finite element analyses of two walls with different dimensions but with equal aspect ratios yielded similar results. This was true in particular of the shape of the base stress distributions and B_e/B values of the walls with aspect ratios (B/H) equal to 0.4 and 0.5.

EFFECTS OF THE PRESENCE OR ABSENCE OF A TOE FILL

The effects of the presence or absence of a toe fill was investigated in this set of analyses. Nodal forces corresponding to nine feet of toe fill were applied on the side of the wall opposite the backfill side, as shown in Fig. 4.33, in much the same manner that the nodal forces corresponding to the placement of the backfill were applied. The wall in this case was 30 feet in height.

The failure regions after application of the full backfill loads calculated from analyses with and without the toe fill are shown in Fig. 4.34. The stabilizing effect of the toe fill is immediately apparent. It may be noted that with the toe fill, no soil elements in the toe area failed, and the failure region beneath the heel was less extensive. The reasons for these occurrences are : (1) The surcharge due to the toe fill increases the confining pressure (and, consequently, the strength) of the elements in the toe area. This also increases the bearing capacity of the foundation. (2) The lateral earth pressure from the toe fill reduces the tendency of the wall to lift off due to the lateral load exerted by the backfill. This would also result in increased confining pressures of the elements in the area beneath the heel.

The base normal and shear stress distributions calculated from these two analyses are

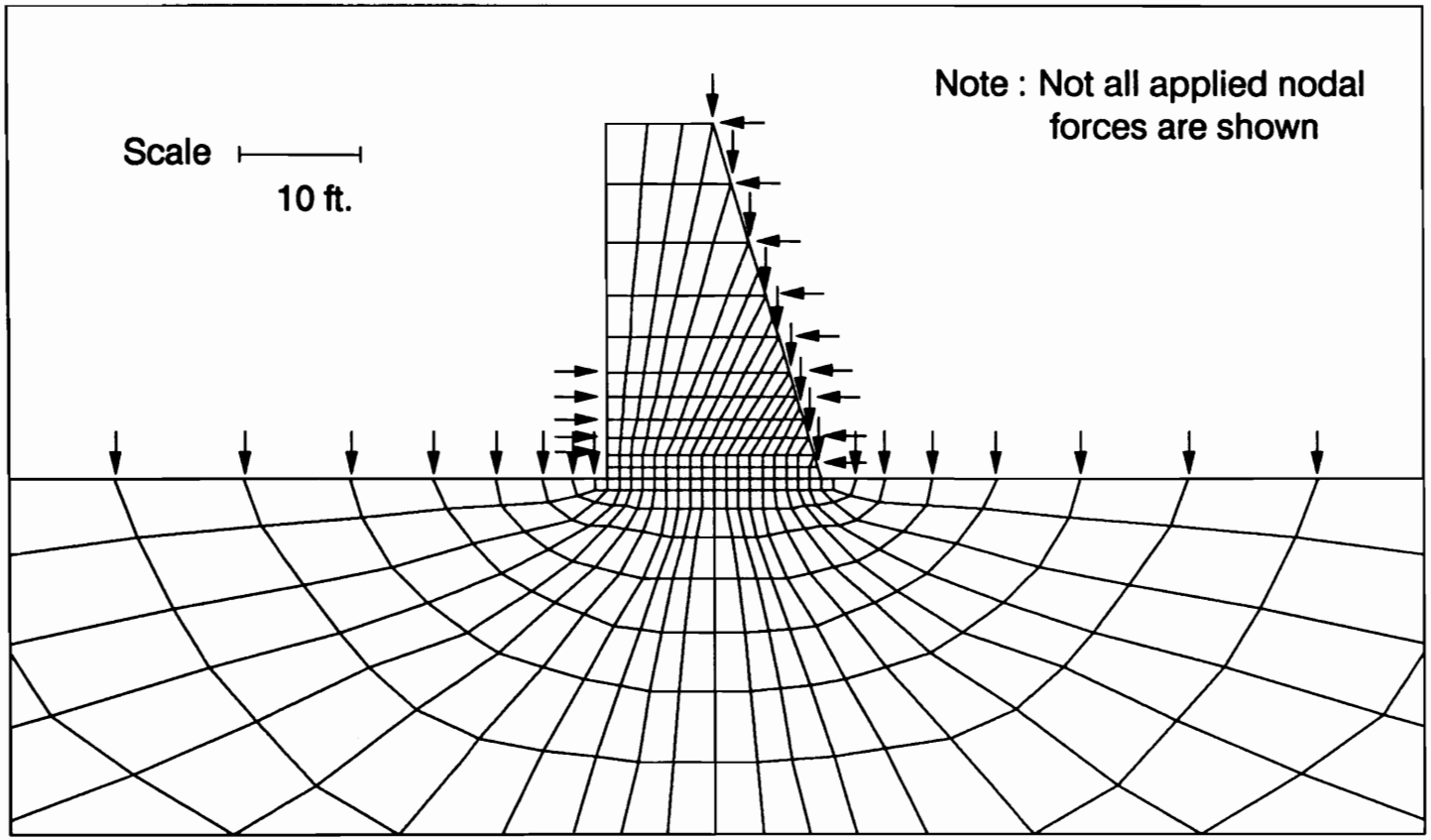

Figure 4.33 - Application of Nodal Forces to Simulate the Placement of both the Toe Fill and the Backfill

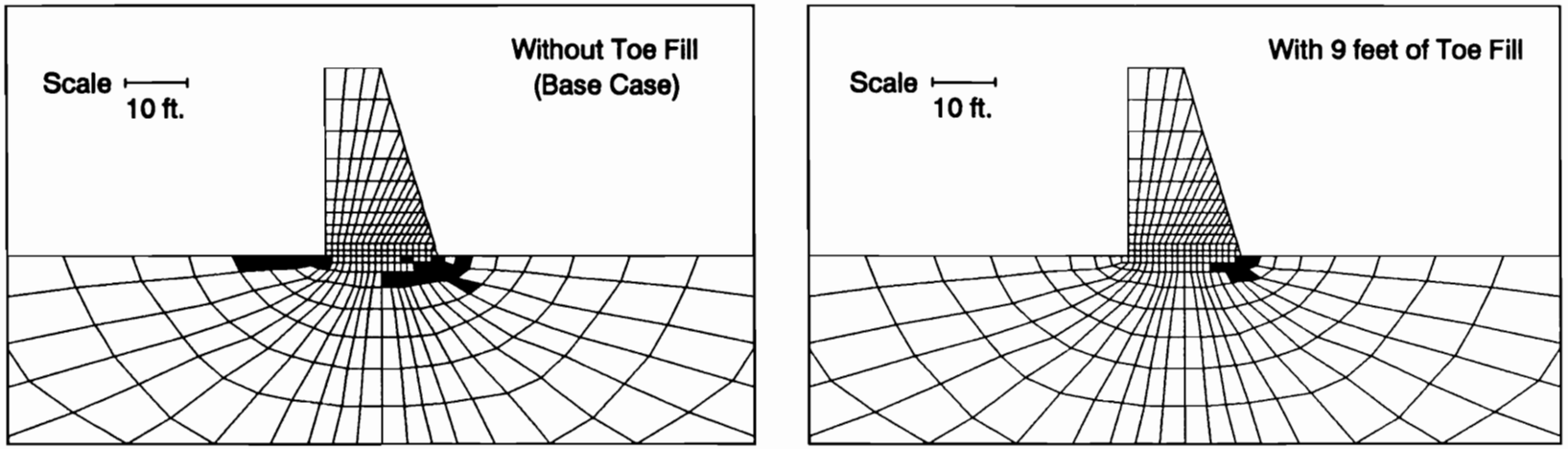

Figure 4.34 - Failure Regions after Full Loading Sequence
- Construction with and without Toe Fill

shown in Fig. 4.35. In the analysis with the toe fill, there is a larger magnitude of both the normal and shear stresses in the toe area, compared to the stresses in the same area without the toe fill. There were no failed soil elements in the toe area and consequently, redistribution of stresses did not occur.

Analyses with and without the toe fill resulted in a base contact area (B_e/B) equal to 93 percent. While it seems that the toe fill had no effect on B_e/B, it is believed that the loss of contact in both analyses is not so much the effect of the forces applied on the wall as it is the effect of the initial stress distribution, which was zero at the heel.

The presence of the toe fill reduced the maximum wall displacement to 40 percent of the value without the toe fill. Maximum displacement (Δ/H) values calculated were : 0.0161 for the analysis without the toe fill and 0.0137 for the analysis with the toe fill.

EFFECTS OF THE METHOD USED IN SIMULATING RETAINING WALL CONSTRUCTION

Prior to backfilling, the foundation was subjected to loads due to the construction of the retaining wall. The method used to simulate the construction of the retaining wall establishes the initial stresses in the interface between the wall base and the foundation, as well as the initial stresses in the soil elements in the foundation. Two methods of simulating the wall construction were used, and the results of the two analyses were compared.

The first method of simulating wall construction is referred to as the "pressure buildup" method. This method was used in the analysis of the Base Case problem and all the analyses discussed thus far. As discussed in Chapter 2, this method involved applying pressure on the interface elements beneath the base of the wall. The pressure distribution is a reflection of the

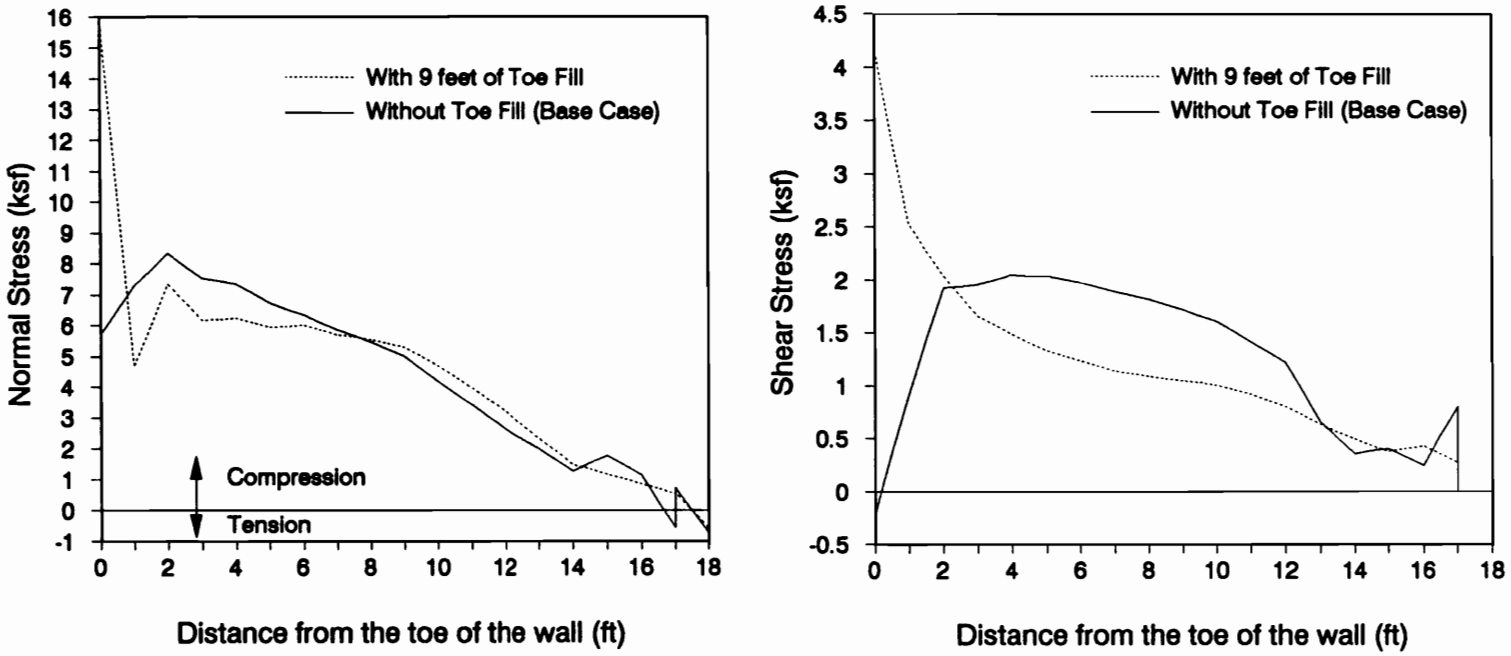

Figure 4.35 - Effect of the Presence or Absence of Toe Fill on the Base Stresses

weight of the wall above the interface and was applied while the elements in the wall still possess the properties of air. As soon as the full pressure distribution was applied, the wall elements were assigned the properties of hardened concrete. This procedure prevents soil-structure interaction from taking place and influencing the stresses in the interface and foundation.

The second method is referred to as the "element buildup" method. In this method, retaining wall construction was simulated by assigning properties of fluid concrete to the elements that make up the wall, layer by layer. After placement, the elements in a layer were assigned the properties of hardened concrete to simulate concrete setting. This is done prior to the placement of the succeeding layer. A total of eleven layers was used to build up the wall. In contrast to the pressure buildup method discussed in the previous paragraph, there will be soil-structure interaction effects in this method of simulating wall construction.

The failure regions immediately after retaining wall construction using these two methods are shown in Fig. 4.36. Both analyses resulted in failure, mostly near the ground surface adjacent to the edges of the wall. The soil elements in these regions failed primarily because of low confining stresses.

The base stresses immediately after wall construction are shown in Fig. 4.37. Using the pressure buildup method, the normal stresses on the wall-foundation interface were equal to the pressure distribution that was applied, as shown in Fig. 4.37(a). Using the element buildup method, soil-structure interaction effects were manifested in the form of "spikes" in the normal stress distribution (Fig. 4.37(a)), particularly in the areas beneath the edges of the wall. The presence of these "spikes" is similar to the large stresses that elastic theory predicts at the edges of a rigid punch on an elastic half-space. Soil-structure interaction effects in the element buildup method are also evident in the resulting shear stress distribution, shown in Fig. 4.37(b). The shear stress in this case varied from -1.8 to + 1.0 ksf. For the pressure buildup method, the

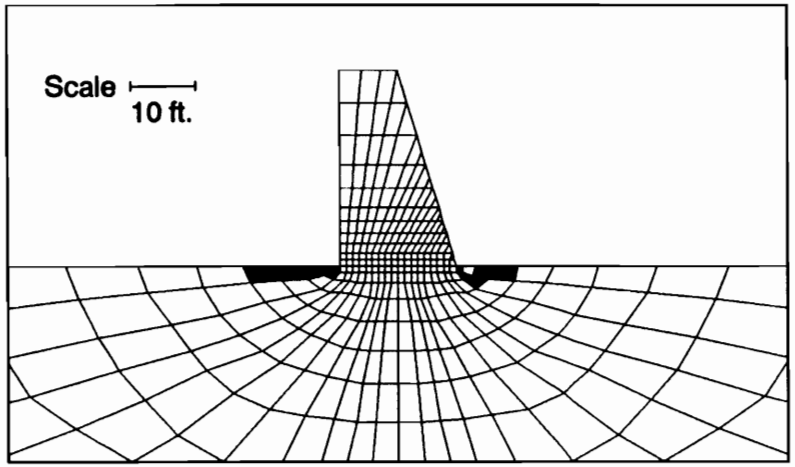

(a) Wall Construction Simulation by Specification of Base Pressure (Base Case)

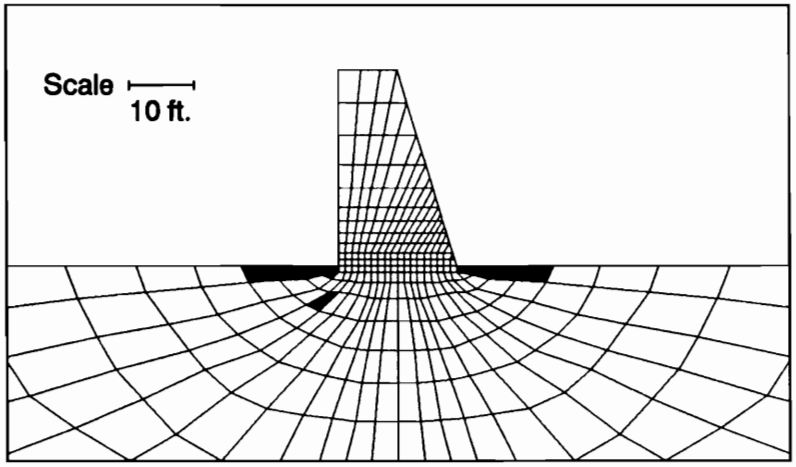

(b) Wall Construction Simulation by Addition of Finite Elements

Figure 4.36 - Failure Regions After Construction of the Retaining Wall for Two Mehtods of Simulating Wall Construction

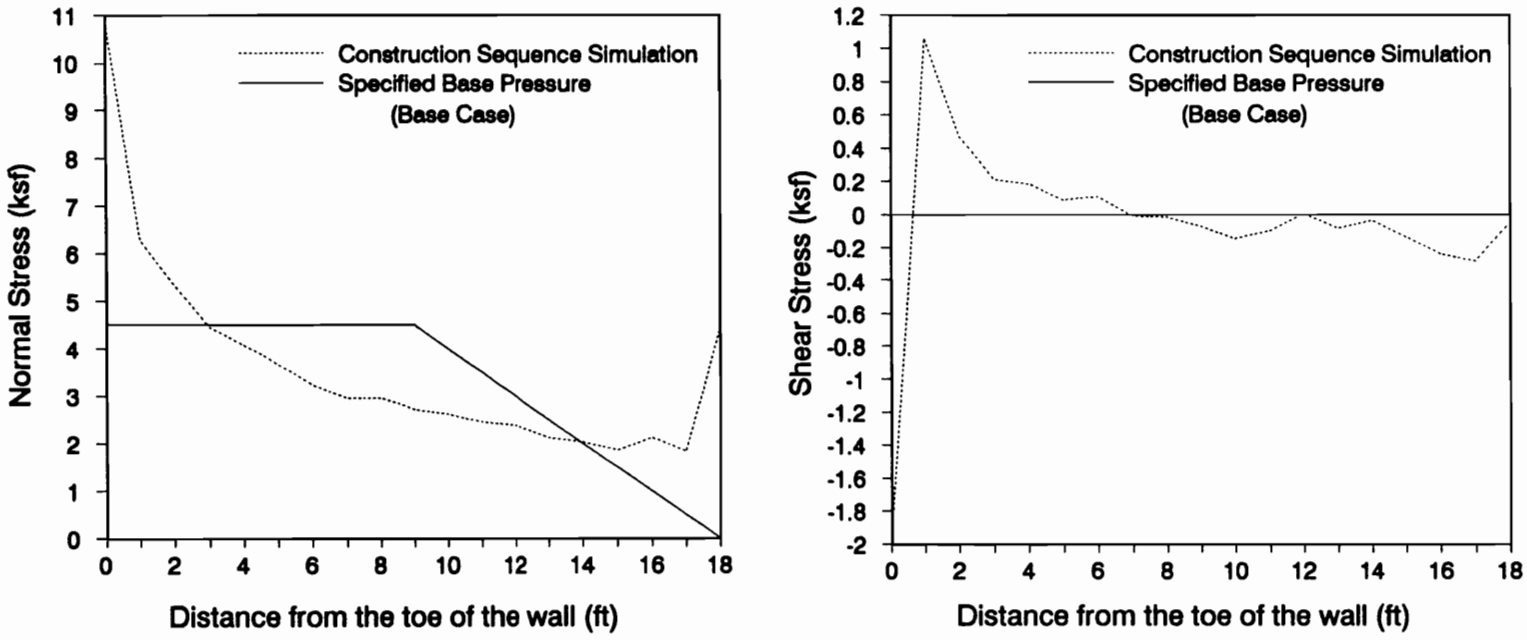

(a) (b)

Figure 4.37 - Base Stresses After Construction of the Retaining Wall for Two Methods of Simulating Wall Construction

shear stress is assumed to be equal to zero everywhere along the base.

The failure regions after the application of the full backfill loads are shown in Fig. 4.38. It can be seen that the failure regions are much more extensive when the retaining wall construction is simulated using the element buildup method. This is true particularly for the area beneath the toe. The system, however, is not yet in a "failure" state. This more extensive failure region associated with the element buildup method resulted in a calculated value of Δ/H equal to 0.0481, about three times the value calculated from the analysis utilizing the pressure buildup method, which is equal to 0.0161.

The base stresses at the end of backfilling are shown in Fig. 4.39. It is interesting to note from Fig. 4.39(a) that the "spike" present in the normal stress distribution after the wall construction which employed the element buildup method is still distinguishable after the application of the full backfill loads. The soil-structure interaction effects resulting from the use of this method are also evident in the shear stress distribution after backfilling, as shown in Fig. 4.39(b). This shear stress distribution is approximately a superposition of the initial non-zero stress distribution using the element buildup method (after wall construction) and the shear stress distribution utilizing the pressure buildup method after backfilling.

The residual effects of the "spikes" are also evident in the base contact areas at the end of backfilling. The effective base widths are 93 percent in the analysis using the pressure buildup method and 98 percent in the analysis using the element buildup method.

SUMMARY

Following load analyses using an updated version of SOILSTRUCT which incorporated the Alpha Method were performed to determine the effects of material, geometric and loading

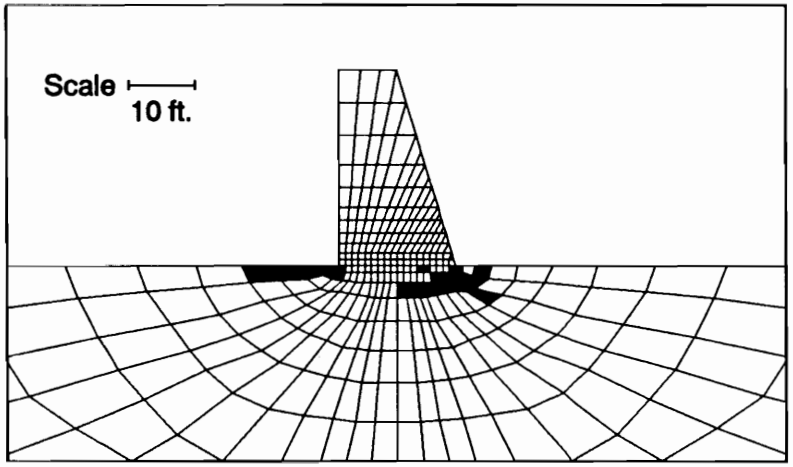

(a) Wall Construction Simulation by Specification of Base Pressure (Base Case)

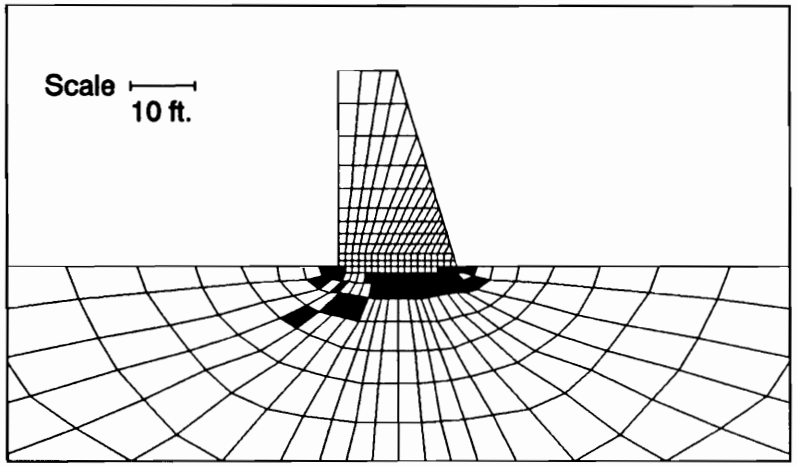

(b) Wall Construction Simulation by Addition of Finite Elements

Figure 4.38 - Failure Regions After Backfilling for Two Methods of Simulating Wall Construction

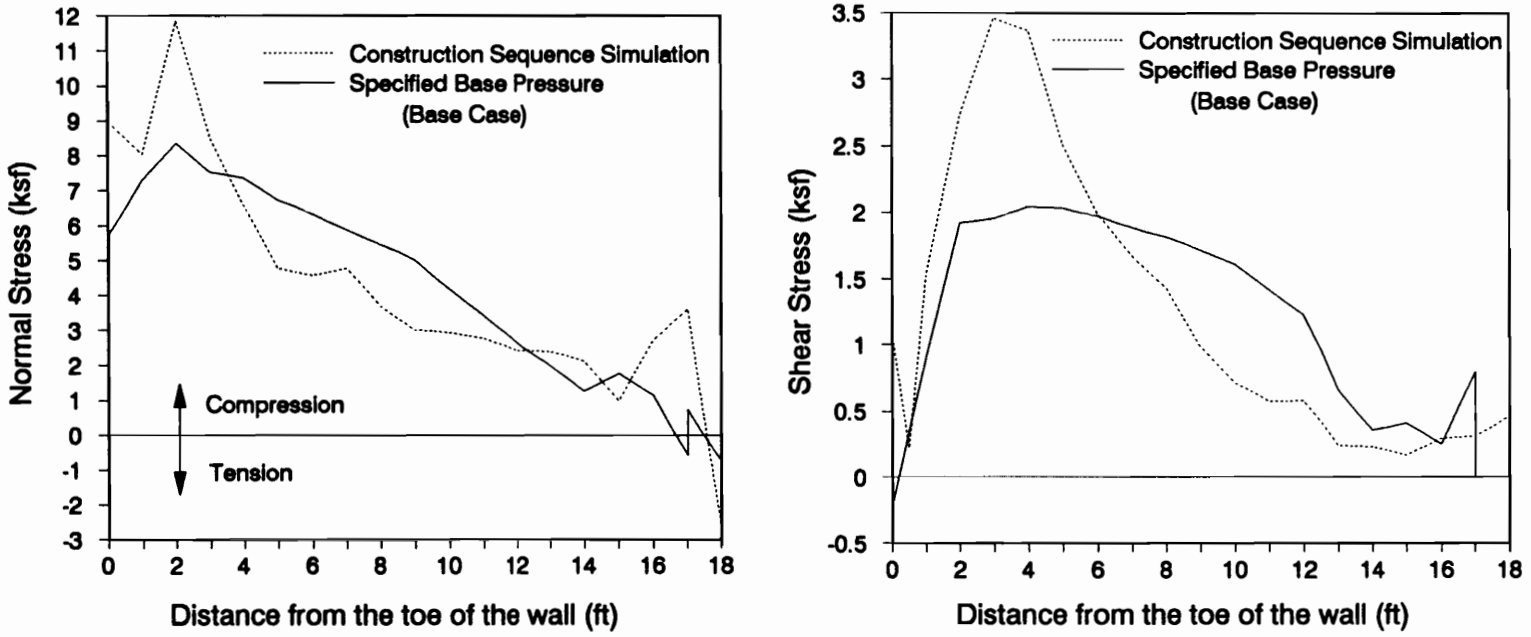

Figure 4.39 - Effect of the Method used for Simulating Wall Construction on the Base Stresses after Backfilling

parameters on the behavior of gravity retaining walls. In the course of this study, it was found that a fairly reliable assessment of the stability of gravity retaining walls on soil can be obtained by analyzing the wall-foundation system as a bearing capacity problem.

Conventional equilibrium analyses of retaining walls implicitly assume a linear variation of pressure at the base with the maximum normal stress at the toe. In the finite element analyses, it was found that stress redistribution occurs in the wall-foundation interface as a result of the failure of soil elements in the foundation. The soil elements beneath the edges of the wall usually fail first, and consequently, the maximum stresses usually do not occur at the toe, but at a location slightly inside the toe of the wall.

Specific conclusions drawn from the analyses are :

Results of Analyses with and without the Alpha Method

The base case problem was analyzed using the original and revised versions of the finite element program SOILSTRUCT. The revised version contains the Alpha Method routine for two-dimensional elements as well as Seed and Duncan's (1983) model for the unload-reload behavior of soil.

The control of overshoot was improved in the analysis using the revised version of the program. This improved result affected the development of the failure regions, which in turn influenced the base normal and shear stress distributions, as well as the amount of wall movement. The analyses with both the original and the revised versions of the program indicate that the wall in the base case problem should be stable.

Results of Analyses using different Interface Shear Stiffnesses

Analyses were conducted using three different values of the wall-foundation interface shear stiffness, K_s. Results from this set of analyses indicate that K_s can be varied within a reasonable range of values without affecting the results significantly. However, it should be

emphasized that although this conclusion is valid for following load analyses, it may not be for the case when the backfill is represented by soil elements rather than by nodal forces.

Results of Analyses using different Lateral Earth Pressure Coefficient

The horizontal thrust that the backfill exerts on the retaining wall increases as the value of the lateral earth pressure coefficient, K_h, is increased. Increasing the horizontal thrust tends to concentrate the stresses in the toe area, decreases the effective base contact area, results in a more extensive failure region and increases the displacement at the top of the wall. A sufficiently large K_h value causes instability of the wall.

Results of Analyses using different Poisson's Ratio of the Foundation Soil

Changes in the Poisson's ratio of the foundation soil affects mainly the lateral stresses induced in the soil elements. A decrease in the value of Poisson's ratio resulted in a reduction in the magnitudes of the confining stresses and, consequently, the strength of the soil elements. Analyses have shown, however, that ν_s can be varied within a reasonable range of values without significantly affecting the results.

Results of Analyses using different Relative Densities of the Foundation Soil

Analyses were performed on walls resting on foundation soils with relative densities equal to 25, 50, 75 and 100 percent. It was concluded from the results of the finite element analyses that the relative density of the foundation soil is of major importance in the overall stability of retaining walls. Failure regions in the foundation developed more rapidly as the density of the foundation soil decreased. This led to lower factors of safety against bearing capacity failure. The wall displacements did not differ significantly during the early backfilling stages, when wall movement was in the direction of the backfill. In all four cases analyzed, wall movement away from the backfill commenced when the backfill height was about 60 to 65 percent of the wall

height. Beyond this stage, the wall movements increased more rapidly as the factor of safety against bearing capacity failure decreased, particularly for smaller relative densities.

Results of Analyses using different Foundation Soil Thicknesses

The thickness of the foundation soil influenced the extent of the failure regions in the foundation soil to a small degree. Both extremely thin and extremely thick foundation soil layers tend to have more extensive failure regions, although the nature of the forces that cause the failures is different in these cases.

Although there were differences in the extent of the failure regions calculated from the analyses of the different foundation soil thicknesses, these differences were slight, and as such, they did not significantly affect displacements, base stresses and the overall stability of the wall. It is therefore reasonable to conclude that thickness of the foundation soil is of minor importance in influencing the behavior of gravity retaining walls.

Results of Analyses of Different Wall Dimensions

Two sets of analyses were performed to determine how wall dimensions affected its behavior. In the first set of analyses, the width of the wall base was kept constant (B = 18 feet), while the height was varied (H = 15, 30, 36 and 45 feet). In the second set of analyses, the height was kept constant (H = 30 feet), while the width of the base was varied (B = 12, 15, 18 and 21 feet). Results show that it is not solely the dimension B or the dimension H which affects the behavior of the wall, but rather the aspect ratio B/H.

In general, a wall becomes more unstable as B/H decreases. On a medium dense sand foundation, a retaining wall is unstable for B/H ratios of 0.5 or less when subjected to lateral loads corresponding to $K_h = 0.37$.

It was found that when the wall starts moving away from the backfill, there is a unique relationship between the factor of safety against bearing capacity failure and Δ/H, independent

of the value of the aspect ratio of the wall, B/H.

Results of Analyses with and without a Toe fill

The placement of a toe fill improves the overall stability of a retaining wall. In conventional analyses, the stabilizing effects of a toe fill are accounted for by a lateral earth force exerted by the toe fill on the wall. This force counteracts the forces exerted by the backfill, which tend to overturn the wall.

Finite element analyses of a wall founded on soil have shown that the stabilizing effects of a toe fill arise from increased bearing capacity of the foundation. This increase in bearing capacity is due to the increase in confining pressure and strength of the underlying soil. A comparison of the finite element analyses with and without the toe fill show that with the toe fill, there is a significant reduction in the number of failed soil elements in the heel area, as well as an absence of failed soil elements in the toe area.

Results of Analyses using Two Methods of Simulating Wall Construction

Two methods were utilized to simulate construction of the retaining wall. These were referred to as the "pressure buildup" method and the "element buildup" method. The "pressure buildup" method was used to simulate wall construction in all of the analyses previously discussed.

The main difference between the two methods is that the element buildup method models soil-structure interaction between the wall and the foundation soil while the pressure buildup method does not. This difference is evident in the interface stresses immediately after wall construction, shown in Fig. 4.31, particularly the "spikes" in the normal stress distribution occurring at the edges of the retaining wall. As shown in Fig. 4.33, these spikes are still evident, even after backfilling.

The element buildup models the wall construction sequence, and the base stresses after

wall construction calculated by this method are probably more realistic. A further drawback of the pressure buildup method is that, if the magnitude of the pressure in the heel area is small, there is always a small amount of wall-foundation separation at the end of backfilling which is not believed to be realistic. This was the case even in the analysis of a short, stocky wall with a base-to-height ratio equal to 1.2. However, the amount of separation (usually six to seven percent of the base width) did not adversely affect the overall stability of the wall and was considered tolerable.

CHAPTER 5

ANALYSES OF GRAVITY RETAINING WALLS FOUNDED ON SOIL USING THE BACKFILL PLACEMENT METHOD

INTRODUCTION

This chapter discusses the results of parameter studies performed on gravity retaining walls on soil using the "backfill placement" method of analysis. The term "backfill placement" was used by Ebeling et al. (1988) to refer to the mode of analysis whereby the soil backfill is represented by finite elements which are added to the mesh layer by layer. The forces exerted by the backfill on the wall-foundation system are determined by the backfill properties and the wall movements, and the analysis thus accounts for soil-structure interaction effects. In this respect these analyses differ from following load analyses, in which the backfill is represented by nodal forces whose magnitudes are pre-determined. The backfill placement method is considered to provide a more realistic model of the backfilling process.

CHANGES IN THE COMPUTER PROGRAM SOILSTRUCT

The following load analyses discussed in the previous chapters utilized a version of SOILSTRUCT which computed soil element stiffnesses based on the elastic parameters E_t (tangent modulus) and ν_s (Poisson's ratio). The value of ν_s was assumed to be constant. The backfill placement analyses described in this and the following chapter were performed using the bulk modulus formulation developed by Duncan, et al. (1980), which is believed to afford a

somewhat better representation of the stress-strain behavior of soil.

Filz et al. (1990) developed SSB, a version of SOILSTRUCT which utilizes the bulk modulus formulation developed by Duncan, et al (1980). In addition, the following changes related to stress-strain behavior were incorporated in SSB by Filz, et al (1990) :

(a) The "stress state" concept for 2D soil elements (discussed in Chapter 2) was adapted for use in interface element stiffness computations.

(b) The "stress state" concept for 2D elements was modified to extend its applicability to cohesive soils. The original stress-state concept was developed for cohesionless soils and was found to be unsuitable for modeling the behavior of a soil with significant values of cohesion intercept.

(c) Constraints on the value of the bulk modulus B_{mod} were included. These constraints were based on the discussion in Duncan et al. (1980). In addition, Filz et al. (1990) introduced a constraint on B_{mod} based on an unloading parameter, K_2, discussed by Seed and Duncan (1986). This constraint lowered the minimum possible value of ν_s to that corresponding to the following formula :

$$(\nu_s)_{min} = K_2/(1 + K_2) \tag{5.1}$$

Consequently, the minimum permissible value of B_{mod} is reduced.

These changes were incorporated in the version of SOILSTRUCT with the Alpha Method for interface and 2D elements, and was used in the backfill placement analyses.

HYPOTHETICAL STRUCTURES AND LOADING CONDITIONS USED IN THE BACKFILL PLACEMENT ANALYSES

The hypothetical wall-foundation system which was analyzed is shown in Fig. 5.1. The geometry is the same as for the wall which was analyzed using the following load method. Because the backfill is represented by finite elements, additional interface elements were placed on the wall-backfill, the wall-toefill and the foundation-backfill interfaces.

The values of the material and geometric parameters used in the backfill placement analyses are listed in Table 5.1. The analysis designated as Run BFBC is referred to as the base case backfill placement run, the results of which are used for reference in evaluating the effects of changes in the parameter values.

The geometry for the base case is shown by the finite element mesh in Fig. 5.2. It consists of 40 interface elements, 474 two-dimensional elements and 548 nodes. The mesh is designed so that the backfilling process can be simulated using ten 3-foot thick lifts.

As in the following load analyses, the stresses in the foundation prior to the construction of the wall and backfill correspond to at-rest conditions. The construction of the wall was simulated using the "pressure buildup" method discussed in Chapters 2 and 4.

Fig. 5.3 illustrates how the placement of backfill was simulated in the backfill placement method. Fig. 5.3 (a) shows the finite element mesh after the construction of the wall, with the backfill elements still assigned the properties of air. These "air elements" are shown with dotted boundaries. A lift is placed by changing the properties of the elements in that lift from those of air to those of soil. Fig. 5.3(b) shows the mesh after the first lift was placed. The 2D soil elements in this lift drawn with solid lines. When backfill elements are first placed, they are modeled so as to behave as a dense fluid with low moduli. They are allowed to harden in subsequent construction steps, and their moduli during these later steps are computed using the

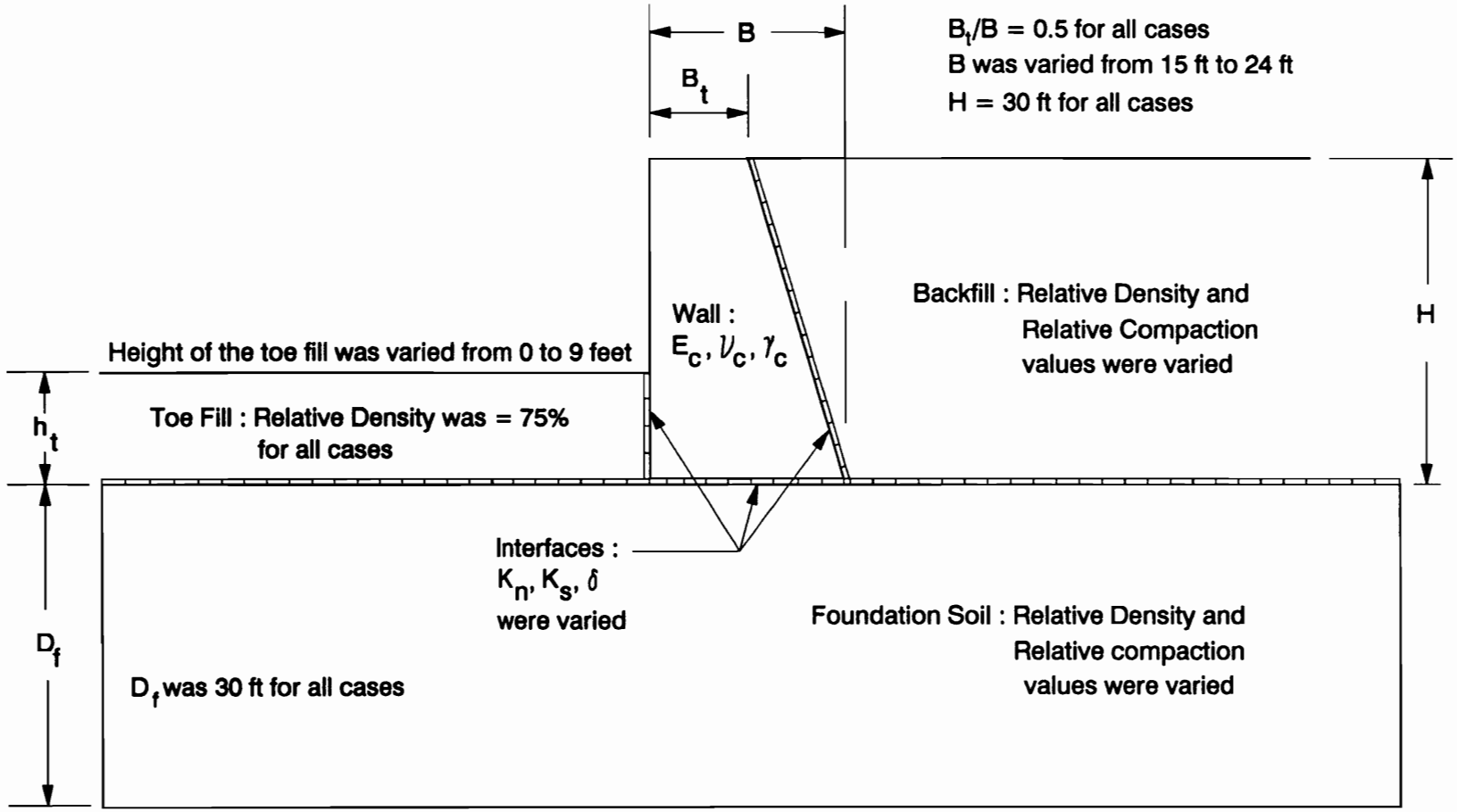

Figure 5.1 - Hypothetical Wall-Foundation System used for Backfill Placement Analyses Showing Parameters

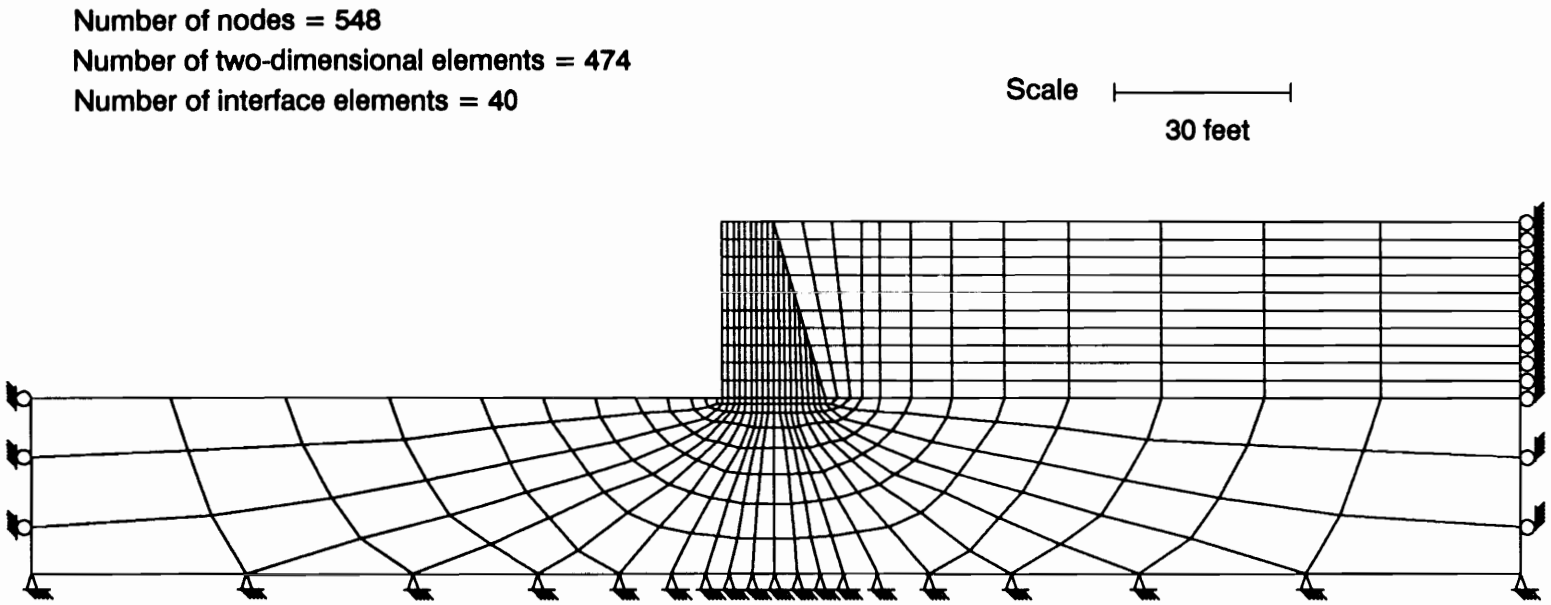

Figure 5.2 - Finite Element Mesh for the Base Case Wall-Foundation System - Backfill Placement Analyses

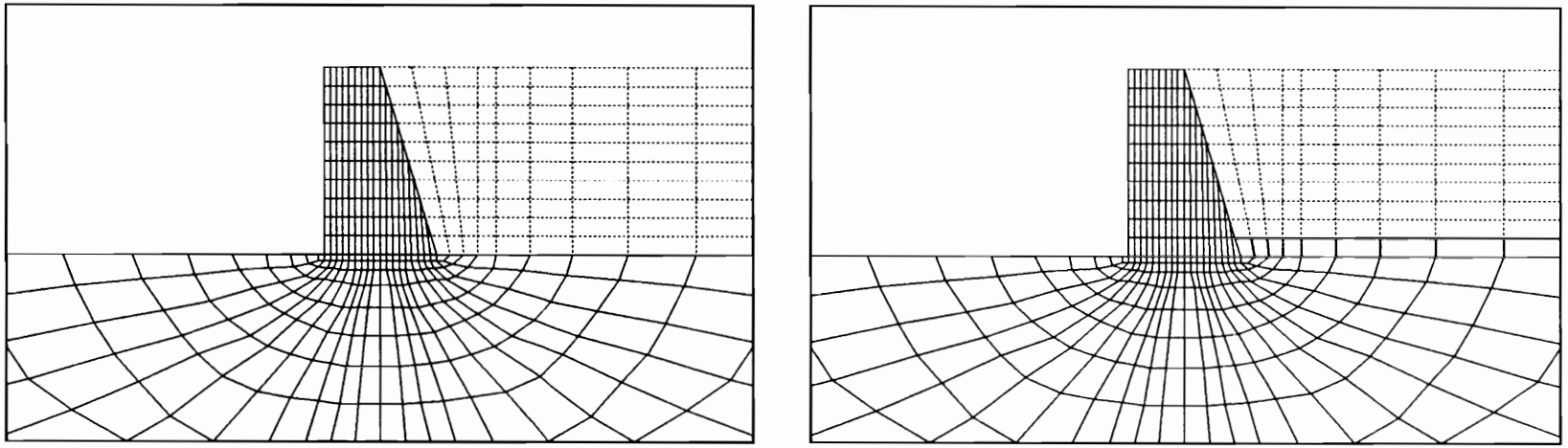

(a) Mesh prior to backfilling - air element boundaries shown as dotted lines

(b) Mesh after placement of first lift

Figure 5.3 - Transformation of Air Elements to Soil to Simulate Backfilling

hyperbolic stress-strain model.

PARAMETER STUDIES USING THE BACKFILL PLACEMENT METHOD

The material and geometric parameters shown in Fig. 5.1 were varied systematically in the backfill placement analyses. The parameters that were varied are the following :

(1) The shear stiffness of the interface elements at the base of the wall

(2) The relative density of the foundation soil (for a cohesionless foundation soil)

(3) The relative compaction and compaction water content of the foundation soil (for a cohesive foundation soil)

(4) The relative compaction and water content of the backfill (for a cohesive backfill)

(5) The relative density of the backfill (for a cohesionless backfill)

(6) The presence/absence of a toe fill

(7) The base-to-height ratio of the wall

The ranges of values used for these parameters are listed in Table 5.1.

Using the results of the finite element analyses, the following aspects of the retaining wall behavior were evaluated :

(1) The extent of the zones of failure within the foundation and backfill

(2) The horizontal displacement of the top of the wall

(3) The stress resultants on key planes along the wall surface and within

Table 5.1 - Parameter Values used in the Backfill Placement Analyses

Constant Parameters

Geometric

- $H = D_f = 30$ ft
- B_t/B = Ratio of width of top of wall to width of base of wall = 0.5

Material

- K_n = Normal stiffness of wall-base interface elements = 5.18×10^9 pcf
- γ_c = Unit weight of concrete = 150 pcf
- E_c = Modulus of elasticity of concrete = 4.3×10^8 pcf
- ν_c = Poisson's ratio of concrete = 0.20

Variable Parameters

Geometric

- B = Base width of wall
- h_t = Height of toe fill

Material

- K_s = Shear stiffness of wall-base interface elements elements
- D_r = Relative density for cohesionless backfill/ foundation soils
- RC, w% = Relative Compaction and Water content for cohesive backfill/foundation soils

Run No.	Base Int. El. K_s (pcf)	Fd'n D_r	Backfill D_r	Fd'n RC	Backfill RC	B (ft)	h_t (ft)	Comments
BFBC	1.64×10^5	75	75	-	-	18	0	Base Case
BF1A	(1.10×10^5)	75	75	-	-	18	0	Low K_s
BF1B	(2.20×10^5)	75	75	-	-	18	0	High K_s
BF2A	1.50×10^5	(50)	75	-	-	18	0	Medium Dense Sand Foundation
BF2B	1.80×10^5	(100)	75	-	-	18	0	Very Dense Sand Foundation
BF2C	1.64×10^5	75	75	-	-	18	0	Water Table at ground level
BF3A	1.64×10^5	75	(25)	-	-	18	0	Loose Sand Backfill
BF3B	1.64×10^5	75	(50)	-	-	18	0	Medium Dense Sand Backfill
BF3C	1.64×10^5	75	(100)	-	-	18	0	Very Dense Sand Backfill
BF3D	1.64×10^5	75	75	-	-	18	(9)	With Toe Fill
BF4A	1.64×10^5	75	75	-	-	(15)	0	B/H = 0.5
BF4B	1.64×10^5	75	75	-	-	(21)	0	B/H = 0.7
BF4C	1.64×10^5	75	75	-	-	(24)	0	B/H = 0.8
BF5A	1.42×10^5	-	75	(100)	-	18	0	SM-SC Foundation, 2% dry of opt.
BF5B	1.42×10^5	-	75	(95)	-	18	0	SM-SC Foundation, 2% wet of opt.
BF5C	1.54×10^5	-	75	(100)	-	18	0	CL Foundation, 2% dry of opt.
BF5D	1.30×10^5	-	75	(95)	-	18	0	CL Foundation, 1% wet of opt.
BF6A	1.64×10^5	75	-	-	(100)	18	0	SM-SC Backfill, 2% dry of opt.
BF6B	1.64×10^5	75	-	-	(95)	18	0	SM-SC Backfill, 2% wet of opt.
BF6C	1.64×10^5	75	-	-	(100)	18	0	CL Backfill, 2% dry of opt.
BF6D	1.64×10^5	75	-	-	(95)	18	0	CL Backfill, 1% wet of opt.

Note : Values in ( ) indicate a value other than the base case value

Hyperbolic parameters/properties used for soils

USC Class.	RC	w (%)	D_r (%)	K	n	K_b	m	ϕ	K_o	γ_s (pcf)	R_f
SW, SP	-	-	100	600	0.4	175	0.2	42°	0.33	145	0.70
SW, SP	-	-	75	450	0.4	125	0.2	39°	0.37	140	0.70
SW, SP	-	-	50	300	0.4	75	0.2	36°	0.41	135	0.70
SW, SP	-	-	25	200	0.4	50	0.2	33°	0.46	130	0.70
SM-SC	100	2% dry of opt	-	700	0.4	300	0.2	33°	.46	130	0.80
SM-SC	95	2% wet of opt	-	150	0.8	100	0.8	33°	.46	125	0.65
CL	106	2% dry of opt	-	700	0.1	350	0.0	30°	.50	115	0.70
CL	102	1% wet of opt	-	150	0.5	200	0.0	30°	.50	110	0.60

the backfill

(4) The displacements of the ground surface

SIGNIFICANCE OF STRESS RESULTANTS ON "KEY" PLANES

Fig. 5.4 shows the "key" planes in the wall-foundation system where stress resultants are computed. Key planes located within the backfill are the following :

(1) A vertical plane passing through the heel of the wall. This is designated as plane A-A.

(2) A vertical plane close to the rightmost boundary of the mesh. This is designated as plane B-B.

Key planes along the surface of the wall are as follows :

(1) A plane through the wall-backfill interface. This is designated as plane C-C.

(2) A plane through the base of the wall. This is designated as plane D-D.

(3) If a toefill is present, a plane on the wall-toefill interface. This is designated as plane E-E.

A vertical plane within the toe fill designated as plane F-F is also defined when a toe fill is present. This key plane is located near the leftmost boundary of the mesh.

The stress resultants on these planes are resolved into normal and shear components.

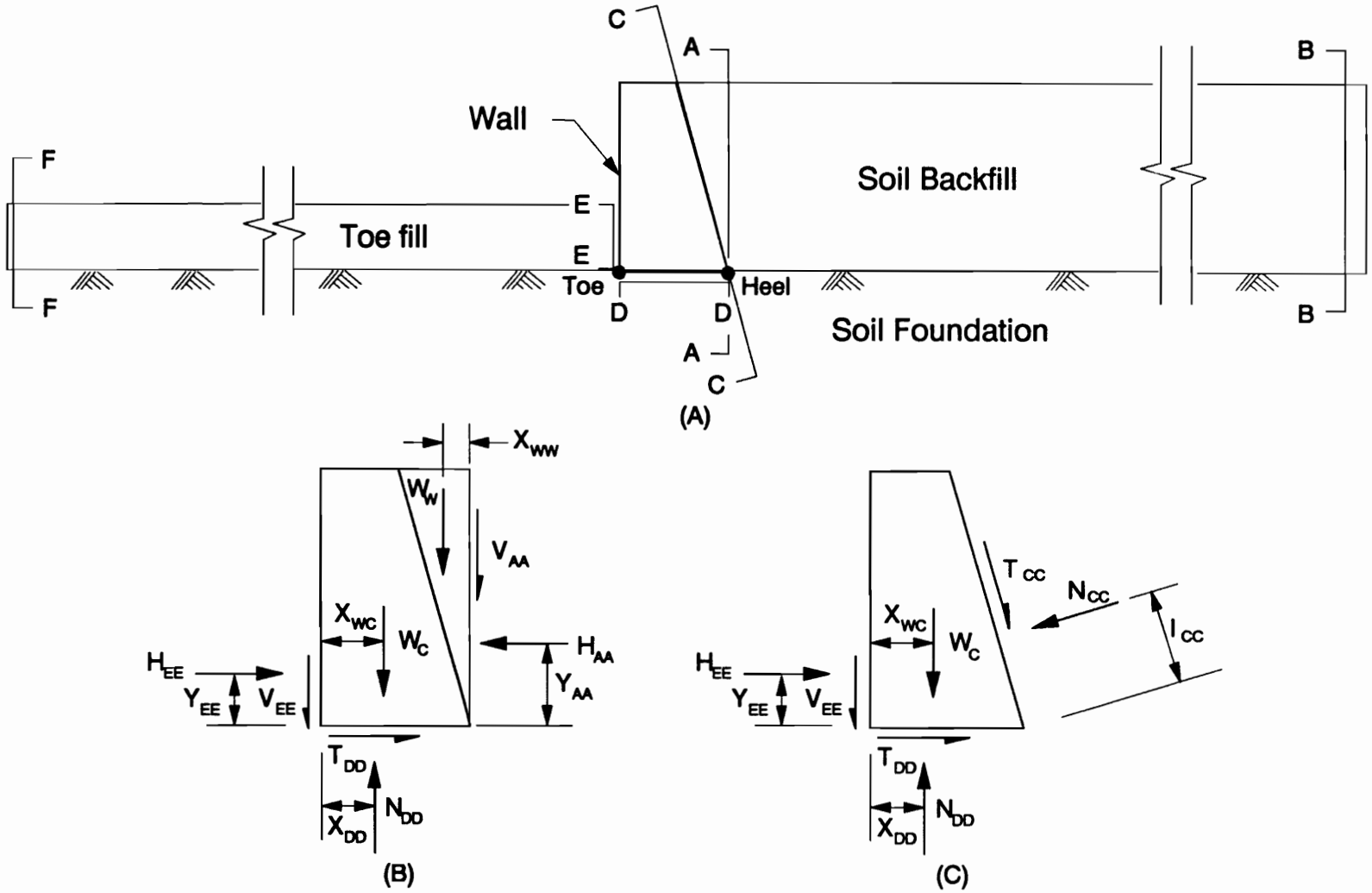

Figure 5.4 - Free Body Diagrams showing Resultant Forces on Planes along the Surfaces of the Wall and within the Backfill and Toe Fill

The labels used for these forces are summarized in Table 5.2.

The resultant forces on vertical planes within the backfill are used to calculate the values of the earth force coefficients K_v, K_h and the earth pressure index EPI. These coefficients have the following definitions :

$$K_v = F_v/(\tfrac{1}{2}/\gamma_s H^2) \tag{5.2}$$

$$K_h = F_h/(\tfrac{1}{2}/\gamma_s H^2) \tag{5.3}$$

$$EPI = \frac{K_o - K_h}{K_o - K_a} \tag{5.4}$$

where F_v is the normal (horizontal) force on the vertical plane and F_h is the shear (vertical) force on the vertical plane. These coefficients provide convenient measures of the magnitudes of the earth pressures calculated in the analyses.

K_v is the vertical shear stress coefficient defined by Ebeling et al. (1988). In conventional analyses of retaining walls, K_v is implicitly assumed to be equal to zero, since shear stresses within the backfill are neglected. However, Ebeling et al. (1988) found that when there is significant differential settlement within the backfill, these shear stresses should are appreciable. The vertical shear force on plane A-A is an important factor in the overall stability of the retaining wall.

K_h is the lateral earth pressure coefficient. The value of this coefficient can range from the at-rest value K_o, when there is no movement of the wall, to the active value K_a, when sufficient wall movement away from the backfill has occurred so as to mobilize the strength of the soil in the backfill.

The index EPI was defined by Ebeling et al. (1988) as an indicator of the extent to which wall movement affected the lateral earth pressure in the backfill. A value of EPI equal to zero (i.e., $K_h = K_o$) indicates that wall movement did not affect the lateral earth pressure.

Table 5.2 - Labels used to Characterize Forces on the Key Planes

Plane	A-A	B-B	C-C	D-D	E-E	F-F
Orientation & Location	Vertical Plane in backfill through heel of wall	Vertical Plane in backfill near right end of the mesh	Parallel and Coincident w/ wall-backfill Interface	Horizontal; Coincident with the wall base	Vertical; Coincides w/ wall-toe fill Interface	Vertical Plane in toe fill near left end of the mesh
Normal Force	H_{AA}	H_{BB}	N_{CC}	N_{DD}	H_{EE}	H_{FF}
Line of action of Normal Force	Y_{AA}	Y_{BB}	I_{CC}	X_{DD}	Y_{EE}	Y_{FF}
Shear Force	V_{AA}	V_{BB}	T_{CC}	T_{DD}	V_{EE}	V_{FF}

In the other extreme, an EPI value equal to 1.0 (i.e., $K_h = K_a$) is indicative of the condition where the effect of wall movement has reached its maximum. Intermediate values reflect the level of soil-structure interaction taking place in the vicinity of the plane where EPI is evaluated.

In their evaluation of EPI, Ebeling et al. (1988) used values of K_o obtained from a plane within the backfill where there is negligible horizontal movement, and stresses are therefore representative of at-rest conditions. In the key planes previously mentioned, planes B-B and F-F fit this category. Therefore, K_o was evaluated using the equation

$$K_o = H_{BB}/(\tfrac{1}{2}\gamma_s H^2) \tag{5.5}$$

for the backfill and

$$K_o = H_{FF}/(\tfrac{1}{2}\gamma_s H^2) \tag{5.6}$$

for the toe fill.

ANALYSES OF THE BASE CASE PROBLEM - COMPARISON OF FOLLOWING LOAD AND BACKFILL PLACEMENT ANALYSES

The results of backfill placement and following load analyses of the base case problem are presented and compared in this section. As mentioned previously, the major difference between the following load method and the backfill placement method is that the former does not account for soil-structure interaction effects in the backfilling process while the latter does.

While the geometry of the base case problem analyzed is the same for both methods, there are several differences between the manner in which the following load method was used to analyze the problem (Run FOL1A in Chapter 2) and the backfill placement analysis of the same problem (Run BFBC in this chapter). These differences are :

(1) A different version of the program SOILSTRUCT was used in Run FOL1A. The version used for Run BFBC contains the bulk modulus formulation and modifications of the modulus calculation routines discussed previously.

(2) The lift thicknesses used during the backfilling process are not the same for the two analyses because of differences in mesh design.

(3) A more conservative backfill unit weight of 140 pcf. was used in the backfill placement analysis, compared to 135 pcf used in the following load analysis.

While these inconsistencies may be of minor importance, eliminating them may yield a more meaningful comparison of the two methods of analyses. For this reason, a new following load analysis was performed utilizing the same version of SOILSTRUCT that was used in the backfill placement analyses. The mesh used for this analysis is the same as the mesh shown in Fig. 5.2, without the backfill elements. The nodal forces used to represent the backfill were calculated based on a backfill unit weight of 140 pcf.

The ground surface profiles calculated in the following load and the backfill placement analyses analyses are shown in Fig. 5.5. The two profiles are basically the same beyond the boundaries of the wall base. However, it is evident that with the following load analysis, the wall has a greater tendency to tilt than in the backfill placement analysis.

The backfill placement analysis resulted in less severe failure regions within the foundation, as shown in Fig. 5.6. This may be attributed to, among other things, the reduced tendency of the wall to tilt and separate from the foundation, resulting in greater confining pressures for the soil elements, especially in the vicinity of the heel. The average stress levels for

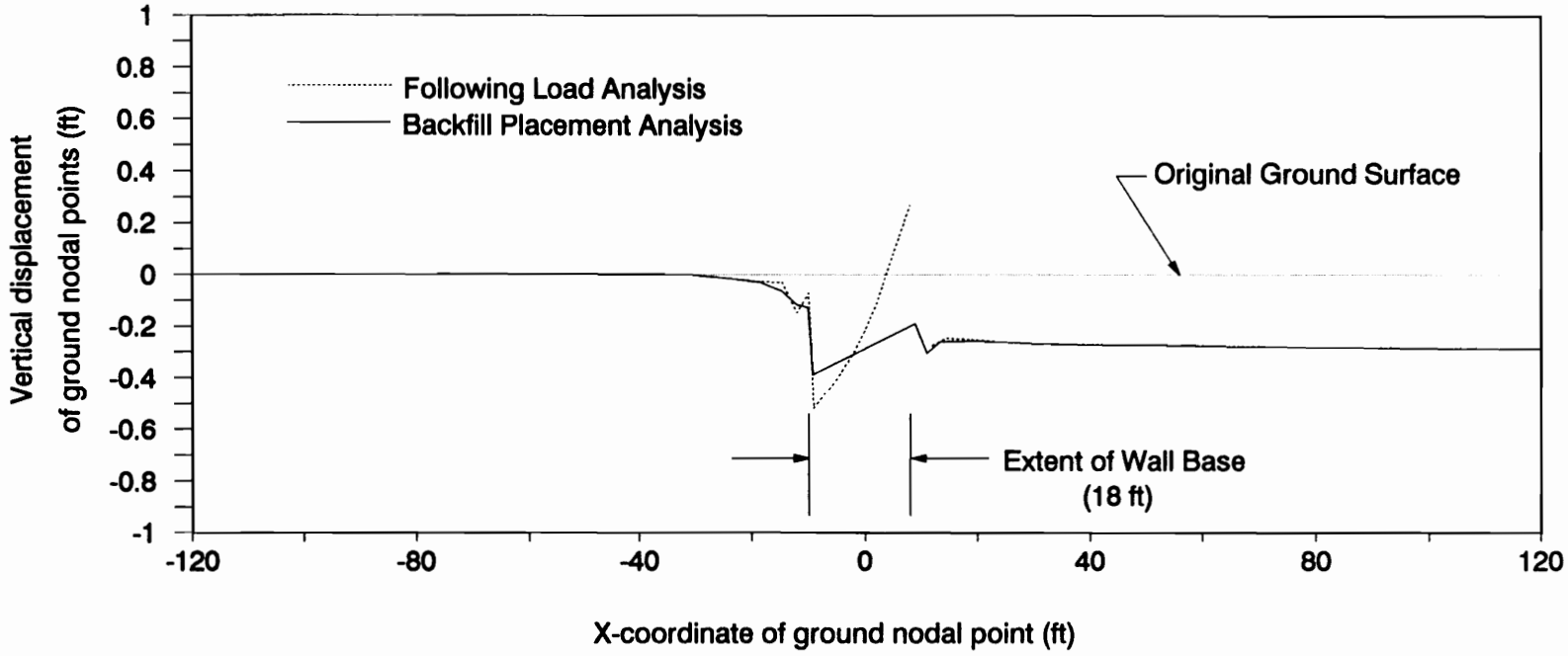

Figure 5.5 - Ground Surface Profiles After Backfilling for Following Load and Backfill Placement Analyses

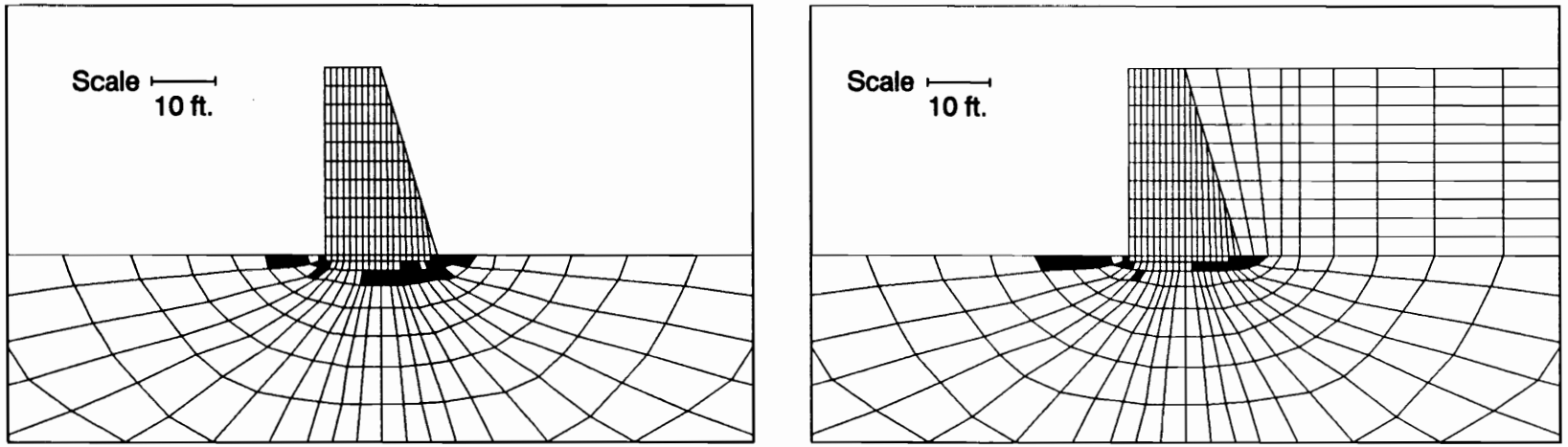

(a) Failure Regions - Following Load Analysis

(b) Failure Regions - Backfill Placement Analysis

Figure 5.6 - Failure Regions within the Foundation - Following Load and Backfill Placement Analyses

the failed elements within the foundation were 1.17 for the backfill placement analysis and 1.20 for the following load analysis. These low average values indicate the effectiveness of the Alpha Method in controlling overshoot in two-dimensional soil elements.

Figure 5.7 shows how the lateral earth force on the wall, H_{AA}, varied with the normalized wall displacement, Δ/H, for the two analyses. It can be seen that the results are very similar. In the early stages of loading, the wall tilts back in both cases. In the latter stages it tilts forward. The maximum earth load in the backfill placement analysis was smaller than the maximum used in the following load analysis, which was based on at-rest pressures.

Table 5.3 summarizes the characteristics of the forces on the key planes and their related indices. On plane A-A, the lateral earth pressure coefficient, $K_h{}^{AA}$, obtained from Run BFBC is equal to 0.27, and the earth pressure index, EPI, is equal to 0.70, indicating a significant level of soil-structure interaction.

The value of the vertical shear force coefficient $K_v{}^{AA}$ obtained from Run BFBC is equal to 0.07. In his analyses of walls on rock, Ebeling (1988) found that K_v for similarly located planes was about 0.14. These results are consistent with the manner in which the wall moves in relation to the backfill. On a rock foundation there is very little, if any, settlement of the wall. The tendency therefore is for a wall on rock to rotate about its toe. This rotation increases the relative vertical displacement and shear forces between the backfill and the wall. When the wall is on a relatively soft foundation, as in the cases analyzed in this study, the relative vertical displacement is smaller. A gravity wall on a relatively soft foundation tends to settle along with the backfill and rotation about its toe is less pronounced than for a wall founded on rock.

Referring again to Table 5.3, the $K_h{}^{BB}$ and $K_v{}^{BB}$ values obtained from the backfill placement analysis clearly indicate that the earth pressures correspond to at-rest conditions at this location in the backfill. K_h is equal to the K_o value according to Jaky's formula, while K_v

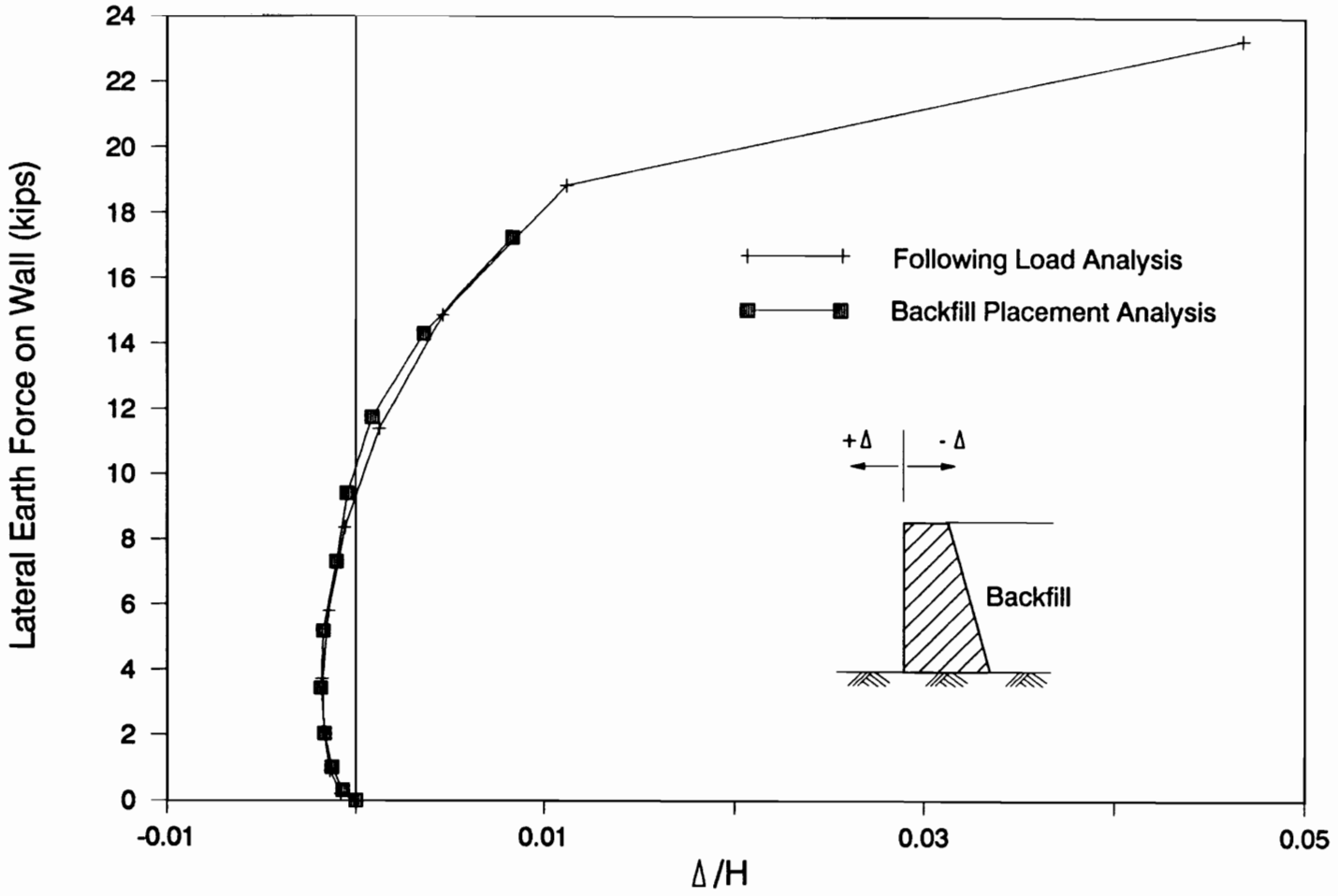

Figure 5.7 - Variation of Normalized Wall Displacements with the Lateral Earth Force on the wall - Following Load and Backfill Placement Analyses

Table 5.3 - Comparison of Forces on Key Planes for the Following Load and Backfill Placement Analyses of the Base Case Problem

Note : All forces in pounds, all lengths are in feet

Run No.	Following Load	BFBC B'fill Placement
Plane A-A		
H_{AA}	23,310	17,270
V_{AA}	-	4,190
Y_{AA}	10.00	10.97
K_h	0.37	0.27
K_v	-	0.07
Plane B-B		
H_{BB}	-	23,450
V_{BB}	-	70
Y_{BB}	-	10.03
K_h	-	0.37
K_v	-	0.00
Plane D-D		
N_{DD}	79,650	82,190
T_{DD}	23,310	17,270
X_{DD}	6.0	6.7
X_{DD}/ B	0.33	0.37
δ_{mob} / $\phi_{foundation}$	0.42	0.30

is equal to zero.

Some soil elements within the backfill failed during backfill placement, as shown in Fig. 5.8. The figure shows that Plane A-A intersected these failed elements. Fig. 5.9 shows the distribution of normal and shear stresses on plane A-A. Redistribution of stresses occurred as a result of the failure of some of the soil elements, and the larger stresses occur in the stronger, unfailed elements. However, in spite of the erratic distribution of the normal stresses, the position of the line of action of the resultant normal force (Y_{AA}) is equal to $0.37*H$, which is close to that for a triangular stress distribution ($0.33*H$). Also shown on Fig. 5.9 are the normal and shear stresses for plane B-B at the far end of the backfill. The nearly triangular normal stress and near-zero shear stress distributions on this plane are manifestations of the lack of soil-structure interaction effects in locations sufficiently far from the wall.

A comparison of the base forces in Table 5.3 show that the base normal force obtained using the backfill placement method is about 4 percent larger than its counterpart obtained using the following load method. The difference is due to the "downdrag" effect of the settling backfill on the wall which is accounted for in the backfill placement method. Fig. 5.10 shows the distribution of stresses along the base of the wall. In Fig. 5.10(a) it can be seen that the maximum normal stress is higher using the following load approach. This higher maximum normal stress indicates that a greater degree of stress redistribution is obtained using this method. This difference in stress redistribution between the two methods is also apparent in the base shear stress distributions shown in Fig. 5.10(b). The backfill placement analysis tends to yield a smoother, more even shear stress distribution.

Table 5.3 also lists the effective base width, B_e/B, as 92 percent for the following load method and 95 percent for the backfill placement method.

The main conclusion that can be drawn from these analyses is that the use of the following load method or the equivalent hand calculation approach discussed in Chapter 3 yields

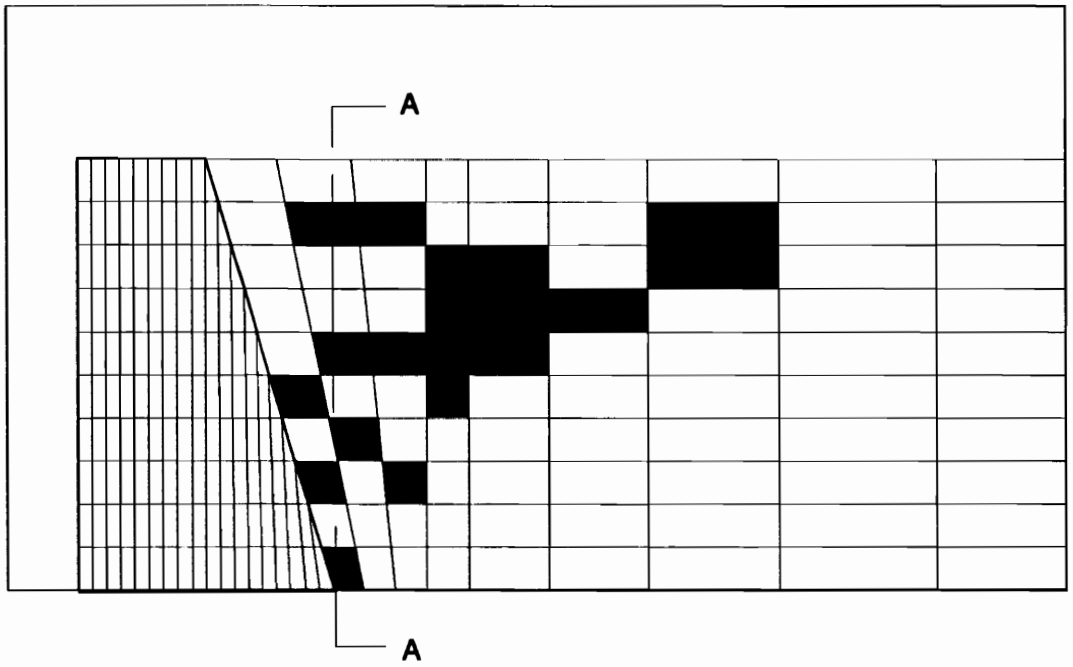

Figure 5.8 - Failure Regions within the Backfill for the Base Case Problem

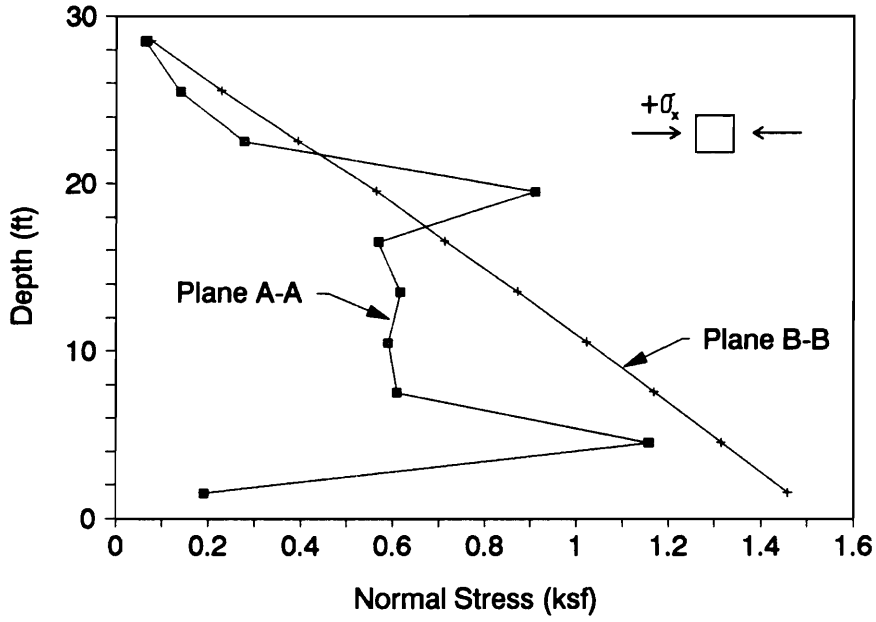

(a)

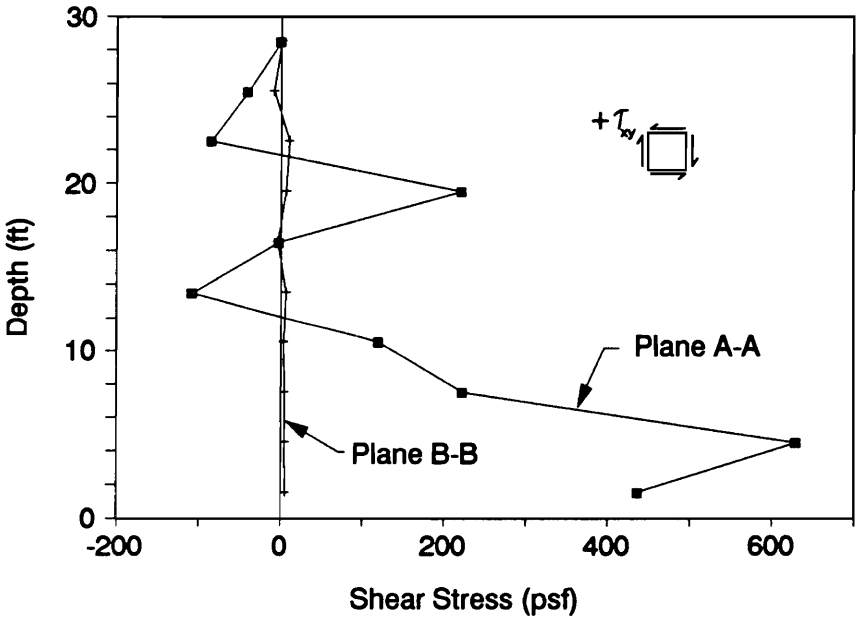

(b)

Figure 5.9 - Variation of Normal and Shear Stresses on the Vertical Planes A-A and B-B

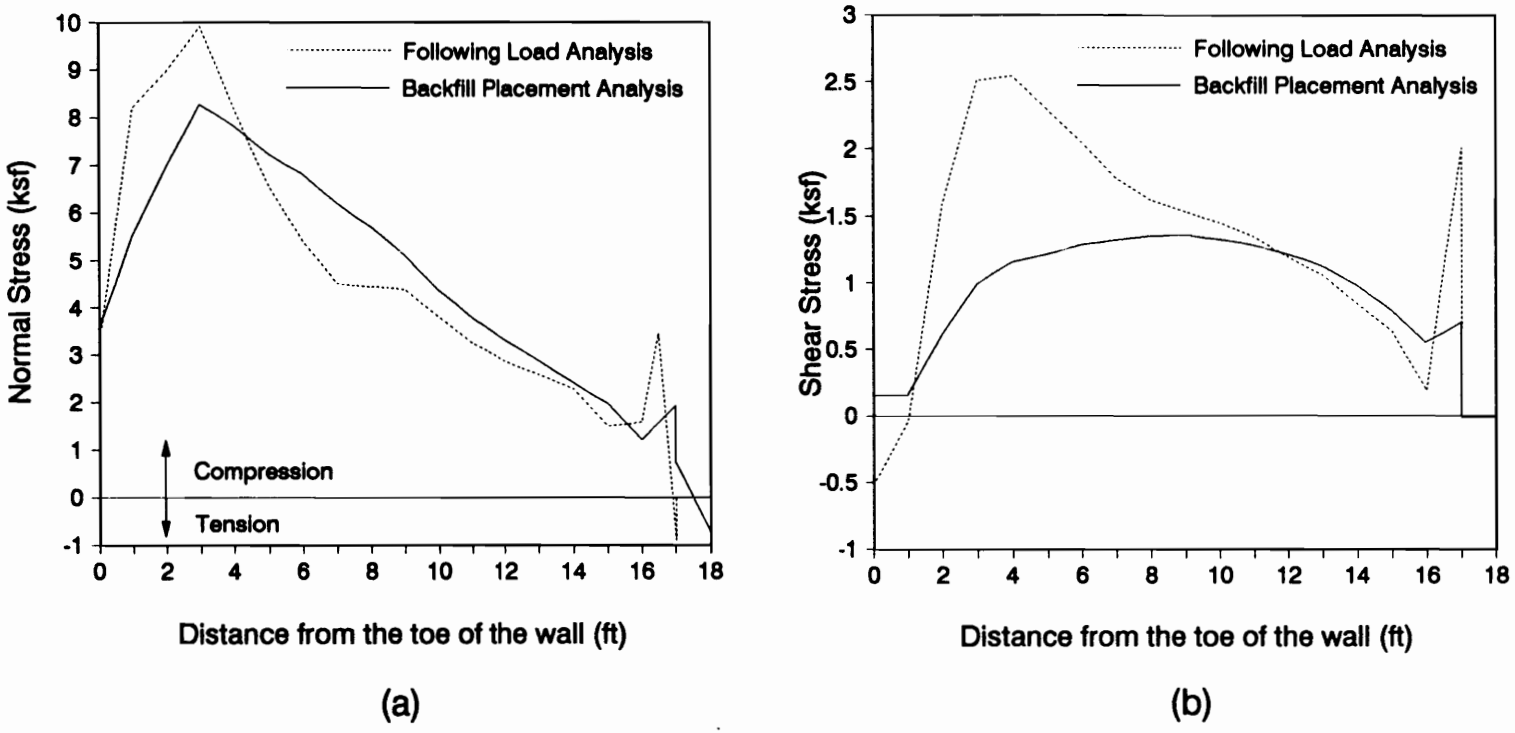

Figure 5.10 - Base Stresses After Backfilling for Following Load and Backfill Placement Analyses

conservative results. The retaining wall is more stable than the following load method would indicate. The use of the backfill placement method for walls on soil resulted in smaller displacements, less extensive failure regions and reconfirmed the presence of stabilizing shear loads on the back of the wall due to soil-structure interaction.

INVESTIGATION OF A MODIFIED ALPHA METHOD FOR 2D ELEMENTS

The idea behind the Alpha Method for 2D elements discussed in Chapter 2 is to systematically apply reduced loads on the system such that the amount of overshoot in the soil elements is minimized. The worst stressed soil element in the mesh determine the appropriate value of the load reduction factor α which, when applied to the load, ensures that failure takes place only in this worst stressed element. The procedure for determining α is illustrated in Fig. 2.9. The value of α is such that the Mohr's circle for the worst stressed element is tangent to the Mohr-Coulomb failure envelope. While this method greatly improved the control of overshoot, results indicated that an average of 10 to 20 percent overshoot could still occur in failed soil elements. These results led to the idea that the Alpha Method could be improved further.

A modified Alpha Method that was investigated is based on the idea of computing the factor α based on reduced values of the soil strength parameters C and Φ. As shown on Fig. 5.11(A), the $C-\Phi$ envelope is the basis for determining the stress level of a soil element. For the purpose of determining the values of α for load apportionment, however, factored values of the soil strength parameters are used, as shown in Fig. 5.11(B). The reduction factor for the strength parameters is labeled λ. The idea is to obtain a smaller value of α such that the load on the worst stressed soil element will bring it close to a failure state, that is, a value of stress

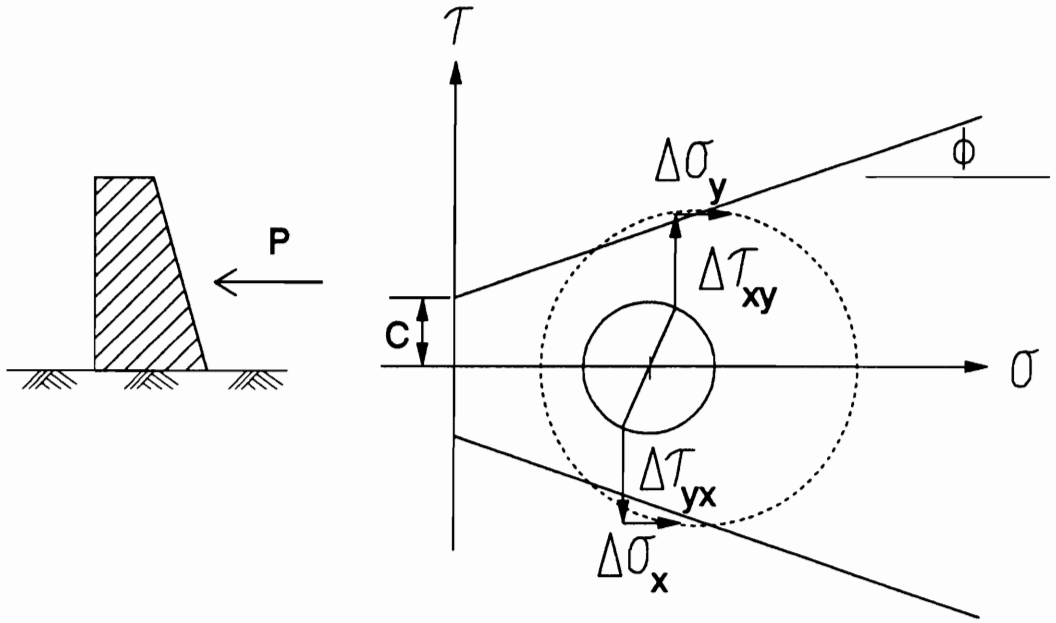

(a) Application of Full load and Corresponding Stress Component Increases in a Soil Element

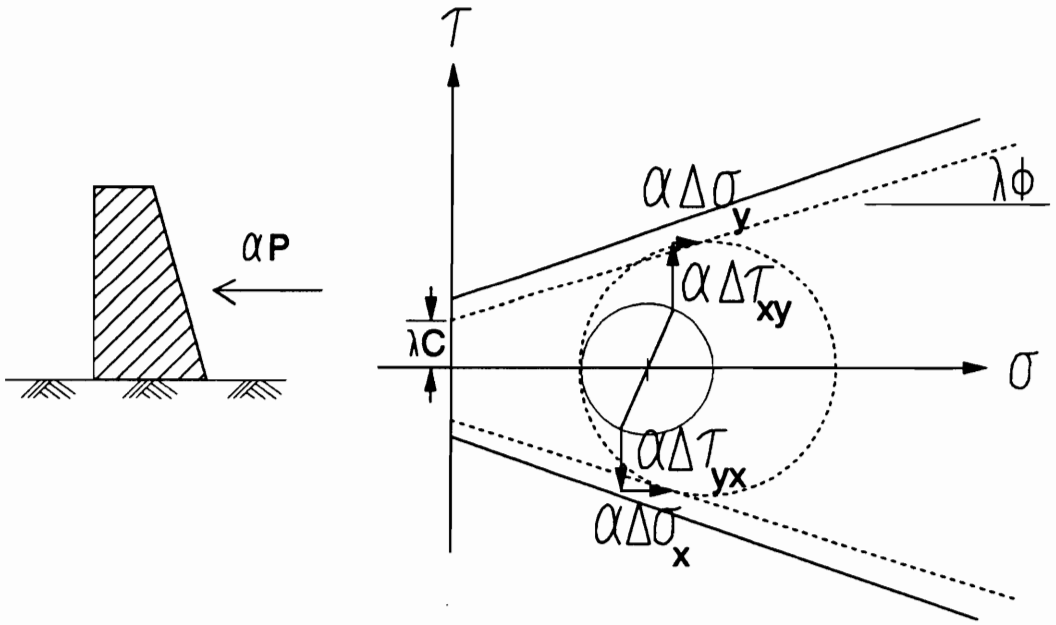

(b) Factored Load and Corresponding Stress Component Increases in a Soil Element

Figure 5.11 - Calculation of Alpha based on Factored Soil Strength Parameters

level (based on unfactored values of C and Φ) less than but close to unity. Note that for λ equal to 1.00, the procedure becomes the original α-method.

The base case problem was analyzed using the modified α-method, with λ equal to 0.95. Table 5.4 shows some results of this run, along with those obtained from the analysis using the original Alpha Method (λ equal to 1.00). It can be seen that the use of λ=0.95 decreased the number of failed elements only by a small number. The standard deviation of the SL values (s_{SL}) indicate a reduction in the scatter for λ=0.95. There is, however, no improvement in the mean value of the stress levels ($\overline{x}_{SL}$). A major difference between the two analyses is the runtime. For λ=1.00, the runtime was only three (3) minutes while for λ=0.95, the runtime was 115 minutes. Considering the enormous time requirements and the resulting slight improvement in the control of overshoot, the use of a value of λ less than 1.00 is not practical.

EFFECTS OF VARYING THE SHEAR STIFFNESS OF THE BASE INTERFACE ELEMENTS

The stress-displacement model that characterized the behavior in shear of the interface elements described in Chapter 4 is essentially the same model utilized by the version of SOILSTRUCT for the analyses described in this chapter. This updated version of SOILSTRUCT includes the stress-state concept developed by Filz, et al. (1990) for use in modeling interface element unload-reload behavior.

In the analyses described in this section, the shear stiffness of the base interface elements, K_s, was varied while the values of all other material, geometric and loading parameters were unchanged. The objective was to determine the effects of varying degrees of concrete-foundation interface roughness. For this purpose, three values of K_s were used to model rough (maximum

Table 5.4 - Some Results of Analyses of the Base Case Problem using the Original and the Modified Alpha Method for 2D Elements

λ	No. of failed elements excluding those in tension	x_{SL} for failed elements	s_{SL} for failed elements	No. of elements in tension	Maximum SL for "strong"* elements
1.00	41	1.14	0.31	2	2.05
0.95	38	1.14	0.22	1	1.79

* - The definition of "strong" elements is given in Chapter 2

K_s value), intermediate (base case K_s value) and smooth (minimum K_s value) interface conditions. It should be pointed out that in later analyses, the value of K_s also changes when the type of foundation soil changes.

Figures 5.12 to 5.14 compare various results from the analyses of the three cases. The following observations can be made :

(1) In Fig. 5.12, which shows the failure regions at the end of backfilling, there appears to be no significant differences between the failure regions within the foundation and backfill for the three cases.

(2) The ground surface profiles for the three cases, shown in Fig. 5.13, are practically the same.

(3) The base stresses shown in Fig. 5.14 are quite close, with all three cases yielding an effective base width, B_e/B, equal to 95 percent.

The variation of lateral earth force with wall displacement during backfilling for the three cases are shown in Fig. 5.15. At the end of backfilling, Δ/H values are, for practical purposes, all essentially equal to 0.008 for the minimum, intermediate, and maximum K_s values.

Table 5.5 summarizes the forces on the key planes resulting from the three analyses. On plane A-A, $K_h{}^{AA}$ varied only slightly from 0.26 to 0.27. The EPI values ranged from 70 to 77 percent, indicating similar behavior for all three cases. The vertical shear force coefficient $K_v{}^{AA}$ varied slightly from 0.05 to 0.07. Similar small variations can be observed in the results for the rest of the key planes.

With these results, it may be concluded that with all other parameters unchanged, the assumption of whether the concrete-foundation interface is smooth or rough does not significantly affect the results.

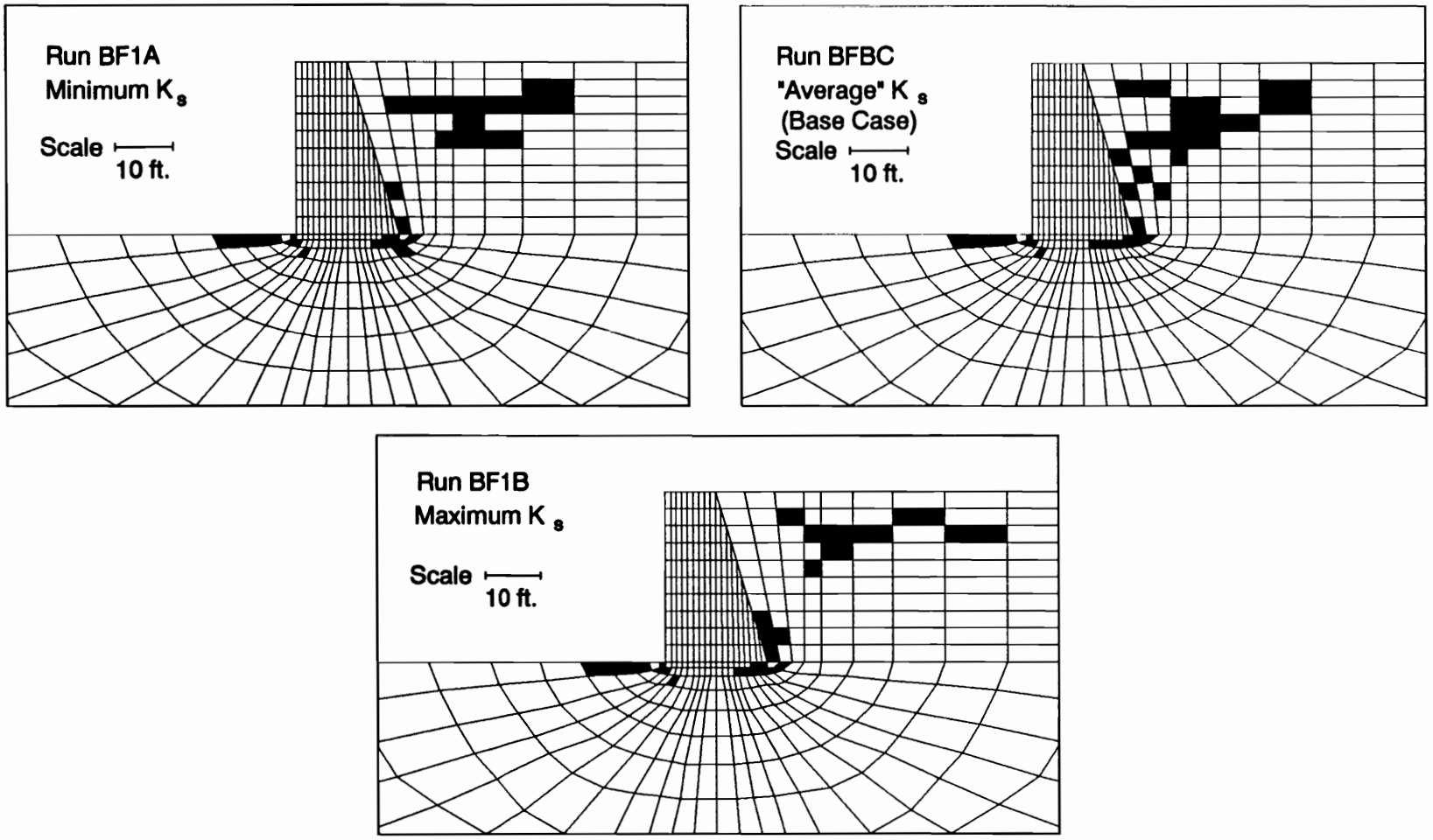

Figure 5.12 - Failure Regions within the Foundation and Backfill - different Base Interface Shear Stiffnesses

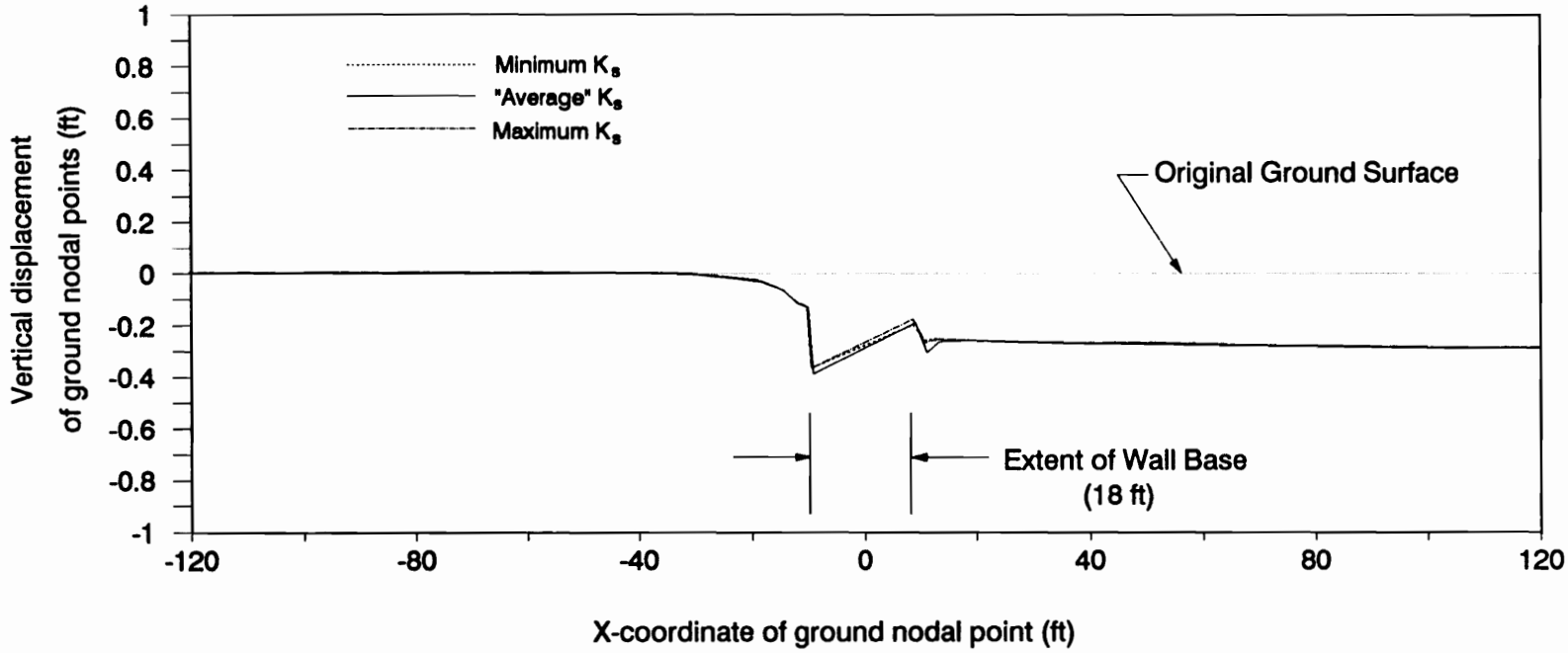

Figure 5.13 - Ground Surface Profiles after Backfilling for different Base Interface Shear Stiffnesses

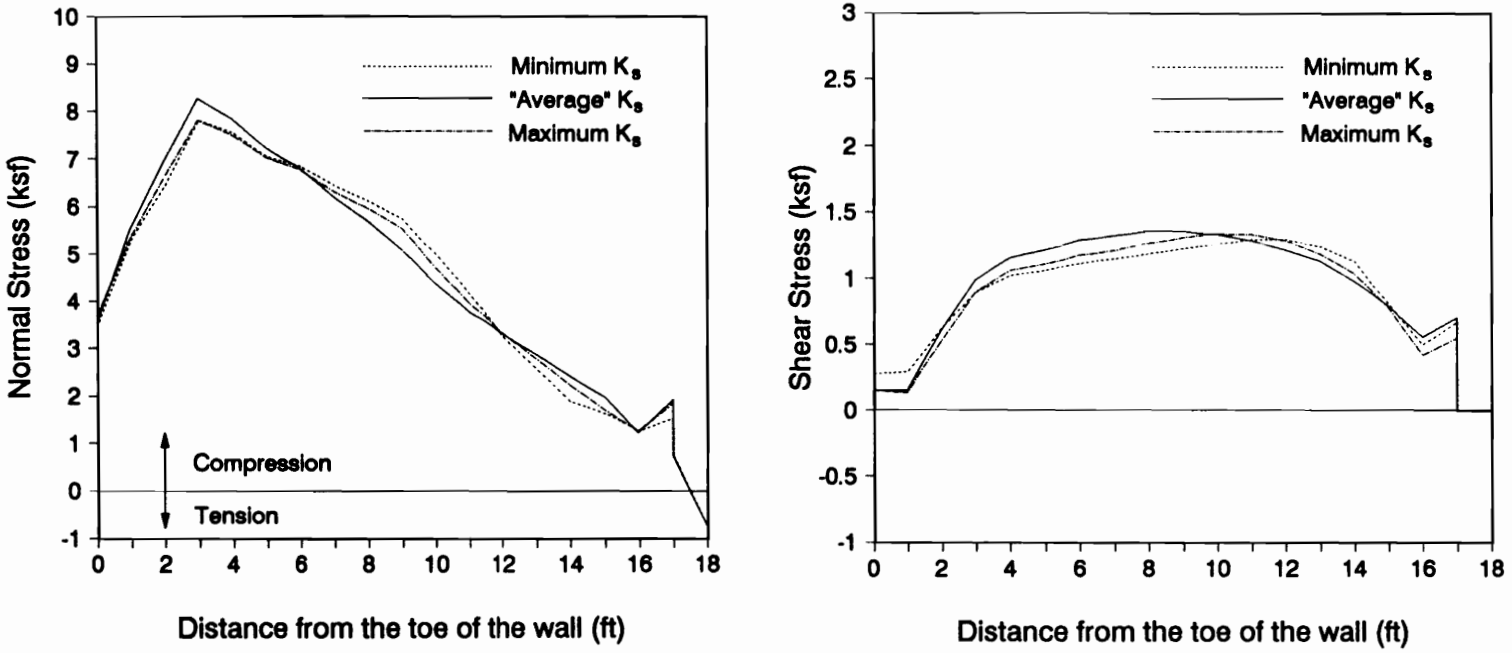

Figure 5.14 - Base Stresses After Backfilling for Different Base Interface Shear Stiffnesses

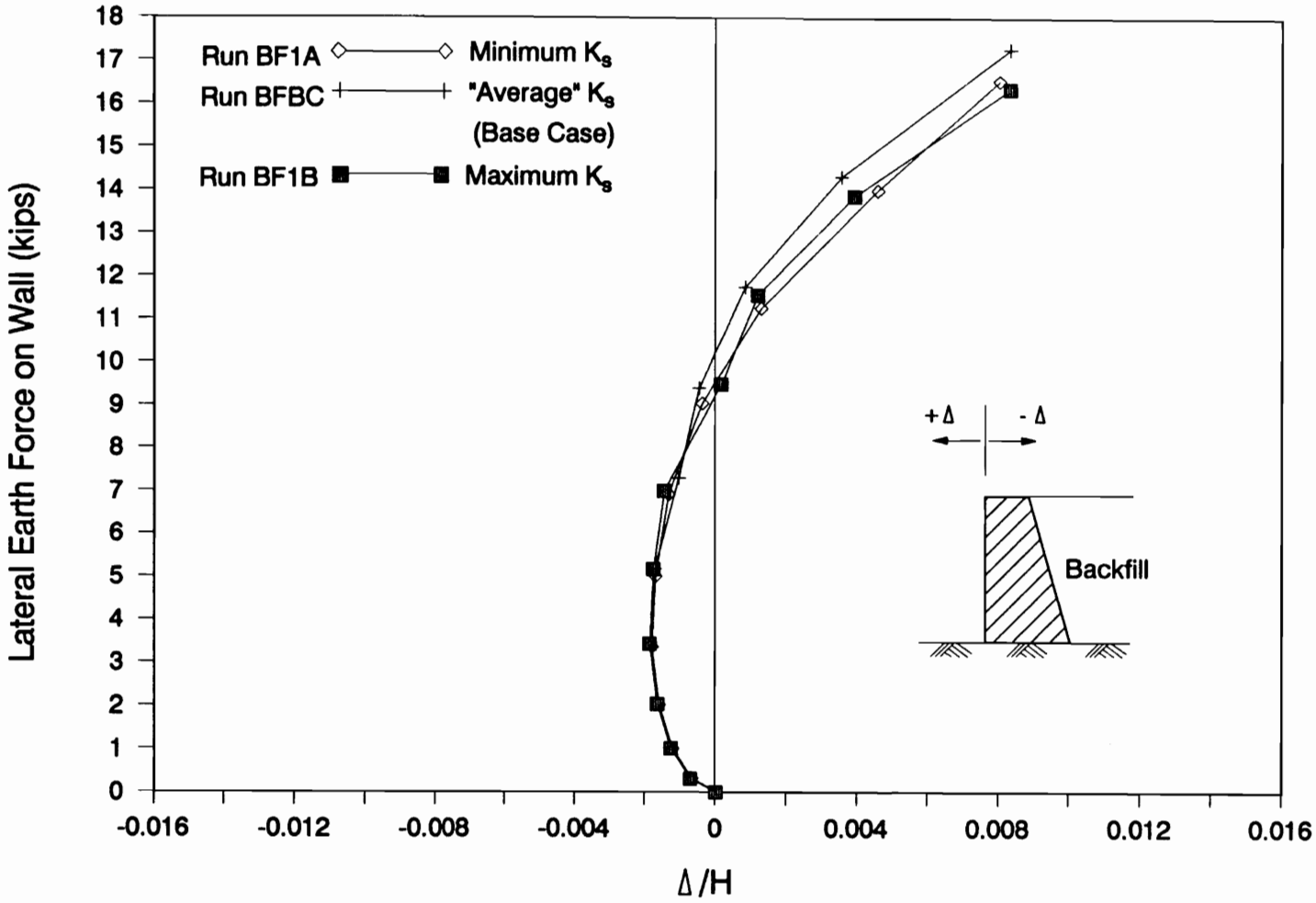

Figure 5.15 - Variation of Normalized Wall Displacements with the Lateral Earth Force on the wall - Different Base Interface Shear Stiffnesses

Table 5.5 - Forces on Key Planes for various Base Interface Shear Stiffnesses

Note : All forces in pounds, all lengths are in feet

Run No.	BF1A (Min. K_s)	BFBC (Ave. K_s)	BF1B (Max. K_s)
Plane A-A			
H_{AA}	16,530	17,270	16,240
V_{AA}	3,485	4,190	3,280
Y_{AA}	10.67	10.97	10.79
K_h	0.26	0.27	0.26
K_v	0.06	0.07	0.05
EPI	0.77	0.70	0.77
Plane B-B			
H_{BB}	23,390	23,450	23,390
V_{BB}	66	70	72
Y_{BB}	10.07	10.03	10.07
K_h	0.37	0.37	0.37
K_v	0.00	0.00	0.00
Plane C-C			
N_{CC}	21,830	22,700	21,685
T_{CC}	15,220	15,580	15,315
l_{CC}	11.6	11.6	11.6
l_{CC}/l	0.37	0.37	0.37
$\delta_{mob} / \phi_{backfill}$	0.90	0.88	0.90
Plane D-D			
N_{DD}	81,600	82,190	81,650
T_{DD}	16,530	17,270	16,370
X_{DD}	6.7	6.7	6.7
X_{DD}/B	0.37	0.37	0.37
$\delta_{mob} / \phi_{foundation}$	0.30	0.30	0.29

EFFECTS OF VARYING THE RELATIVE DENSITY OF THE FOUNDATION SOIL

To determine the effects of the density of the foundation soil on the behavior of the system, the foundation was assigned strength and stiffness parameters corresponding to relative densities of 50, 75 (the base case value) and 100 percent. These cases were designated as Runs BF2A, BFBC and BF2B, respectively. The strength and stiffness properties used in each case are given in Table 5.1.

The failure regions obtained from the three analyses are shown in Fig. 5.16. This figure clearly shows the high degree of instability of the wall when the foundation soil has a relative density equal to 50 percent.

Fig. 5.17 shows the development of the lateral force on the wall (H_{AA}) and the corresponding displacement of the crest of the wall (Δ/H) during backfilling. At the end of the backfilling process, Run BF2B (D_r equals 100 percent) yielded a Δ/H value equal to 0.003 while Run BFBC (D_r equals 75 percent) yielded a value of 0.011. In the case of Run BF2A (D_r equals 50 percent), large wall displacements occurred during the tenth and final layer of backfill, reaching a value of 2.8 at the crest feet upon application of the full backfill load.

The conditions at the end backfilling obtained from the analysis involving a foundation soil with 50 percent relative density are unacceptable from a design standpoint and should be considered a failure state for practical purposes. Large areas of soil failure occurred in both the foundation and the backfill, and the results could reflect numerical inaccuracies as a result.

Fig. 5.18 show how the ground surface displaced vertically for D_r equal to 75 and 100 percent. With increasing stiffness, the both the ground settlement and the wall tilt became less severe. Because of extensive soil element failure near the surface, the displacements obtained in

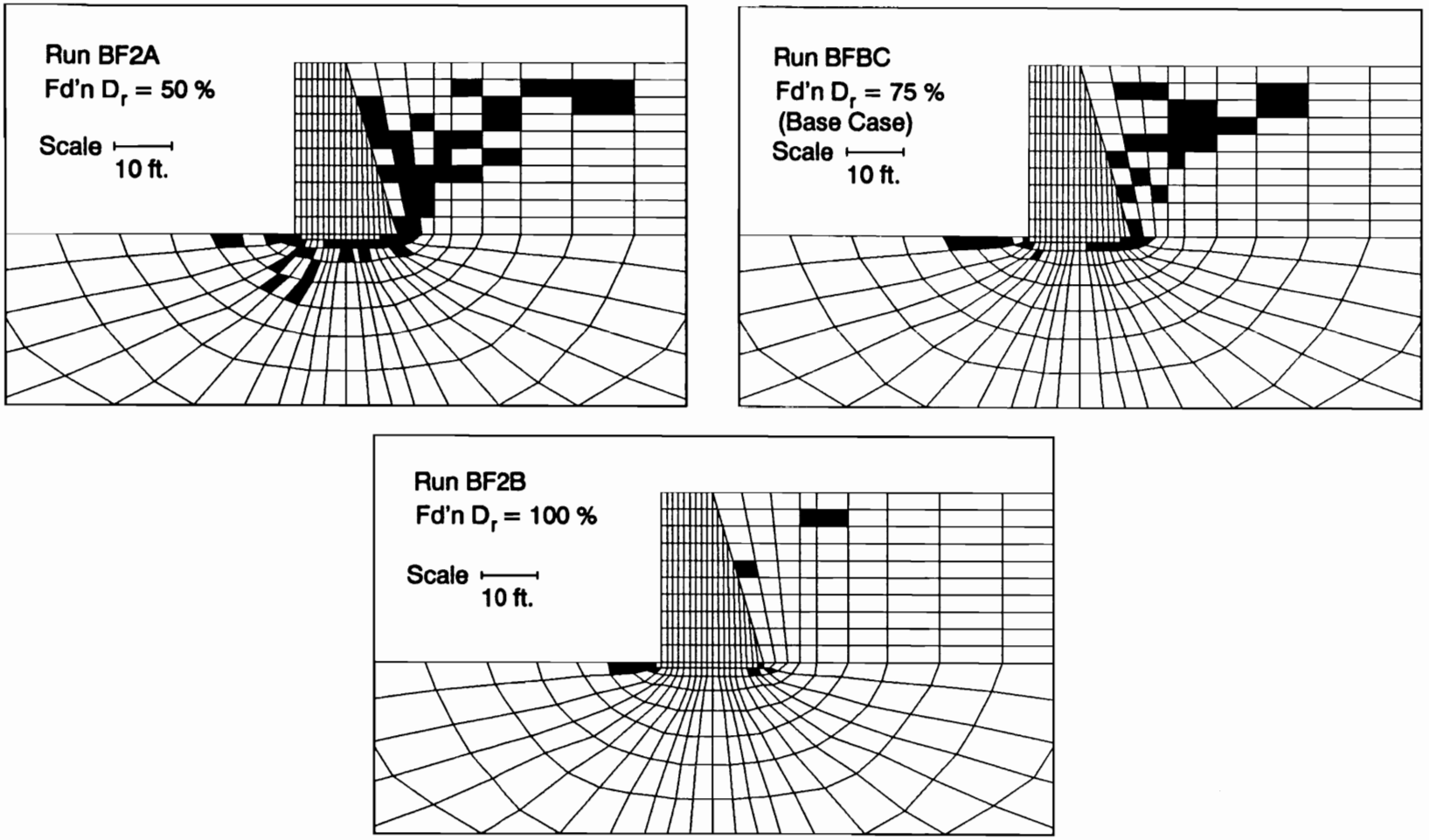

Figure 5.16 - Failure Regions within the Foundation and Backfill - different Foundation Relative Densities (Cohesionless Foundation Soil)

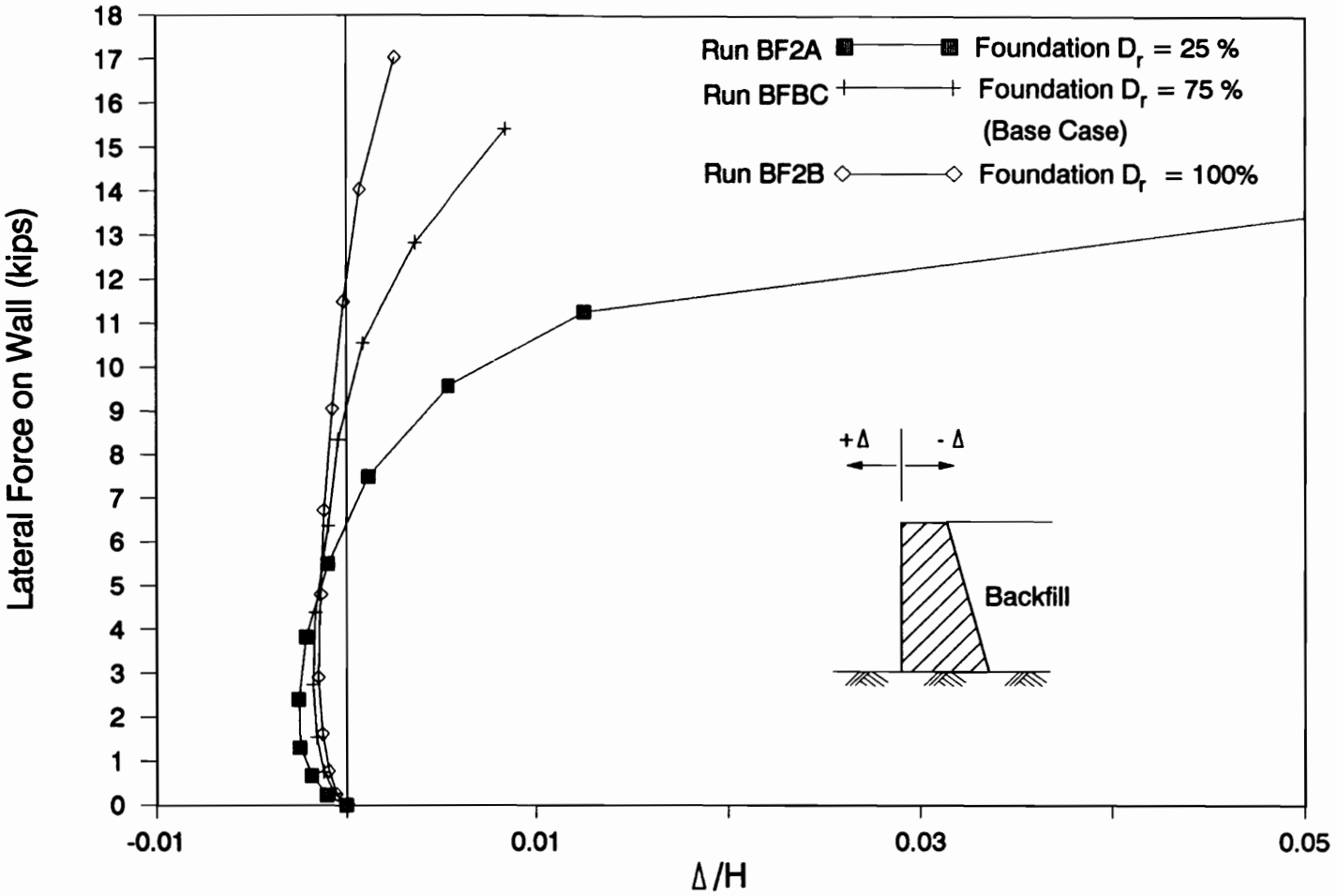

Figure 5.17 - Variation of Normalized Wall Displacements with the Lateral Earth Force on the wall - Different Foundation Soil Relative Densities (Coehesionless Foundation Soil)

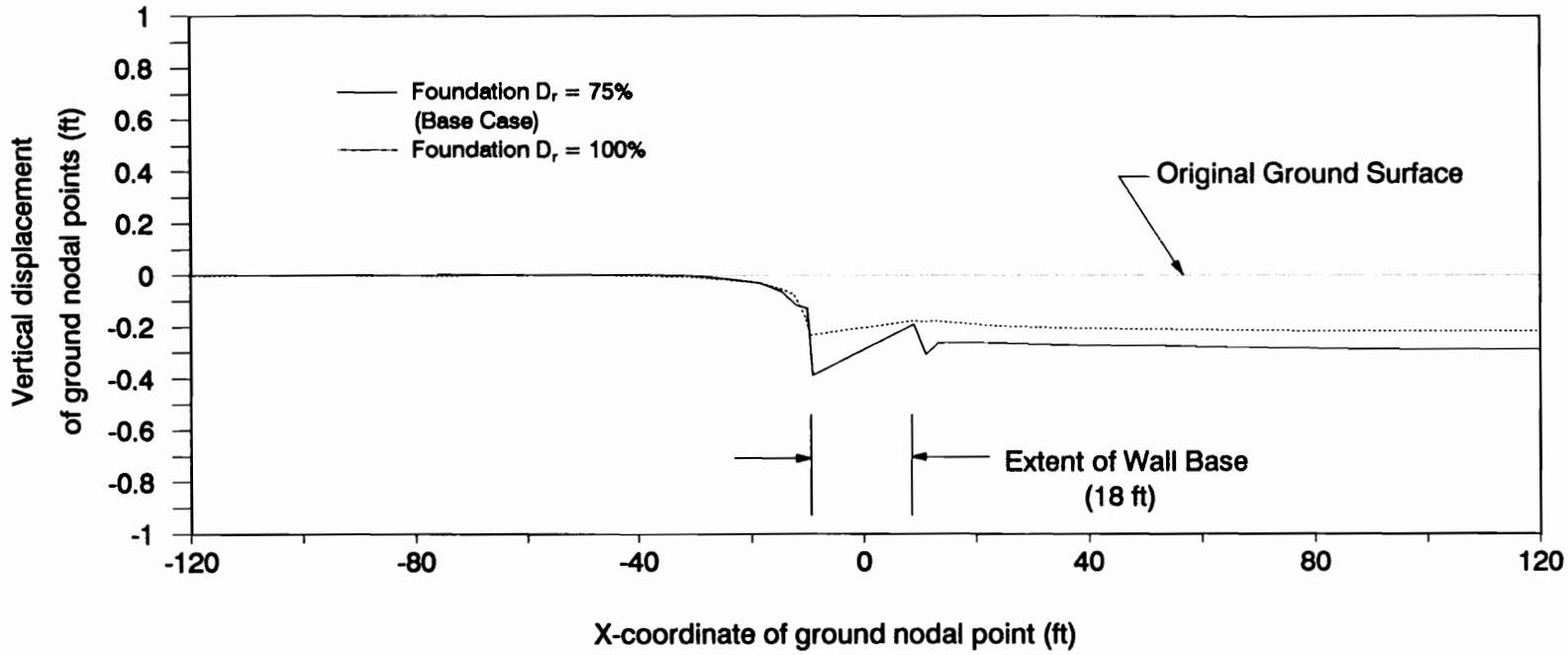

Figure 5.18 - Ground Surface Profiles after Backfilling for different Foundation Relative Densities

the case of D_r equal to 50 percent were unrealistic and so the result for this run was omitted from the figure.

Fig. 5.19 shows the stress distributions along the base at the end of backfilling for the three cases. The stiffer the soil, the greater the tendency for a concentration of normal stresses to occur in the toe area. In all three cases, B_e/B was equal to 95 percent. With the unstable conditions in Run BF2A, the fact that the same effective base width was obtained for all three analyses seem to indicate that massive soil failure would occur before severe base separation takes place for a wall on soil.

Table 5.6 summarizes the forces on the key planes for the three runs. $K_h{}^{AA}$ ranged from 0.27 to 0.29, corresponding to a range of EPI values ranging from 0.56 to 0.70. K_v varied only slightly from 0.07 to 0.08. On this same plane, it may be noted that Y_{AA}, which defines the line of action of the lateral earth force H_{AA}, moves down with increasing foundation stiffness. Y_{AA} ranged from $0.42H$ for D_r equal to 25 percent to $0.34H$ for D_r equal to 100 percent. There are no appreciable difference in the results obtained for the other key planes.

It is to be expected that the wall would be less stable as the foundation soil becomes looser. Displacements become larger and failure regions more widespread with looser foundation soil. This trend toward instability is due to failure within the foundation rather than wall-foundation base separation, as is assumed in conventional equilibrium analyses.

EFFECTS OF SUBMERGENCE OF THE FOUNDATION SOIL

The effects of submergence of the foundation soil were investigated in the analysis designated as Run BF2C. The water table was assumed to be at the ground surface, decreasing the effective stresses of the soil elements within the foundation. The saturated unit weight of

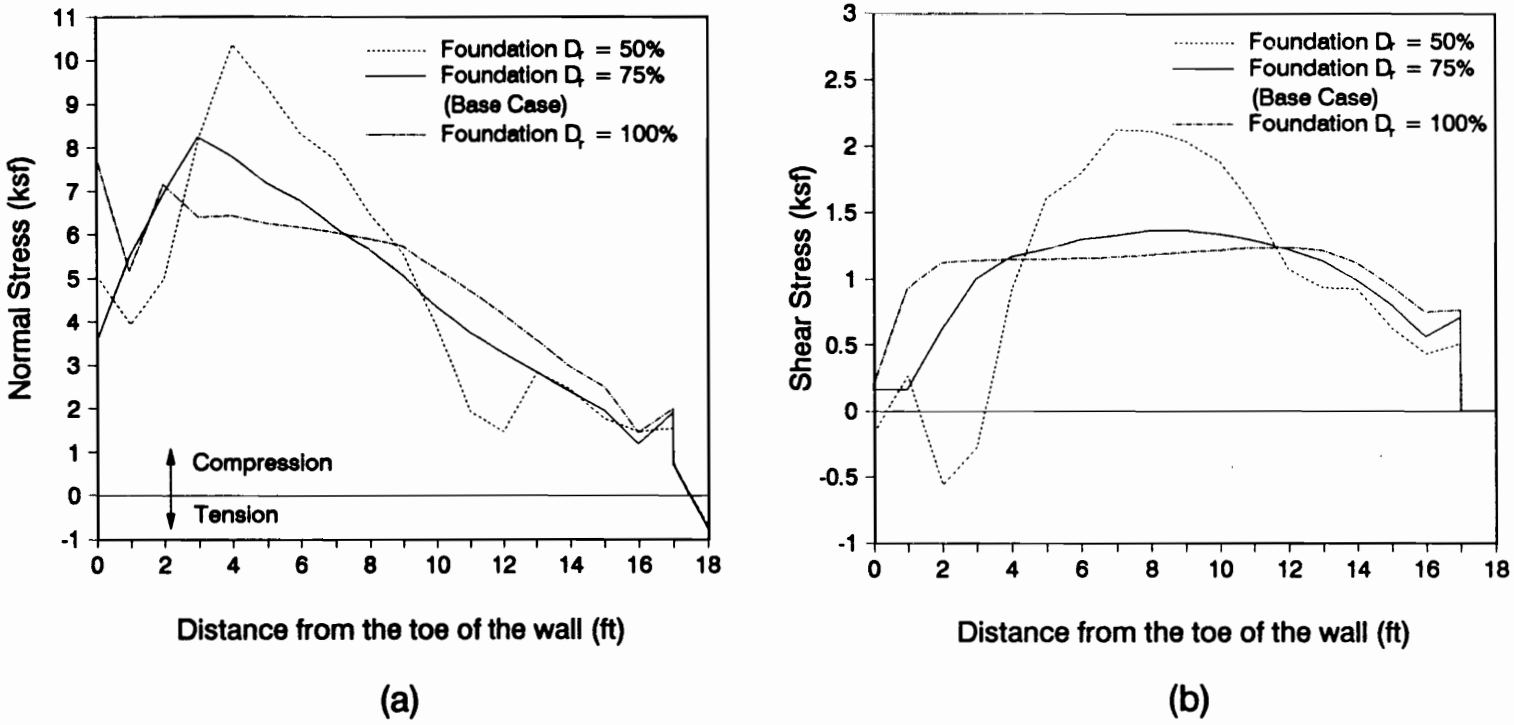

Figure 5.19 - Base Stresses After Backfilling for Different Foundation Relative Densities (Cohesionless Foundation Soil)

Table 5.6 - Forces on Key Planes for various Foundation Relative Densities

Note : All forces in pounds, all lengths are in feet

Run No.	BF2A (Fd'n D_r=50%)	BFBC (Fd'n D_r=75%)	BF2B (Fd'n D_r=100%)
Plane A-A			
H_{AA}	17,620	17,270	18,350
V_{AA}	5,190	4,190	5,190
Y_{AA}	12.63	10.97	10.18
K_h	0.28	0.27	0.29
K_v	0.08	0.07	0.08
EPI	0.63	0.70	0.56
Plane B-B			
H_{BB}	23,490	23,450	23,660
V_{BB}	50	70	45
Y_{BB}	10.09	10.03	10.03
K_h	0.37	0.37	0.38
K_v	0.00	0.00	0.00
Plane C-C			
N_{CC}	23,580	22,700	24,420
T_{CC}	17,270	15,580	17,520
l_{CC}	12.7	11.6	10.7
l_{CC}/l	0.41	0.37	0.34
$\delta_{mob} / \phi_{backfill}$	0.93	0.88	0.92
Plane D-D			
N_{DD}	84,070	82,190	84,550
T_{DD}	17,620	17,270	18,350
X_{DD}	6.5	6.7	7.0
X_{DD}/B	0.36	0.37	0.39
$\delta_{mob} / \phi_{foundation}$	0.33	0.30	0.29

the foundation soil was assumed to be equal to 150 pcf. The rest of the parameters that described the base case were utilized in the analysis.

The consequence of the decrease in effective stress within the foundation was a decrease in strength, leading to the widespread failure region shown in Fig. 5.20. This extensive failure resulted in large wall displacements as early as the 8th lift, as shown in the force-displacement curves in Fig. 5.21.

Other results obtained upon application of the full backfill load were considered unreliable because of the numerical inaccuracies resulting from the occurrence of extensive failure. These results are not presented. The main conclusion that can be made from this analysis is that submergence of a cohesionless foundation is detrimental to the overall stability of the wall system.

EFFECTS OF VARYING THE RELATIVE DENSITY OF THE BACKFILL

The series of analyses discussed in this section is aimed at determining the effects of utilizing cohesionless soils of various relative densities as backfill. Four cases were analyzed, using backfill relative densities of 25, 50, 75 (the base case) and 100 percent. The strength and stiffness parameters corresponding to each case are listed in Table 5.1.

A summary of the forces and related indices on the key planes for each of the four analyses is given in Table 5.7.

The horizontal normal force on plane A-A increased in magnitude with decreasing relative density. This trend is attributable to the fact that the looser soil has higher at-rest pressures, and also that the earth pressure drops less rapidly as the wall deflects, due to the fact that looser soil is less stiff. The earth pressure index, EPI, varied only slightly from 0.70 to 0.71,

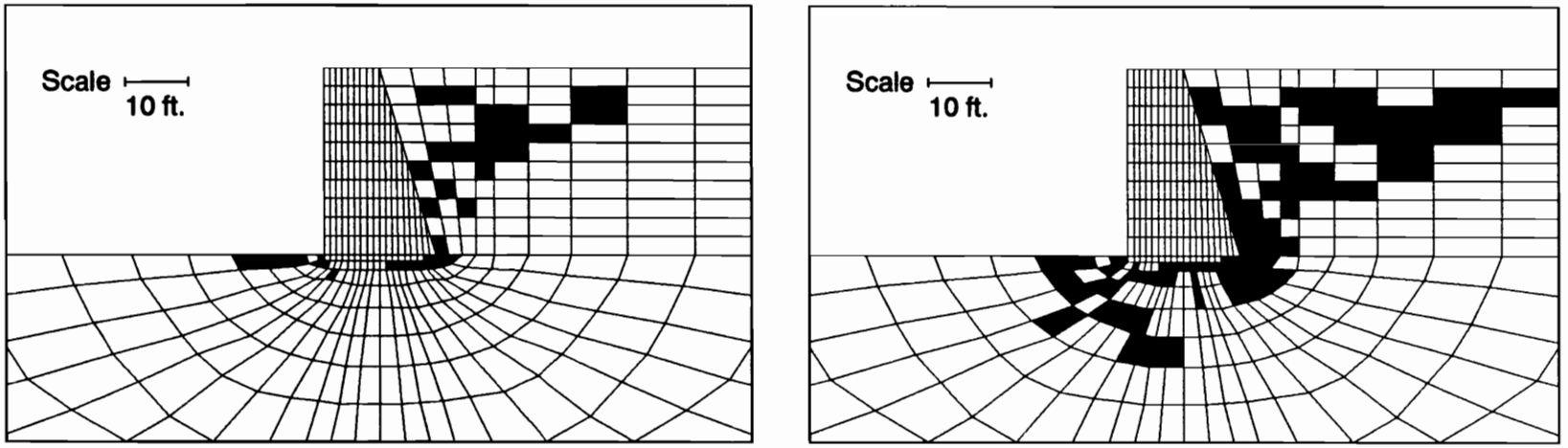

(a) Failure Regions - Dry Foundation Soil

(b) Failure Regions - Submerged Foundation Soil

Figure 5.20 - Failure Regions within the Foundation and Backfill - Dry and Submerged Foundation Soils

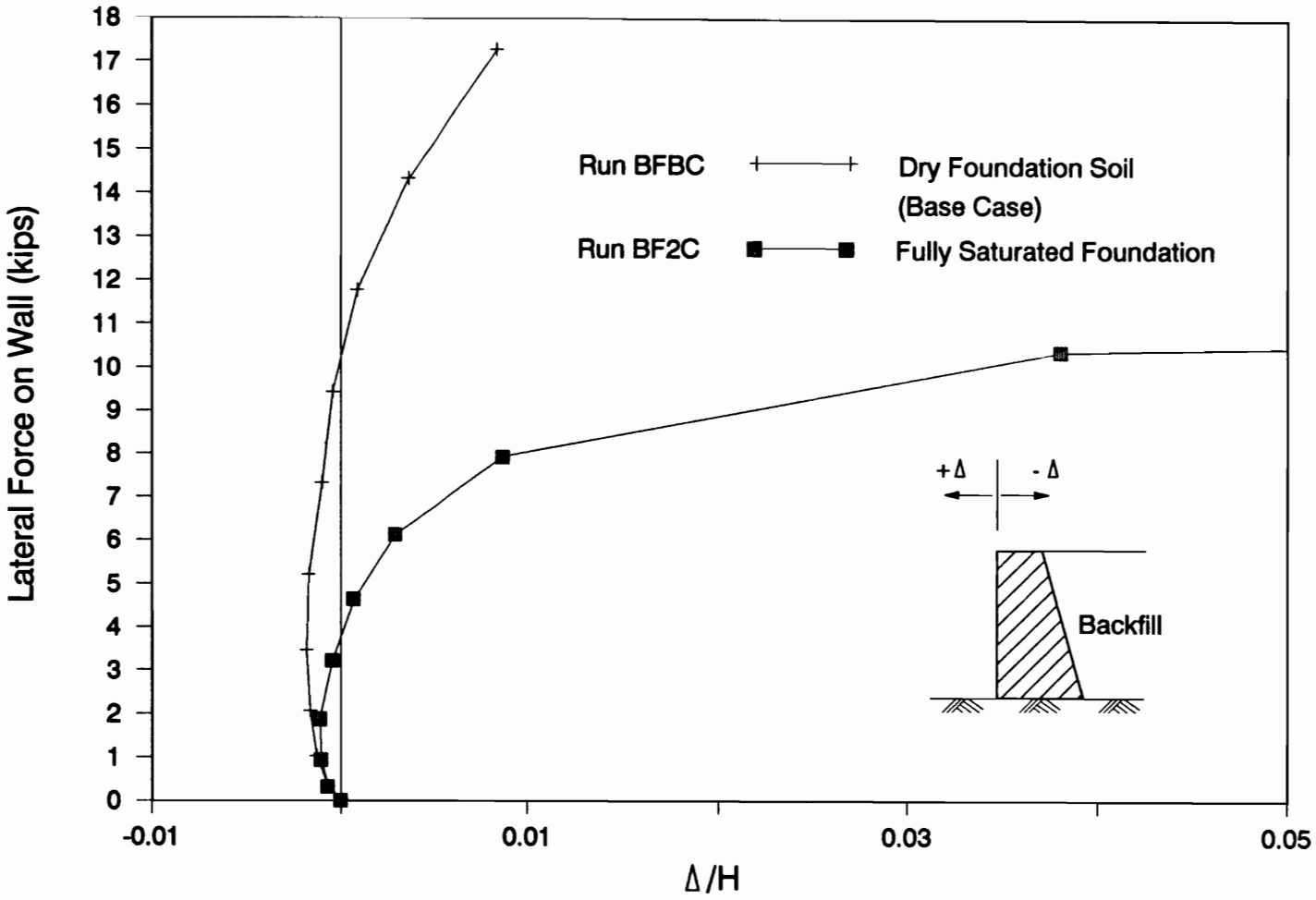

Figure 5.21 - Variation of Normalized Wall Displacements with the Lateral Earth Force on the wall - Dry and Fully Saturated Foundation Soil

Table 5.7 - Forces on Key Planes for various Backfill Relative Densities

Note : All forces in pounds, all lengths are in feet

Run No.	BF3A (D_r=25%)	BF3B (D_r=50%)	BFBC (D_r=75%)	BF3C (D_r=100%)
Plane A-A				
H_{AA}	19,980	18,000	17,270	15,300
V_{AA}	2,940	4,080	4,190	2,760
Y_{AA}	9.87	10.63	10.97	10.82
K_h	0.34	0.30	0.27	0.24
K_v	0.05	0.07	0.07	0.04
EPI	0.71	0.71	0.71	0.70
Plane B-B				
H_{BB}	26,060	24,060	23,450	22,450
V_{BB}	50	45	70	85
Y_{BB}	9.98	10.01	10.03	9.93
K_h	0.45	0.40	0.37	0.34
K_v	0.00	0.00	0.00	0.00
Plane C-C				
N_{CC}	25,260	23,610	22,700	20,670
T_{CC}	14,650	16,030	15,580	15,650
l_{CC}	10.1	10.7	11.6	12.0
l_{CC}/l	0.32	0.34	0.37	0.38
$\delta_{mob} / \phi_{backfill}$	0.91	0.95	0.88	0.88
Plane D-D				
N_{DD}	82,040	82,890	82,190	81,675
T_{DD}	19,980	18,000	17,270	15,300
X_{DD}	6.8	6.9	6.7	6.8
X_{DD}/B	0.38	0.38	0.37	0.38
$\delta_{mob} / \phi_{foundation}$	0.35	0.32	0.30	0.27

indicating a similar degree of soil-structure interaction in all four cases. A slight variation was also observed in the line of action of H_{AA}, ranging from 33 to 36 percent of the wall height.

The shear force coefficient, $K_v{}^{AA}$, was found to be equal to 0.07 for the backfills of D_r equal to 50 and 75 percent. A lower value of 0.05 was obtained for D_r equal to 25 percent. This lower value may be due to the soil's decreased capacity to generate shear stresses, being less stiff in shear than soils of higher relative densities. However, an even smaller value of 0.04 was obtained for the case where D_r is equal to 100 percent, which represents the stiffest backfill analyzed in this series. The decrease in shear force in this case is due to the smaller settlement of the backfill relative to the wall. The ground surface profile in Fig. 5.22. show that less severe wall tilt as well as smaller differential settlement in the heel vicinity occurred in the case where the backfill D_r was 100 percent. This smaller tilt is due to the smaller lateral force generated in this particular case.

The stiffness of the backfill soil also affected the extent of the failure regions within the backfill, as shown in Fig. 5.23. The stiffer the soil, the more extensive are the failure regions in the backfill, because failure occurs at smaller strains in the stiffer soil. However, the effects on the failure regions in the foundation are minimal. The failure regions in the backfill directly affect the stress distributions in plane A-A, as shown in Fig. 5.24 and Fig. 5.25. Note that the resultants of the normal stress distributions have lines of action that are quite close, even though the distributions are quite different from each other.

The forces in plane B-B again demonstrate the absence of soil-structure interaction effects at distances sufficiently far from the wall. The locations of the resultant lateral force, Y_{BB}, are very close to the lower third point that corresponds to a triangular pressure distribution. The values of $K_h{}^{BB}$ are very nearly equal to the K_o-values as computed by Jaky's formula.

The normal force on the back of the wall, N_{CC}, decreases with increasing relative density, as would be expected. The shear force, T_{CC}, varied only slightly, with only a 10

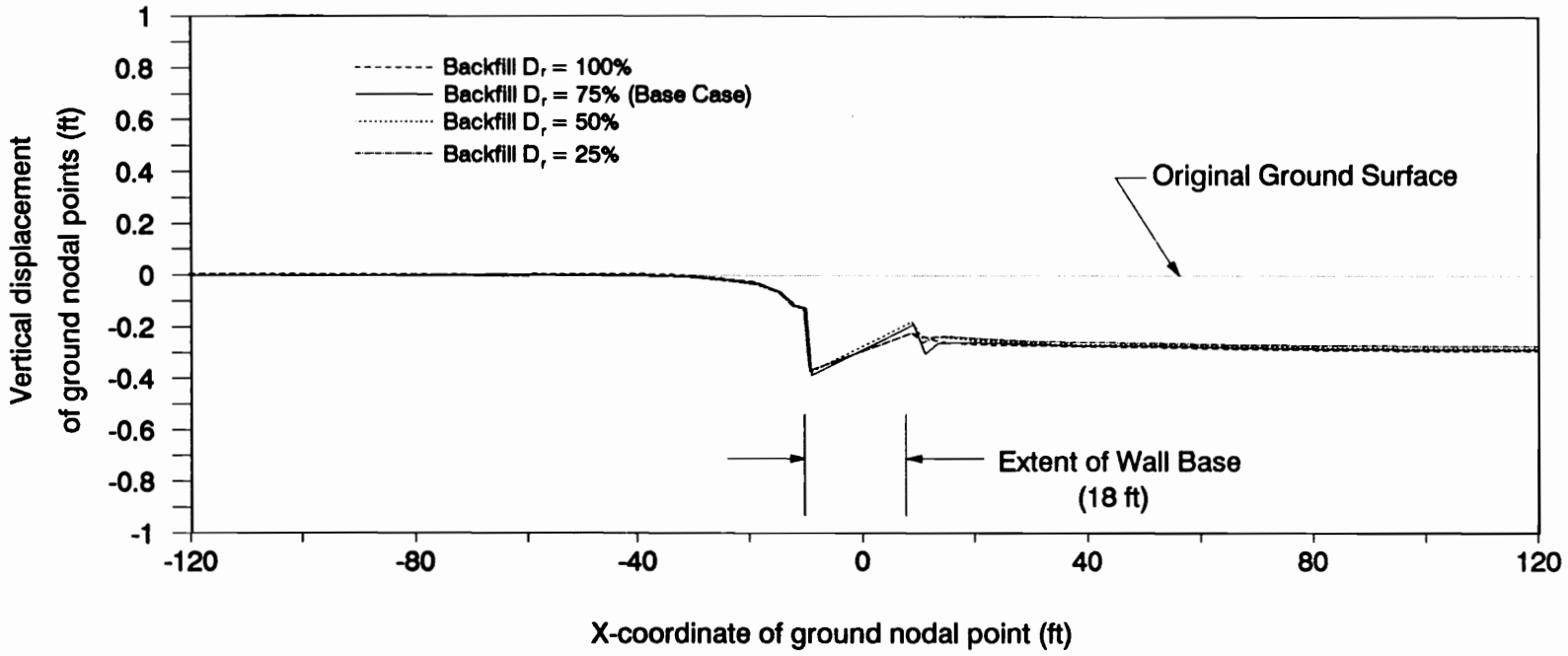

Figure 5.22 - Ground Surface Profiles after Backfilling for different Backfill Relative Densities

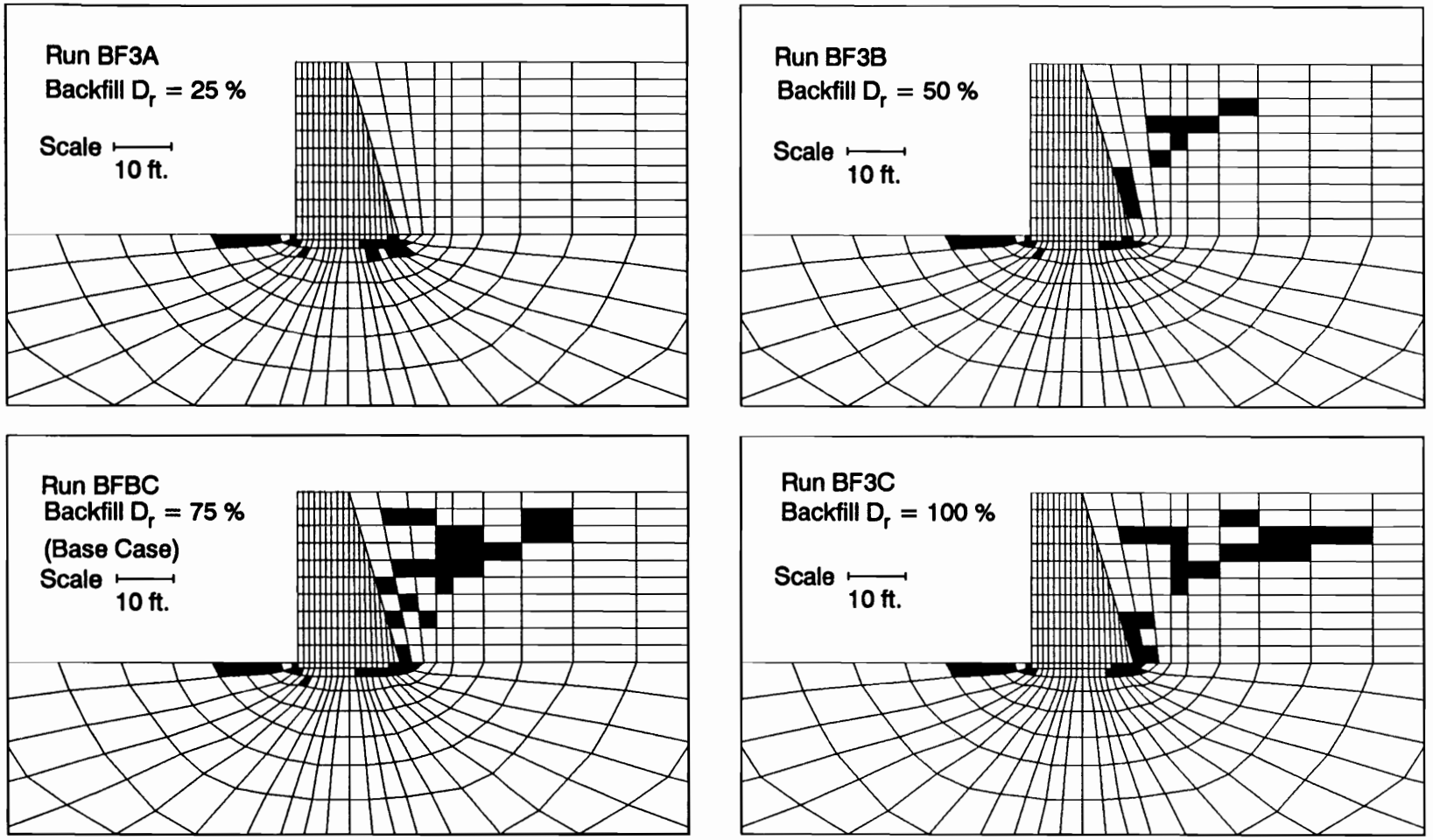

Figure 5.23 - Failure Regions within the Foundation and Backfill - different Backfill Relative Densities (Cohesionless Backfill)

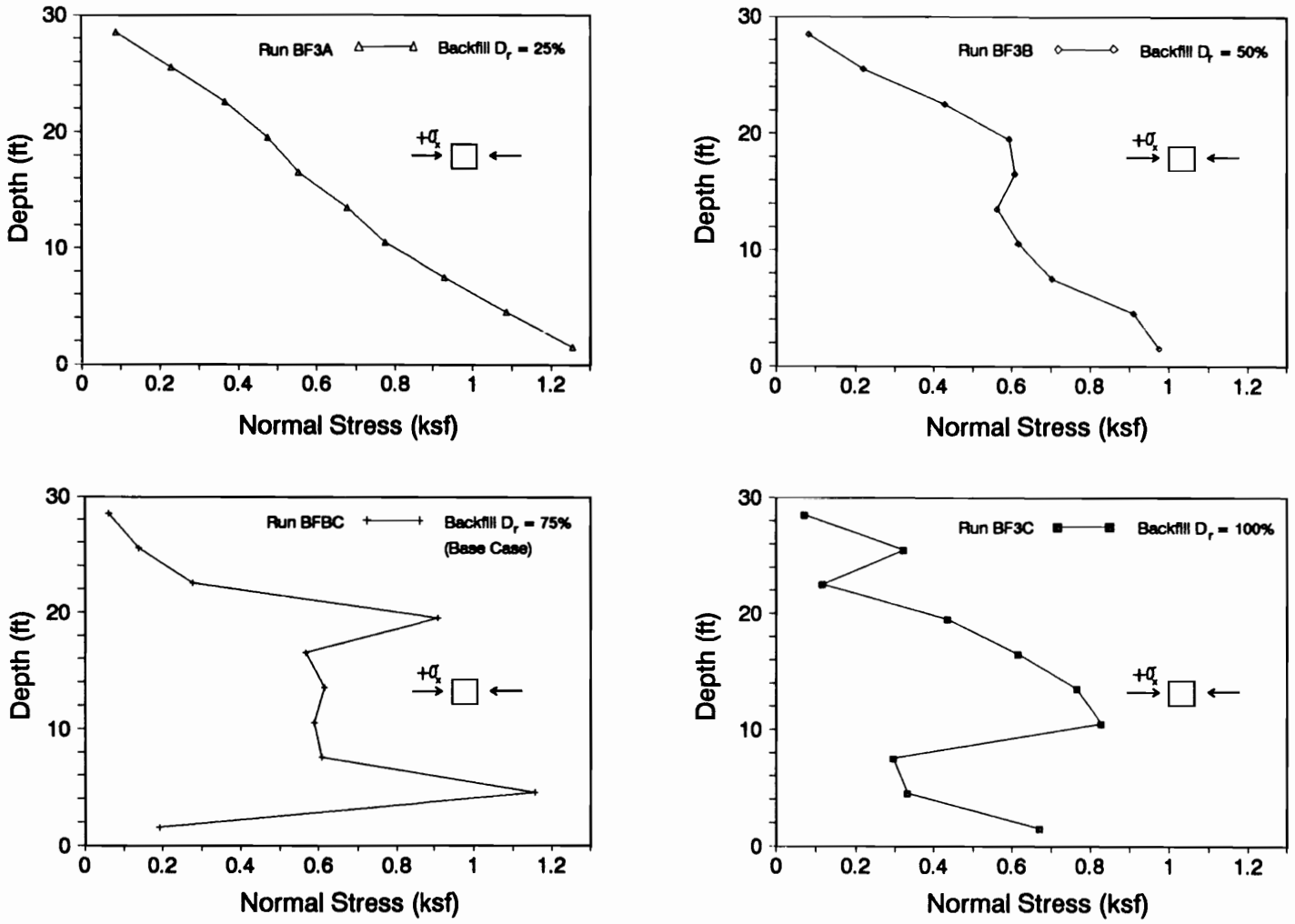

Figure 5.24 - Variation of Normal Stresses on the Vertical Plane A-A for different Backfill Relative Densities

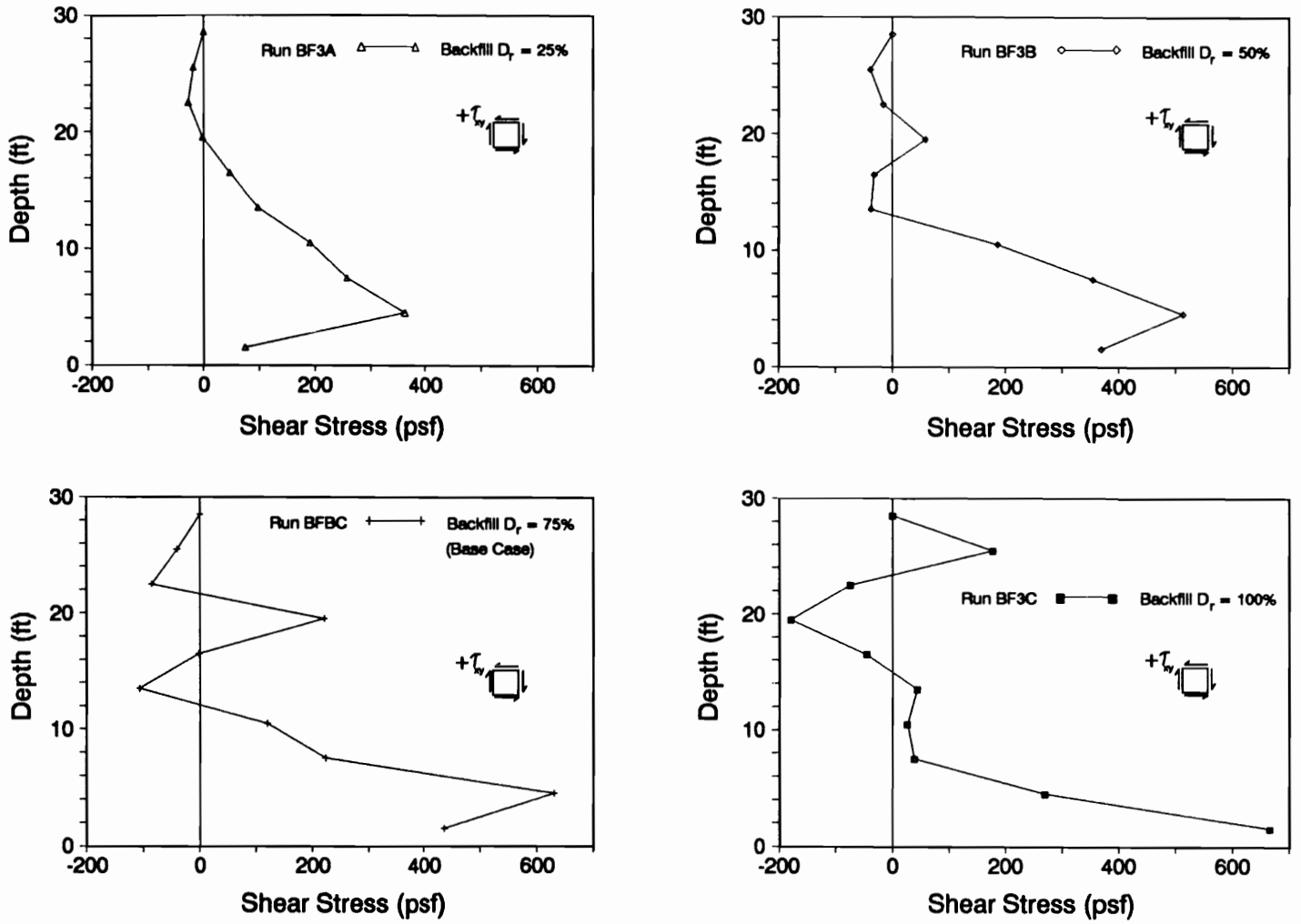

Figure 5.25 - Variation of Shear Stresses on the Vertical Plane A-A for different Backfill Relative Densities

percent difference between the largest and smallest values. Considering the entire length of the wall-backfill interface, the values of the ratio $\delta_{mob}/\Phi_{backfill}$ ranged from 0.88 to 0.95.

Because there is no toe fill, the shear force on the base of the wall, T_{DD}, is equal to the lateral force , H_{AA}. Slightly higher peak values of shear stress occurred for the less dense backfills, as shown in Fig. 5.26. The largest value of mobilized friction on the base correspond to a ratio $\delta_{mob}/\Phi_{foundation}$ equal to 0.35. All the walls had an effective base width, B_e/B equal to 95 percent.

The normalized displacements of the top of the wall, Δ/H, with their corresponding backfill relative densities are : 0.013 for D_r equal to 25 percent, 0.009 for D_r equal to 50 percent, 0.008 for D_r equal to 75 percent and 0.005 for D_r equal to 100 percent. It may be concluded that less dense backfills would lead to larger displacements because of the greater lateral pressures that are generated. The variation of Δ/H with the lateral earth force on the wall for the cases analyzed are given in Fig. 5.27.

EFFECTS OF THE PRESENCE OF A TOE FILL

An analysis was performed wherein 9 feet of soil (toe fill) was placed in front of the wall. This toe fill was represented by finite elements, and consists of sand of 75 percent relative density. The toe fill consisted of three 3-foot thick lifts, and was placed simultaneously with the backfill to a depth of 9 feet, as shown in Fig. 5.28.

The force-displacement behavior for the two cases are shown in Fig. 5.29. With a toe fill, the wall moves toward the backfill during backfilling until the placement of the last lift. The Δ/H values at the end of construction are 0.0005 with a toe fill, and 0.008 without. There is also a greater tendency of the wall to settle uniformly when there is a toe fill, as shown in Fig.

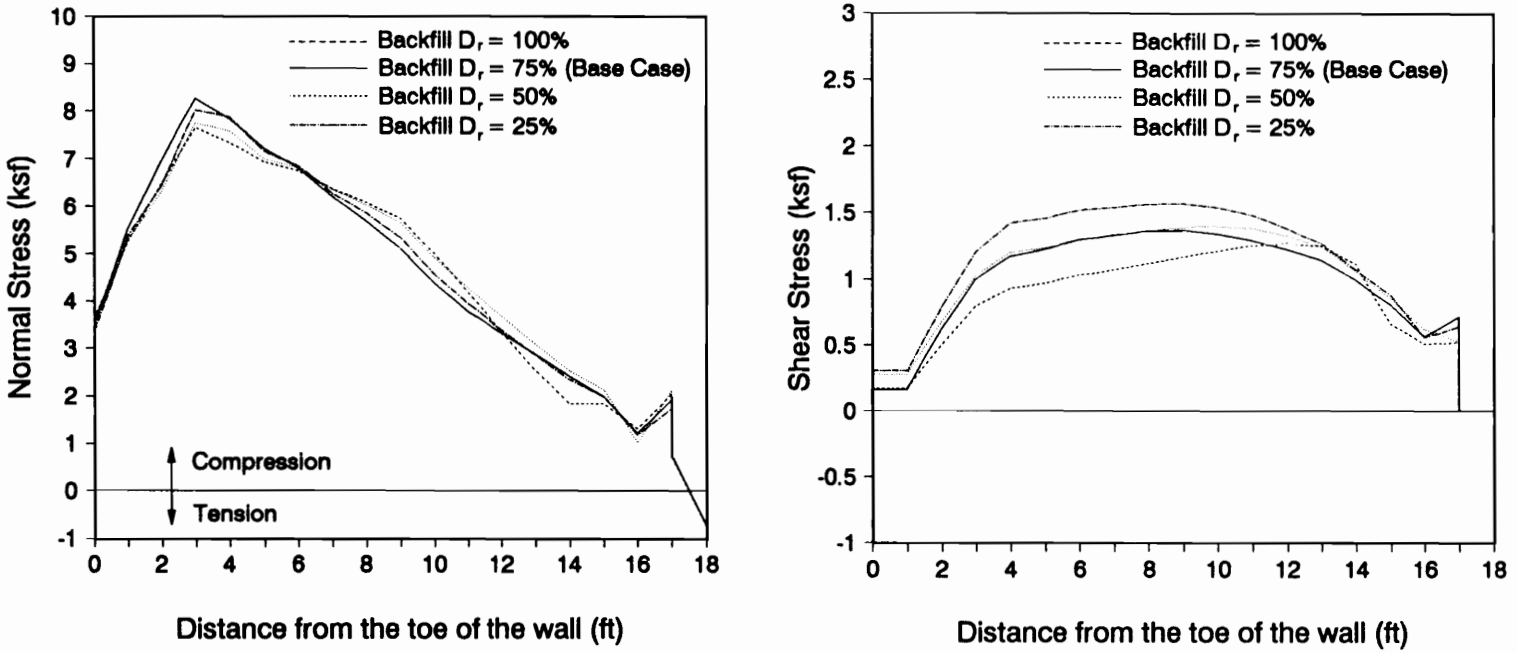

Figure 5.26 - Base Stresses After Backfilling for Different Backfill Relative Densities (Cohesionless Backfill)

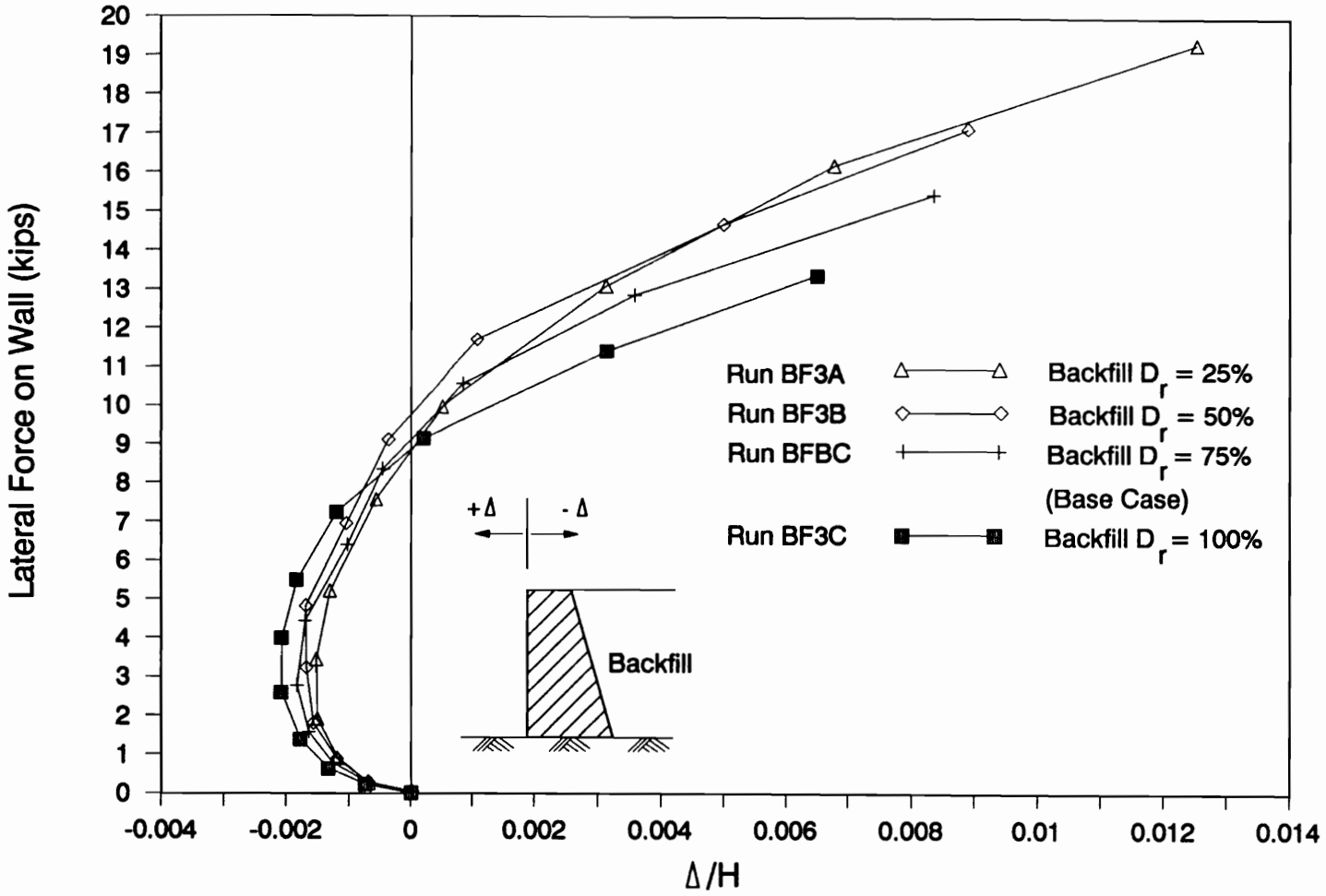

Figure 5.27 - Variation of Normalized Wall Displacements with the Lateral Earth Force on the wall - Different Backfill Relative Densities (Cohesionless Backfill)

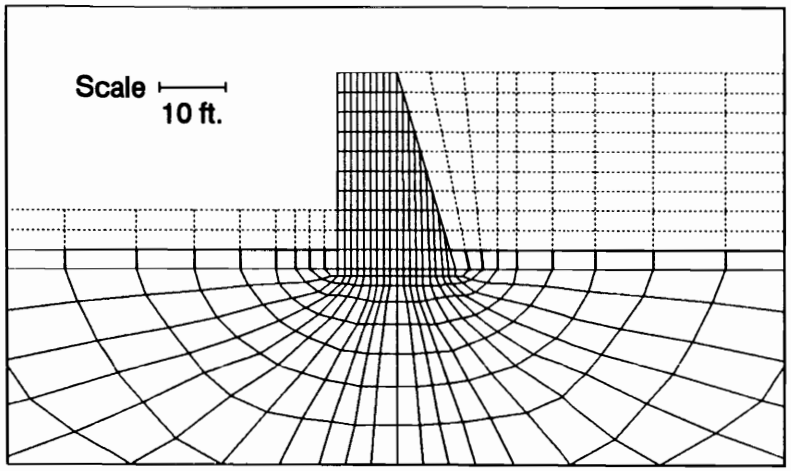

(a) After placement of first lift

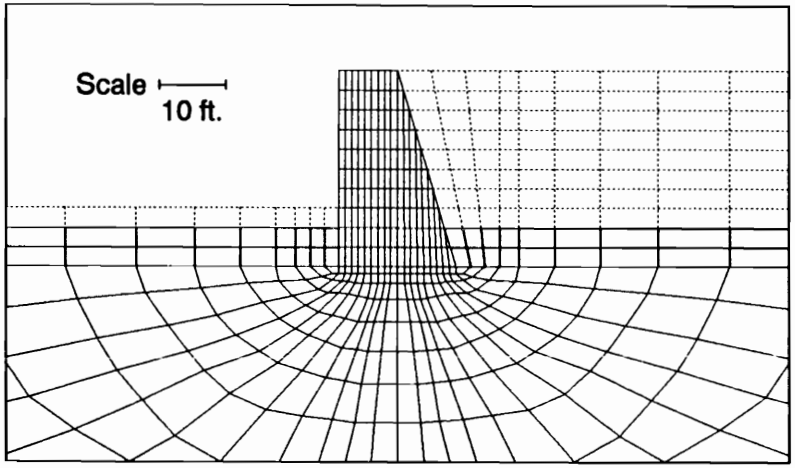

(b) After placement of second lift

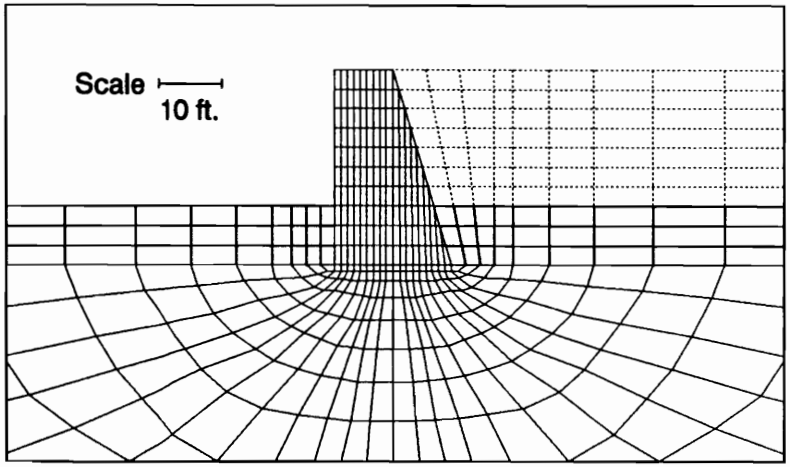

(b) After placement of third lift

Figure 5.28 - Simultaneous Placement of Backfill and Toe Fill

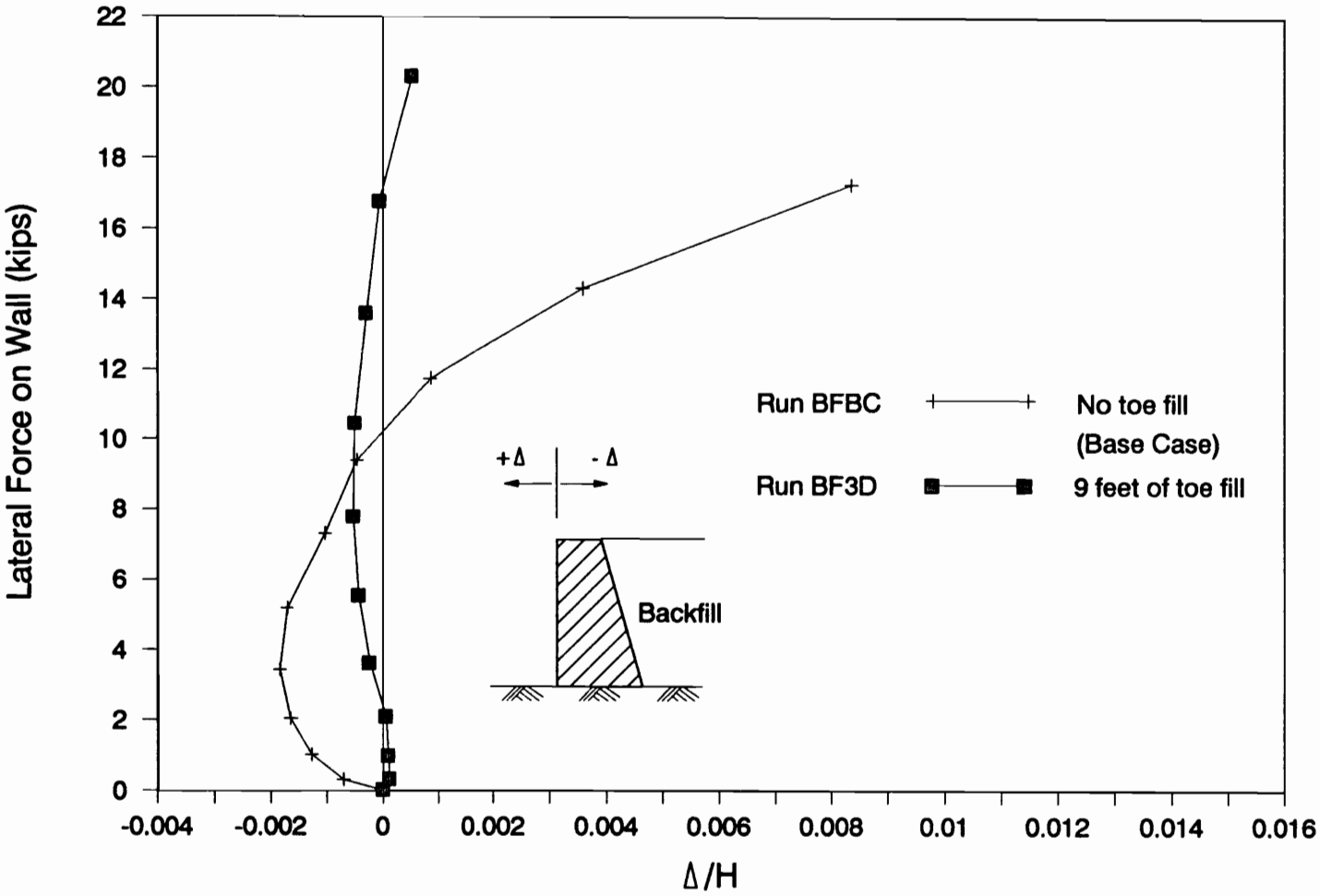

Figure 5.29 - Variation of Normalized Wall Displacements with the Lateral Earth Force on the wall - with and without Toe Fill

5.30.

Fig. 5.31 compares the failure regions for analyses with and without a toe fill. The number of failed elements in both the foundation and backfill is significantly less with a toe fill, due to the accompanying increase in confining pressures. In fact, not a single backfill soil element was in a state of failure at the end of backfilling with a toe fill. Consequently, smoother stress distributions were obtained on plane A-A compared to those obtained in the base case, where backfill soil failures led to stress redistribution, as shown in Fig. 5.32. A summary of the stress resultants in this plane as well as in other key planes are given in Table 5.8.

The $K_h{}^{AA}$ value increased from 0.27 for the case without a toe fill to 0.32 for the case with a toe fill. This increase is to be expected because the wall does not deflect as far when there is a toe fill. Consequently, the EPI for in plane A-A decreased from 0.70 to 0.39. There is also an increase in the vertical shear force coefficient K_v from 0.07 for the base case to 0.10 with the toe fill. This increase is possibly due to the increase in stiffness of the soil elements in the backfill, which allowed them to develop larger shear stresses as a result of differential settlements between the backfill and the wall.

The stresses at the base of the wall are as shown in Fig. 5.33. Because there was not extensive failure in the toe area, the foundation soil is stiff and stress concentrations occurred in this vicinity. However, in spite of the improved stability, the effective base width B_e/B was 95 percent for both cases. This re-confirms the findings of the following load analyses discussed in Chapter 4 that even for stable walls, a small amount of base separation would occur because of the manner in which the base pressure was established by simulating the buildup of the wall.

A summary of the forces on the key planes within the toe fill is given in Table 5.9. On plane E-E, which is the interface between the wall and the toe fill, the horizontal normal force H_{EE} corresponds to a K_h value of 1.48. This relatively high K_h value is the result of movement of the wall toward the toe fill during backfilling. The force H_{EE} improves the

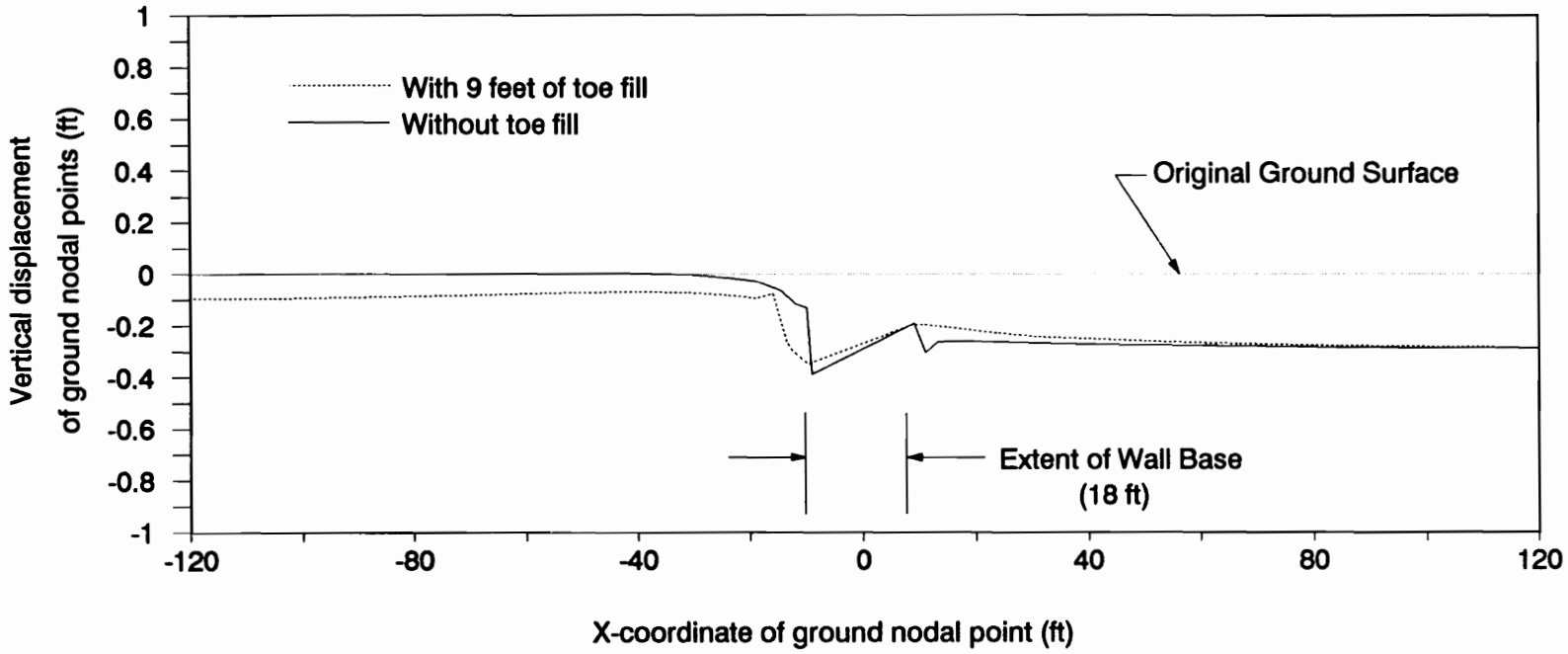

Figure 5.30 - Ground Surface Profiles after Backfilling - with and without Toe Fill

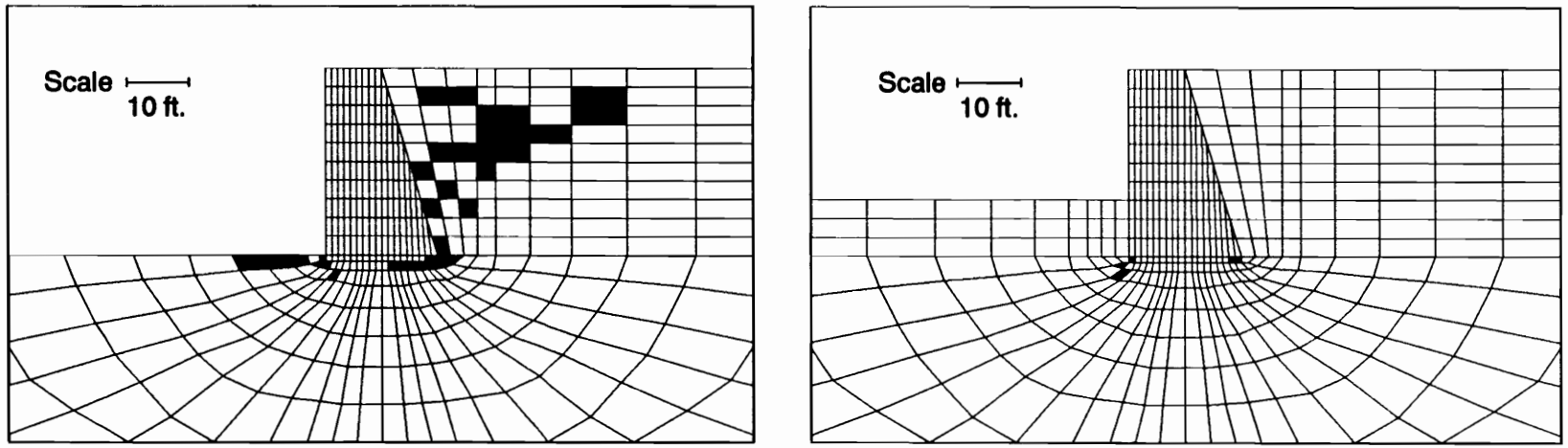

(a) Failure Regions for Base Case - no toe fill

(b) Failure Regions - with 9 feet of toe fill

Figure 5.31 - Failure Regions within the Foundation and Backfill - Analyses with and without Toe Fill

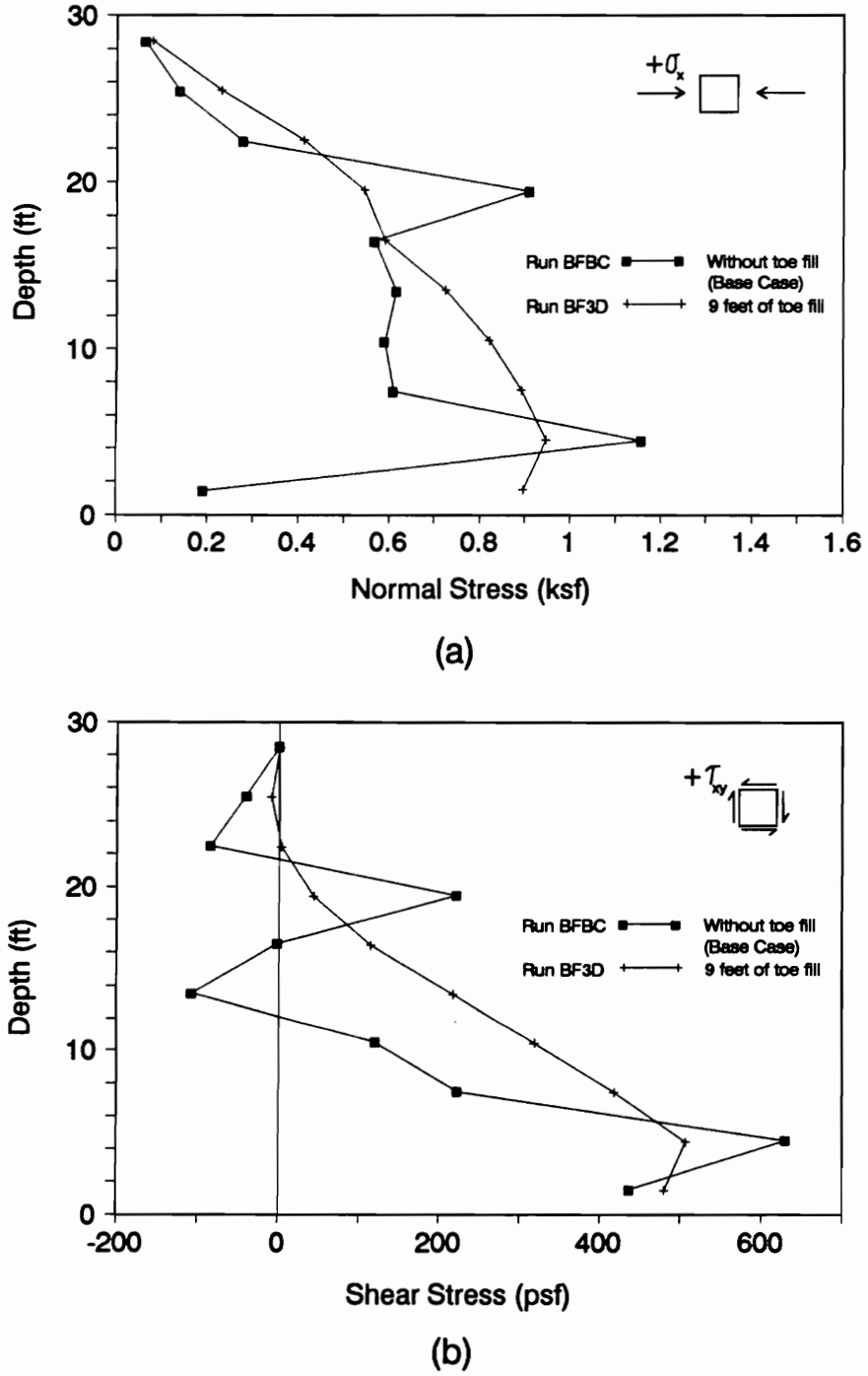

Figure 5.32 - Variation of Normal and Shear Stresses on the Vertical Plane A-A for Analyses with and without Toe Fill

Table 5.8 - Forces on Key Planes in the Backfill for analyses with and without a Toe Fill

Note : All forces in pounds, all lengths are in feet

Run No.	BFBC (No toe fill)	BF3D (With toe fill)
Plane A-A		
H_{AA}	17,270	20,290
V_{AA}	4,190	6,250
Y_{AA}	10.97	10.09
K_h	0.27	0.32
K_v	0.07	0.10
EPI	0.71	0.39
Plane B-B		
H_{BB}	23,450	23,740
V_{BB}	70	5
Y_{BB}	10.03	9.96
K_h	0.37	0.38
K_v	0.00	0.00
Plane C-C		
N_{CC}	22,700	26,520
T_{CC}	15,580	17,790
l_{CC}	11.6	10.7
l_{CC}/l	0.37	0.34
$\delta_{mob} / \phi_{backfill}$	0.88	0.87
Plane D-D		
N_{DD}	82,190	85,050
T_{DD}	17,270	11,865
X_{DD}	6.7	6.2
X_{DD}/B	0.37	0.34
$\delta_{mob} / \phi_{foundation}$	0.30	0.20

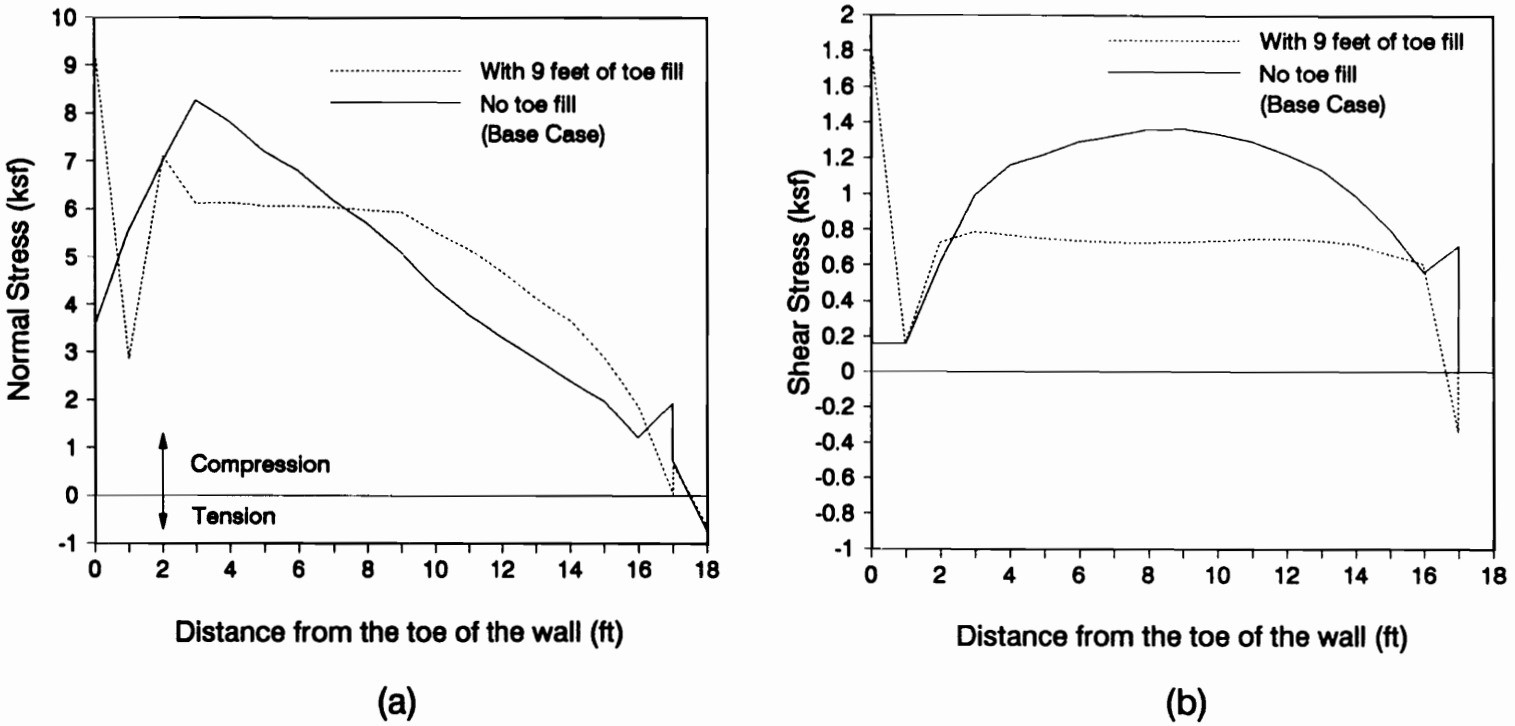

Figure 5.33 - Base Stresses After Backfilling - with and without Toe Fill

Table 5.9 - Forces on Key Planes in the Toe Fill

Note : All forces in pounds, all lengths are in feet

Run No.	BF3D (With toe fill)
Plane E-E	
H_{EE}	8,425
V_{EE}	370
Y_{EE}	4.05
K_h	1.48
K_v	0.07
δ_{mob} / $\phi_{toefill}$	0.07
Plane F-F	
H_{FF}	2,630
V_{FF}	5
Y_{FF}	3.01
K_h	0.46
K_v	0.00

stability of the wall with respect to sliding as well as overturning.

In plane F-F at the far end of the toe fill, the calculated value of $K_h{}^{FF}$ was equal to 0.46. This K_h value is higher than the K_o-value from Jaky's formula, which is equal to 0.37. Ebeling et al. (1988) observed a similar phenomenon in the toe fill in their analyses of walls on rock. They found that the average K_h value decreases as the number of layers increase. The fact that a layer is placed as a dense fluid with K_o equal to 1.00 increases the average value of K_h for a smaller number of lifts. In this case, $K_h{}^{FF}$ in the far end of the toe fill is about 25 percent larger than $K_h{}^{BB}$. The ratio $K_h{}^{EE}/K_h{}^{FF}$ is about 3.19, indicating a high degree of lateral resistance at the wall-toe fill interface.

EFFECTS OF VARYING THE WALL ASPECT RATIO B/H

Four analyses were conducted to determine the influence of the wall base-to-height ratio on its stability. These analyses were carried out by varying the base width of the wall. Base widths equal to 15, 18 (the base case), 21 and 24 feet were considered. With the wall height, H, equal to 30 feet, these base width values correspond to B/H ratios of 0.5, 0.6, 0.7 and 0.8.

It is immediately apparent from the failure regions in Fig. 5.34 how the aspect ratio of the wall affects its stability. For a medium dense foundation (D_r equal to 75 percent), extensive soil failure occurred for run BF4A, where B/H was equal to 0.5. Ebeling et al. (1988) analyzed stable walls on rock that had B/H ratios equal to 0.4 The extensive failure in run BF4A led to large wall displacements commencing on the placement of the 8th lift, as shown in the Δ/H vs H_{AA} plots in Fig. 5.35. Because of this early failure, results obtained after the placement of the entire backfill were considered unreliable and were therefore omitted from the figures and tables to follow. Tolerable wall displacements were obtained from the other three cases. The

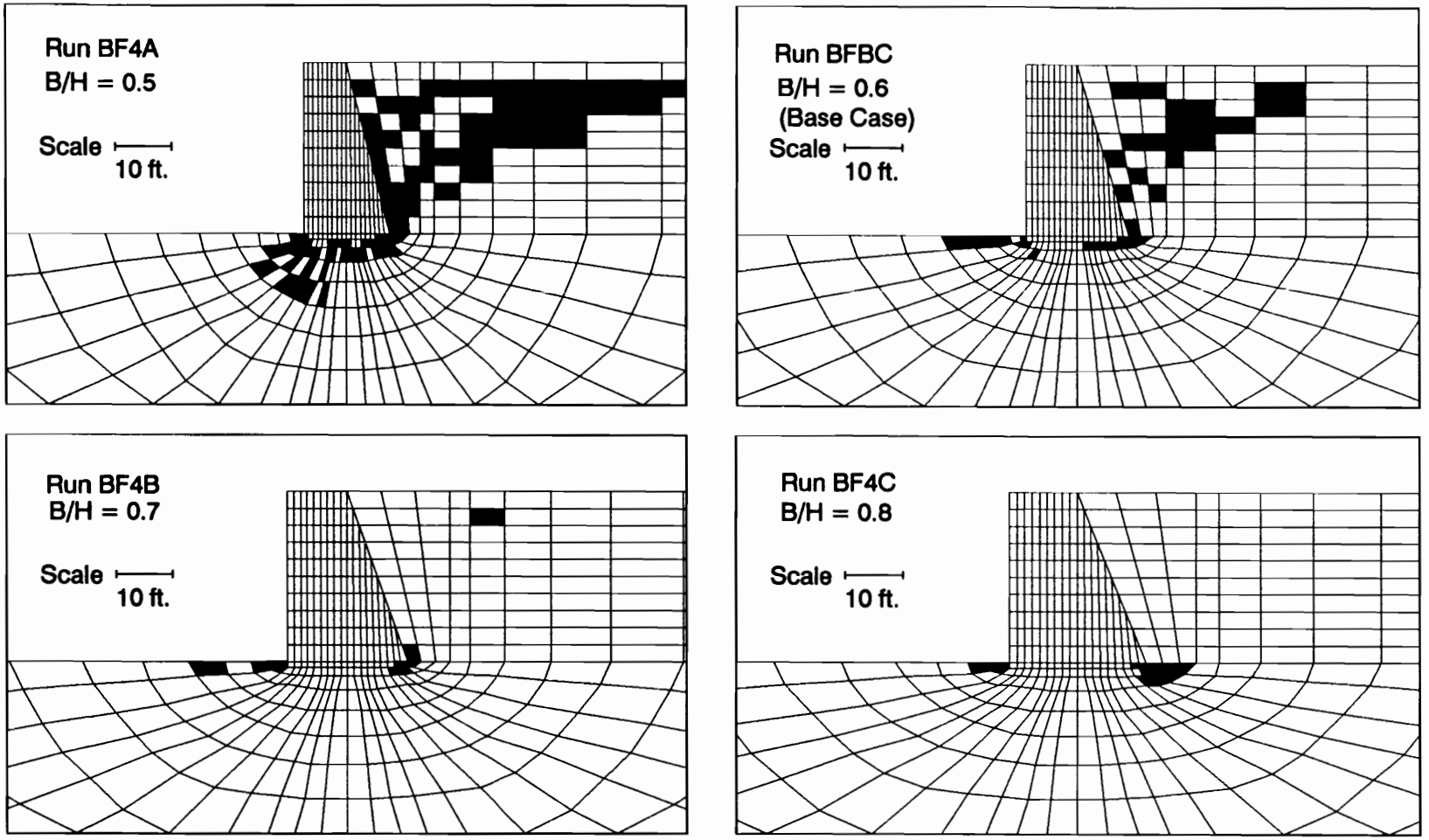

Figure 5.34 - Failure Regions within the Foundation and Backfill - different Wall Base-to-Height Ratios

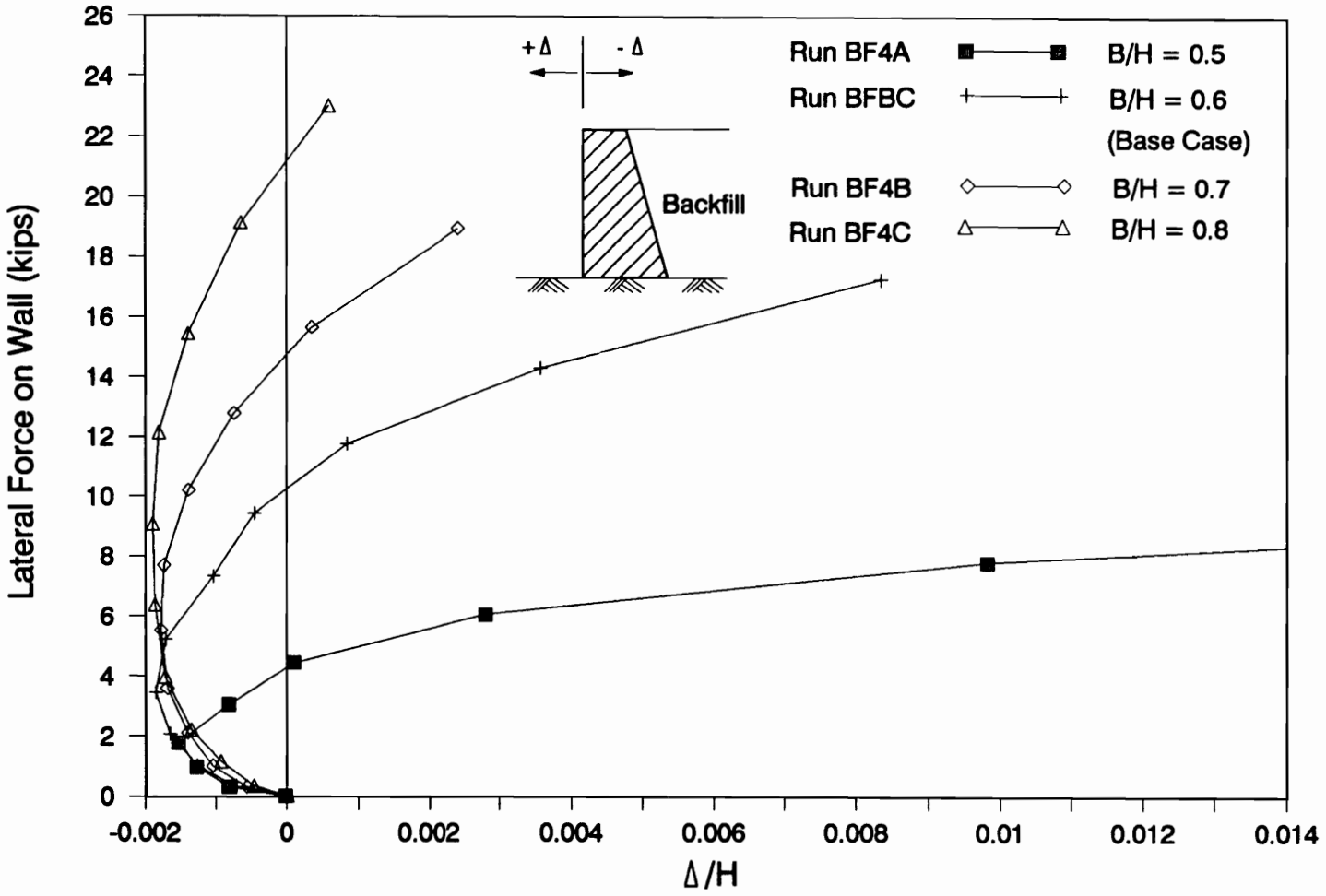

Figure 5.35 - Variation of Normalized Wall Displacements with the Lateral Earth Force on the wall - Different Wall Base-to-Height Ratios

normalized displacements, Δ/H, were as follows : 0.008 for B/H equal to 0.6, 0.002 for B/H equal to 0.7 and 0.0006 for B/H equal to 0.8. Note that with each step increase in B/H, the value of Δ/H is decreased by about 70 percent. This trend is in line with the variations in the calculated ground surface profiles shown in Fig. 5.36 for the different B/H values. It can be seen from this figure that the wider the base, the greater is the tendency of the wall to settle uniformly and the less severe is its tilt.

Table 5.10 summarizes the forces on the key planes for the runs BFBC, BF4B and BF4C. The results obtained in Run BF4A (B/H equal to 0.5) were considered unreliable and are not included in the table.

Considering the forces in plane A-A for the three cases summarized, it may be noted that there is a steady increase in ${K_h}^{AA}$ from 0.27 for B/H equal to 0.6 to 0.37 for B/H equal to 0.8. This steady increase is due to the improved stability of the wall and foundation. The more stable is the system, the smaller are the resulting wall displacements which then allow larger lateral pressures to develop within the backfill. With this steady increase in ${K_h}^{AA}$, the EPI decreased from 0.70 for B/H equal to 0.6 to 0.07 for B/H equal to 0.8. Note also, from Fig. 5.37, that the increase in strength within the backfill brought about a more "regular" distribution of stresses in plane A-A. The location of the line of action, Y_{AA}, of the resultant force H_{AA}, was consistently close to the lower third point of the wall height.

The change in ${K_v}^{AA}$ was more abrupt than the change in ${K_h}^{AA}$. A ${K_v}^{AA}$ value of 0.07 was obtained for B/H equal to 0.6 and 0.7. This value more than doubled to 0.15 in the increase in aspect ratio from 0.7 to 0.8.

The normal and shear stresses on the base of the wall (plane D-D) are shown in Fig. 5.38 and Fig. 5.39, respectively. It may be noted from the plots that the tendency is for the stresses to become more uniform as the aspect ratio B/H is increased. This trend is also reflected in the movement of the resultant normal force on the base, N_{DD}. Its line of action, defined by the

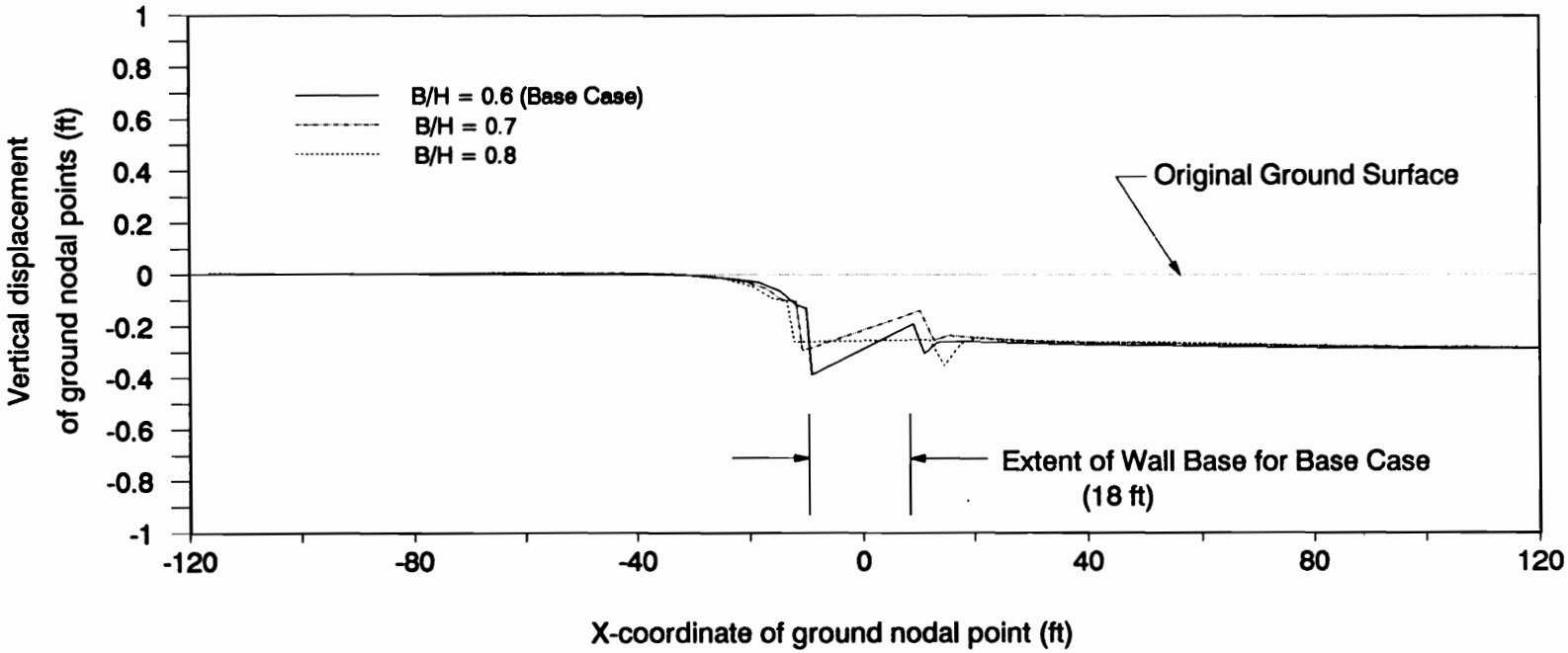

Figure 5.36 - Ground Surface Profiles after Backfilling for different Wall Base-to-Height Ratios

Table 5.10 - Forces on Key Planes for various Wall Aspect Ratios B/H

Note : All forces in pounds, all lengths are in feet

Run No.	BFBC (B/H=0.6)	BF4B (B/H=0.7)	BF4C (B/H=0.8)
Plane A-A			
H_{AA}	17,270	18,990	23,010
V_{AA}	4,190	4,320	9,180
Y_{AA}	10.97	10.36	10.11
K_h	0.27	0.30	0.37
K_v	0.07	0.07	0.15
EPI	0.70	0.52	0.07
Plane B-B			
H_{BB}	23,450	23,730	23,880
V_{BB}	70	50	40
Y_{BB}	10.03	10.04	10.04
K_h	0.37	0.38	0.38
K_v	0.00	0.00	0.00
Plane C-C			
N_{CC}	22,700	26,390	33,770
T_{CC}	15,580	17,910	22,480
I_{CC}	11.6	11.2	10.6
I_{CC} / I	0.37	0.35	0.33
δ_{mob} / $\phi_{backfill}$	0.88	0.88	0.86
Plane D-D			
N_{DD}	82,190	96,495	114,420
T_{DD}	17,270	18,990	23,000
X_{DD}	6.7	8.5	10.5
X_{DD}/ B	0.37	0.41	0.44
δ_{mob} / $\phi_{foundation}$	0.30	0.29	0.29

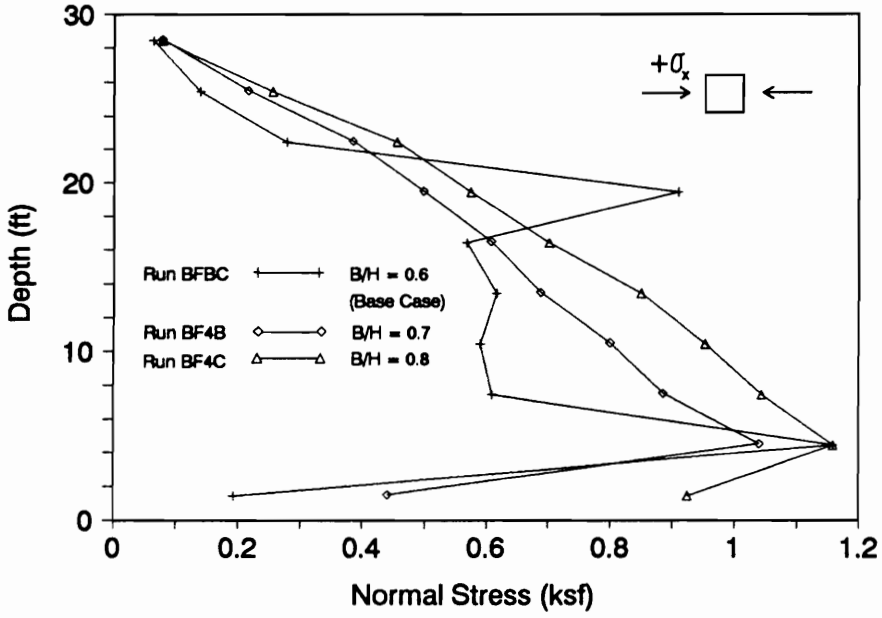

(a)

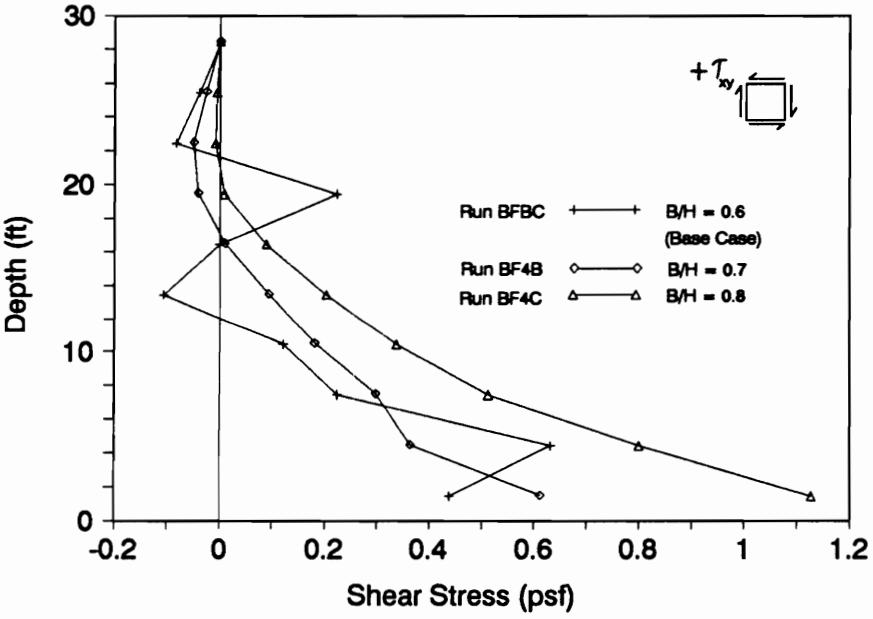

(b)

Figure 5.37 - Variation of Normal and Shear Stresses on the Vertical Plane A-A for various Wall Base-to-Height Ratios

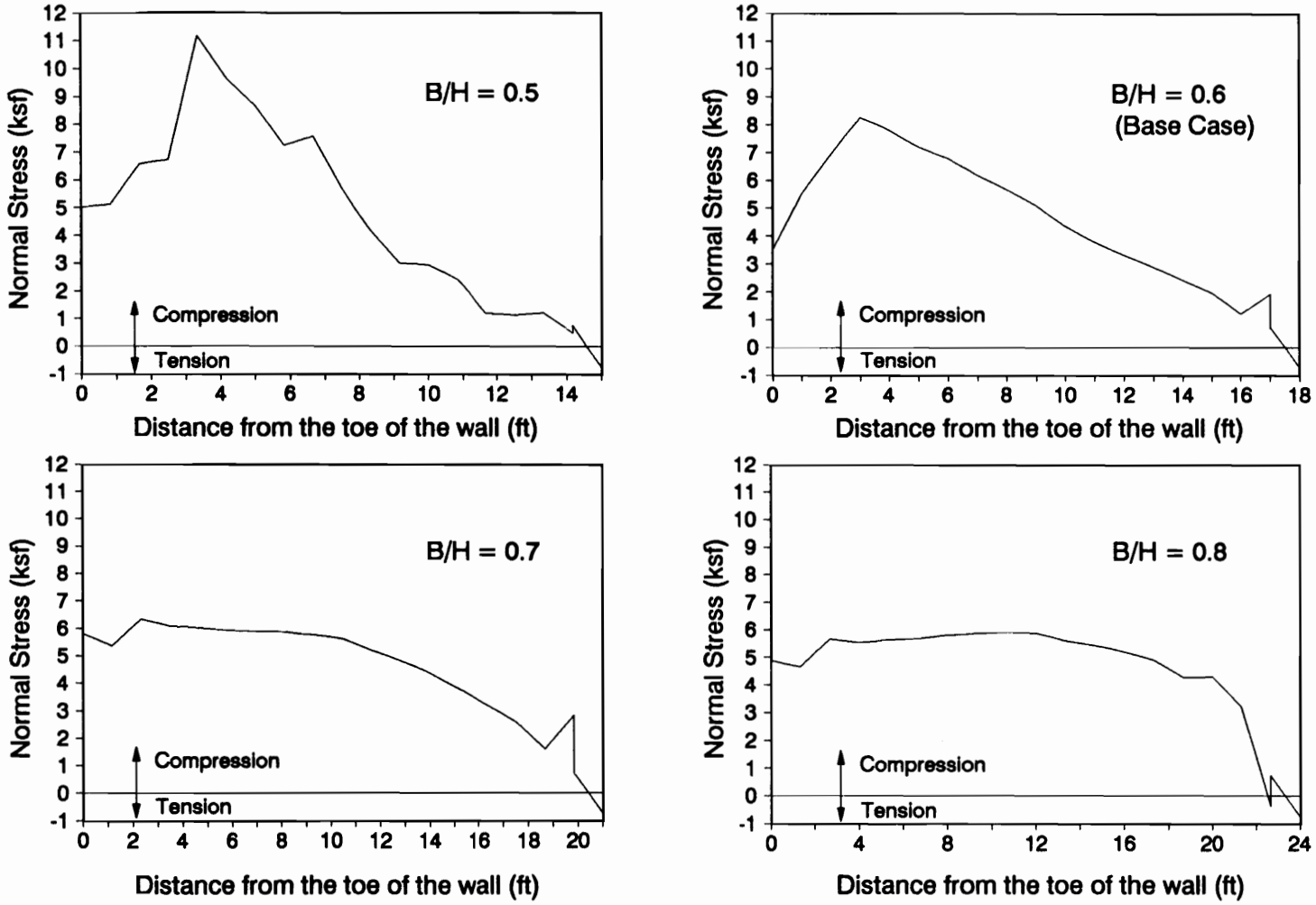

Figure 5.38 - Base Normal Stresses After Backfilling for Different Wall Base-to-Height Ratios

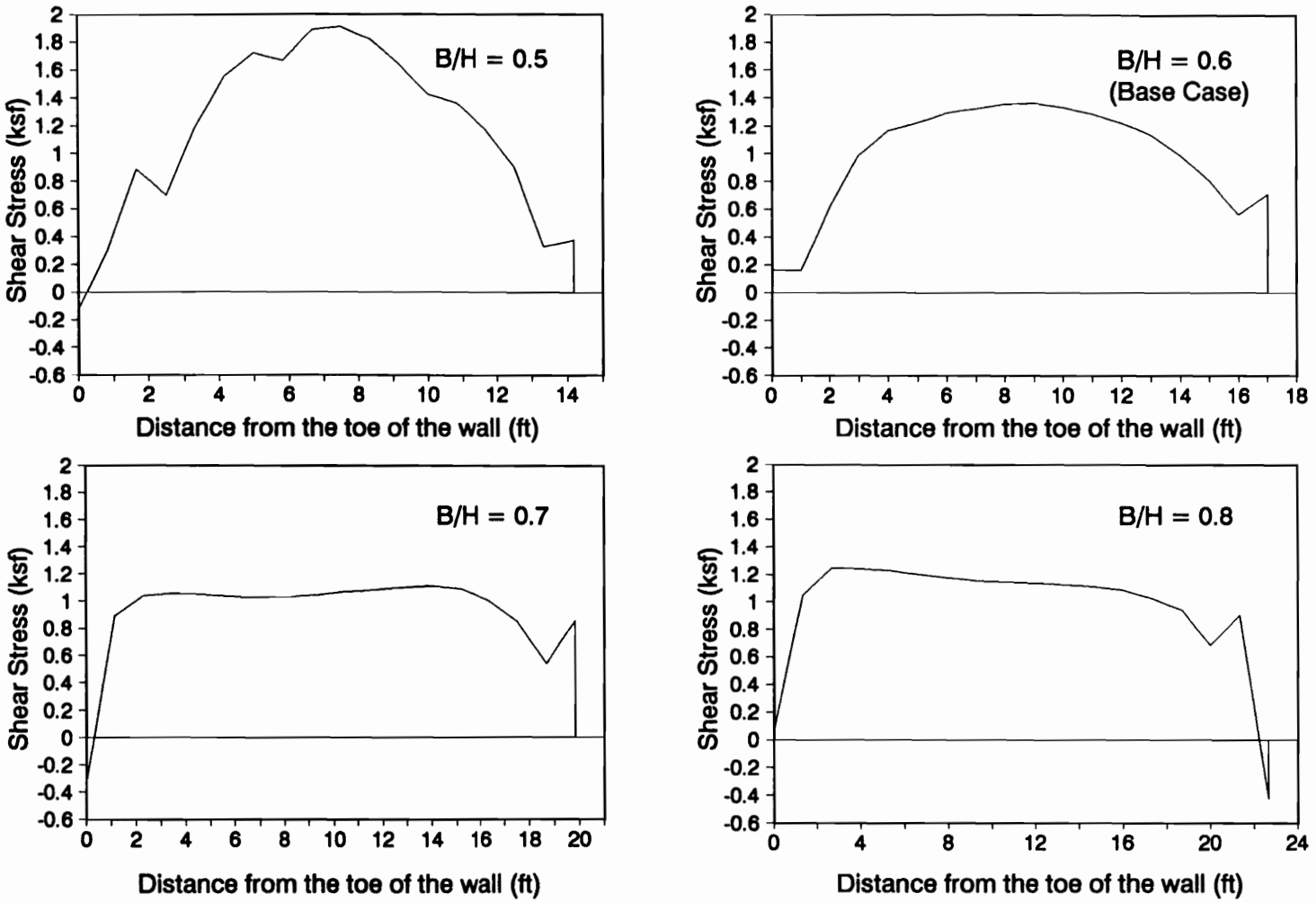

Figure 5.39 - Base Shear Stresses After Backfilling for Different Wall Base-to-Height Ratios

distance X_{DD} measured from the toe, moves toward the center of the base as B/H is increased. A B_e/B value of 95 percent was obtained for the aspect ratios B/H equal to 0.5, 0.6 and 0.7 and a slightly smaller value of 94 percent was obtained for B/H equal to 0.8.

There is a significant difference between the minimum required wall aspect ratio for stability on a soil foundation and what would be required for walls on rock. It has been shown (Ebeling et al., 1988) that walls on rock with B/H ratios equal to 0.4 are stable. On a soil foundation, the required aspect ratio would depend on the strength and stiffness characteristics of the soil. The preceding results show that a B/H ratio of at least 0.6 is required for stability on a medium dense cohesionless foundation. A foundation soil in a looser state would require a higher B/H value.

EFFECTS OF A COHESIVE FOUNDATION

The nature of the problems that need to be addressed when dealing with cohesive soils are quite different from those involving cohesionless soils. Consolidation, swell and creep may be significant in cohesive soils. SOILSTRUCT does not have the capability to model any of these phenomena.

Two soils types were considered in this investigation : USC classification SM-SC (SIlty/Clayey Sand) and USC classification CL (Clay of low plasticity). The strengths and stiffnesses of these soils vary with the Relative Compaction (RC) and water content ($w\%$). For each soil type, two cases were considered : (1) High strength and stiffness (High RC, low $w\%$), and (2) Low strength and stiffness (Low RC, high $w\%$). The run designations and the corresponding foundation soil types are as follows :

(1) Run BF5A - SM-SC, 100% RC, 2% dry of optimum

(2) Run BF5B - SM-SC, 95% RC, 2% wet of optimum

(3) Run BF5C - CL, 100% RC, 2% dry of optimum

(4) Run BF5D - CL, 95% RC, 1% wet of optimum

The strength and stiffness parameters for these foundation soils are listed in Table 5.1. These values were derived from the experimental results conducted on silty clayey sand from the Mica Dam core and Canyon Dam silty clay by Duncan, et al. (1980). The RC values for both the SM-SC and CL soils were based on the Standard AASHO compaction procedure.

The ground surface profiles for the above four cases are shown in Fig. 5.40. For comparison purposes, the base case result was included. The soils subjected to a higher compactive effort and compacted on the dry side underwent smaller settlements. The soils compacted on the wet side heaved just beyond the toe. This heaving may be attributed to the combination of low stiffness and relatively high bulk modulus. The failure regions resulting from the four analyses are given in Fig. 5.41. Extensive failures within the backfill were present for the "wet" foundations. Note the absence of extensive failure within the foundations, especially near the surface. This absence of failure regions is due to the cohesive nature of the soils which gives them to substantial strength near the surface where confining pressures are low.

The development of lateral forces and crest displacements during backfilling are shown in Fig. 5.42. For the foundations compacted on the wet side, the Δ/H values were 0.015 for Run BF5B and 0.016 for Run BF5D. Although from Fig. 5.40 the settlements beneath the wall for the wet foundations were larger than the rest, the corresponding horizontal movement of the top were not very large. These small displacements of the crest are due to the fact that even though the wall settlements were large, wall tilting was not as severe in both cases. This can be observed from the relative vertical positions of the points on the ground surface directly beneath the toe and the heel. Note from the base case ground profile that the wall appears to have a

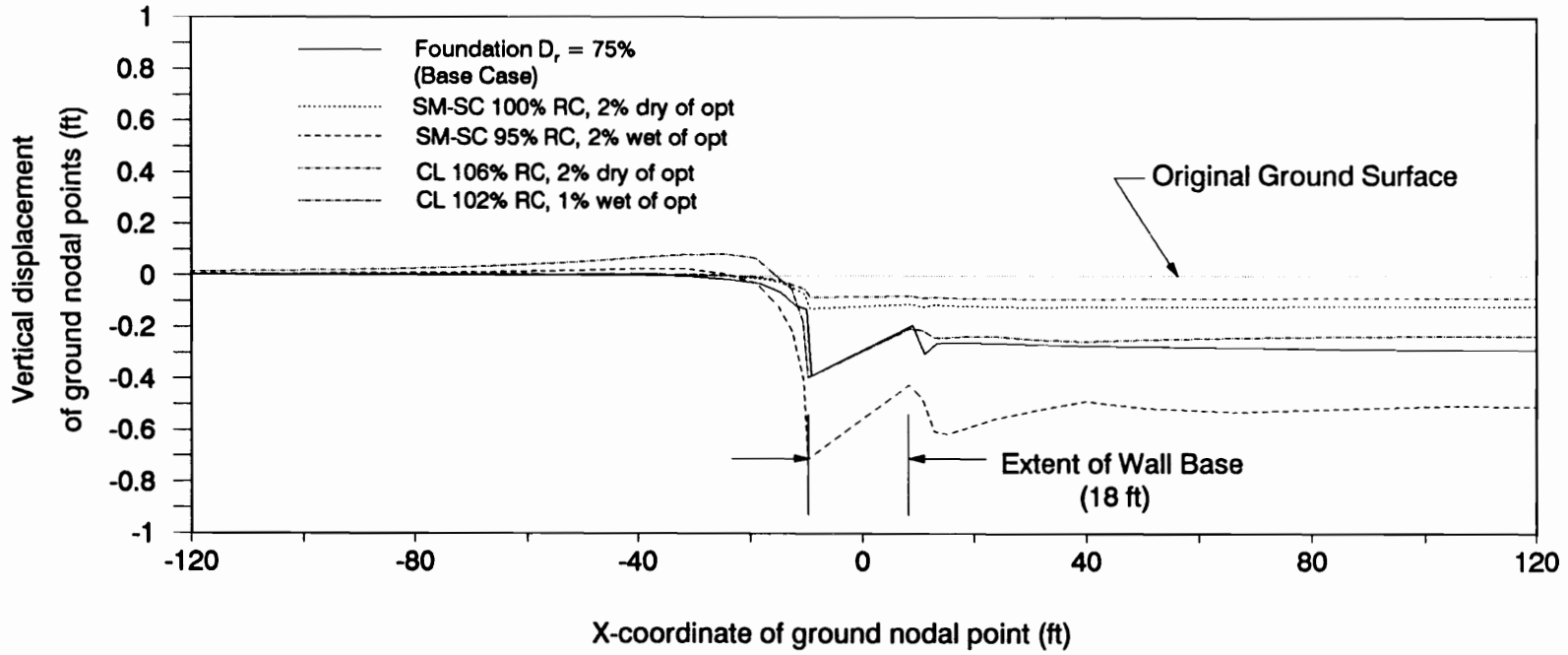

Figure 5.40 - Ground Surface Profiles after Backfilling for Cohesive Foundations with various Relative Compactions and Compaction Water Contents

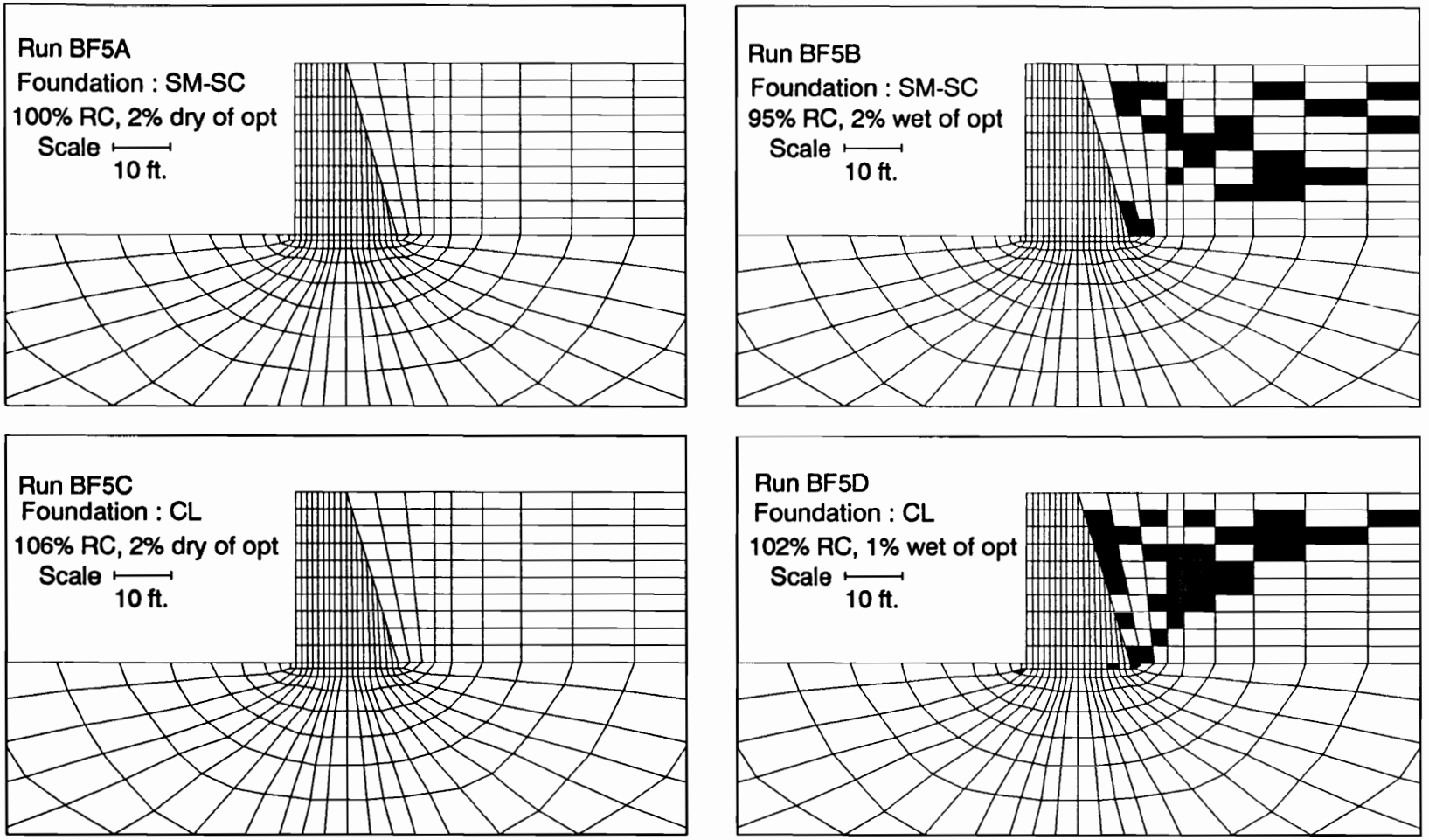

Figure 5.41 - Failure Regions within the Foundation and Backfill - Cohesive Foundation Soils with different Relative Compactions and Compaction Water Contents

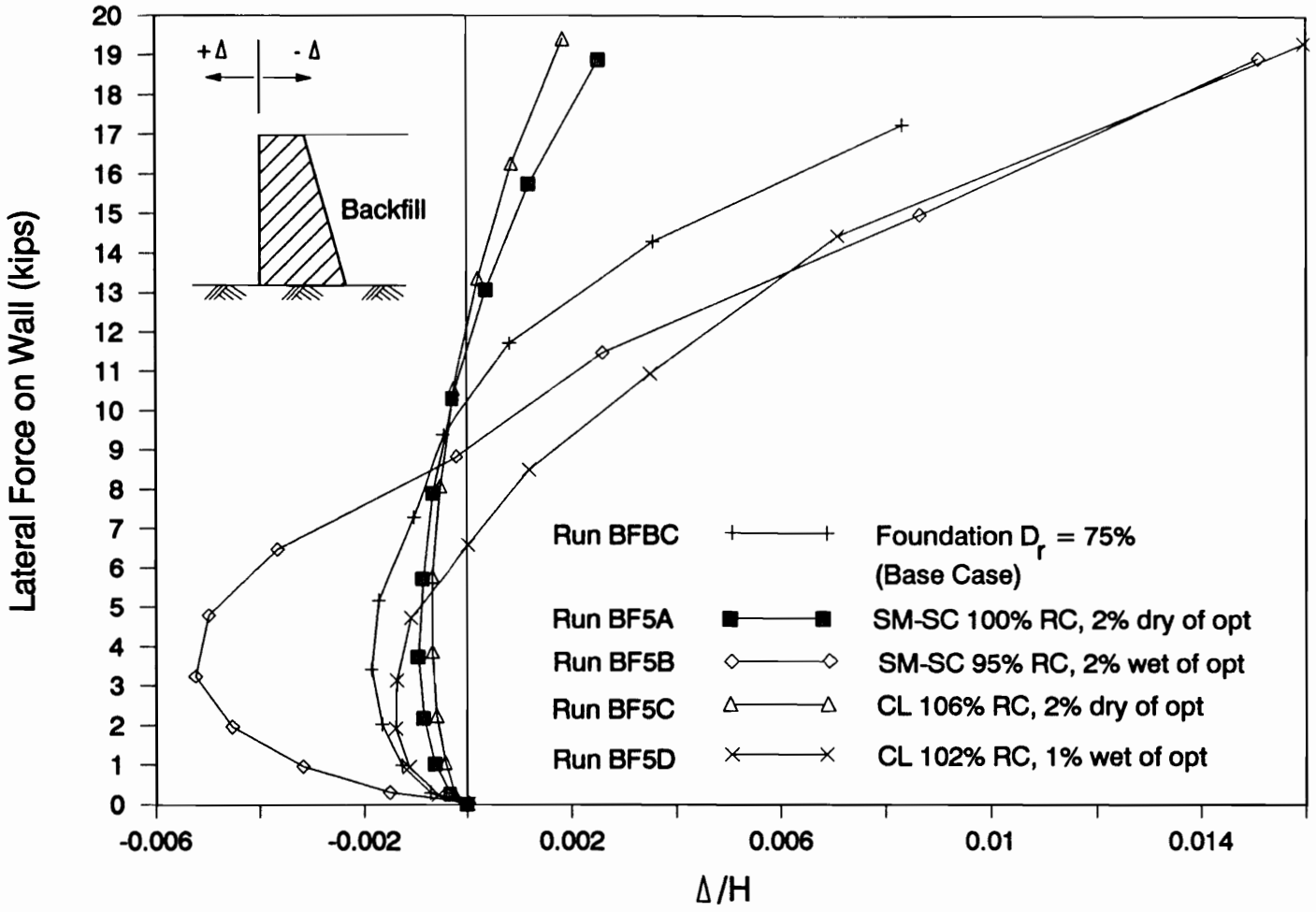

Figure 5.42 - Variation of Normalized Wall Displacements with the Lateral Earth Force on the wall - Cohesive Foundation Soils

more severe tilt in this case. Recall that in the base case analysis, Δ/H was equal to 0.008, a value which does not differ significantly from those resulting from Runs BF5B and BF5D. On the other hand, the soils compacted on the dry side were stiffer and resulted in smaller settlements. The wall displacements were also smaller : Δ/H equals 0.003 for Run BF5A and Δ/H equals 0.002 for Run BF5C.

The forces on the key planes are summarized in Table 5.11. Note that the *EPI*'s indicates a very similar level of soil-structure interaction for all four cases. There was only a 9% percentage difference between the *EPI*'s of the dry and wet SM-SC foundations and only an 11% percentage difference between the *EPI*'s of the dry and wet CL foundations. The shear force coefficient $K_v{}^{AA}$ varied slightly from 0.08 to 0.10. The $K_v{}^{AA}$ and $K_h{}^{AA}$ values for the cases involving cohesive foundations were consistently greater than the base case values and those obtained from similar cases involving cohesionless foundations.

The base stresses given in Fig. 5.43 show that all four analyses yielded very similar normal and shear stress distributions. Again, stress concentrations occurred near the toe because there was no extensive foundation soil failure. B_e/B was equal to 95 percent in all four cases.

The conclusion that may be drawn from this set of analyses is that if the problems of consolidation, creep and heave have been addressed, and appropriate compaction procedures are utilized to bring about sufficient strength and stiffness, cohesive soils could be acceptable foundations. The earth pressure indices (*EPI*) indicate lower degrees of soil-structure interaction (higher earth pressures from the backfill) than for the base case involving a sand foundation. Lateral and shear forces generated in the vertical plane through the heel of the wall (plane A-A) were higher than the values for walls on sand. Experience indicates that virtually all problems with retaining walls involve clay backfills, clay foundations, or a combination of both (Duncan, et al., 1990). The failure to model creep and swelling is believed to limit the ability of these analyses to model some of the important aspects of the behavior of clay

Table 5.11 - Forces on Key Planes for various Cohesive Foundation Soils

Note : All forces in pounds, all lengths are in feet

Run No.	BF5A (SM-SC, 100% RC, 2% dry of optimum)	BF5B (SM-SC, 95% RC, 2% wet of optimum)	BF5C (CL, 106% RC 2% dry of optimum)	BF5D (CL, 102% RC 1% wet of optimum)
Plane A-A				
H_{AA}	18,880	18,900	19,400	19,300
V_{AA}	5,840	5,380	5,900	6,800
Y_{AA}	10.12	10.65	10.12	11.88
K_h	0.30	0.30	0.31	0.31
K_v	0.09	0.08	0.09	0.10
EPI	0.49	0.45	0.42	0.38
Plane B-B				
H_{BB}	23,450	22,900	23,300	22,530
V_{BB}	50	185	40	150
Y_{BB}	9.99	10.07	9.92	10.02
K_h	0.37	0.36	0.37	0.36
K_v	0.00	0.00	0.00	0.00
Plane C-C				
N_{CC}	24,880	24,830	25,440	25,560
T_{CC}	17,200	16,980	17,300	18,030
l_{CC}	10.9	11.3	10.9	11.9
l_{CC}/l	0.35	0.36	0.35	0.38
$\delta_{mob} / \phi_{backfill}$	0.89	0.88	0.88	0.90
Plane D-D				
N_{DD}	84,370	84,140	84,640	85,360
T_{DD}	17,200	17,000	17,300	18,000
X_{DD}	6.9	6.7	6.8	6.6
X_{DD}/B	0.38	0.37	0.38	0.37

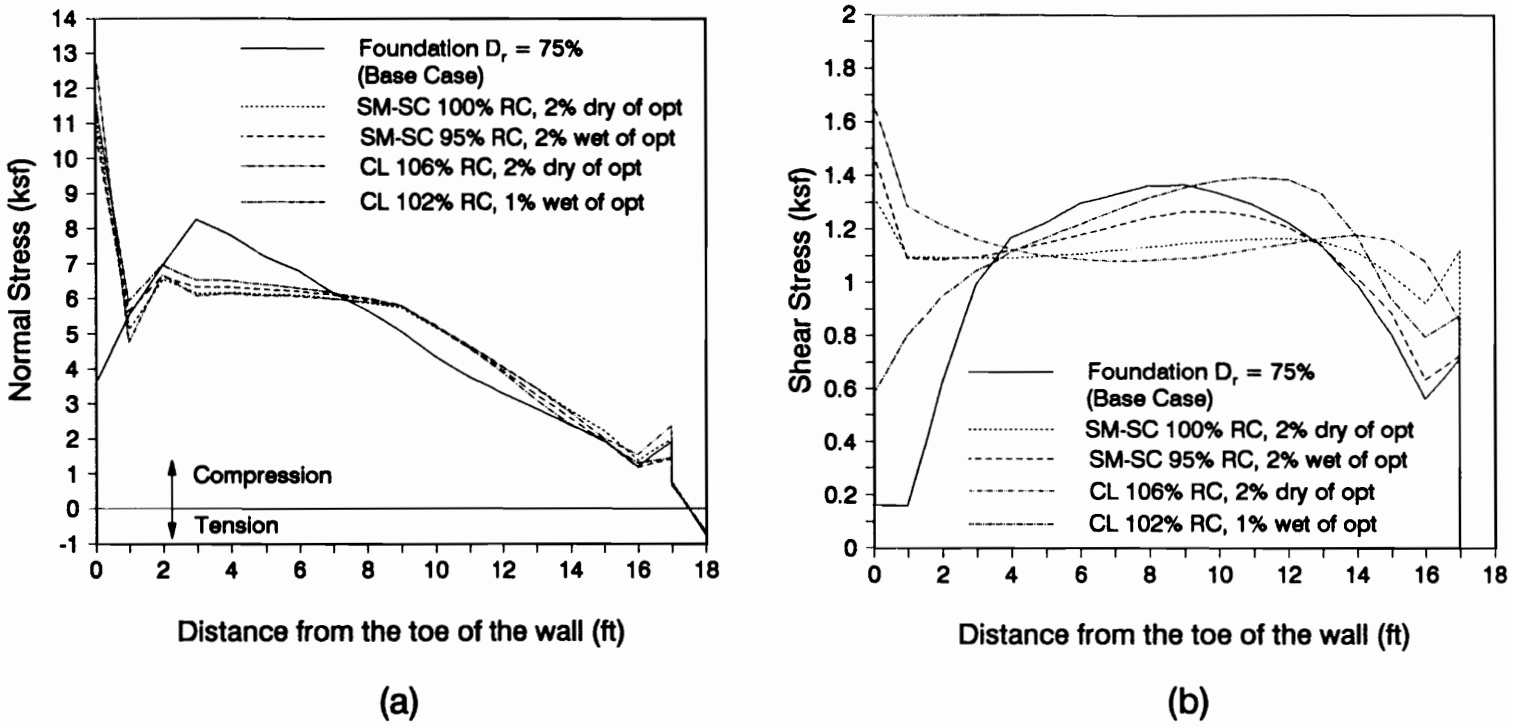

Figure 5.43 - Base Stresses After Backfilling for Cohesive Foundations with various Relative Compactions and Compaction Water Contents

foundations.

EFFECTS OF UTILIZING A COHESIVE BACKFILL

This series of analyses focuses on the effects of using a cohesive backfill. Four analyses were performed, with each analysis utilizing one of the four cohesive soils described in the previous section. As with the analyses in the previous section, the problems of creep, consolidation and heave are not addressed.

Fig. 5.44 shows the failure regions resulting from the four analyses. Note that there is no element in the backfill that is in a state of failure in any of the cases. Equally interesting is the fact that the failure regions within the foundation in all four cases are less extensive than the failure region resulting from the base case analysis (see, for example, Fig. 5.7) where a sand backfill was used. This is especially notable in the heel area. This indicates that a backfill with sufficient strength and stiffness to keep internal failure from developing improves the stability of the foundation soil as well.

The ground surface profiles for the four analyses, together with the base case results, are shown in Fig. 5.45. The settlements that occurred beyond the heel of the became smaller as the unit weight of the backfill used in the analysis decreased. Improved foundation stability from the use of cohesive backfills also led to more uniform wall settlements and less severe wall tilts than those that resulted from the base case analysis.

H_{AA} versus Δ/H plots for all four cases as well as for the base case are given in Fig. 5.46. Note that larger lateral forces and wall displacements developed when the cohesive backfill is compacted wet of optimum. In fact, with the cohesive backfills compacted dry of optimum, the wall tilted toward the backfill. The normalized crest displacements for backfills compacted

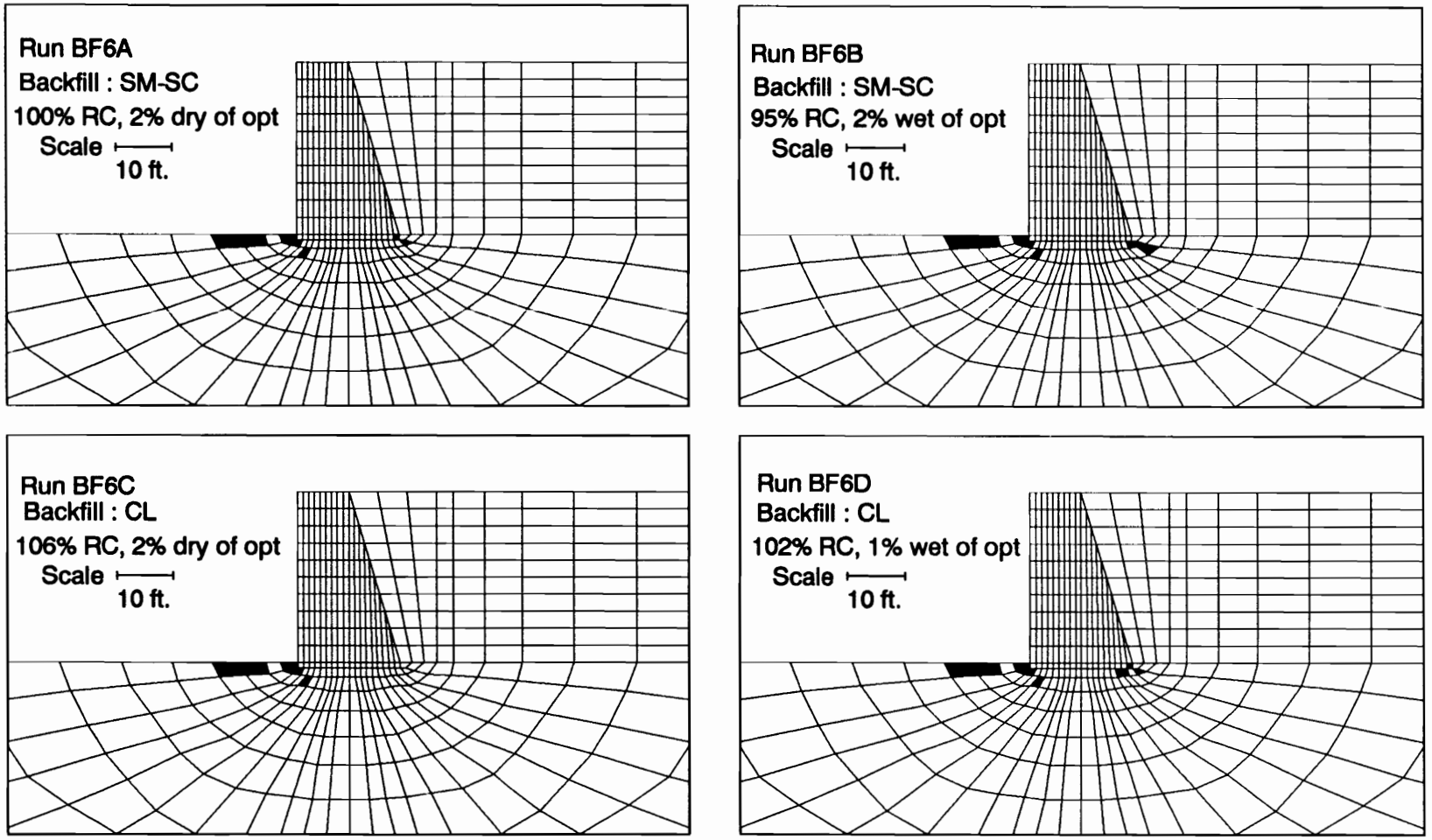

Figure 5.44 - Failure Regions within the Foundation and Backfill - Cohesive Backfills with different Relative Compactions and Compaction Water Contents

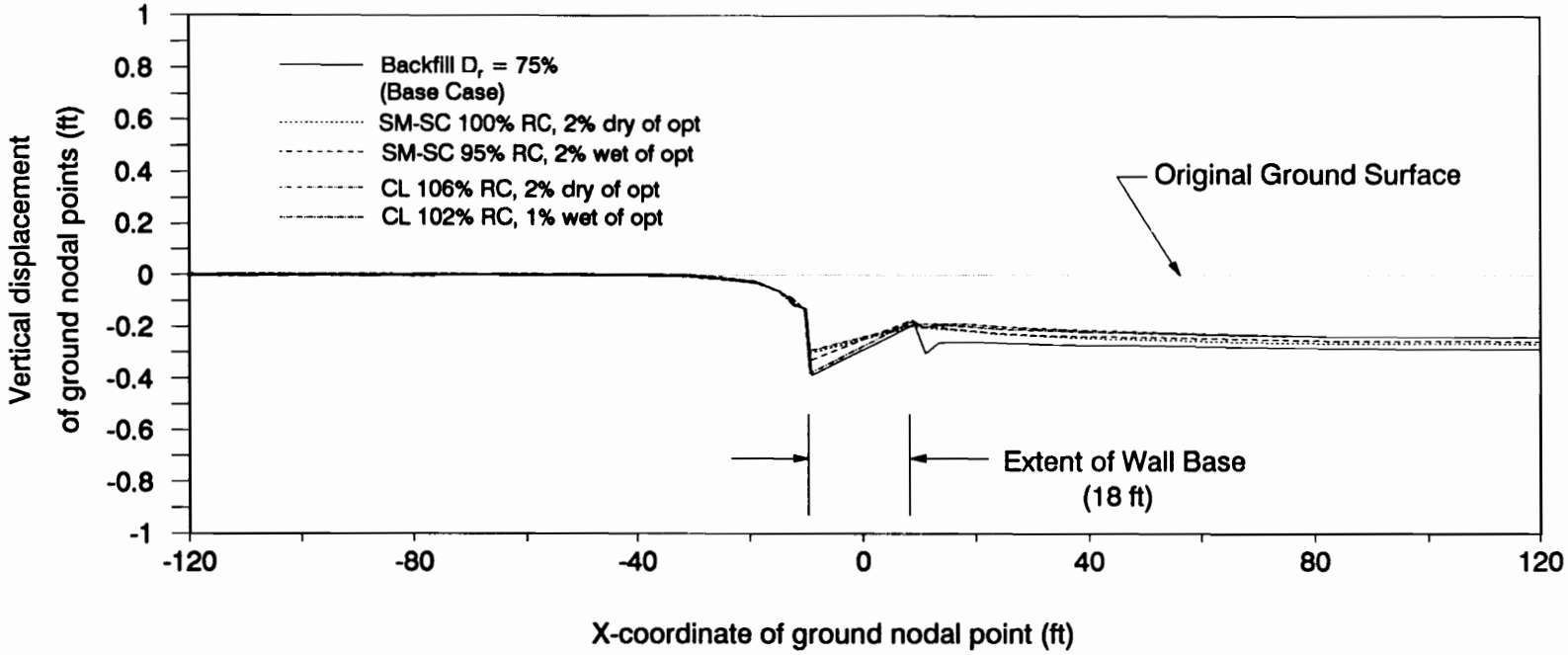

Figure 5.45 - Ground Surface Profiles after Backfilling for Cohesive Backfills with various Relative Compactions and Compaction Water Contents

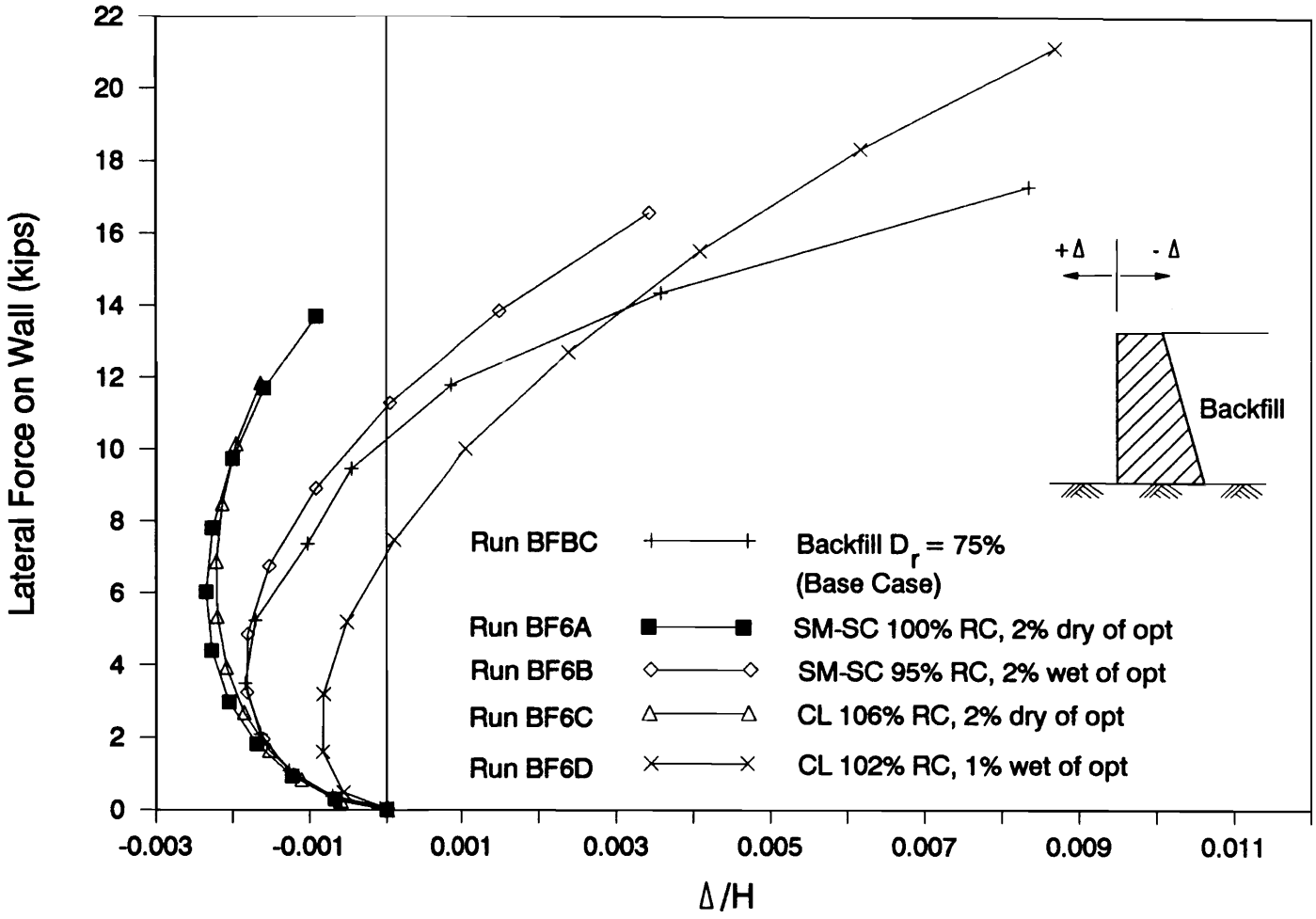

Figure 5.46 - Variation of Normalized Wall Displacements with the Lateral Earth Force on the Wall - Cohesive Backfills

wet of optimum were as follows : Δ/H was equal to 0.003 for Run BF6B and Δ/H was equal to 0.009 for Run BF6D. In both cases, the wall moved away from the backfill. For the backfills compacted dry of optimum, the Δ/H values were: -0.001 for Run BF6A and -0.002 for Run BF6C. These values were for movements toward the backfill.

The forces on the key planes are summarized in Table 5.12. Because of the nonzero cohesion intercept, there is a difficulty in evaluating K_A for use in the formula for EPI given in Equation 5.3. For this reason, no EPI values were given.

The ${K_h}^{AA}$ values for the backfills compacted dry of optimum were both equal to 0.23. For the backfills compacted wet of optimum, the ${K_h}^{AA}$ values were 0.29 for the SM-SC backfill and 0.43 for the CL backfill. The relatively high ${K_h}^{AA}$ value for the wet CL backfill was mainly due to the large lateral force in this case but was also influenced by the low γ_s of the soil. The ${K_v}^{AA}$-values varied from 0.16 to 0.22, the highest value obtained in the case utilizing the "wet" CL backfill.

In the far end of the soil backfill, plane B-B, the same trend was observed in the value of ${K_h}^{BB}$. The less tiff, "wet" soils exerted greater lateral forces than their "dry" counterparts.

The normal and shear stress distributions for the cases utilizing cohesive backfills are plotted in Fig. 5.47. For comparison, the stress distributions from the base case analysis are included. The base stresses are more nearly uniform for the cohesive soils than for the base case. This was especially true for the normal stresses, where the locations of the resultants, defined by X_{DD}/B, varied from 0.41 to 0.46 for the four cases. These locations are all closer to the center of the wall base than the base case result of 0.37. Note also that the distributions from using the "dry" backfills were "more uniform" than their wet backfill counterparts.

Of the four analyses involving cohesive backfills, Run BF6D probably comes closest to representing actual field behavior, considering how creep in a cohesive backfill influences behavior. Because of creep, the strength of cohesive soils cannot be relied upon permanently.

Table 5.12 - Forces on Key Planes for various Cohesive Backfill Soils

Note : All forces in pounds, all lengths are in feet

Run No.	BF6A (SM-SC, 100% RC, 2% dry of optimum)	BF6B (SM-SC, 95% RC, 2% wet of optimum)	BF6C (CL, 106% RC 2% dry of optimum)	BF6D (CL, 102% RC 1% wet of optimum)
Plane A-A				
H_{AA}	13,690	16,550	11,860	21,110
V_{AA}	9,465	9,240	9,115	10,750
Y_{AA}	9.68	10.58	9.30	8.61
K_h	0.23	0.29	0.23	0.43
K_v	0.16	0.16	0.18	0.22
Plane B-B				
H_{BB}	23,720	25,760	21,360	34,610
V_{BB}	80	40	45	110
Y_{BB}	9.84	9.88	9.59	10.05
K_h	0.41	0.46	0.41	0.70
K_v	0.00	0.00	0.00	0.00
Plane C-C				
N_{CC}	20,530	23,200	18,140	27,740
T_{CC}	20,790	19,720	19,190	19,010
l_{CC}	9.2	9.9	8.8	9.5
l_{CC}/l	0.29	0.32	0.26	0.30
Plane D-D				
N_{DD}	86,565	86,310	84,350	86,930
T_{DD}	13,690	16,540	11,860	21,110
X_{DD}	8.1	7.6	8.2	7.3
X_{DD}/B	0.45	0.42	0.46	0.41
$\delta_{mob} / \phi_{foundation}$	0.23	0.28	0.21	0.35

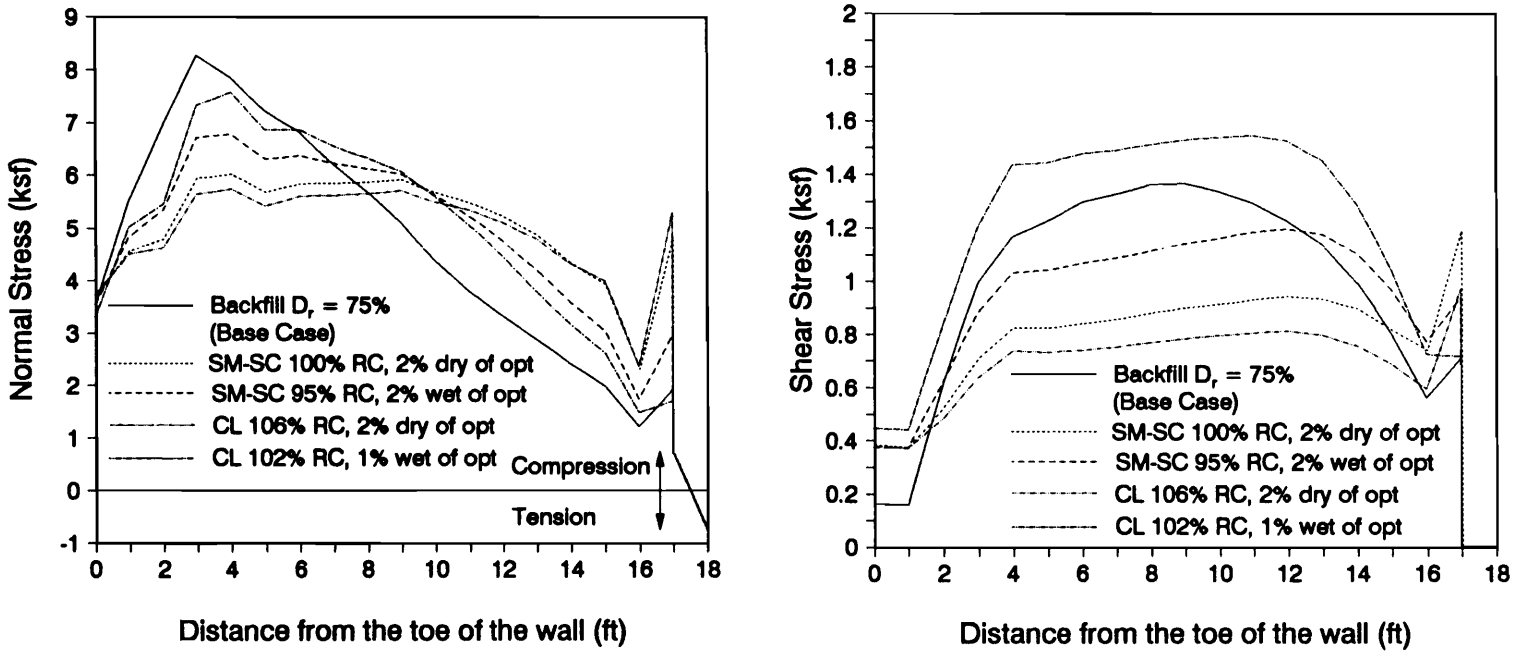

Figure 5.47 - Base Stresses After Backfilling for Cohesive Backfills with various Relative Compactions and Compaction Water Contents

As a result, design earth pressures used for cohesive backfills are higher than active. These higher design pressures are based on "equivalent fluid" unit weights which, in the case of clays of low plasticity, range from 45 to 50 pcf. For γ_s equal to 110 pcf, this would correspond to a value of K_h equal to 0.45.

SUMMARY

The primary objective in performing the analyses presented in this chapter was to examine the factors that affect the stability of gravity retaining walls on soil, considering soil-structure interaction effects. For this purpose, the backfill placement method of analysis was utilized.

Analyses of a base case problem using both the following load and the backfill placement methods reveal that the use of the following load method yields more conservative results than the backfill placement method. The results of the backfill placement analysis further confirmed a conclusion made earlier that the critical mode of failure for walls on soil would be bearing capacity failure of the foundation rather than overturning or sliding.

Parameters that describe the wall-foundation system were varied systematically in the analyses. These analyses confirm the existence of a shear force on the vertical plane in the backfill passing through the heel of the wall. This vertical force and its corresponding shear force coefficient, K_v, were found to depend on the properties of the foundation and the backfill. The magnitude of wall tilt, the uniformity of ground settlements, and the stiffness and strength of the backfill soil all affect the K_v value. Generally, for cohesionless backfills, K_v is about 0.07 or higher for stable walls on soil. Cohesive backfills yield K_v values of 0.15 or higher but the

long-term presence of the corresponding shear force is questionable because of possible creep strength loss.

The value of $K_h{}^{AA}$ is generally lower for walls on soil than the $K_h{}^{AA}$ values for similar systems founded on rock. Ebeling et al (1988) found that, in most cases, $K_h{}^{AA}$ for walls on rock correspond to an EPI of not more than 0.25. $K_h{}^{AA}$ values for walls on soil correspond to an EPI no greater than 0.50 for walls that are stable and no greater than 0.80 for walls that are in a near-unstable condition. Bearing capacity failure in the foundation would occur before the system reaches an active state.

On plane C-C, the wall-backfill interface, the mobilized friction angle for sand backfills corresponded to a ratio of $\delta_{mob}/\Phi_{backfill}$ ranging from 0.86 to 0.9 5. In all of the analyses, the maximum friction angle of the sand-concrete interface, δ, was equal to $0.85*\Phi_{backfill}$. The results therefore indicate that enough relative slip took place to generate forces that correspond to mobilized friction angles greater than the strength. This condition was true regardless of the degree of stability of the wall, although the lower values of $\delta_{mob}/\Phi_{backfill}$ were obtained for the "more stable" systems. It can be concluded that for walls on soil utilizing a sand backfill, severe slip along the backfill-wall interface is inevitable due to the tendency of the wall to tilt and the tendency of the ground behind the wall to settle.

In all of the stable cases, X_{DD}, which defines the line of action of the normal force on the base, N_{DD}, is within the middle third of the base. These results satisfy current Corps of Engineers standards for overturning. Furthermore, these results are conservative, considering that in the analyses, there is usually a 5 percent base separation in the vicinity of the heel because of the manner in which the base pressure due to wall buildup was specified.

Unlike walls on rock, the maximum normal stress for walls on soil usually does not occur at the toe. Failure of foundation soil elements in the toe area results in a stress redistribution which moves the maximum normal stress closer to the center of the base. Cases when the

maximum did occur at the toe are the analyses where either a toe fill was present or the wall was built on a cohesive backfill. In these cases, there was sufficient strength and stiffness at the toe area for the maximum normal stress to occur there. The normal stress distribution tends to be more uniform as the wall aspect ratio B/H increases, with all other parameters held constant. The shear stress distribution, on the other hand, is approximately uniform for all stable cases analyzed.

Although results of analyses involving cohesive soils indicate that they can be good backfill or foundation material, these results are, at best, still inconclusive. As previously mentioned, experience indicates that all retaining wall problems involve clay backfills, clay foundations or both. Creep and swelling in cohesive soils represent important aspects in its behavior, and failure to model these phenomena may lead to unrealistic results.

CHAPTER 6

ANALYSES OF CANTILEVER AND STEPPED-FACE RETAINING WALLS FOUNDED ON SOIL USING THE BACKFILL PLACEMENT METHOD

INTRODUCTION

This chapter presents the results of analyses performed to investigate the behavior of walls with various shapes. Two types of walls were considered : cantilever walls and stepped-face walls. The backfill placement method discussed in Chapter 5 was utilized in the analyses of these walls. The material and loading parameters were the same as those used in the backfill placement base case analysis designated as Run BFBC in Chapter 5.

HYPOTHETICAL STRUCTURES AND LOADING CONDITIONS USED

A. CANTILEVER WALLS

The parameters that characterize the cantilever wall-soil system are shown in Fig. 6.1 and are summarized in Table 6.1. The material parameters that describe the foundation, backfill, wall and interface elements are constant for all analyses and are the same as those used in the base case backfill placement analysis in Chapter 5. The shape of the cantilever wall is defined by the following dimensions:

B = width of base slab

H = overall height of the wall

t_b = thickness of the base slab

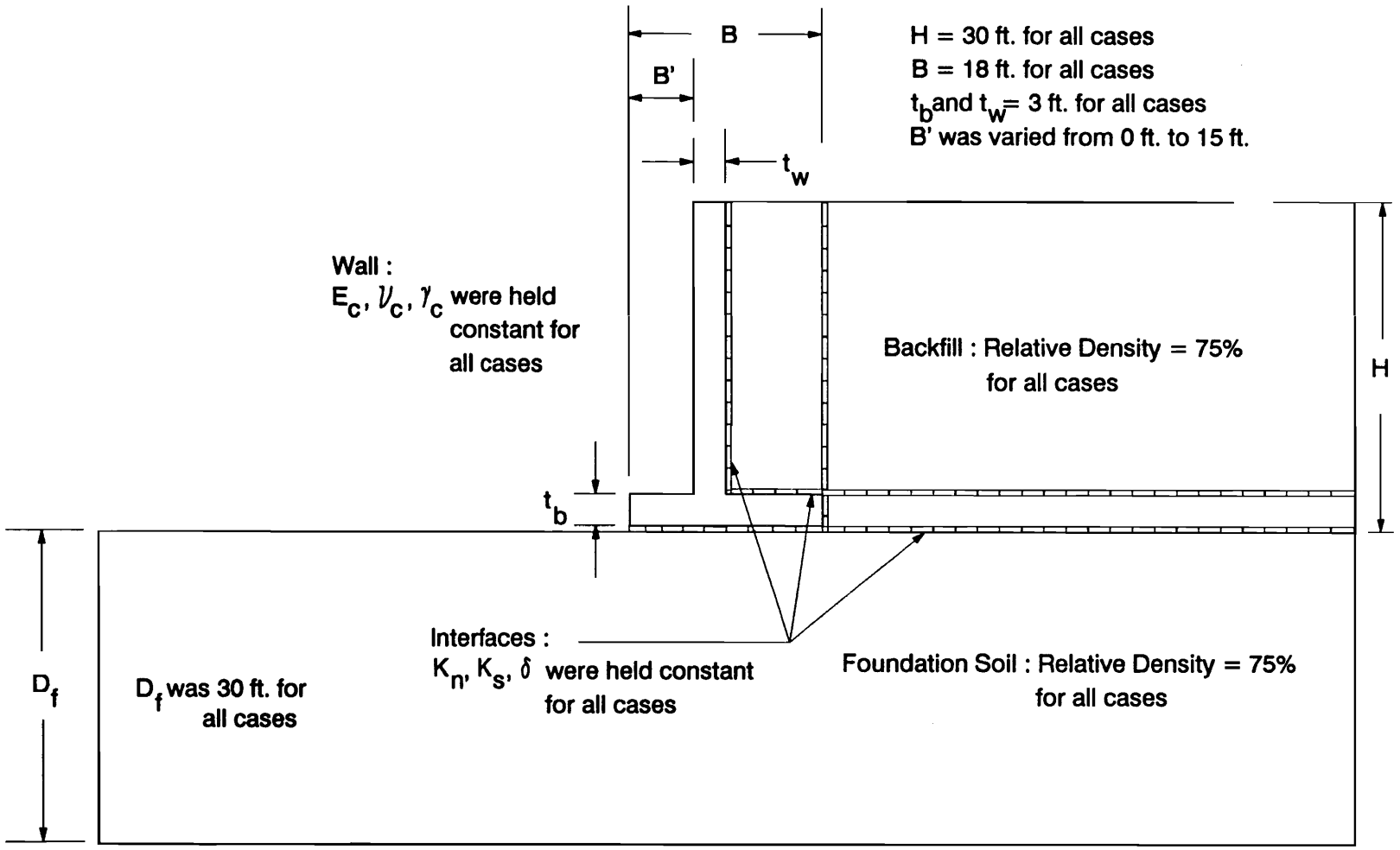

Figure 6.1 - Hypothetical Wall-Foundation System used for Backfill Placement Analyses of Cantilever Retaining Walls

Table 6.1 - Parameter Values used in the Backfill Placement Analyses of Cantilever and Stepped-face Walls

Constant Parameters

Geometric

- H = Overall height of the wall = 30 feet
- B/H = Ratio of width of base of wall to the height of wall = 0.6
- t_b/H = Ratio of the thickness of the base slab to the height of the wall = 0.1 (cantilever walls only)
- t_w/H = Ratio of the thickness of the wall stem to the height of the wall = 0.1 (cantilever walls only)

Material

- K_n = Normal stiffness of wall-base interface elements = 5.18×10^9 pcf
- K_s = Shear stiffness of wall-base interface elements = 5.18×10^9 pcf
- γ_c = Unit weight of concrete = 150 pcf
- E_c = Modulus of elasticity of concrete = 4.3×10^8 pcf
- ν_c = Poisson's ratio of concrete = 0.20
- D_r = Relative density for cohesionless backfill/ foundation soils = 75 %

Variable Parameters

Geometric

- B' = Length of toe projection (Cantilever Walls only)
- n_s = Number of "steps" on wall face (Stepped-face walls only)

Run No.	B'(ft)	n_s	Comments
BF7A	0	-	Cantilever Wall; B'/B = 0.00
BF7B	3	-	Cantilever Wall; B'/B = 0.17
BF7C	6	-	Cantilever Wall; B'/B = 0.33
BF7D	9	-	Cantilever Wall; B'/B = 0.50
BF7E	12	-	Cantilever Wall; B'/B = 0.67
BF7F	15	-	Cantilever Wall; B'/B = 0.83
BF8A	-	2	Stepped-face Wall; n_s = 2
BF8B	-	5	Stepped-face Wall; n_s = 5
BF8C	-	10	Stepped-face Wall; n_s = 10

B'= length of the toe projection

t_w=thickness of the wall stem

The aspect ratio B/H is constant and equal to 0.60 for all analyses. The thicknesses of the wall stem and base slab are both equal to $H/10$ and are uniform along their entire lengths. The toe projection B' is the only dimension varied in the analyses.

Interface elements were placed on the wall-backfill, wall-foundation and backfill-foundation interfaces. Connectivity requirements within the mesh led to extending some rows of interface elements into the backfill.

A typical finite element mesh for the cantilever wall analyses is shown in Fig. 6.2. The number of elements and nodes vary depending on the geometry of the wall. The mesh is designed so the buildup of either the wall or the backfill may be accomplished in ten (10) construction steps, using ten 3 foot thick lifts.

The "pressure buildup" method described in Chapters 2 and 4 is a method for simulating construction of a retaining wall by applying a pressure distribution on the wall base-foundation interface. In this approach the vertical pressure applied at any point on the base is proportional to the height of the wall directly above this particular point. Notably, use of the pressure buildup method in this problem in its "pure" form would lead to extremely high gradients in the base pressure distribution near the wall extremities. Such conditions would not be present in reality because of soil-structure interaction effects. To minimize this effect, a combination of the pressure buildup and the "element buildup" method described in Chapter 2 was used for the wall construction simulation. In this combination, the pressure buildup method was used to simulate the construction of the base slab only. The construction of the vertical slab was accomplished using the element buildup method. These construction steps are illustrated in Fig. 6.3.

The placement of backfill was accomplished using the same procedure for simulating the

Note : Due to space constraints, not all the symbols that represent the boundary conditions were included

B'/B	2-d Elements	Interface Elements	Nodes
0.00	590	63	711
0.17	572	61	691
0.33	554	59	671
0.50	536	57	651
0.67	518	55	631
0.83	500	33	589

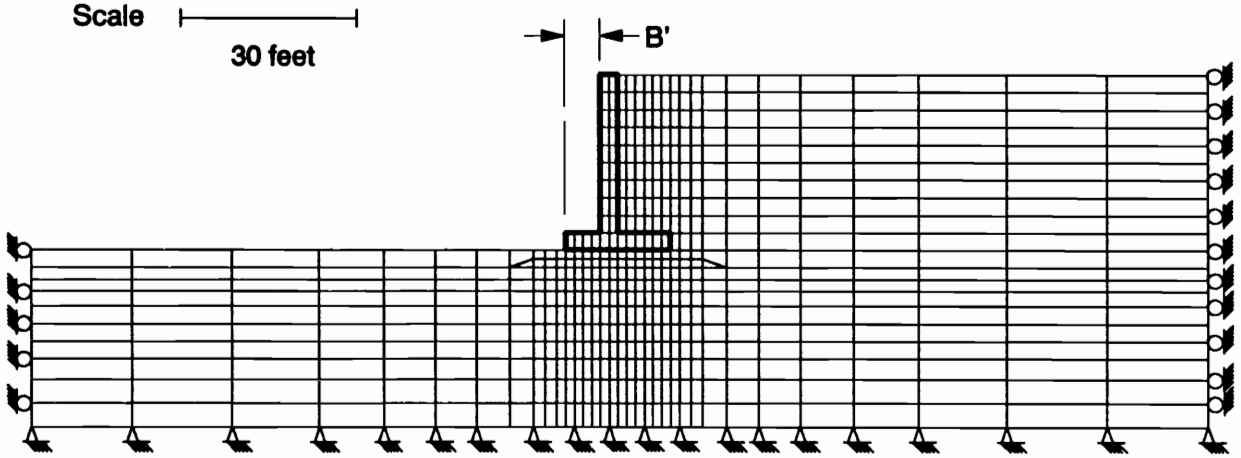

Figure 6.2 - Example of a Finite Element Mesh used in the Analyses of Cantilever Retaining Walls

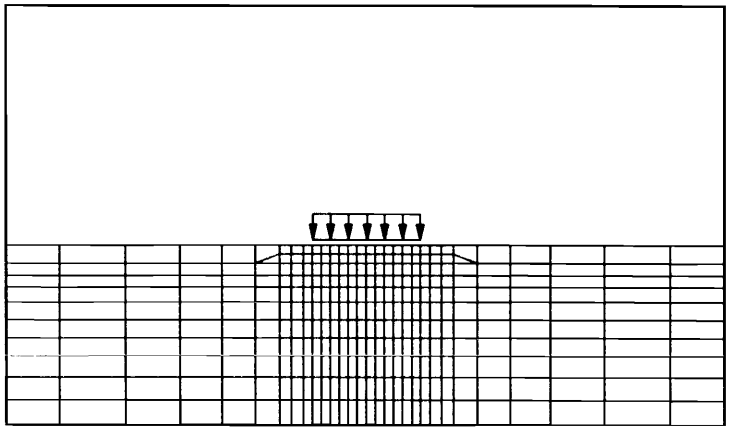

(A) Apply a pressure distribution equivalent to the weight of the base slab

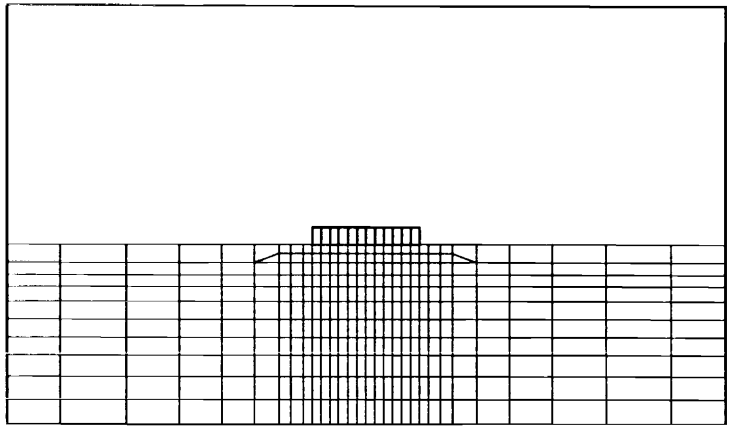

(B) Specify a material type change (from air to concrete) for the elements representing the base slab

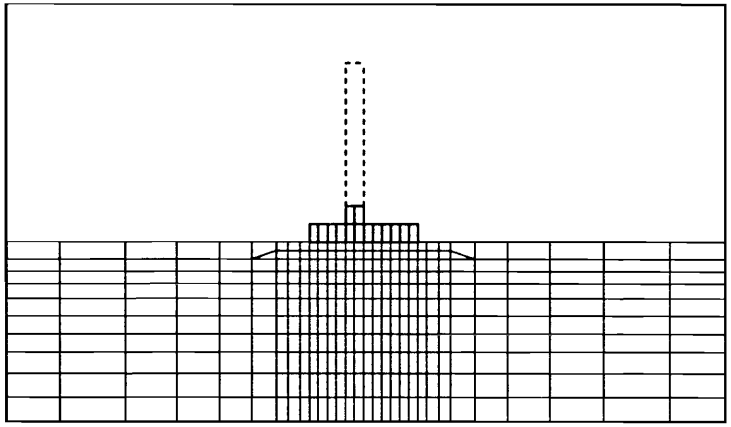

(C) "Place" elements that represent the vertical slab

Figure 6.3 - Cantilever Wall Construction Simulation

backfilling operation described in Chapter 5. In this procedure, the backfill is initially represented by "air elements", and a lift is placed by changing the properties of the elements in that lift from those of air to those of soil.

The geometry of a cantilever wall is such that if it is not properly designed, failure due to bending is possible. The analyses conducted in this report assume that the wall has been designed to provide sufficient strength so as not to be overstressed in bending.

Conventional methods were used to assess the stability of the cantilever wall-soil systems considered in this chapter. Figure 6.4 shows how the factor of safety against sliding varied with the assumed lateral earth pressure coefficient for six cantilever wall geometries. The factor of safety against sliding is given by

$$FS_{sliding} = \frac{tan(\delta)}{tan(\frac{T_{DD}}{N_{DD}})} \tag{6.1}$$

where T_{DD} and N_{DD} are the shear and normal forces acting on the base, and δ is the maximum wall-foundation soil friction angle, assumed to be equal to $0.8*\Phi_{foundation}$. According to Figure 6.4, a wall with B'/B equal to 0.67 may be either safe or unsafe against sliding depending on the value of K_h assumed in the analysis. The wall with B'/B equal to 0.83 has a $FS_{sliding}$ less than unity for any value of K_h greater than K_a.

Figure 6.5 shows the variation of the maximum base normal stress with the assumed lateral earth pressure coefficient for the same six walls. Utilizing the modified Vesic's method discussed in Chapter 3 to compute the ultimate bearing capacity for the worst cases (i.e., K_h equal to 0.28 for B'/B equal to 0.67 and K_h equal to 0.36 for B'/B equal to 0.0, 0.17, 0.33, 0.50), the factor of safety against bearing capacity ranged from 1.6 to 2.2. It was also found that for all stable configurations, B_e/B is equal to 100 percent.

The above results indicate that cantilever walls are more likely to fail by sliding rather

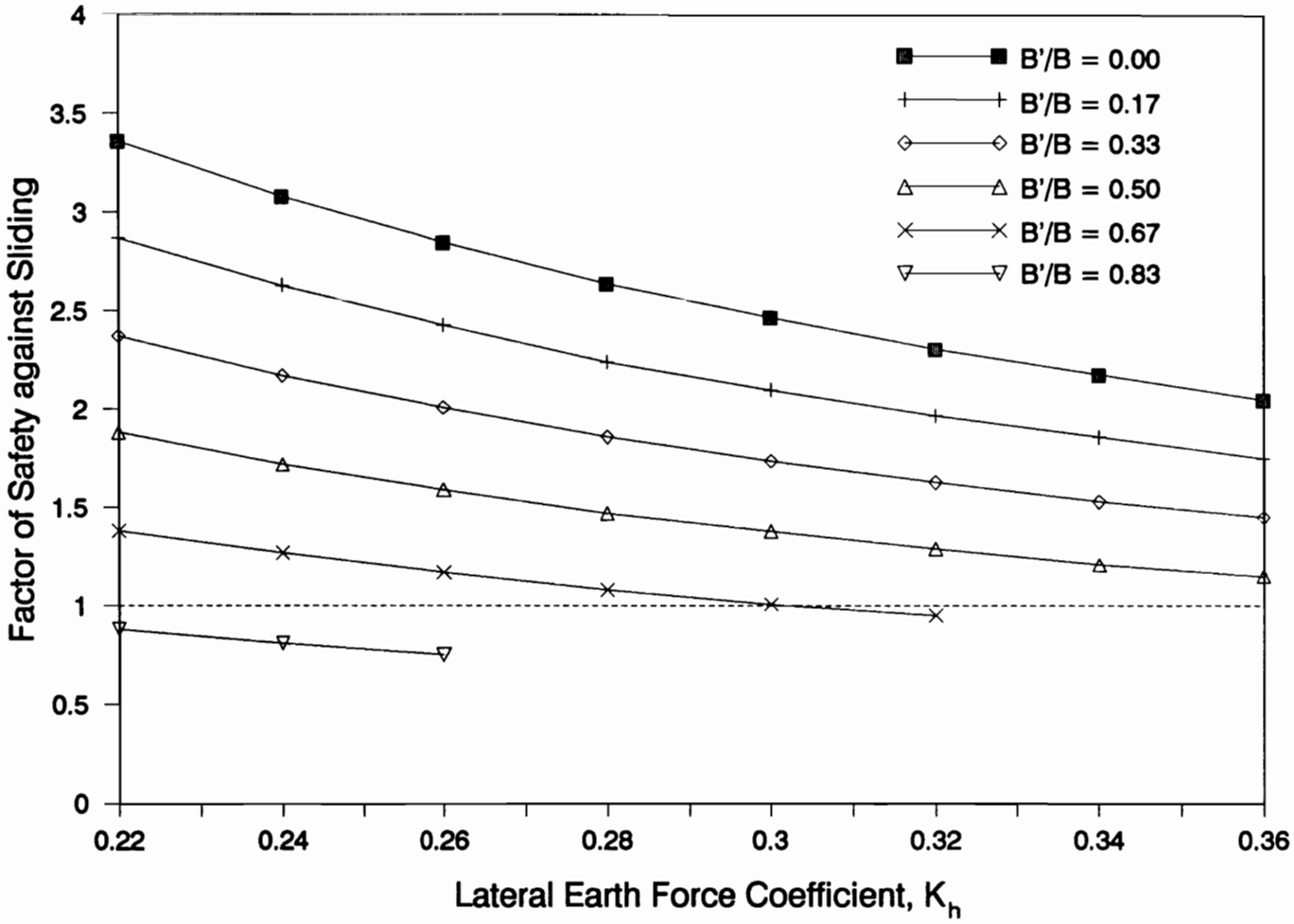

Figure 6.4 - Factor of Safety against Sliding along the Base obtained from Conventional Analyses of Cantilever Walls

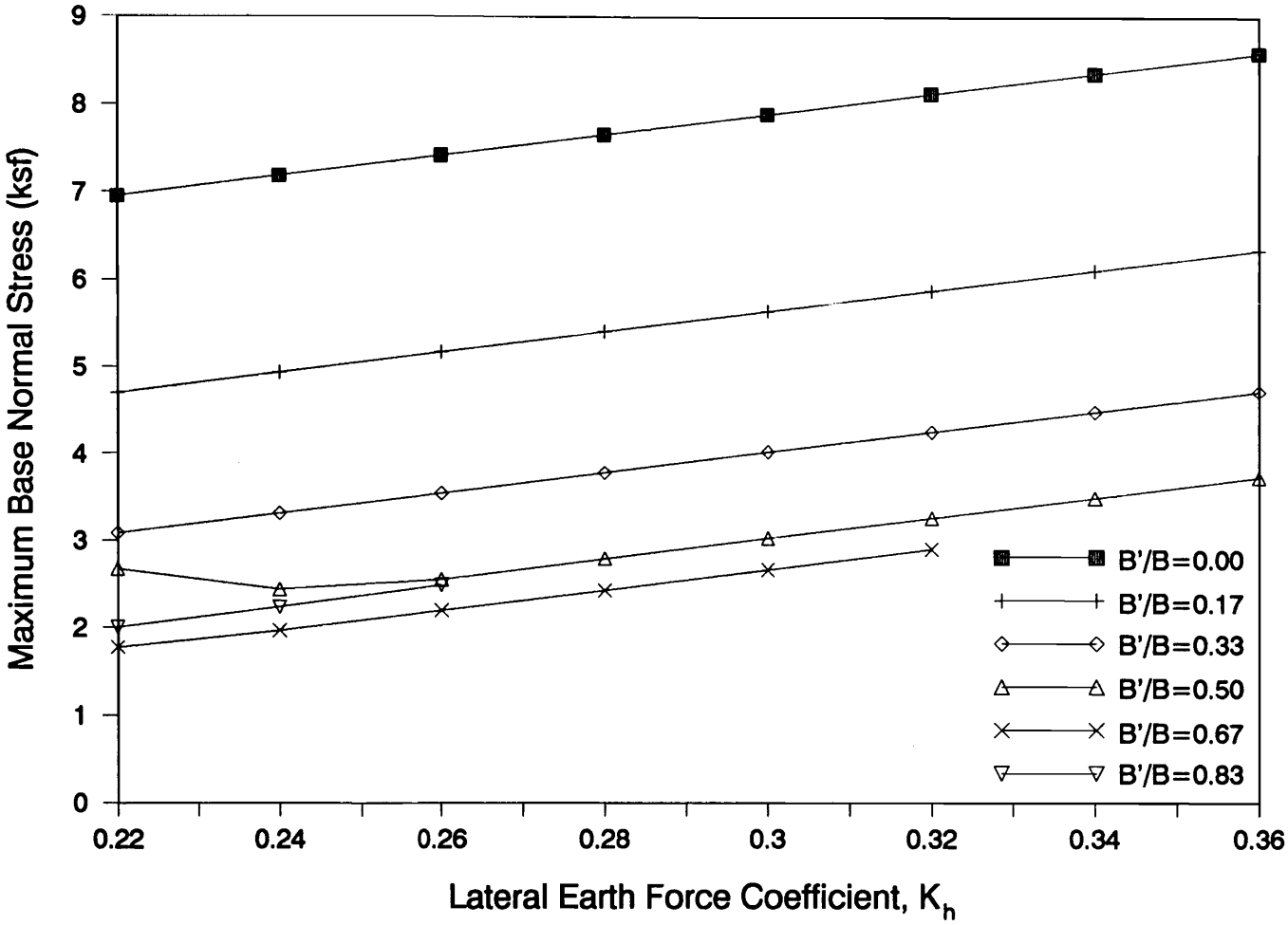

Figure 6.5 - Maximum Normal Stress on the Wall Base obtained from Conventional Analyses of Cantilever Walls

than by bearing capacity.

B. STEPPED-FACE WALLS

Fig. 6.6 shows the parameters that characterize the wall-foundation system for the analyses of stepped-face walls. The values of the material and geometric parameters are listed in Table 6.1. As with the cantilever wall analyses, the material parameters of the different components are constant for this set of analyses. The shape of the stepped-face wall, which is varied in the analyses, is described by the following parameters :

B = width of the base

H = overall height of the wall

n_s = number of "steps"

Again, the ratio B/H is constant and equal to 0.60. The parameter n_s determines the number of "steps" the face of the retaining wall is divided into, as shown in Fig. 6.6. Each "step" has a height equal to H/n_s and a width equal to B/n_s.

An example of a finite element mesh for this set of analyses is given in Fig. 6.7. In this example, n_s is equal to five. As with cantilever walls, the mesh is designed to allow the buildup of either the wall or the backfill to be accomplished in ten (10) construction steps.

Construction of the wall was simulated using the same combination of the pressure buildup and element buildup methods described in the analyses of cantilever retaining walls. Similarly, the method used for simulating backfill placement for the analyses of stepped-face walls is the same as the method used for the cantilever walls.

Conventional design methods indicate that the stepped-face walls analyzed in this chapter are safe against both sliding and bearing capacity failure. The calculated factors of safety against sliding are plotted in Figure 6.8, and it can be seen that $FS_{sliding}$ is at least equal to 2.0. The maximum base normal stress for the same walls are plotted in Figure 6.9. Using the

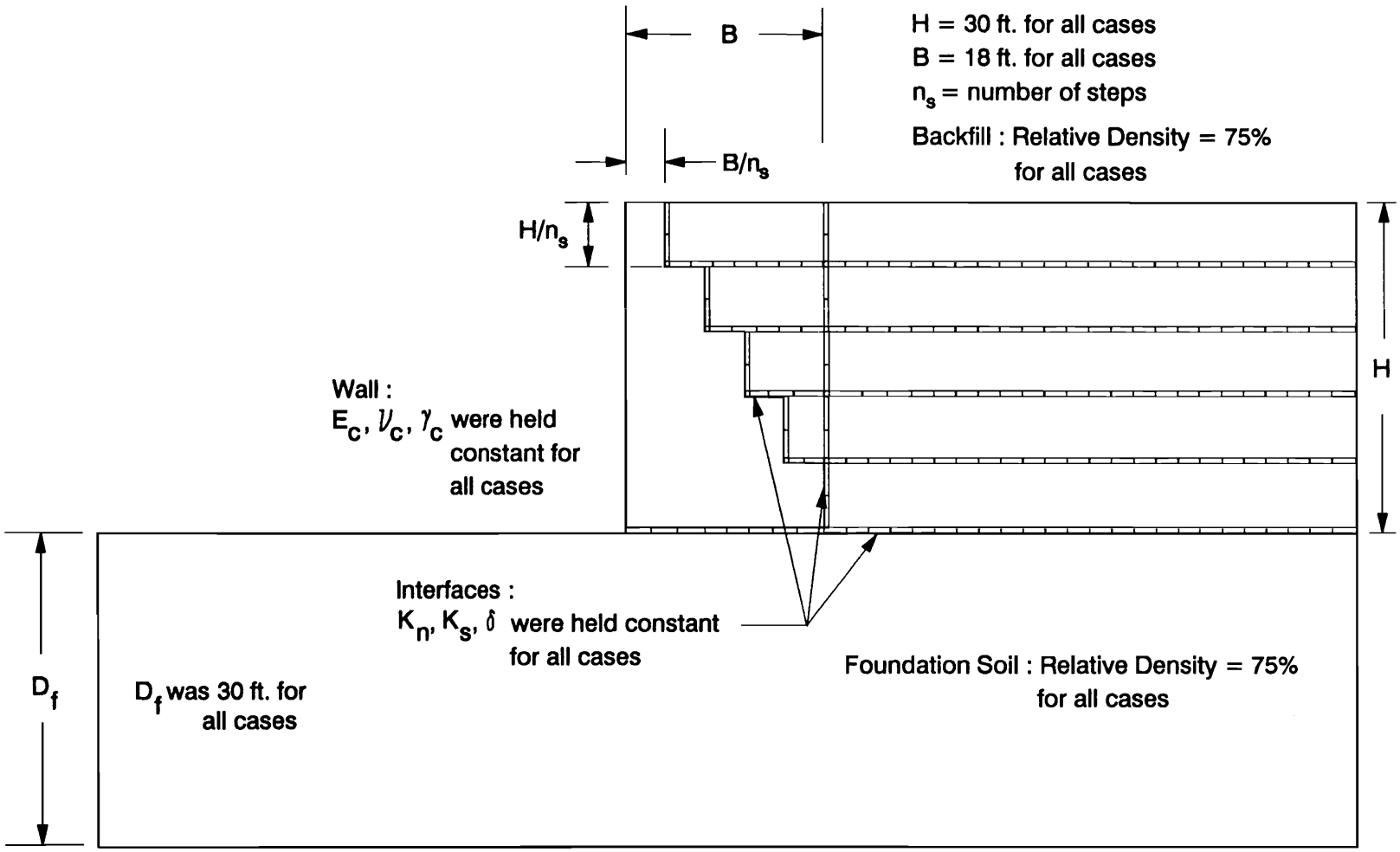

Figure 6.6 - Hypothetical Wall-Foundation System used for Backfill Placement Analyses of Stepped-face Walls

Note : Due to space constraints, not all the symbols that represent the boundary conditions were included

n_s	2-d Elements	Interface Elements	Nodes
2	590	56	704
5	590	125	785
10	590	240	940

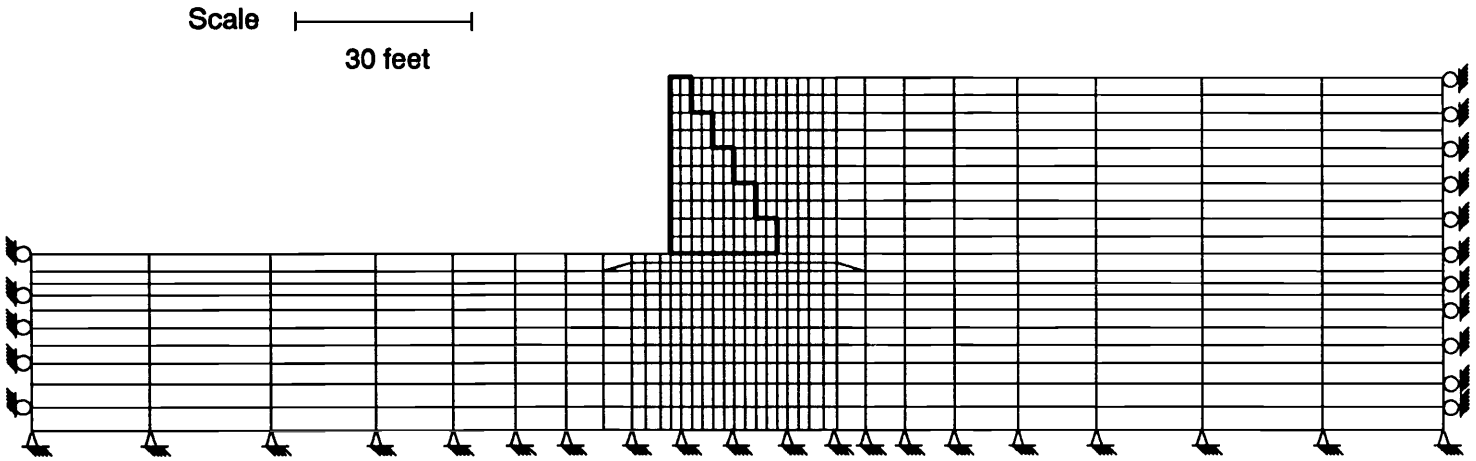

Figure 6.7 - Example of a Finite Element Mesh used in the Analyses of Stepped-face Walls

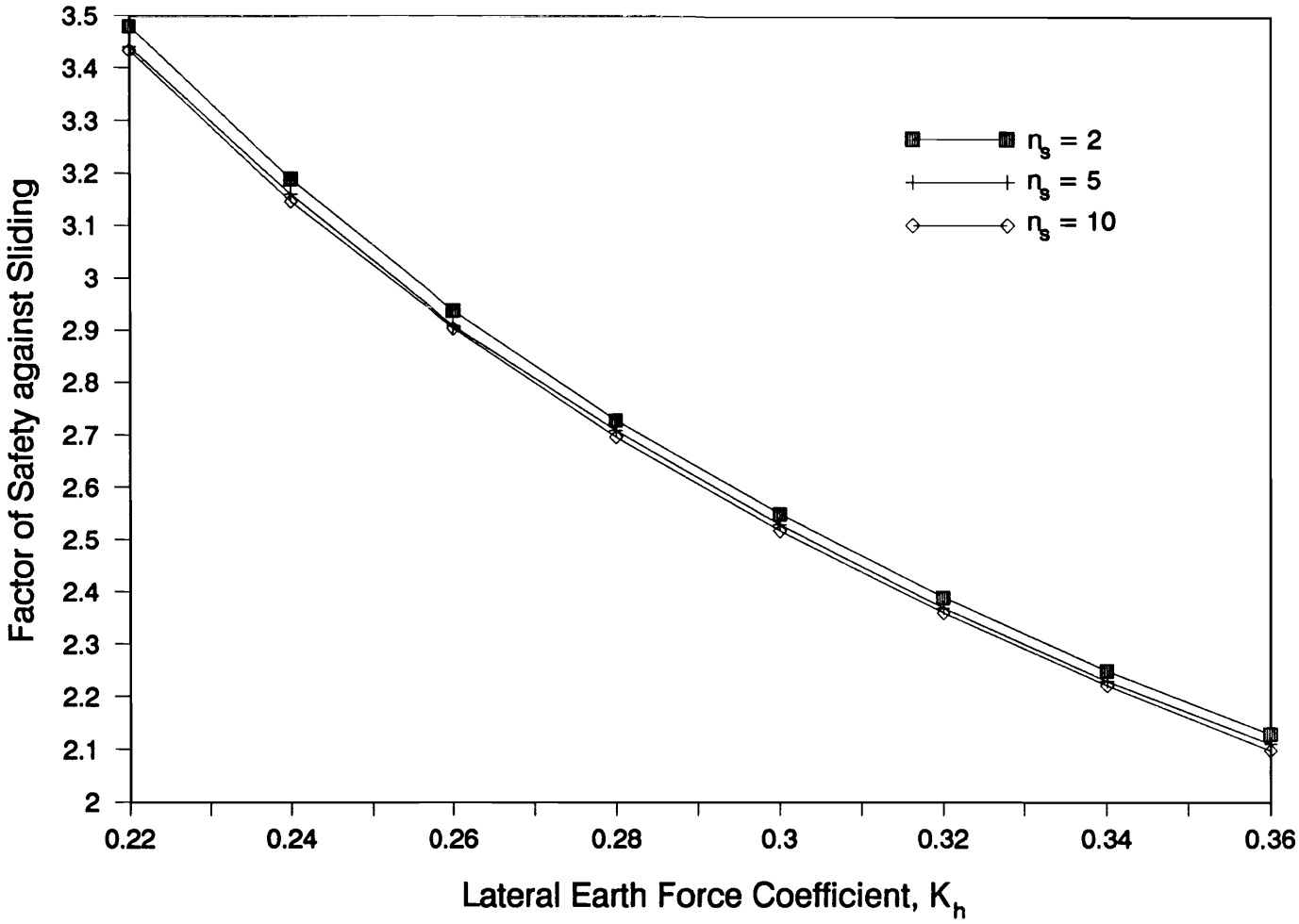

Figure 6.8 - Factor of Safety against Sliding along the Base obtained from Conventional Analyses of Stepped-face Walls

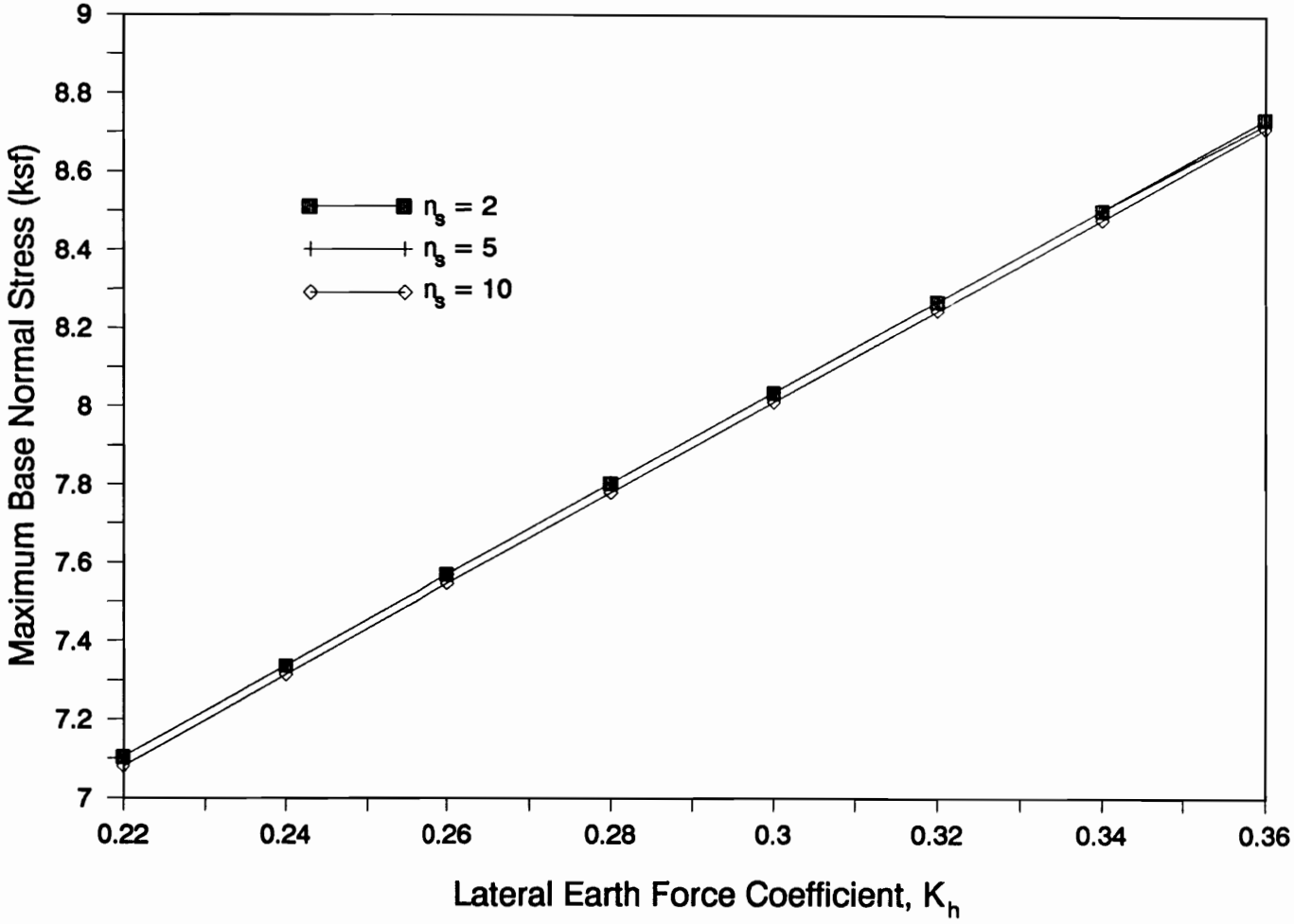

Figure 6.9 - Maximum Normal Stress on the Wall Base obtained from Conventional Analyses of Stepped-face Walls

same approach for calculating the bearing capacity as that used for the cantilever walls, the factor of safety against bearing capacity failure is 2.1 for the three walls.

FORCES ON "KEY" PLANES

In Chapter 5, the term "key" planes was used to refer to planes, either on the surface of the wall or within the backfill, where the stresses are significant in terms of evaluating the response of the wall-foundation system to loading. The locations of these planes for cantilever walls and stepped-face walls are shown in Fig. 6.10 and Fig. 6.11. The names assigned to these planes and the forces that act on them are in accordance with the labels summarized in Table 5.2.

RESULTS OF ANALYSES OF CANTILEVER WALLS

Six analyses were performed on cantilever walls. With all other dimensions of the wall held constant, the length of the toe projection B' was varied from 0 ft. to 15 ft. in 3-foot increments. These values correspond to B'/B ratios equal to 0.00, 0.17, 0.33, 0.50, 0.67 and 0.83. These analyses were designated as BF7A, BF7B, BF7C, BF7D, BF7E and BF7F, respectively.

The variations of the maximum wall displacement, Δ/H, with the lateral earth force, H_{AA}, during backfilling for the six analyses are shown in Fig 6.12. It can be seen that in the initial stages of backfilling the walls move in the direction of the backfill but in the latter stages the walls moves away from the backfill. The maximum wall displacements of the walls with B'/B less than or equal to 0.67 indicate that the geometry of these walls result in a stable

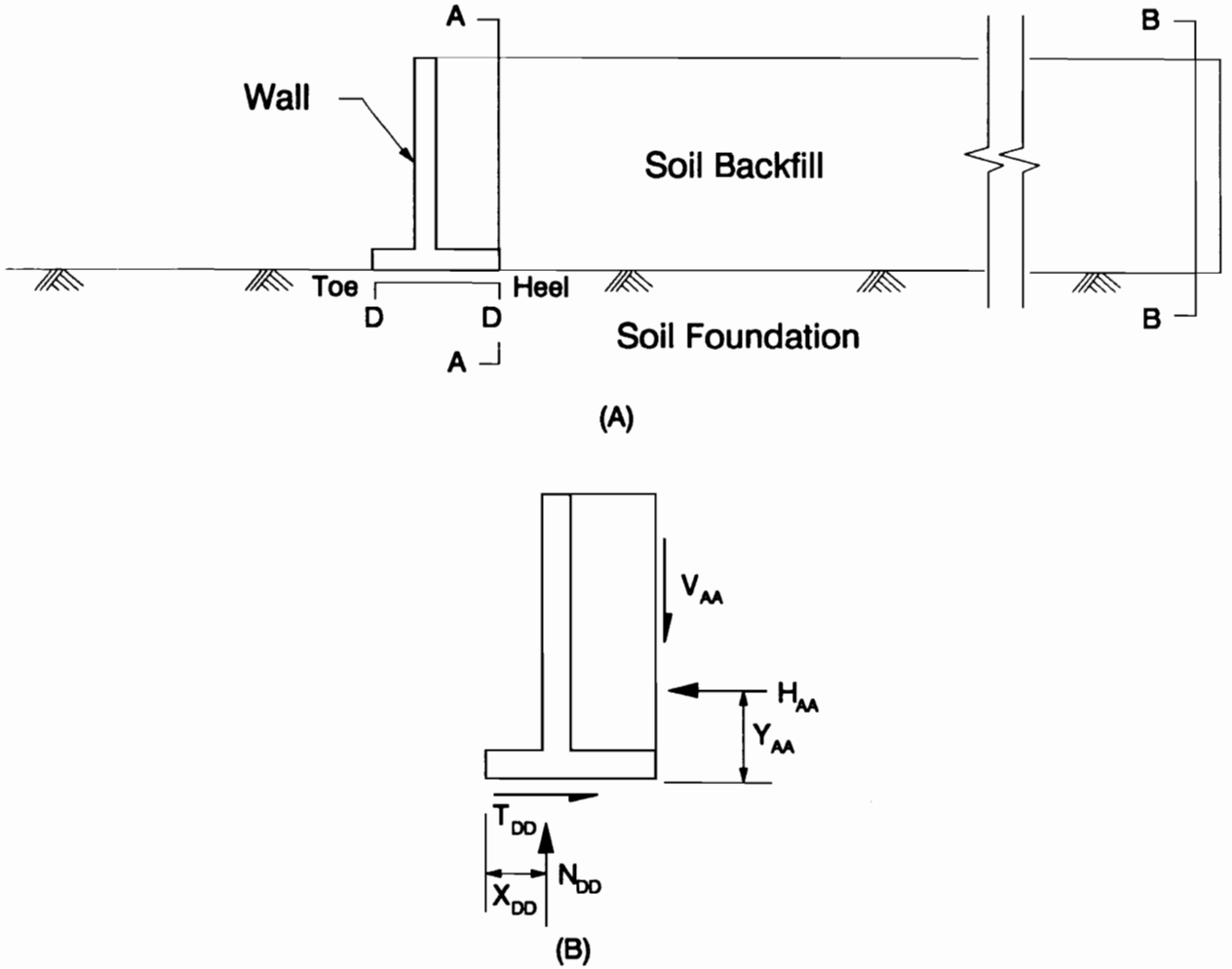

Figure 6.10 - Resultant Forces on Selected Key Planes on the Wall and within the Backfill - Cantilever Walls

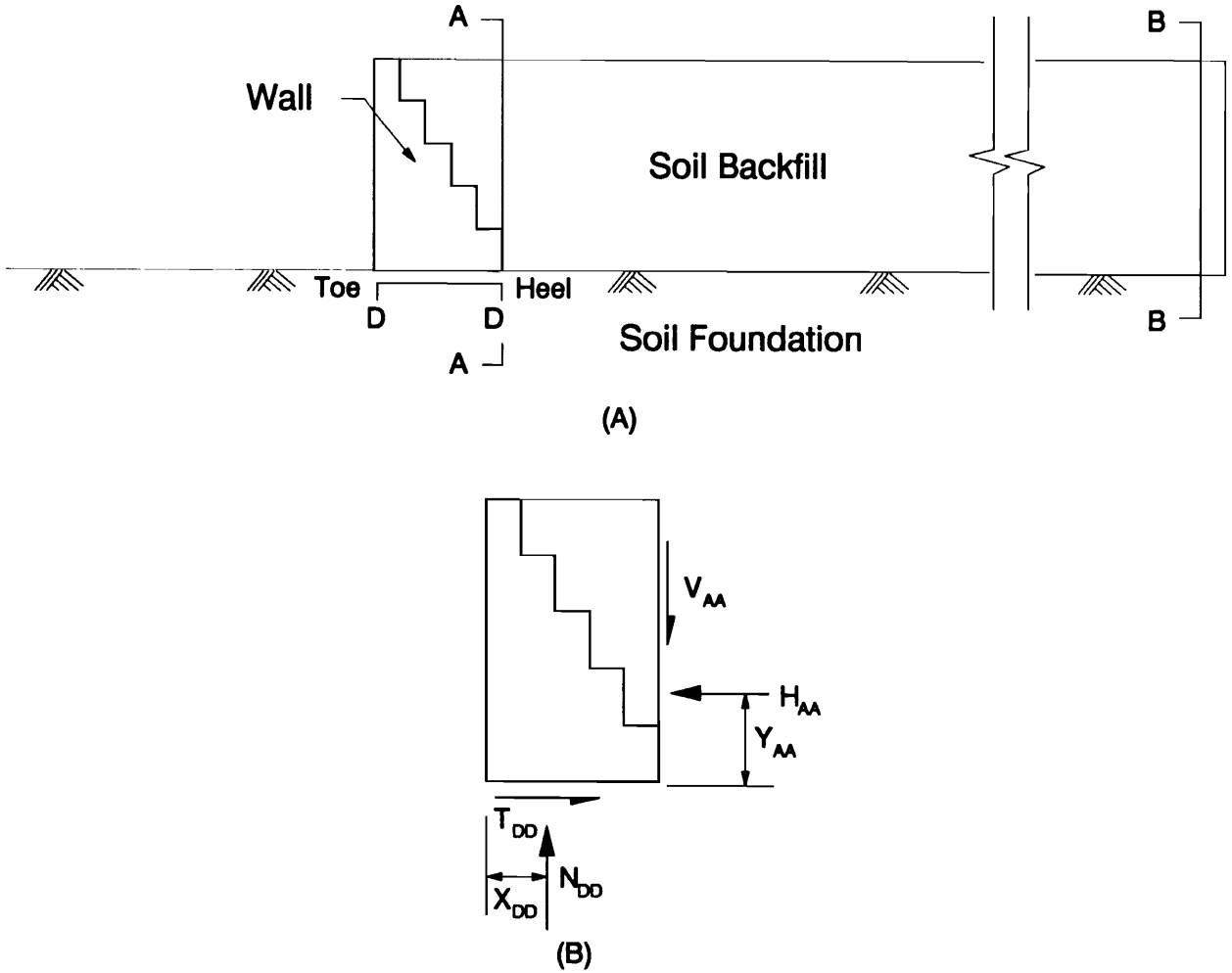

Figure 6.11 - Resultant Forces on Selected Key Planes on the Wall and within the Backfill - Stepped-face Walls

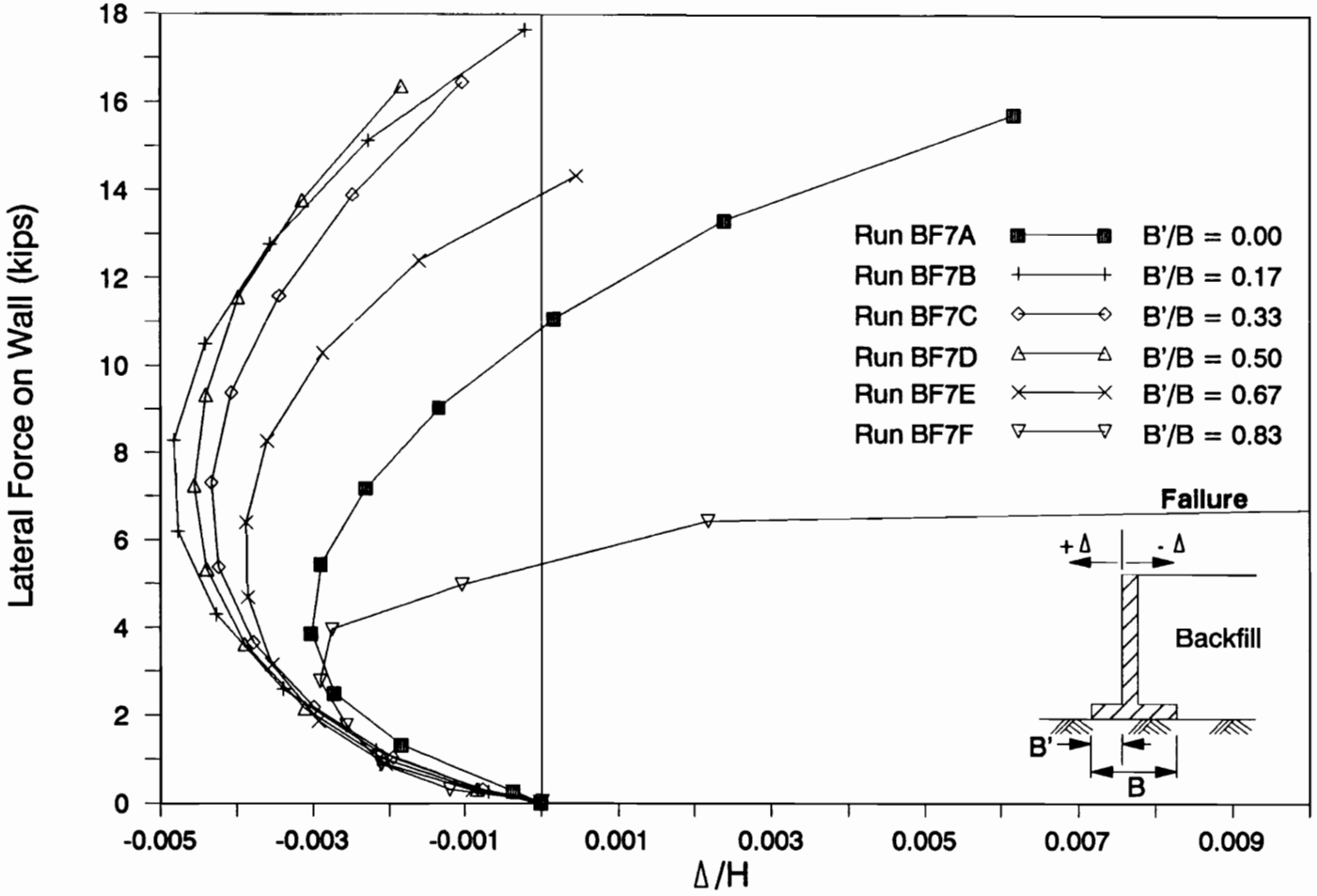

Figure 6.12 - Variation of Normalized Wall Displacements with the Lateral Force on the wall - Different Cantilever Wall Geometries

condition since the final Δ/H values are small. However, the case of B'/B equal to 0.83 (Run BF7F) yields large wall movements prior to the completion of backfilling. This behavior is primarily due to reduction of the contact pressure between the wall base and foundation, which in turn, causes wall sliding and tilting. The conditions at the end of backfilling for Run BF7F for practical purposes represent a failure state.

The variation of the Δ/H after full loading with the ratio B'/B is shown in Fig. 6.13 (the data point in Fig. 6.13 obtained from Run BF7F corresponds to the large wall movement which has occurred prior to the application of the full backfill load). When the wall stem is positioned close to the center of the base slab (B'/B values equal to 0.17, 0.33 and 0.50), the final deflection of the stem is towards the backfill. Only for the cases with the wall stem located in extreme positions on either side of the base slab does the wall end up displaced away from the backfill.

In the cases whereby the final displacement of the wall stem is in the direction of the backfill (Runs BF7B, BF7C and BF7D), it might at first seem that the lateral earth load should be greater than that of an at-rest condition. However, the results for these cases indicate that the earth loads are less than the at-rest magnitude and are close to that corresponding to an active state. The reason for the "lower than at-rest" earth loads is that even though the wall has moved backward, it actually moved away from the backfill in a relative sense because the displacements in the backfill are such that it moved away from the wall. As an illustration, consider the results of Run BF7C. The lateral earth pressure coefficient for this run is $K_h = 0.26$, which is less than K_o. Figure 6.14 shows the relative locations of a line parallel to the displaced position of the wall stem passing through the heel of the wall and a line containing the nodes of the interface elements that define Plane A-A. The former is labeled line AB while the latter is labeled line CD. Clearly, the nodes in the lower portion of line AB moved away from CD. In the upper portion, CD appears to have "moved toward" the wall stem. However,

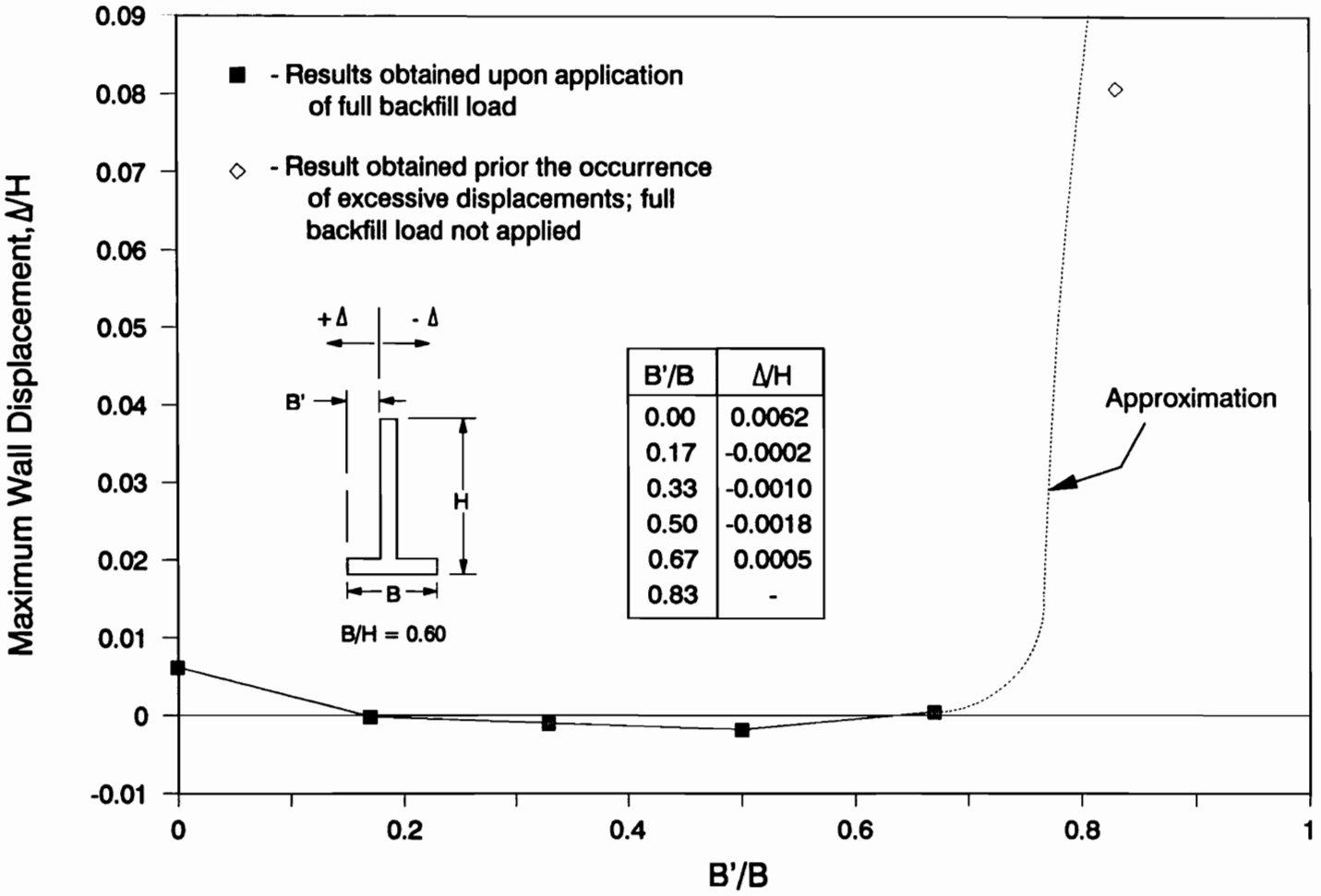

Figure 6.13 - Variation of Maximum Wall Displacement with Cantilever Wall B'/B Ratios

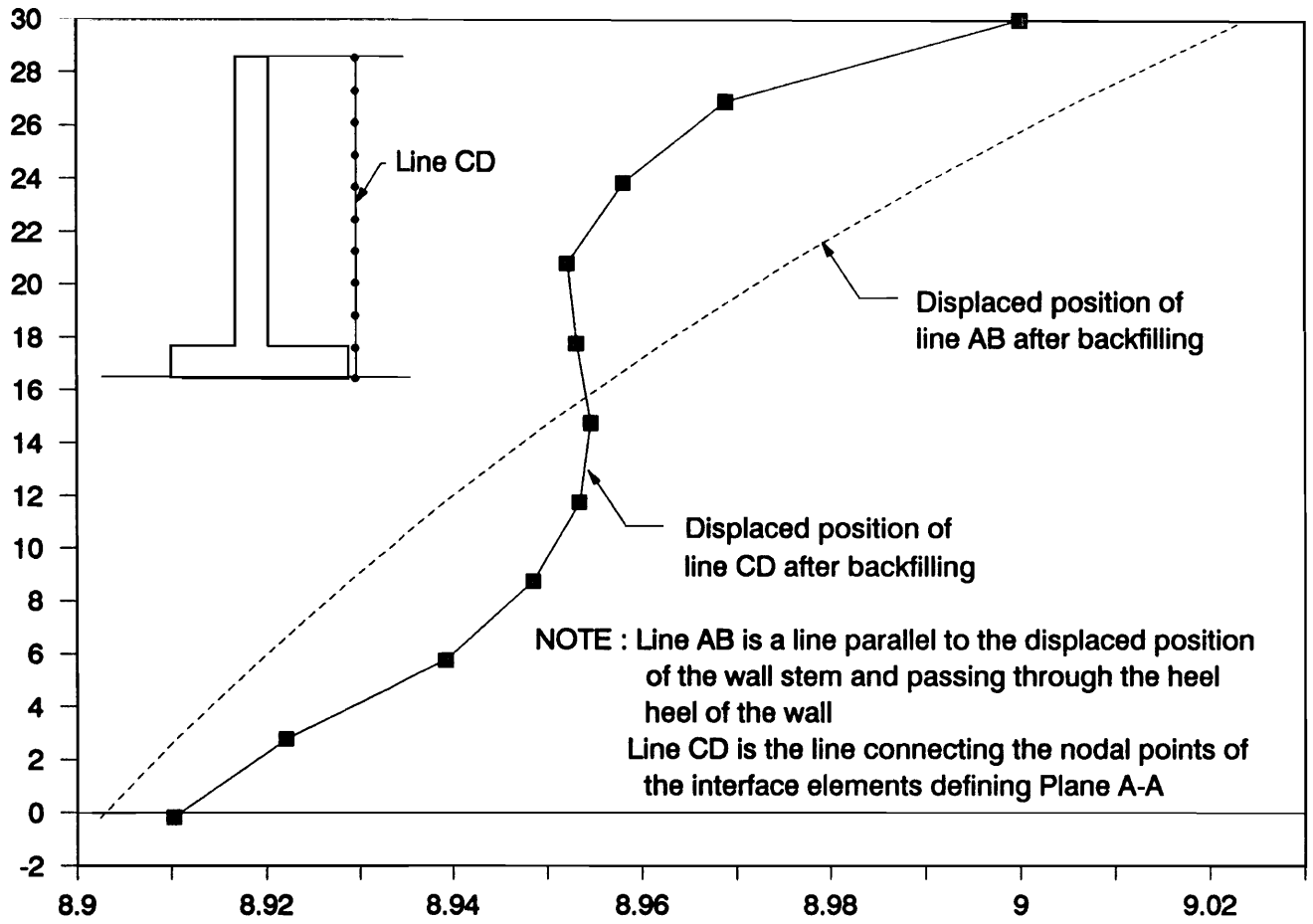

Figure 6.14 - Relative Positions of a Line through the Heel of the Wall Parallel to the Displaced Position of the Stem and the Line Connecting the nodes of the Interface Elements that define Plane A-A - Run BF7C

the resulting relative location of the lines in the upper portion is merely the residual effect of the procedure whereby the nodal displacements of newly-placed backfill elements are zeroed out. The σ_x-σ_y stress paths for several backfill elements in the vicinity of Plane A-A are plotted in Figure 6.15. It is clear that at the end of backfilling, none of the elements developed lateral pressures greater than the at-rest pressure.

Fig. 6.16 shows the ground surface profiles for analyses BF7A to BF7E. It can be seen that as the toe projection length, B' is increased, the tendency of the wall to rotate in the direction of the backfill also increases. A nearly uniform wall settlement was achieved for B'/B equal to 0.17 (Run BF7B). In the case of the wall with B'/B equal to 0.67 (Run BF7E), even though the ground surface profile for this analysis suggests that the wall rotated towards the backfill, Fig. 6.13 indicates that the final position of the top of the wall is to the left of its original position, which is away from the backfill. This would mean that the movement of the wall away from the backfill is due to sliding along the base rather than by rotation of the wall.

The forces on the key planes are summarized in Table 6.2. On plane A-A, the lateral earth force coefficient $K_h{}^{AA}$ ranged from 0.23 to 0.28. The highest $K_h{}^{AA}$ was obtained from Run BF7B (B'/B equal to 0.17). The earth pressure index in this case was equal to 0.59. On the other extreme, the lowest $K_h{}^{AA}$ value was obtained from Run BF7E (B'/B equal to 0.67). The corresponding EPI was equal to 0.98, indicating a condition which is very close an active state. The position of the line of action, Y_{AA}, of the lateral earth pressure force, varied only slightly from $0.36*H$ to $0.38*H$. Also on plane A-A, the vertical shear force coefficient, $K_v{}^{AA}$, ranged from 0.06 to 0.11. The lowest $K_v{}^{AA}$ value was obtained from Run BF7A (B'/B equal to 0.00). The variation of $K_v{}^{AA}$ for B'/B values between 0.17 and 0.67 was minimal, $K_v{}^{AA}$ ranging only from 0.09 to 0.11 (compared to 0.11 to 0.14 for gravity walls on rock and 0.07 to 0.10 for gravity walls on soil). The variation of both $K_h{}^{AA}$ and $K_v{}^{AA}$ with B'/B are plotted in Fig. 6.17.

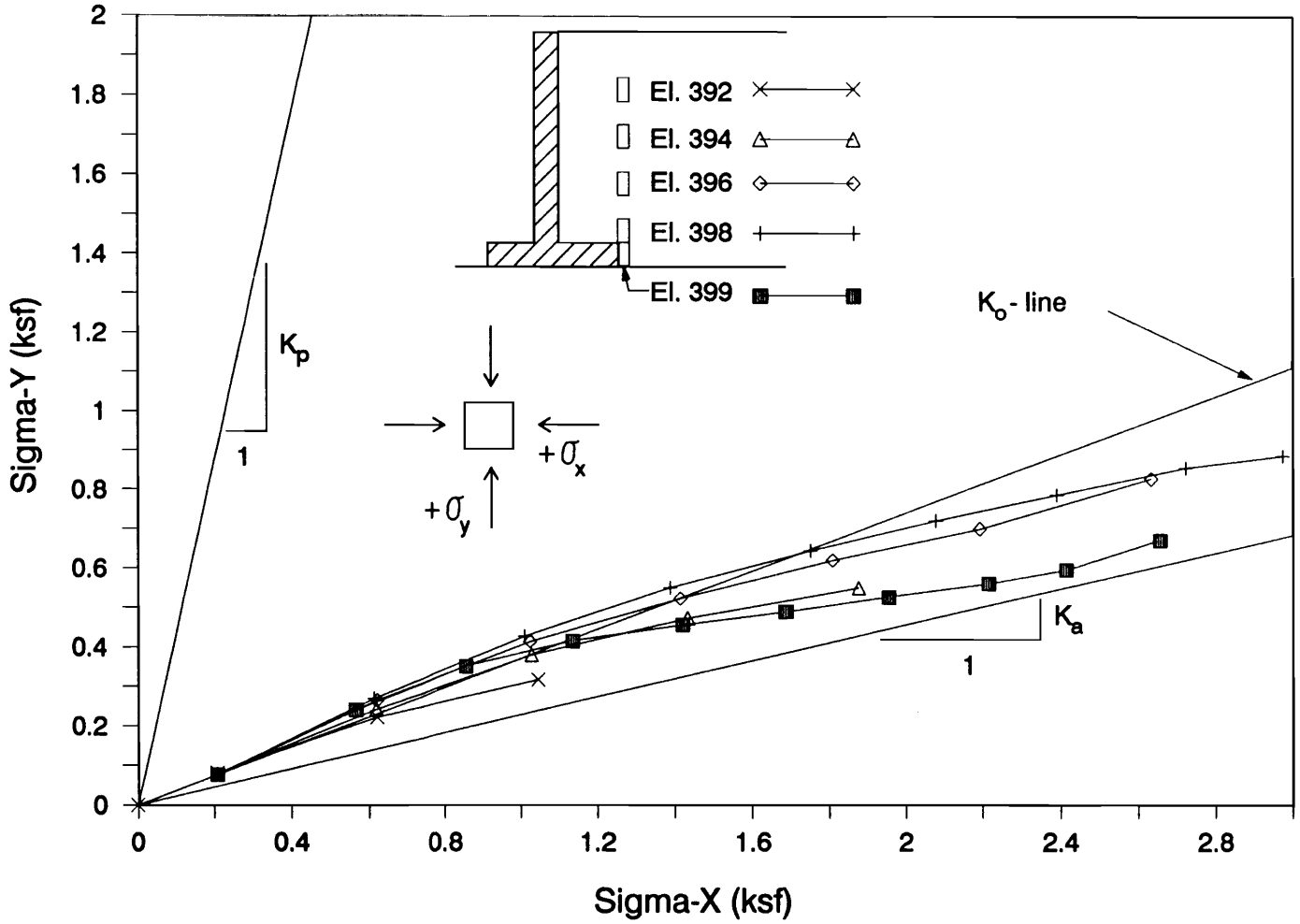

Figure 6.15 - Sigma-X vs. Sigma-Y Stress Paths for Backfill Soil Elements 392, 394, 396, 398 and 399 for Run BF7C

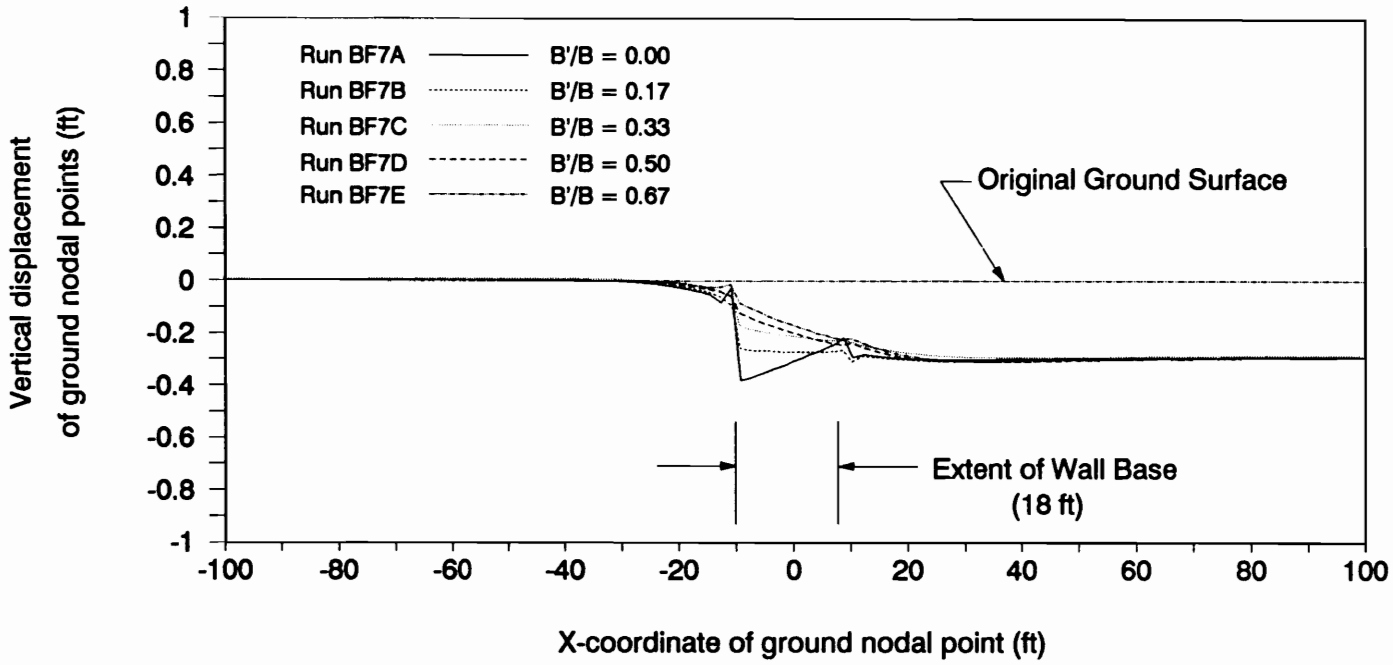

Figure 6.16 - Ground Surface Profiles Resulting from the Analyses of Cantilever Retaining Walls with Different Geometries

Table 6.2 - Forces on Key Planes from the Analyses of Cantilever Walls

Note : All forces in pounds, all lengths are in feet

Run No.	BF7A B'/B = 0.00	BF7B B'/B=0.17	BF7C B'/B=0.33	BF7D B'/B=0.50	BF7E B'/B=0.67
Plane A-A					
H_{AA}	15,740	17,655	16,415	16,335	14,310
V_{AA}	3,930	6,180	5,435	6,400	6,770
Y_{AA}	11.51	11.14	11.23	11.00	10.73
K_h	0.25	0.28	0.26	0.26	0.23
K_v	0.06	0.10	0.09	0.10	0.11
EPI	0.83	0.59	0.75	0.75	0.98
Plane B-B					
H_{BB}	22,550	22,390	22,590	22,540	22,460
V_{BB}	90	77	30	32	60
Y_{BB}	9.97	9.91	9.92	9.95	10.00
K_h	0.36	0.36	0.36	0.36	0.36
K_v	0.00	0.00	0.00	0.00	0.00
Plane D-D					
N_{DD}	80,880	71,790	59,705	49,330	38,365
T_{DD}	15,740	17,655	16,415	16,330	14,310
X_{DD}	7.1	8.2	9.0	9.7	10.2
X_{DD}/ B	0.40	0.45	0.50	0.54	0.57
δ_{mob} / $\phi_{foundation}$	0.28	0.35	0.39	0.47	0.52

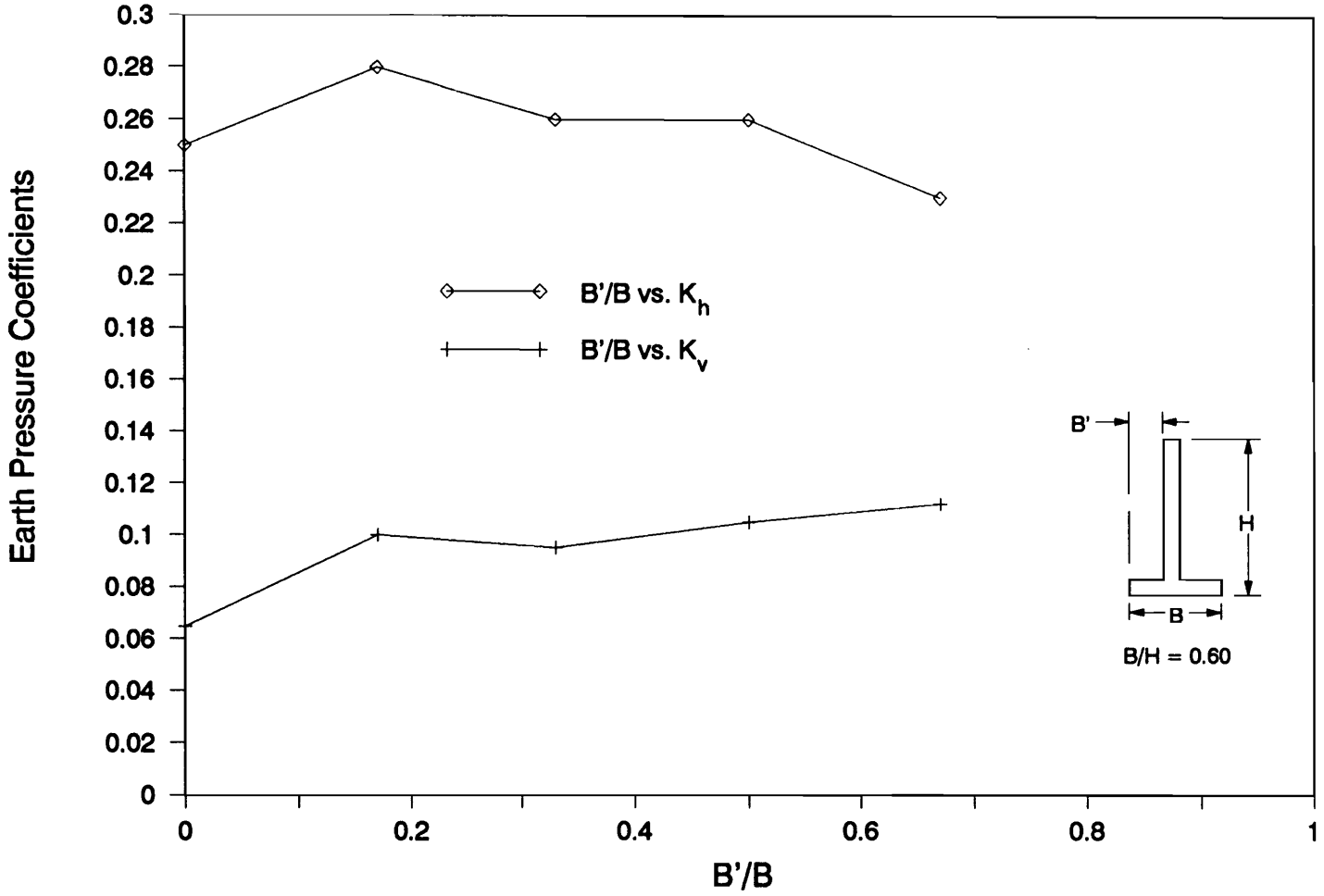

Figure 6.17 - Variation of Earth Pressure Coefficients with Cantilever Wall B'/B Ratios

The regions in the foundation and backfill which reached a condition of failure are shown in Fig. 6.18. The failure regions for B'/B equal to 0.00 (Run BF7A) and B'/B (Run BF7E) equal to 0.67 appear to be the most extensive among the five results. These results are consistent with findings presented earlier indicating that the walls in these two cases underwent the largest displacements relative to and away from the backfill. However, the mechanisms that brought about these movements are different for the two cases. For Run BF7A, movement away from the backfill is primarily due to rotation of the wall away from the backfill as suggested by the ground surface profile for this run. As previously discussed, the wall in Run BF7E moved away from the backfill primarily by sliding along the base.

The normal stress distributions on the base of the wall (plane D-D) are shown in Fig. 6.19. Note that the normal stresses in the toe area decreases with increasing B'/B ratio. This reduction in the base normal stresses has a positive and a negative consequences from the standpoint of stability. On the positive side is the reduction itself of the contact pressure between the base and the foundation. The negative consequence is the accompanying decrease in the confining pressures within the foundation soil, which then reduces its bearing capacity. Results of the analyses indicate that the reduction in the base pressure did not adversely affect wall stability for walls with B'/B ratios up to 0.67. For B'/B equal to 0.67, the wall base appears to be close to losing contact with the foundation soil in the vicinity of the toe. Using a K_h equal to 0.23, a conventional analysis of this wall does not result in base separation either in the toe or heel area. Also, use of the conventional methods yield a normal stress at the toe of approximately 1.8 ksf. There is some base separation in the heel area for B'/B equal to 0.00 and B'/B equal to 0.17. In both of these cases, B_e/B was equal to 90 percent. Conventional results, on the other hand, indicate full base contact. A nearly uniform stress distribution was achieved for B'/B equal to 0.33. Fig. 6.20 shows the corresponding shear stress distributions on the base for these same five analyses. The differences between these stress distributions are not

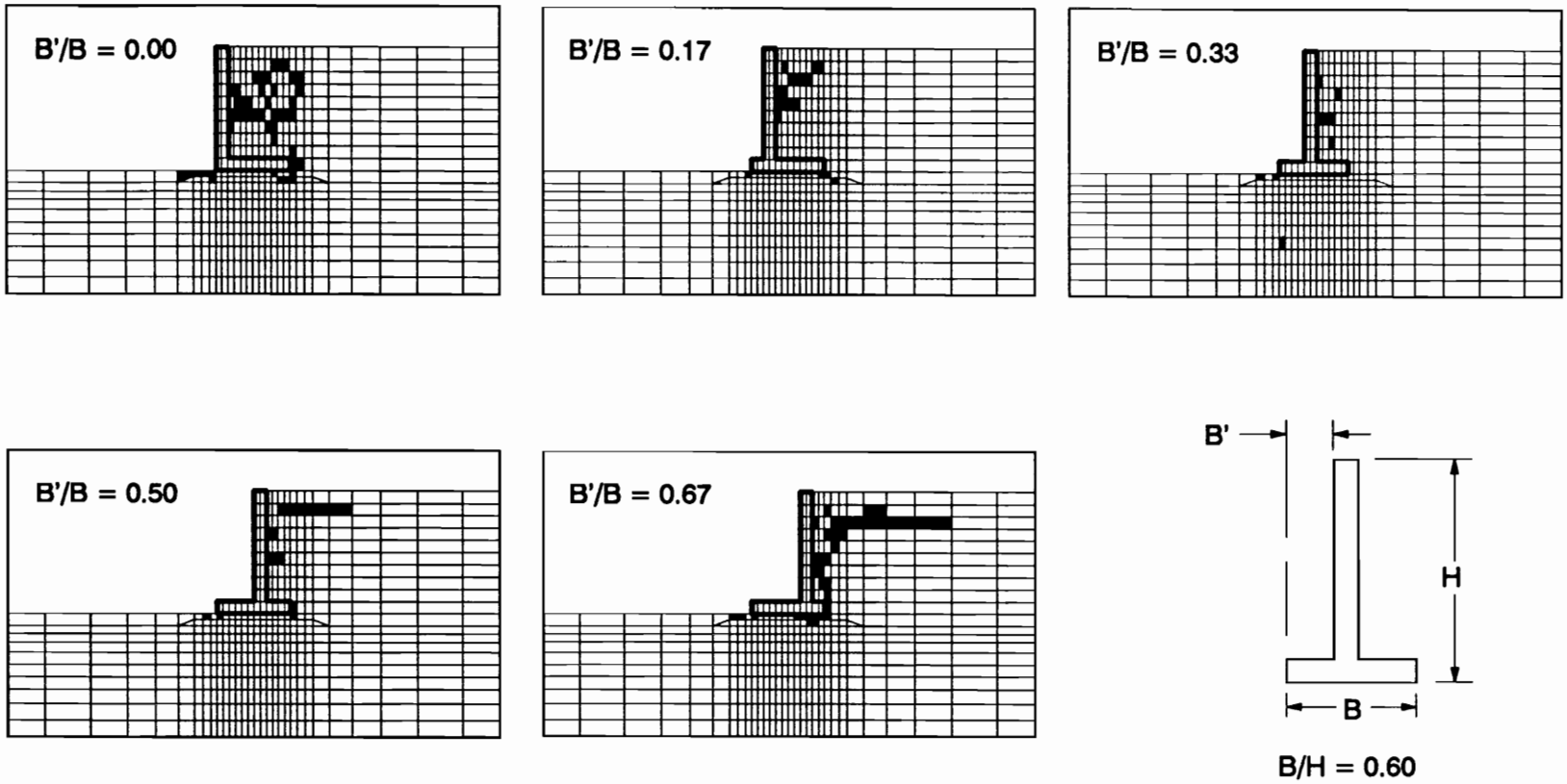

Figure 6.18 - Failure Regions for various Cantilever Wall Geometries

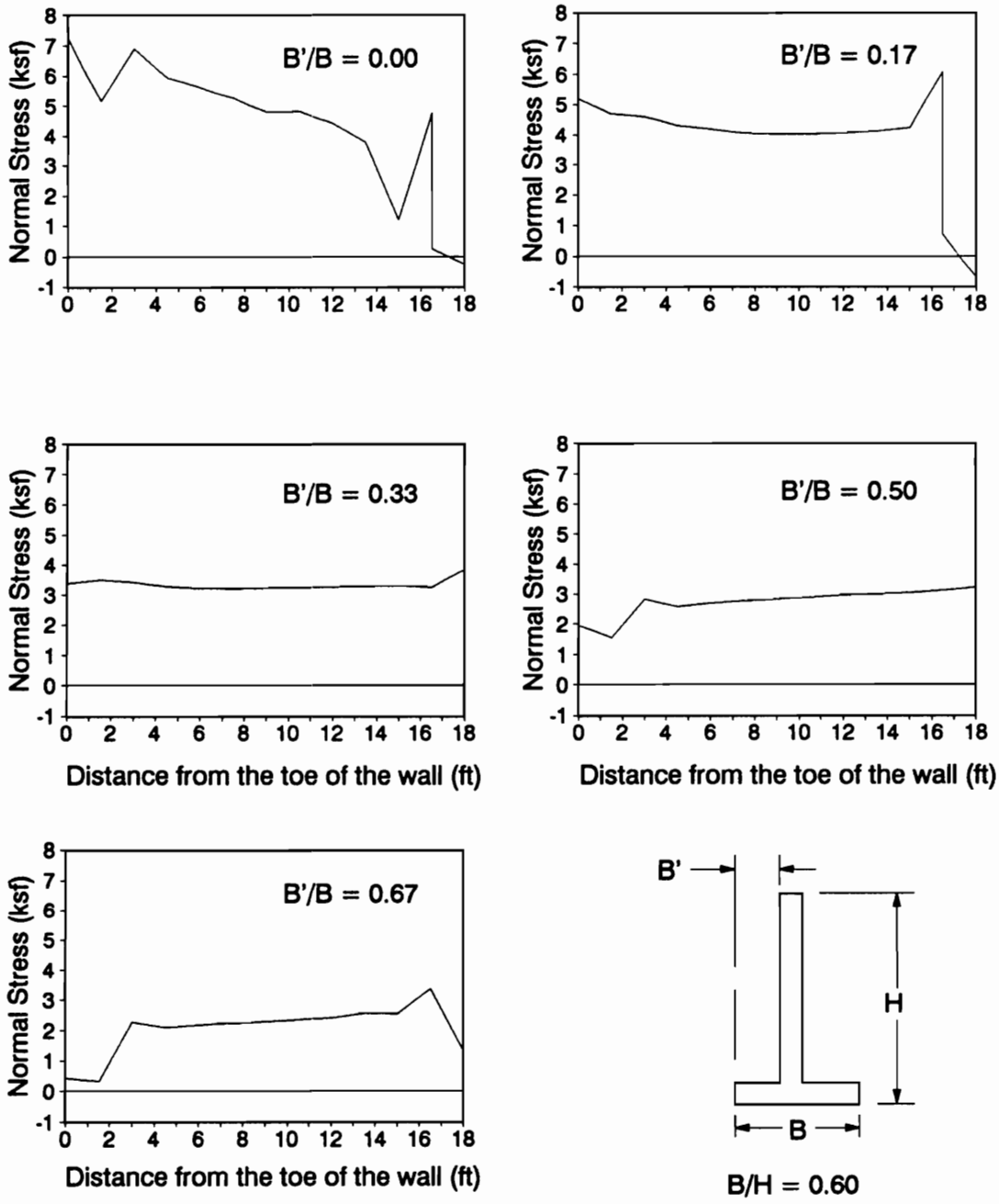

Figure 6.19 - Base Normal Stress Distributions for various Cantilever Wall Geometries

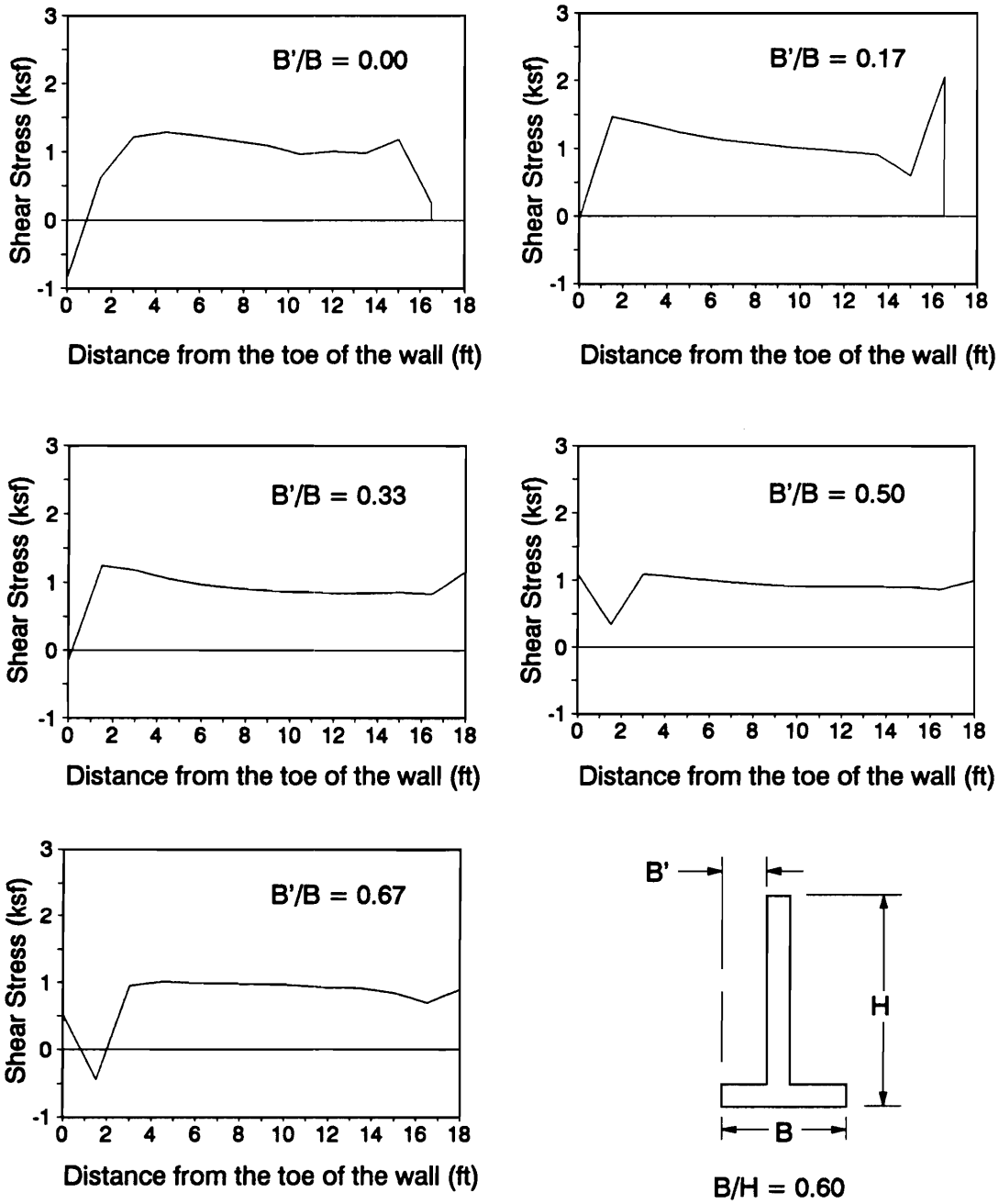

Figure 6.20 - Base Shear Stress Distributions for various Cantilever Wall Geometries

very significant.

On the wall base-foundation interface (Plane D-D), the magnitude of the resultant normal force (N_{DD}) decreased with B'/B. This is mainly due to the decrease in the volume of backfill overlying the base slab. The position of the line of action of N_{DD}, which is defined by the quantity X_{DD}, moved toward the heel as the length of the toe projection was increased. The normalized quantity X_{DD}/B ranged from 0.40 for BF7A to 0.57 for BF7E. The resulting mobilized friction angles on plane D-D for these five runs were normalized by the internal angle of friction of the foundation soil, $\Phi_{foundation}$, which is equal to 39^o. With the maximum interface friction angle, δ, assumed to be equal to $0.8*\Phi_{foundation}$, the smallest factor of safety against sliding was calculated from the results of Run BF7E (B'/B equal to 0.67) and found to be equal to 1.64 (compared to 1.4 from conventional analysis using K_h equal to 0.23). This low value indicates a high likelihood that longer toe projections would result in sliding failure, which was the finding in Run BF7F (B'/B equal to 0.83).

RESULTS OF ANALYSES OF STEPPED-FACE WALLS

Analyses were performed on walls with n_s-values equal to two, five and ten. These analyses were designated Runs BF8A, BF8B and BF8C, respectively.

Fig. 6.21 shows the ground surface profiles that resulted after backfilling. It can be seen that as the number of steps, n_s, is increased, there is a slightly greater tendency of the wall to rotate away from the backfill. This is influenced primarily by the distribution of the weight of the wall, which tends to be concentrated more in the toe area with an increased number of wall steps.

The failure regions within the backfill and foundation after backfilling for the three

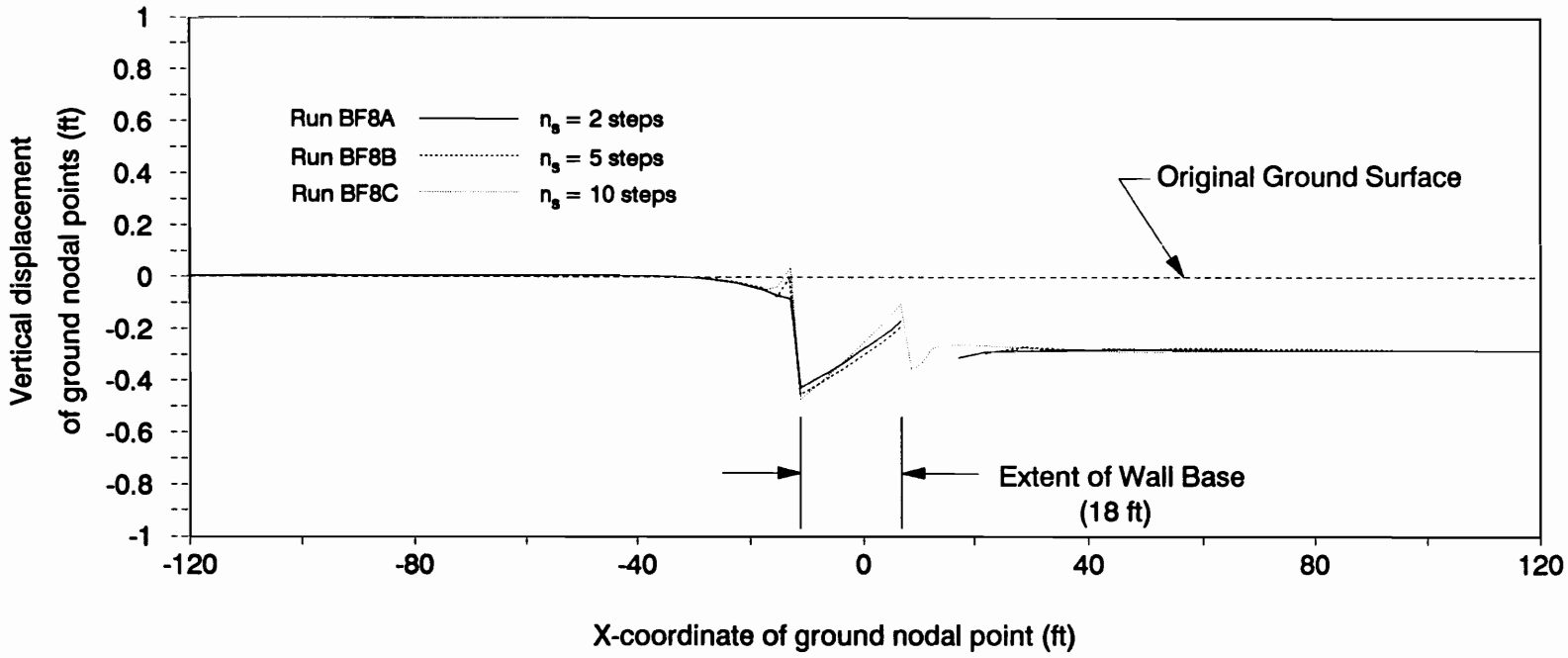

Figure 6.21 - Ground Surface Profiles Resulting from the Analyses of Stepped-face Walls

analyses are shown in Fig. 6.22. Within the backfill, these regions tend to be less extensive as the number of steps is increased. This trend indicates that smaller lateral movements occur for larger n_s-values. It will also be evident in the results to follow that the potential for localized movements within the soil mass directly above the wall also increases with the number of steps.

The characteristics of the forces on the key planes are summarized in Table 6.3. It may be noted that the vertical shear force coefficient, K_v^{AA}, becomes larger as the number of wall steps decrease. The differences in K_v^{AA}-values are significant, with K_v^{AA} equal to 0.20, 0.13 and 0.10 for n_s-values equal to 2, 5 and 10 respectively. This variation is due to localized movements within the soil mass directly above the wall, which tends to be more prominent as the number of wall steps increase. This occurrence is evident in the shear stress distributions on plane A-A (Fig. 6.23). The sign convention for shear stress is given alongside the plots. As the sign convention indicates, shear stress is negative if the backfill to the left of the plane (the soil mass directly above the wall) is moving downward relative to the backfill to the right of the plane. Negative shear stresses near the surface indicates that in these locations, there is downward movement within the soil mass directly above the wall. It may be noted that as the number of wall steps increase, a larger portion of the soil mass moves downward. In relation to the K_v^{AA} values that were obtained for these runs, it is interesting to note that the gravity wall analyzed in the base case problem in Chapter 5 (Run BFBC) resulted in a K_v^{AA}-value of 0.07. The gravity wall in this base case problem may be considered to be a stepped-face wall with an infinite number of steps on its wall-backfill interface.

The variation of the wall displacement, Δ/H, with the lateral earth force, H_{AA}, is given in Fig. 6.24. The maximum wall displacements after backfilling are : -0.0114, -0.0075 and -0.0028 for n_s equal to 2, 5 and 10 respectively. Note that Δ/H at the end of backfilling decreases as the number of steps increases. This is consistent with the trends discussed previously regarding the failure regions within the backfill. Because Δ/H decreases with the

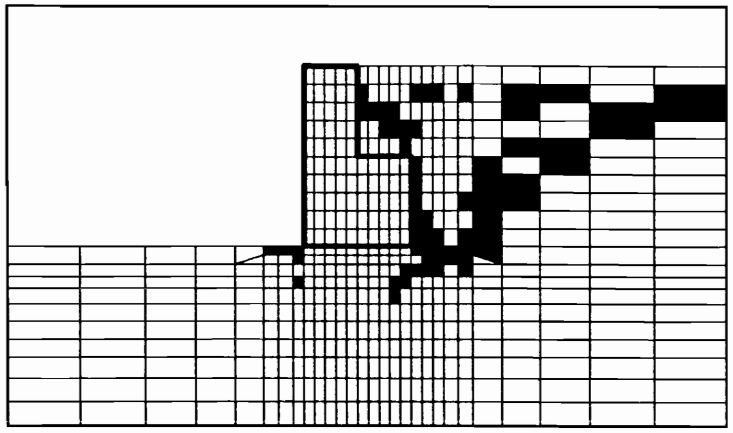

(A) Two (2) steps

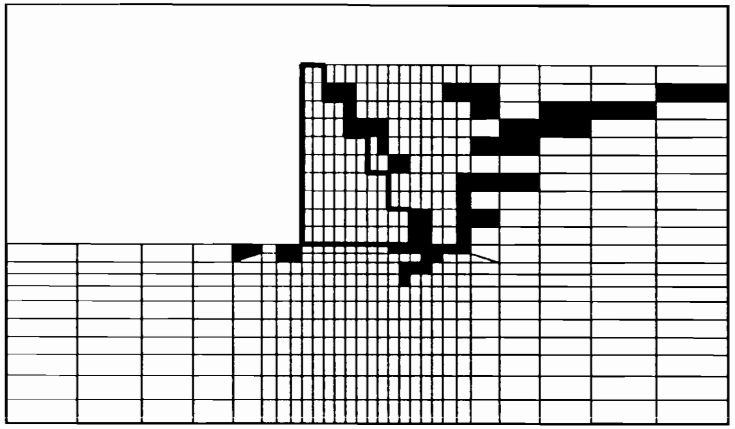

(C) Five (5) steps

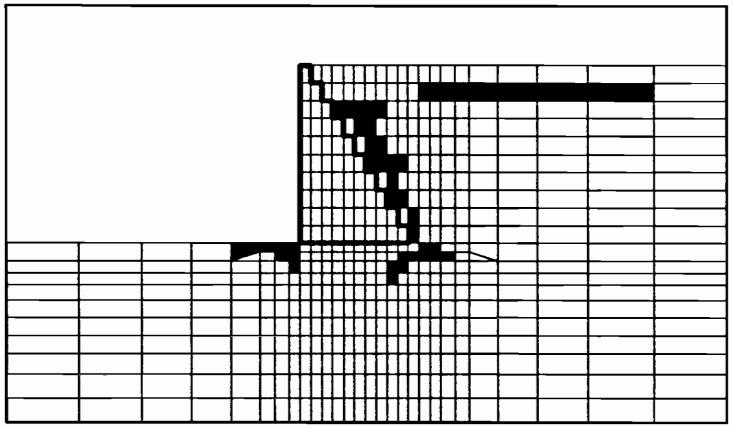

(C) Ten (10) steps

Figure 6.22 - Failure Regions after Backfilling Resulting from the Analyses of Stepped-face Walls

Table 6.3 - Forces on Key Planes from the Analyses of Stepped-face Walls

Note : All forces in pounds, all lengths are in feet

Run No.	BF8A $n_s = 2$	BF8B $n_s = 5$	BF8C $n_s = 10$
Plane A-A			
H_{AA}	21,020	16,945	15,920
V_{AA}	12,720	8,120	6,420
Y_{AA}	11.33	13.21	11.11
K_h	0.33	0.27	0.25
K_v	0.20	0.13	0.10
EPI	0.33	0.69	0.82
Plane B-B			
H_{BB}	23,870	23,190	22,880
V_{BB}	10	62	90
Y_{BB}	10.24	10.14	10.03
K_h	0.38	0.37	0.36
K_v	0.00	0.00	0.00
Plane D-D			
N_{DD}	92,370	86,960	85,000
T_{DD}	21,020	16,945	15,920
X_{DD}	7.6	7.2	7.5
X_{DD}/ B	0.42	0.40	0.42
δ_{mob} / $\phi_{foundation}$	0.33	0.28	0.27

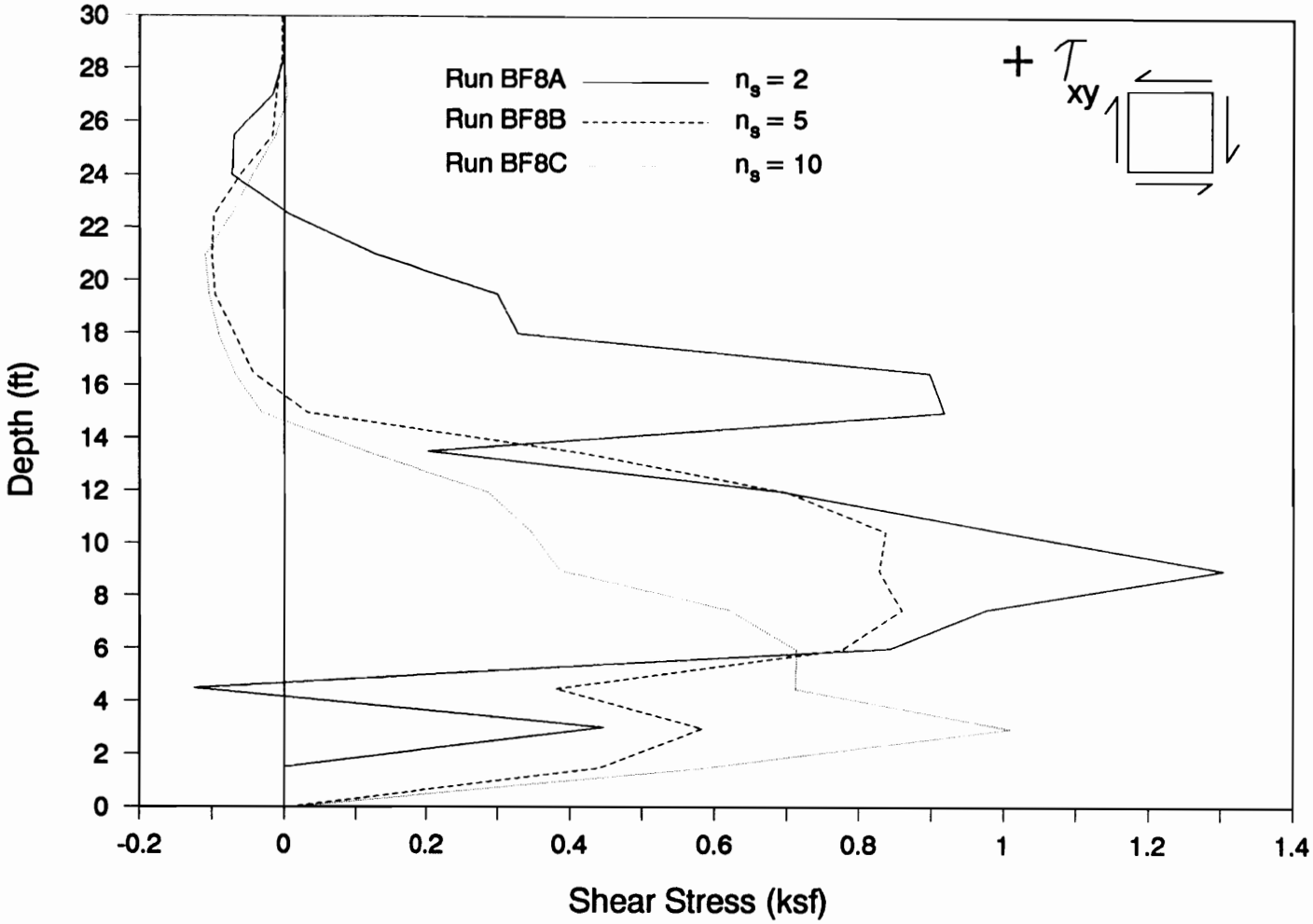

Figure 6.23 - Shear Stress Distribution on Plane A-A from the Analyses of Stepped-face Walls

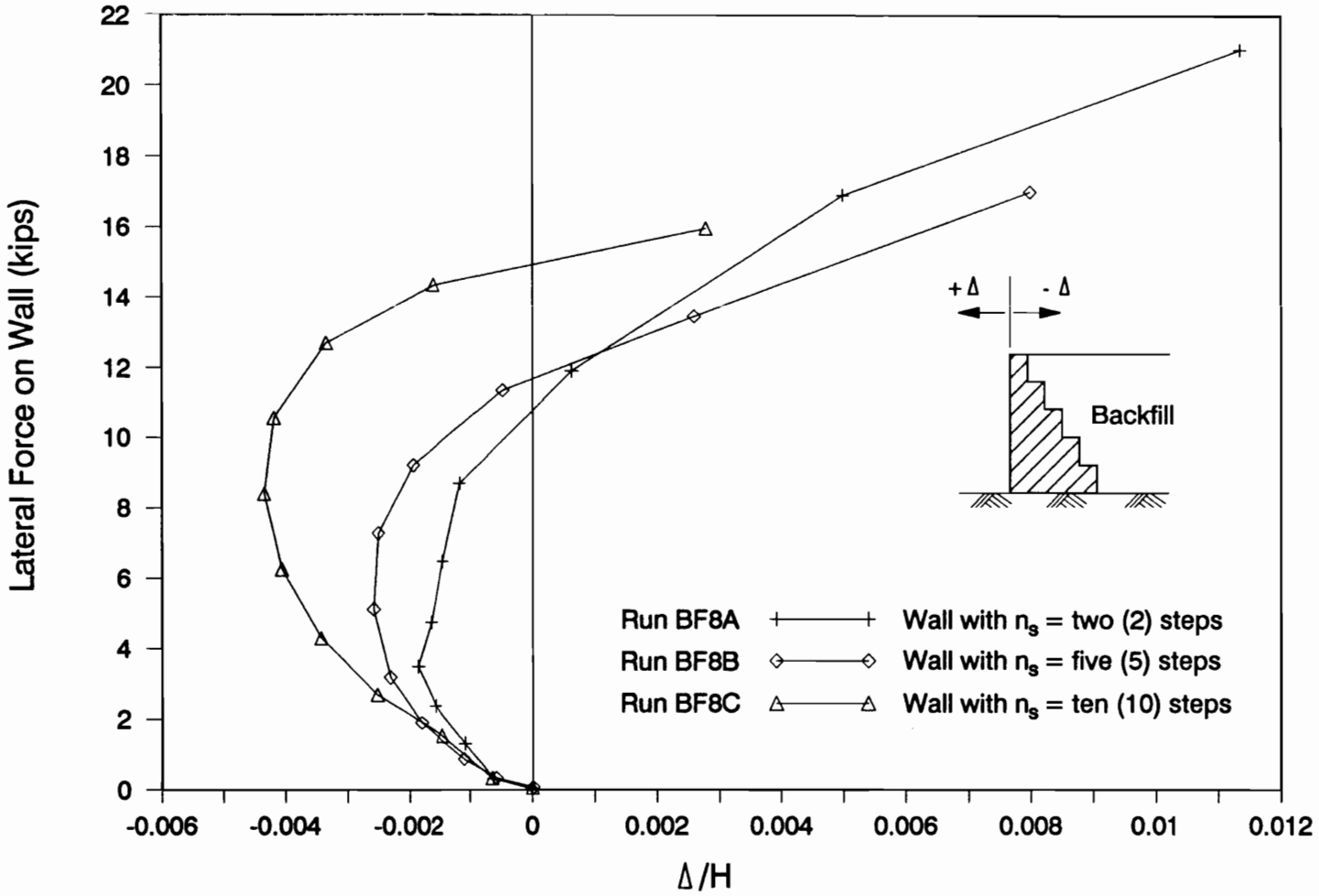

Figure 6.24 - Variation of Normalized Wall Displacements with the Lateral Force on the wall from Analyses of Stepped-face Walls

number of steps, one would infer that the lateral earth force on the wall would increase with n_s. However, Fig. 6.24 and the values of H_{AA} listed in Table 6.3 show otherwise. The results indicate that the lateral force on the wall at the end of backfilling tends to increase as n_s increases. It is believed that this trend may be attributed largely to the increasing local movements within the soil mass directly above the wall for larger n_s-values, rather than the movement of the wall away from the backfill.

Referring again to Table 6.3, the base normal force (on Plane D-D) increases as the number of wall steps decreases. This increase in the normal force is due to the larger magnitude of the "downdrag" force as well as the increased weight of the material directly above the base occurring for the more massive walls (smaller n_s-values).

The base stress distributions for the three runs are given in Fig. 6.25. Base separation in the heel area occurred in the case where n_s equals 10, resulting in some redistribution of stresses. The differences in the magnitude of the stresses were not more than 2 ksf in most locations among the base, a quantity which may, for practical purposes, be considered small.

SUMMARY

The analyses of cantilever walls were aimed primarily at examining the effects of placing the wall stem at different locations along the length of the base slab. This location was defined by the length of the toe projection B'. Results indicate that the wall is generally stable as long as the wall stem is not placed in the vicinity of the heel. The geometry of a cantilever wall is such that it may not be considered "massive". Because of this, it has to rely, to a large extent, on the weight of backfill directly above the base slab in order to have sufficient contact pressure on the wall-foundation interface. If the wall stem is located too close to the heel, the lack of

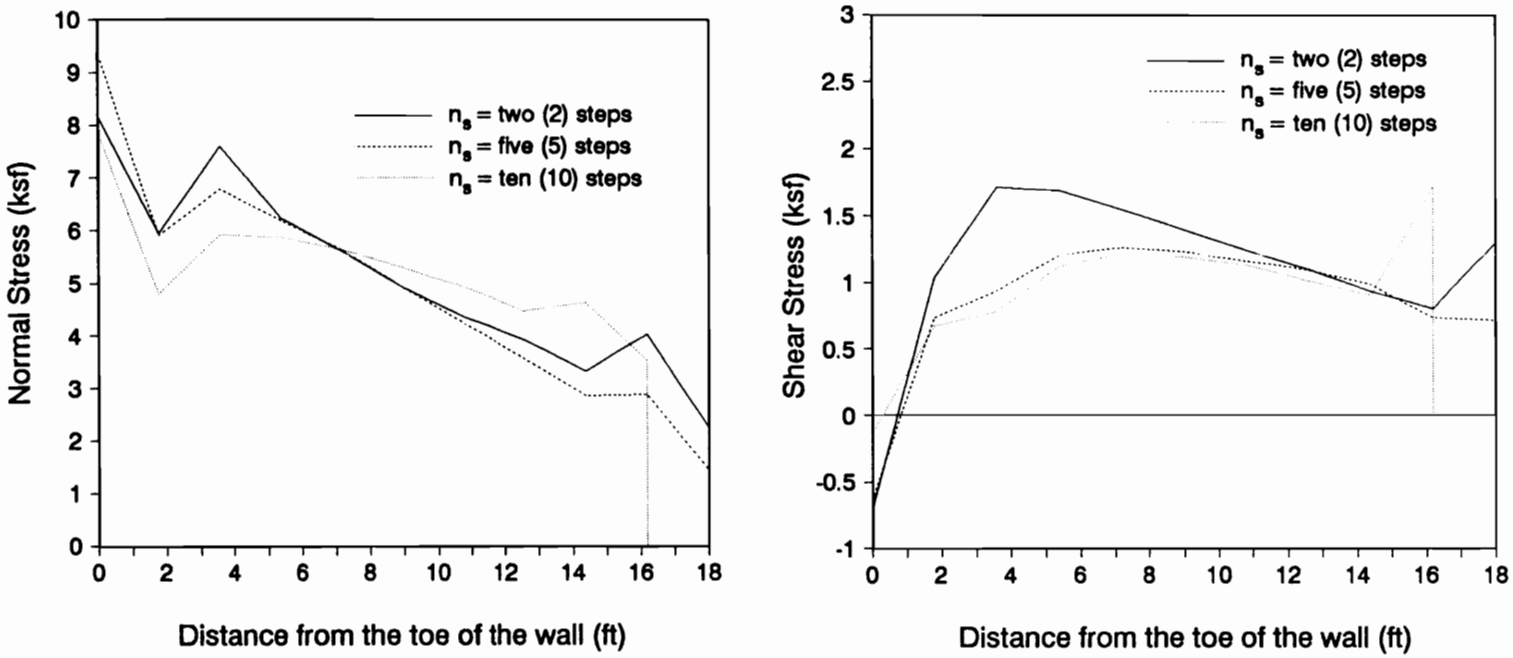

Figure 6.25 - Base Stresses after Backfilling Resulting from the Analyses of Stepped-face Walls

contact pressure may lead to wall instability, as was the result in Run BF7F. Equally interesting is the finding that the shear force coefficient K_v^{AA} varied only slightly (0.09 to 0.11) in cases where the wall stem was not placed in the extreme ends of the base slab.

In the analyses of stepped-face walls, an interesting finding was that there was more pronounced downward movement within the soil mass directly above the wall relative to the rest of the backfill as the number of wall steps, n_s, was increased. This trend resulted in a decrease in the shear force coefficient K_V^{AA} with an increase in the number of wall steps. It is also believed that these localized movements are the main reason why, for higher values of n_s, the lateral force on the wall tends to decrease in spite of the smaller magnitudes of wall movements in these cases.

CHAPTER 7

COMPARISON OF FINITE ELEMENT RESULTS WITH CONVENTIONAL DESIGN PROCEDURES

COMPARISON WITH COULOMB ACTIVE EARTH PRESSURE CONDITIONS

It is interesting to compare the results of Coulomb analyses of retaining walls with the results obtained using the finite element method. For this purpose, walls considered previously (the gravity wall with a sloping back face, the gravity walls with stepped back faces, and the cantilever walls) were analyzed using Coulomb active earth pressures, and the results were compared with the results of the finite analyses discussed previously.

In the Coulomb analyses, it is necessary to assume the location of the failure plane along the back of the wall, and the value of the wall friction angle, δ. The assumed failure planes for the retaining walls analyzed are shown in Fig. 7.1. A value of $\delta=\Phi$ was used in the cases when most of the failure plane passes through soil. Where the failure plane was along the back of the wall, a value of δ equal to 0.67Φ was used.

Comparisons of the Coulomb active with the finite element results were made on the basis of the earth force coefficients K_h and K_v, the maximum base pressure q_{max}, the location of the base normal force, X_{DD}, and the mobilized angle of friction between the base of the wall and the foundation. The procedure used to determine equivalent values of K_h and K_v values for the Coulomb analyses is shown in Fig. 7.2. Fig. 7.2(a) shows a free body diagram of a wedge of backfill bounded by the wall-backfill interface (a failure plane), the top of the backfill, and a vertical plane passing through the heel of the wall. The force polygon for this system of

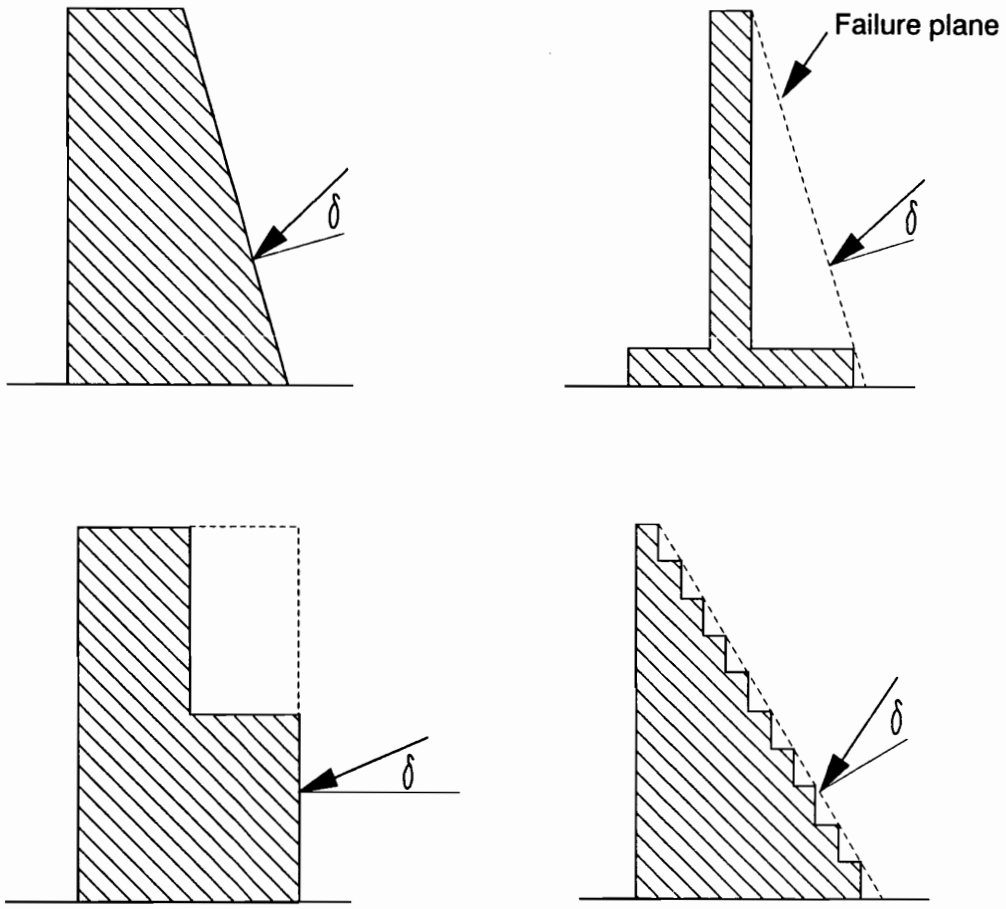

Figure 7.1 - Failure Planes assumed in the Coulomb Analyses of various Wall Shapes

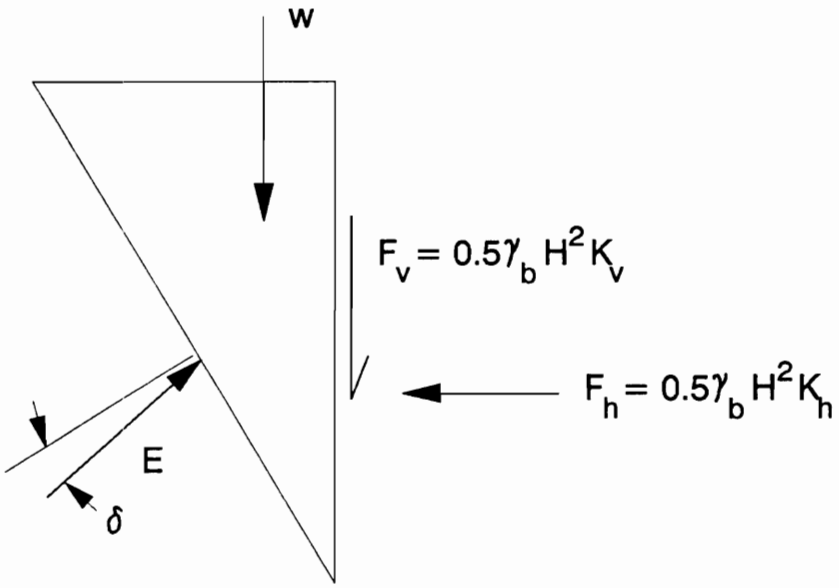

(a) Free body diagram of backfill wedge

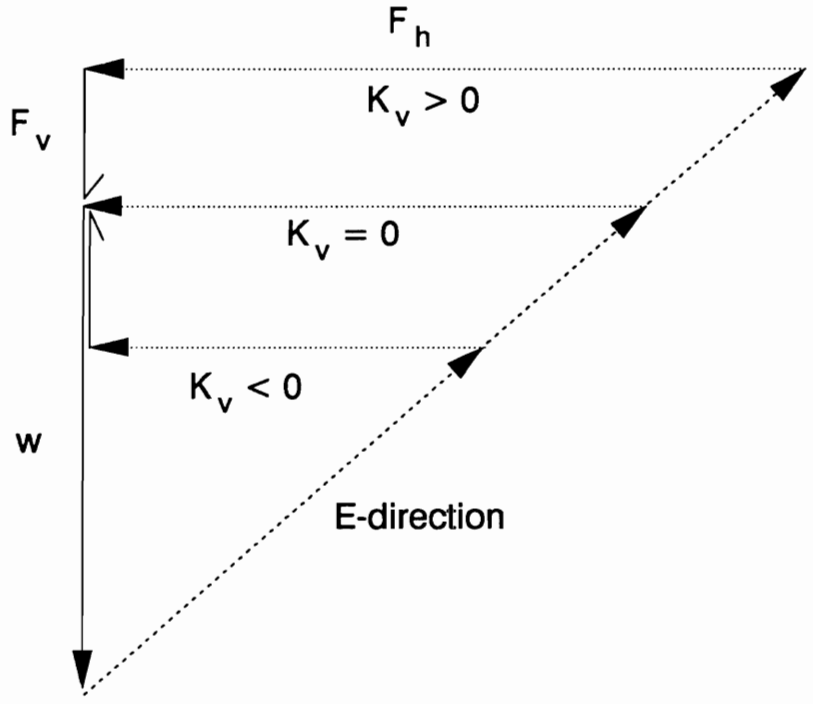

(b) Force polygon for the backfill wedge

Figure 7.2 - Relationships between Forces acting on the Backfill Wedge

forces is shown in Fig. 7.2(b). In this polygon, the "fixed" quantities are the weight of the backfill wedge W and the direction of the force E, which makes an angle of δ with the normal to the wall-backfill interface. It can be seen that, depending on the magnitude of the horizontal earth pressure force, F_h, closure of this polygon may lead to either a positive (downward), zero, or negative (upward) shear force F_v. For the active condition, there is a unique value of F_h, and therefore, a unique equivalent value of K_v. These values of K_v can be compared with those obtained from finite element analyses.

Coulomb analyses were performed for this wall using $\delta = \Phi$ and δ=0.67Φ. The resulting values of K_v and K_h are shown in Fig. 7.3. A friction angle equal to 39 degrees resulted in a positive K_v-value (point (1a)) while a friction angle equal to 26 degrees resulted in a negative K_v-value (point (1b)). Values of K_h and K_v corresponding to at-rest conditions are shown at point (2) in the same figure. K_v=0 for the at-rest condition. The values of K_h and K_v obtained from the finite element analysis of the wall are shown by point (3). It can be seen that the finite element value of K_v is larger than that from the Coulomb analyses or the at-rest conditions.

To assess the significance of these findings, the maximum base pressures, the positions of the resultants, and the mobilized friction angle on the base of the wall were calculated for the Coulomb and finite element earth pressures. Surprisingly, although the earth pressures from the finite element analysis are about 23 percent higher than the active values, the maximum base pressure and the position of the resultants are not much different. The mobilized friction angles are such that the factor of safety against sliding from the Coulomb analyses is about 18 percent higher than the finite element result. Thus, although the Coulomb analyses assume full mobilization of the shear strength of the backfill, and (for δ=39°) full mobilization of friction along the back of the wall, the resulting forces on the base of the wall are not much different from those using the finite element analyses, where the backfill strength is not fully mobilized.

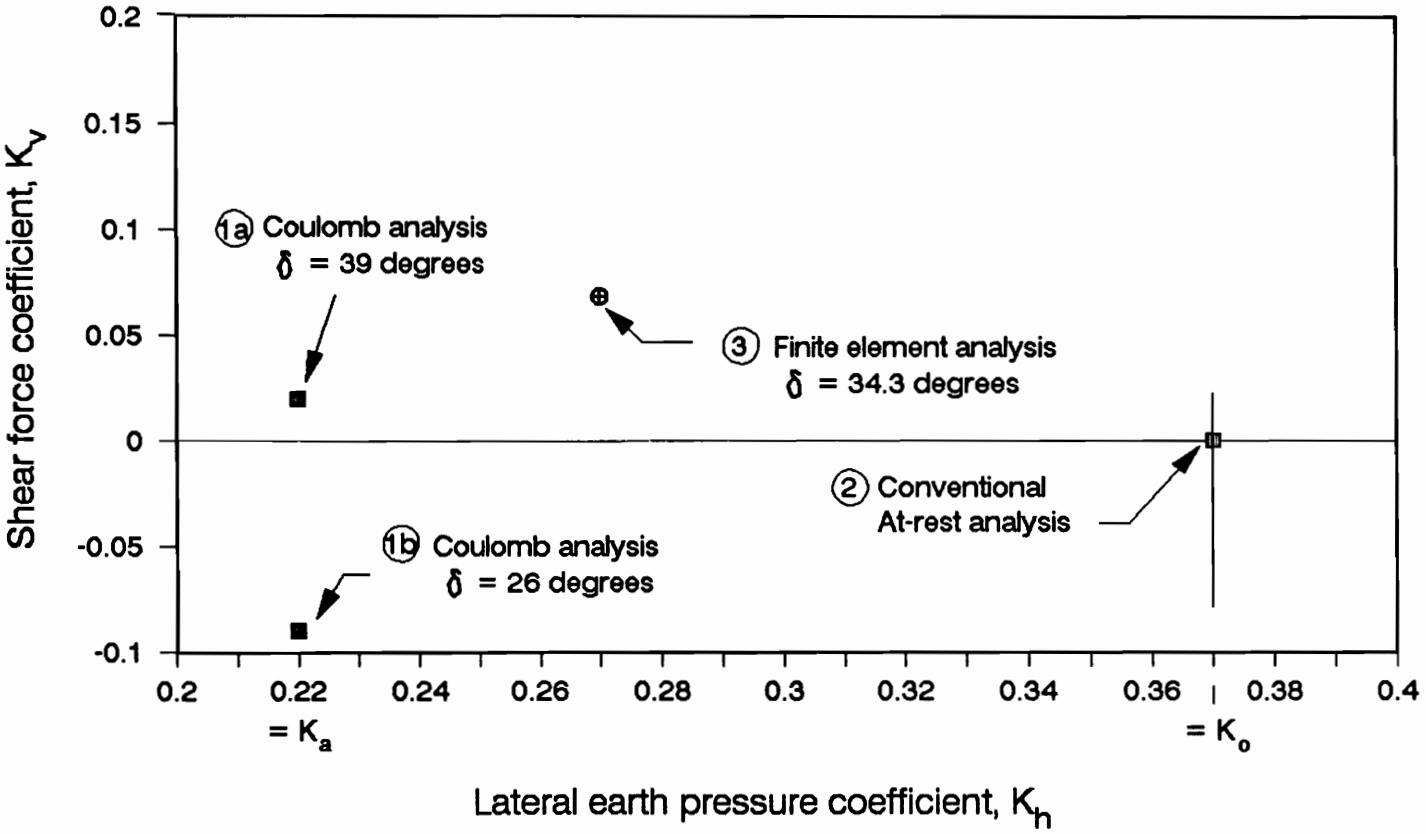

Figure 7.3 - Relationships between K_h and K_v for various Analyses of the Base Case Problem

These results illustrate the fact that higher values of K_v (larger values of shear forces on the vertical plane through the heel) compensate for higher values of K_h (larger horizontal forces on the vertical plane through the heel).

As shown in Table 7.1, the analyses of the other wall geometries gave similar results. Only in the case of the stepped-face wall with n_s=2, where the finite element value of K_h was 50 percent higher than the value of K_a, was the maximum base pressure much different. In this case the maximum base pressure from the finite element analyses was about 20 percent higher than the values from the Coulomb analyses. Even in this case the positions of the resultant on the base were not much different.

The mobilized friction angles from the finite element analyses were higher than those from the Coulomb analyses. The values of the friction angles were generally small, with the exception of those for the cantilever walls with B'/B equal to 0.50 and 0.67. In these cases, the walls have smaller margins of safety against sliding because they are relatively "light". With a Coulomb analysis, it is possible to get results that are appreciably unconservative for lighter walls.

Thus, it appears that conventional analyses using the Coulomb active earth pressure theory, with δ=0.67Φ to δ=Φ, will result in forces on the base of the wall that are not significantly different from those derived from finite element analyses. Although the values of both K_h and K_v differ for these two types of analyses, the differences compensate with regard to the magnitudes and locations of the forces on the base of the wall. Both the K_v and K_h coefficients are higher for the finite element analyses than the Coulomb analyses.

Table 7.1 - Results from Coulomb and Finite Element Analyses

Wall type	K_v	X_{DD}/B	q_{max}(psf)	K_h/K_a	δ_{base}
Gravity Wall					
Coulomb with $\delta = 26^\circ$	-0.09	0.36	7,590	1.00	11.1
Coulomb with $\delta = 39^\circ$	0.02	0.41	7,040	1.00	9.6
FEA	0.07	0.37	8,070	1.23	11.3
Cantilever Wall					
B'/B=0.33					
Coulomb with $\delta = 39^\circ$	0.01	0.52	3,730	1.00	13.3
FEA	0.09	0.50	3,320	1.18	15.2
B'/B=0.50					
Coulomb with $\delta = 39^\circ$	0.03	0.55	3,450	1.00	14.7
FEA	0.10	0.54	3,380	1.18	18.3
B'/B=0.67					
Coulomb with $\delta = 39^\circ$	0.09	0.57	3,010	1.00	17.6
FEA	0.11	0.57	2,990	1.05	20.3
Stepped-face wall					
$n_s = 2$					
Coulomb with $\delta = 26^\circ$	0.09	0.45	6,260	1.00	8.4
Coulomb with $\delta = 39^\circ$	0.14	0.46	6,180	1.00	7.1
FEA	0.20	0.42	7,530	1.50	13.0
$n_s = 5$					
Coulomb with $\delta = 39^\circ$	0.01	0.45	6,650	1.00	8.5
FEA	0.13	0.40	7,730	1.22	11.0
$n_s = 10$					
Coulomb with $\delta = 39^\circ$	0.01	0.48	5,320	1.00	9.2
FEA	0.10	0.42	7,080	1.14	10.5

NOTE : Downward shear forces are indicated by positive shear force coefficients

FEA - Finite element analysis

COMPARISONS WITH AT-REST EARTH PRESSURE CONDITIONS

Even at-rest earth pressure conditions, with K_v=0, correspond to non-zero values of the wall friction angle, δ. In analyses performed using at-rest earth pressures, the wall and the backfill directly above the wall are usually drawn together as one free body, as shown in Fig. 7.4(a). With the assumptions that K_v=0 and K_h=K_o, the force acting on the vertical plane through the heel of the wall (plane A-A) is the lateral earth force, F_h. If the backfill wedge is drawn as a separate free body, as shown in Fig. 7.4(b), equilibrium conditions require a vertical and horizontal component of force on the wall-backfill interface. This means that, in general, there is a non-zero wall friction angle, δ, implicit in the use of at-rest earth pressure conditions with K_v=0. The magnitude of the implicit value of δ depends on the assumed value of the at-rest coefficient, K_o, and the dimensions of the backfill wedge, D and H. The variation of δ for various values of K_o are shown in Fig. 7.4(c). It can be seen that the implicit values of δ are not larger than could reasonably be mobilized on the interface.

Similar analyses were performed to evaluate values of δ implicit in at-rest earth pressure conditions (with K_v=0) for the other walls analyzed using the finite element method. The results are shown in Table 7.2. It can be seen that the implicit values of δ are not unreasonably large, and are within a range of values than could reasonably be mobilized.

The results of at-rest and finite element analyses are compared in Table 7.3. On the average, the at-rest earth pressure coefficient K_o is about 30 percent higher than the value of K_h from finite element analyses. The maximum base pressures, the positions of the resultant on the base and the mobilized base friction angles clearly show that the at-rest analyses are conservative for walls on soil. The finite element analyses yield $FS_{sliding}$ that are 20 to 50 percent higher than those obtained using at-rest pressures. These results are also overconservative for walls on soil, especially since it has been established in earlier chapters that

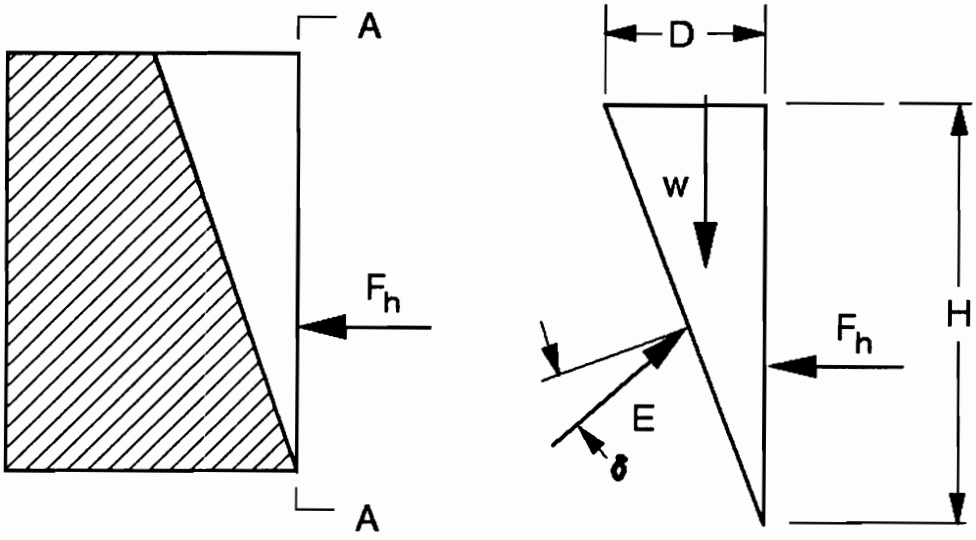

(a) Free body isolated in conventional analyses (not all forces shown)

(b) Free body diagram of backfill wedge showing implicit friction angle

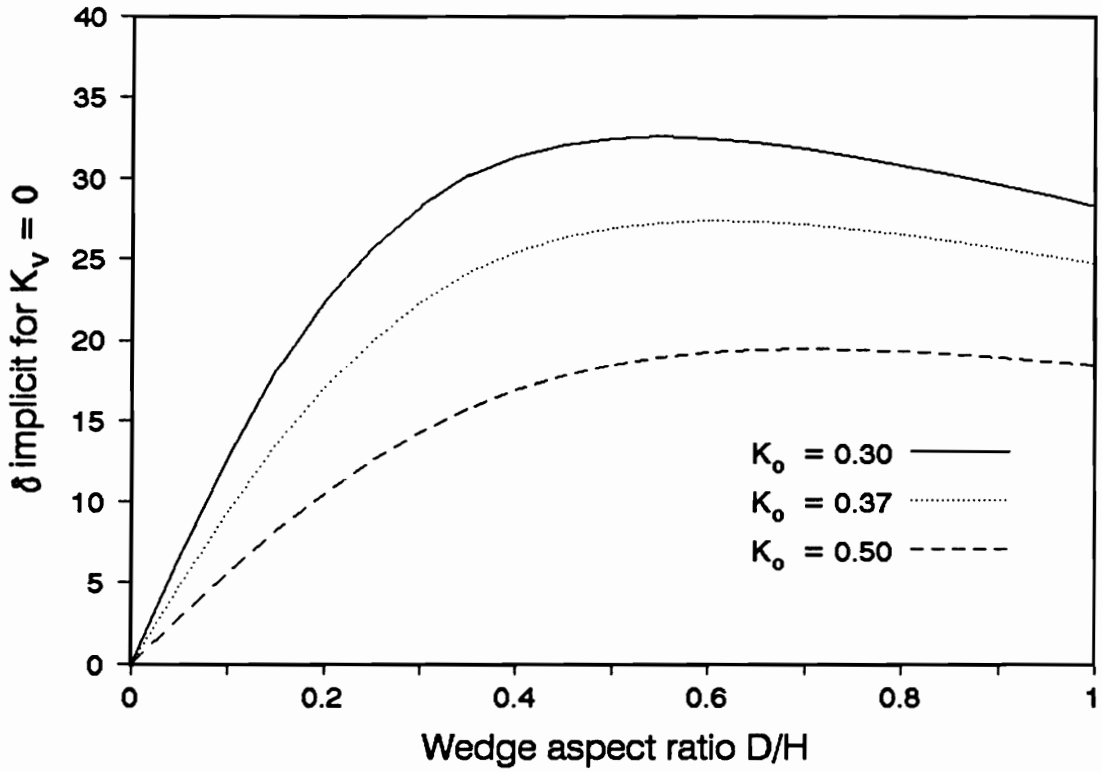

(c) Variation of the implicit friction angle with the aspect ratio D/H

Figure 7.4 - The Implicit Friction Angle in Conventional Analyses

Table 7.2 - Implicit Wall-backfill Friction Angles for At-rest Analyses

$K_o = 1 - \sin(\varphi) = 0.37$

Wall type	Implicit $\delta°$
Gravity Wall	22.3
Cantilever Wall	
B'/B=0.33	23.6
B'/B=0.50	18.5
B'/B=0.67	10.4

Table 7.3 - Results from Conventional At-rest and Finite Element Analyses

Wall type	X_{DD}/B	q_{max}(psf)	K_h/K_o	δ_{base}
Gravity Wall				
At-rest (K_v = 0)	0.36	8,890	1.00	16.3
FEA (K_v = 0.07)	0.37	8,070	0.73	11.3
Cantilever Wall				
B'/B=0.33				
At-rest (K_v = 0)	0.40	4,830	1.00	23.2
FEA (K_v = 0.09)	0.50	3,320	0.70	15.2
B'/B=0.50				
At-rest (K_v = 0)	0.40	3,840	1.00	28.5
FEA (K_v = 0.10)	0.54	3,380	0.70	18.3
B'/B=0.67				
At-rest (K_v = 0)	0.34	3,480	1.00	36.4
FEA (K_v = 0.11)	0.57	2,990	0.62	20.3
Stepped-face wall				
n_s = 2				
At-rest (K_v = 0)	0.33	8,850	1.00	16.3
FEA (K_v = 0.20)	0.42	7,530	0.89	13.0
n_s = 5				
At-rest (K_v = 0)	0.33	8,840	1.00	16.5
FEA (K_v = 0.13)	0.40	7,730	0.73	11.0
n_s = 10				
At-rest (K_v = 0)	0.33	8,830	1.00	16.5
FEA (K_v = 0.10)	0.42	7,080	0.68	10.5

NOTE : All angles are in degrees

FEA - Finite element analysis

massive retaining walls would more likely fail by bearing capacity rather than overturning or sliding.

CONCLUSIONS

The preceding discussions show that analyses of wall stability performed using Coulomb active earth pressures with δ equal to 0.67Φ, or even δ equal to Φ, result in magnitudes and locations of forces on the base that are not much different from those determined by finite element analyses. Even though the Coulomb analyses assume that the strength of the backfill and the strength of the interface are fully mobilized, the forces on the base are not much different from the results of the finite element analyses, where these strengths are not fully mobilized. This is true because the higher values of K_v found from the finite element analyses compensate for the effects of higher values of K_h.

Use of at-rest earth pressures with K_v=0, are considerably more conservative than either Coulomb analyses of finite element analyses, and are clearly overconservative for walls founded on soil.

CHAPTER 8

SUMMARY, CONCLUSIONS AND RECOMMENDATIONS

The main objective of this research is to examine how foundation properties, backfill properties, and wall geometry influence the behavior of gravity retaining walls founded on soil. Finite element analyses of walls founded on soil were performed using the program SOILSTRUCT to study these factors. An earlier study performed on walls founded on rock (Ebeling, et al.) provided the starting point for this investigation. Major questions that were addressed in this investigation were : (1) Can the same analytical procedures be used for walls on soil as were used for walls on rock ? (2) How does the behavior of walls on soil differ from the behavior of walls on rock ?

Initial runs using SOILSTRUCT showed that it would be desirable to improve the procedures used for modeling soil element failure and recovery. This led to the development of the "Alpha Method" for 2D soil elements, which was found to improve the accuracy with which the stress-strain behavior of soil elements is modeled, especially for elements that are in failure or near-failure states. In addition, the "Stress State" concept developed by Seed and Duncan (1983) was incorporated in the program. This model provided a better representation of the stress-strain behavior of soil elements that are recovering from a failure condition.

In order to verify the effectiveness of these changes, SOILSTRUCT was used to analyze the classical Rankine active and passive earth pressure problems for which accurate limit state analyses can be performed. The results of the finite element analyses were found to agree very well with the ideal theoretical solutions. The finite element analyses of the Rankine problems demonstrated that the use of the α-method resulted in excellent control of overshoot.

The first finite element analyses of gravity retaining walls on soil were performed using

the "following load" method of analysis. In this method, backfilling of the wall was simulated by applying forces to the wall. This approach had the advantage of reducing the number of variables involved in the analyses making it easier to isolate effects. An interesting result from these analyses is that the mode of failure of walls on soil is usually bearing capacity failure, rather than overturning or sliding. A reliable assessment of the stability of walls on soil can be made by analyzing the wall-foundation system as a bearing capacity problem. It was found that Vesic's bearing capacity theory provides an effective means of analysis.

Analyses of gravity walls on soil were also performed using the backfill placement method of analysis. In this approach, the backfill was represented by finite elements, and the backfilling operation was modeled by adding the backfill elements one layer at a time. This approach accounts for soil-structure interaction effects and provides a more complete and realistic model of the backfilling process than the following load approach. The results of these analyses confirmed earlier findings that gravity retaining walls on soil will more likely fail by bearing capacity rather than overturning or sliding. The results also showed that shear forces on the vertical plane through the heel of the wall, which were found to be a significant factor in the stability of walls on rock, also exist for walls on soil. In general however, the shear forces for walls on soil are smaller in magnitude than the corresponding forces for similar walls founded on rock. A wall on soil settles more than a wall on rock, thereby reducing the shear forces exerted on the wall by the settling backfill. For cohesionless backfill, the vertical shear force coefficient K_v was found to be 0.10 or higher for walls on rock , while for similar walls on soil , K_v is generally 0.07 or higher. The sets of analyses utilizing the backfill placement method provided a better understanding as to how factors such as wall shape and material properties affect the values of K_v.

Analyses of gravity walls involving either a cohesive backfill or a cohesive foundation indicate that these walls can perform better than walls with only cohesionless soils in the backfill

and foundation. These results are contrary to findings from experience, however, indicating that the finite element analyses of cohesive backfills and foundations are not reliable indicators of long-term behavior. This inconsistency between analytical results and long-term field behavior is attributed to the inability of SOILSTRUCT to model important aspects of the behavior of cohesive soils such as creep and swell.

Backfill placement analyses were also performed to examine the behavior of cantilever and stepped-face walls. It was found that the sliding stability of a cantilever wall decreases as the wall stem is located closer to the heel, and sliding will occur if the wall, together with the prism of backfill that rests on the base slab, is not sufficiently massive. The number of steps (n_s) on a stepped-face wall has little effect on wall stability. However, n_s influences localized movements in the soil mass directly above the wall. More steps of smaller size result in more pronounced local movevents in the backfill, which in turn reduce the horizontal and vertical earth loads on the wall.

Comparisons were made between the results of finite element analyses and the results using two conventional design procedures, the first utilizing Coulomb active pressures and the second utilizing at-rest earth pressures. It was found that Coulomb analyses yielded results that were not much different from finite element analyses results, primarily because of compensating effects resulting from lower values of K_h and K_v in the Coulomb approach. In comparing the finite element results with at-rest analyses, the use of at-rest pressures in design is clearly overconservative for walls on soil.

In view of the findings in this research, it is recommended that :

(1) Finite element procedures for analyzing creep and swell should be developed, so that more realistic analyses can be performed for geotechnical problems involving the long-term behavior of cohesive soils

(2) The possibility of improving the Alpha Method for 2D elements, or of developing more efficient and effective convergence procedures, should be investigated. Efforts should be directed at further reducing the magnitude of overshoot, within a reasonable amount of computer time.

REFERENCES

Clough, G. W., and Duncan, J. M. (1971), "Finite Element Analyses of Retaining Wall Behavior", *Journal of the Soil Mechanics and Foundation Division*, ASCE, Vol. 97, No. SM12, Dec., pp. 1657-1673.

Duncan, J. M., Byrne, P., Wong, K. S. and Mabry, P. (1980), "Strength, Stress-Strain and Bulk Modulus Parameters for Finite Element Analyses of Stresses and Movements in Soil Masses", *Geotechnical Engineering Research Report No. UCB/GT/80-01*, University of California, Berkeley.

Duncan, J.M. and Chang, C. Y. (1970), "Nonlinear Analysis of Stress and Strain in Soils", *Journal of the Soil Mechanics and Foundation Division*, ASCE, No. SM5, Sept., pp. 1629-1653.

Duncan, J. M., Clough, G. W., and Ebeling, R. M. (1990), "Behavior and Design of Gravity Earth Retaining Structures", *Proceedings*, ASCE Specialty Conference on the Design and Performance of Earth Retaining Structures, Cornell University, Ithaca, pp. 251-277.

Ebeling, R. M., Clough, G. W., Duncan, J. M., and Brandon, T. L. (1988), "Methods of Evaluating the Stability and Safety of Gravity Earth Retaining Structures Founded on Rock", Volume I, *Report prepared for the U.S. Army Corps of Engineers*, Waterways Experiment Station, Vicksburg, Miss., Contract No. DACW39-86-K-0007, July.

Filz, G. M., Clough, G. W. and Duncan, J. M. (1990), "User's Manual for SOILSTRUCT", The Charles E. Via, Jr., Department of Civil Engineering, Virginia Polytechnic Institute and State University, Blacksburg.

Hansen, J. B. (1970), "A Revised and Extended Formula for Bearing Capacity", *Bulletin No. 28*, Danish Geotechnical Institute, Copenhagen, pp. 5-11.

Jaky, J. (1948), "Pressure in Silos", *Proceedings*, 2nd International Conference on Soil Mechanics and Foundation Engineering, Vol. 1, pp. 103-107.

Kulhawy, F. H., Trautmann, C. H., Beech, J. F., O'Rourke, T. D., and McGuire, W. (1983), "Transmission Line Structure Foundations for Uplift-Compression Loading", *EPRI Report EL-2870*, Electric Power Research Institute.

Seed, R. B., and Duncan, J. M. (1983), "Soil-Structure Interaction Effects of Compaction-Induced Stresses and Deflections", *Geotechnical Engineering Research Report No. UCB/GT/83-06*, University of California, Berkeley.

Seed, R. B., and Duncan, J. M. (1986), "FE Analyses : Compaction-Induced Stresses and Deformations", *Journal of the Soil Mechanics and Foundations Division*, ASCE, Vol. 112, No. 1, Jan., pp. 23-43.

Vesic, A. S. (1973), "Analysis of the Ultimate Loads of Shallow Foundations", *Journal of the Soil Mechanics and Foundations Division*, ASCE, Vol. 99, No. SM-1, Jan., pp. 45-73.

Vesic, A. S. (1975), "Bearing Capacity of Shallow Foundations", *Chapter 3 in Foundation Engineering Handbook*, Ed. by H. Winterkorn and H. Y. Fang, Van Nostrand Reinhold Company, New York, pp. 121-147.

APPENDIX A

USER'S MANUAL FOR PROGRAM SOILSTRUCT (ISOTROPIC) WITH THE ALPHA METHOD FOR BASE SEPARATION AND CONTROL OF OVERSHOOT IN 2-D SOIL ELEMENTS

INPUT DATA SEQUENCE

1. IDENTIFICATION DATA --- FORMAT (20A4)

Column	Variable	Explanation
1-80	HED	Analysis identification.

2. CONTROL DATA --- FORMAT (13I5)

MESH PARAMETERS

All nodes, two-dimensional and interface elements to be used in the analysis must initially be included in the mesh; additions or deletions are not allowed, but the material parameters can be changed to make them active or inactive. One-dimensional bar elements usually are added in subsequent construction steps, but may initially be included in the mesh.

Column	Variable	Explanation
1-5	NUMNP	Number of nodal points (1000 maximum).
6-10	NUMEL	Number of elements initially in the mesh, excluding bar and beam elements, but including interface elements. NUMEL (1000 maximum), then, includes NUMJT. Interface elements should be numbered first.
11-15	NUMJT	Number of interface elements (400 maximum).
16-20	NUMBAR	Number of bar elements initially in the mesh (60, maximum including elements added in subsequent construction steps).

ANALYSIS PARAMETERS

Column	Variable	Explanation
21-25	NC	Number of loading and construction steps (60 maximum).
26-30	NMOD	Modulus specification code: = 0 if modulus calculation codes entered with

		Loading Information (See Input Data Section 7) = 1 if modulus Calculation codes entered with Modulus Specification Data. (See Input Data Section 8.)
31-35	INIT	Initial stress input code: = -1 If the initial stresses are generated by direct gravity ($\sigma_x = K_o\sigma_y$) assuming a horizontal ground surface. The user specifies the Y-coordinate defining the ground surface and the material number of the soil to be used in the calculations (See Input Data Section 15.) = 0 if external input from data included in input sequence. (See Input Data Section 16.) = 1 if internally generated from gravity turn-on analysis assuming linear elastic response of soil, and using $\nu = K_o/(1 + K_o)$ = 2 if the initial stresses are to be set equal to zero internally
36-40	KI	= 0 if the interface is automatically activated. KI is used when INIT is not equal to 0. If INIT=0, then KI can be left blank.
41-45	IHORIZ	Ground surface inclination code (used only when INIT = 1): = 0 Normally used for horizontal ground surface. Vertical stresses computed from gravity turn-on. Horizontal stresses are computed using K_o. The τ_{xy} shear stress is set to zero. = 1 Normally used for sloping ground surface. Vertical and horizontal stresses are calculated from gravity turn-on analysis. The τ_{xy} shear stress is obtained from the gravity turn-on analysis.

Note: IHORIZ may be 0 or 1 for either level or sloping ground.

OUTPUT PARAMETERS

Column	Variable	Explanation
46-50	ITRD	Analysis printout code: = 0 if initial stresses are to be printed. = 2 if initial stresses are not to be printed
56-60	ILIST	Element and nodal point data printout code: = 0 if not printed.

		= 1 if printed.
61-65	IPINIT	Initial stress disk storage code: = 0 no disk storage. = 1 disk storage of analysis continuation data after calculation of initial stresses.

2. BASIC PARAMETERS --- FORMAT (2F10.4)

The unit weight of water and the atmospheric pressure are included as basic parameters. Either English or SI units can be used, but consistency must be maintained with coordinate, pressure, and material property parameters.

Column	Variable	Explanation
0-10	GAMW	Unit weight of water.
11-20	PATM	Atmospheric pressure.

4. MATERIAL ALLOCATION --- FORMAT (16I5)

All two dimensional material types are assigned numbers first, followed by the interface material types. (Note that bar elements are not assigned a material type number,but are identified solely by their element number.) If a number for NATYP, for example, is not required, assign a value of zero or leave blank.

Column	Variable	Explanation
1-5	NUMMAT	Total number of material types, including both two-dimensional soil or construction material types and interface material types.
6-10	NUMSOL	Total number of material types excluding the interface material types. Thus, (NUMMAT-NUMSOL) must equal the number of interface material types.
11-15	NATYP	Material type number assigned to 2-D elements having the properties of air. Usually, elements that will be built are initially identified as air elements. This material type must be included if excavation is performed.
16-20	NA2TYP	Material type number assigned to interface elements having the properties of air. Usually, elements that will be built are initially identified as air elements. This material type must be included if excavation of interface elements is performed.

21-25	NCTYP	Structural material type, such as concrete. Note that this designation is a matter of convenience in programming. Actually, any material can be a "structural" material. NCTYP simply designates a material which will automatically be considered to have a linear elastic response and may be used in the build-up process. In Input Data Section 8 of this manual an alternative means is available to force linear elastic response on any material.
26-30	NB1TYP	Backfill material type 1. (refer to Input Data Section 13 on fill or concrete placement)
31-35	NB2TYP	Backfill material type 2. (refer to Input Data Section 13 on fill or concrete placement)

5. THE ALPHA METHOD FOR INTERFACE AND 2-D ELEMENTS

(a) FIRST LINE OF DATA — FORMAT(2I5, 20X, 4I5)

The following set of variables control (a) the model of the loss of contact between a structure and its foundation using the Alpha Method for interface elements and (b) the maximum number of iterations for the Alpha Method for 2-D elements in one loading step. For the Alpha Method for interface elements, only horizontal interface elements may be used along the base of the structure.

Column	Variable	Explanation
1-5	NLOOP	Maximum number of iterations using the Alpha Method for interface elements for each loading step. If the Alpha Method for interface elements is not required, a value of zero should be assigned to NLOOP or it may be left blank.
6-10	KEYFRC	Linear stress increment applied to interface elements during transfer of shear stress to adjacent element (zero or blank).
31-35	NOELF1	First horizontal element checked for tension.
36-40	NOELF2	Last horizontal element checked for tension.
41-45	NGROUP	Number of groups of interface elements for which resultant forces are to be computed (See Input Data Section 3(b)).
46-50	NLOOP2	Maximum number of iterations using the

		Alpha Method for 2-d elements for each loading step. If the Alpha Method for 2-d elements is not required, a value of zero should be assigned to NLOOP2 or it may be left blank. NOTE : If both NLOOP and NLOOP2 are non-zero, the smaller of the two will determine the maximum number of iterations using the Alpha Method.

(b) SECOND LINE OF DATA --- FORMAT (2I5)

The following lines specify the element numbers of the interface elements to be grouped for the purpose of computing stress resultants.

Column	Variable	Explanation
1-5	NELGRP(I,1)	First interface element in group I
6-10	NELGRP(I,2)	Last interface element in group I
		Repeat until I is equal to NGROUP sets of interface elements.

6. CONTROL PARAMETERS FOR EXCESSIVE DISPLACEMENT CHECK

(a) FIRST LINE OF DATA --- FORMAT (3I5, 2D10.1, I5)

The following variables control the routines that check if "excessive" incremental displacements have occurred at specified locations in the mesh.

Column	Variable	Explanation
1-5	ICKCOL	Code that specifies the type of incremental displacement check to be performed = 0 if no check is to be made = 1 if the mesh is to be checked for excessive incremental x-displacements. = 2 if the mesh is to be checked for excessive incremental y-displacements. = 3 if the mesh is to be checked for excessive incremental x or y-displacements. If ICKCOL $\neq$ 0, appropriate messages will be printed when excessive incremental displacements occur.

6-10	LODCHK	The number of the load step when a check for excessive incremental displacements will be first performed. The same check will be performed in all subsequent load steps.
11-15	NNDCHK	The total number of nodal points to be checked for excessive incremental displacements. If ICKCOL = 0 or left blank, NNDCHK will not be used. If ICKCOL $\neq$ 0 and NNDCHK = 0, all nodes in the mesh will be checked for excessive incremental displacements.
16-25	XTOL	Tolerance value of incremental x-displacement. Beyond this value, the incremental x-displacement will be considered excessive.
26-35	YTOL	Tolerance value of incremental y-displacement. Beyond this value, the incremental y-displacement will be considered excessive.
36-40	ICOLST	Stop run code = 1 if the program is to stop executing if and when the incremental displacements of specified nodes exceed the tolerance values specified in XTOL and/or YTOL. The stresses and displacements prior to the occurrence of excessive displacement(s) will be printed.

(b) SECOND LINE OF DATA --- FORMAT (16I5)

The following line(s) specify the nodal points that will be checked for excessive incremental displacements.

Column	Variable	Explanation
1-5	NDCHK(I)	Nodal point number of the first node to be checked for excessive incremental displacements. Information on the next 15 nodal points is supplied in the next 15 five-column fields.

7. LOADING INFORMATION DATA --- FORMAT (3I2, 1X, I2, 1X, 5I2, 15A4)

One line of data is supplied for each construction step. One to three loading/construction modes can be included in each construction step. The loading/construction mode codes include:

KCS(MQ,I)	LOADING/CONSTRUCTION MODE
1	Excavation
2	Fill placement
3	Seepage loading
4	Deletion of bar element
5	Installation of bar element
6	Boundary pressure loading
7	Temperature loading
8	Support displacement
9	Concentrated nodal loads
10	Element material type change

As mentioned above, a construction step can include up to three loading/construction modes. The equivalent nodal loads and displacements from all the modes of a construction step are assembled, and any specified material type changes are made prior to assembling the global stiffness vector and solving the assembled equations. The following modes apply loads: excavation, fill, seepage loading, deletion of a bar element, boundary pressure loading, temperature loading, and concentrated nodal loading. The following modes cause material type changes to be made: excavation, fill, and element material type change. The mode for bar installation adds spring elements to the mesh, but it does not apply concentrated nodal loads to the load vector.

All construction modes which generate equivalent nodal loads or support displacements can be applied in a series of equal substeps in order to better track non-linear stress-strain behavior of soil and interface elements. All the assembled loads and displacements of a construction step are divided equally into NUMSS(MQ) substeps.

The following pairs of loading/construction modes cannot be combined in a construction step: deletion of a bar element and fill placement, excavation and material type change, and seepage loading and temperature loading. Generally, problems which involve both seepage and temperature loading require a restart analysis (See Input Data Section 16). Also, if a temperature change is specified, and a given number of substeps is specified, then only temperature loading can be specified in the loading step - i.e., KCS(MQ,2) and KCS(MQ,3) must be set equal to zero, or left blank. If the number of substeps, NUMSS(MQ),is equal to one, then temperature loading can be included with any other loading/construction modes in a load step.

Since the same input format is used and similar operations are performed for loading/construction modes 8 and 9, the following rules in the usage of these two codes apply. If

only concentrated nodal loads are specified, use mode 9. If only support displacements are specified, use mode 8. If both loads and displacements are specified, use mode 8.

Column	Variable	Explanation
1-2	KCS(MQ,1)	First loading/construction mode code.
3-4	KCS(MQ,2)	Second loading/construction mode code.
5-6	KCS(MQ,3)	Third loading/construction mode code. KCS(NC,1), KCS(NC,2), and KCS(NC,3) can be input in any numerical order, but the modes are processed in ascending numerical order. If the second and/or third loading construction modes are not required then KCS(NC,2) and/or KCS(NC,3) should be set equal to zero or left blank.
8-9	NUMIT(MQ)	Number of iterations for the loading step. NUMIT(MQ) applies to each substep if substeps are specified. A maximum of 10 iterations can be specified.
11-12	NUMSS(MQ)	Number of substeps. A maximum of 10 substeps can be specified.
13-14	MOD(1,MQ)	Modulus calculation code: = 1 if a loading modulus is to be calculated = 2 if an unload reload modulus is to be calculated. = 0 if the computer is to decide the type of modulus to be calculated. In this case, if the most recently calculated stress level for an element is less than the critical stress level, an unload-reload modulus is calculated. Otherwise a loading modulus is calculated. Data is required here only if NMOD = 0. All material types, other than interface or bar elements, are given one of the above codes. If NMOD=0 and NC=0, as might be the case for an analysis of initial stresses, MOD(I,1) is set equal to zero, or the computer decides.
15-16	NALFPT(MQ)	Print code for the Alpha Method = 1 information on the results of the Alpha Method analyses will be output for this load step. The information includes which

		element(s) failed, the worst stressed element and the value of the load factor α for this element.
17-18	IPRT(MQ)	Print code for stresses and displacements. = 0 print displacements and stresses for final iteration only. = 1 print interface element stresses for each iteration, and stresses for all elements and displacements for the final iteration only. = 2 print stresses for all elements for each iteration, stresses and displacements for final iteration only. = 3 print stresses and displacements for each iteration.
19-20	IPUN(MQ)	Disk storage code = 0 no disk storage = -1 store analysis continuation data and displacements for plotting prior to implementation of the Alpha Method. = -2 store analysis continuation data prior to implementation of the Alpha Method. = -3 store displacements for plotting prior to implementation of the Alpha Method. = 1 store analysis continuation data and displacements for plotting after the implementation of the Alpha Method. = 2 store analysis continuation data after the implementation of the Alpha Method. = 3 store displacements for plotting after the implementation of the Alpha Method.
21-80	HEDCS(MQ)	Description of loading step.

6. MODULUS SPECIFICATION DATA --- FORMAT (40I2)

This information is required only if NMOD = 1 and NC > 0. A line of data is required for each loading step, 1 to NC. In this option, values of the modulus specification code are specified for all material types (and thus each element, excluding bar and beam elements).

Column	Variable	Explanation
2,4,6,...	MOD(I,NC)	Modulus calculation code for each material type (1 to NUMMAT) for the first load step. Separate lines of data are required for each load step. Columns not used can be left blank.

9. MATERIAL PROPERTIES

These data are used only for two-dimensional elements (e.g., soil, air, concrete); the first and second lines of data must be supplied for each material type, excluding bar and interface material types. The first and second lines of data, as a pair, are supplied in order of material type number N = 1 to NUMSOL. Information or properties not required for a material type can be left blank.

(a) FIRST LINE OF DATA --- FORMAT(I10, 7D10.5)

Column	Variable	Explanation
1-10	IDRAIN(N)	Material behavior code: = 0 if undrained = 1 if drained
11-20	GAM(N)	Total unit weight (always specified, regardless of drained or undrained material behavior).
21-30	COHE(N)	Undrained strength or cohesion.
31-40	PHI(N)	Friction angle in degrees.
41-50	TENS(N)	Minimum allowable value of the minor principal stress for isotropic nonlinear (non-elastic) materials. Enter as a positive value : $0.0 \leq$ TENS(N) $\leq$ COHE(N) / TAN(PHI(N)). May be left blank when XXP(N) = 0.0.
51-60	AO(N)	Coefficient of lateral earth pressure at rest, K_o, pertaining to effective stresses. Must be specified when INIT = 1 and XXP(N) $\neq$ 0.0
61-70	XXP(N)	Exponent n in the initial tangent and unload-reload modulus expressions. Its value is assumed to be independent of loading mode. For a linear elastic material n must be 0. For saturated soils in undrained loading, when PHI(N) = 0., n should normally be 0.0001.
71-80	HCOEF(N)	Coefficient K_m in the initial tangent modulus expression: $$E_i = P_a K_m (\sigma_3 / P_a)^n$$ May be left blank when XXP(N)=0.0

(b) SECOND LINE OF DATA --- FORMAT(8D10.5)

Column	Variable	Explanation
1-10	ULCOEF(N)	Coefficient K_{ur} in the unload-reload modulus expression: $$E_{ur} = P_a K_{ur} (\sigma_3 / P_a)^n$$ May be left blank if XXP(N) = 0.0
11-20	FR(N)	Correlation factor: ratio of measured strength at failure to ultimate hyperbolic strength. May be left blank when XXP(N) = 0.0
21-30	EIMN(N)	Minimum initial tangent modulus for nonlinear (non-elastic) materials. Normally, EIMN(N) > E(N) for XXP(N) $\neq$ 0.0. May be left blank when XXP(N) = 0.0
31-40	XXPB(N)	Exponent for bulk modulus expression. May be left blank when XXP(N) = 0.0
41-50	BCOEF(N)	Bulk modulus coefficient. May be left blank when XXP(N) = 0.0
51-60	E(N)	Tangent modulus at failure for nonlinear (non-elastic) materials, or Young's modulus for elastic materials, i.e., when XXP(N) = 0.0.
61-70	GUE(N)	Poisson's ratio for linearly elastic material. May be left blank when XXP(N) $\neq$ 0.0
71-80	ALPHA(N)	Coefficient of linear thermal expansion for structural element; zero or blank otherwise.

10. INTERFACE PROPERTIES

Two lines of data are supplied for each interface material type, N = 1 to NUMJT = NUMMAT - NUMSOL. If there are no interface materials, no data are required.

(a) FIRST LINE OF DATA --- FORMAT (I10, 3D10.5, I10)

Column	Variable	Explanation
1-10	JDRAIN(N)	Interface behavior code: = 0 if undrained = 1 if drained
11-20	COJ(N)	Interface cohesion.

21-30	PHJ(N)	Interface friction angle in degrees.
31-40	TENSJ(N)	Tensile strength of interface material. Enter tensile strength as a positive value: $0.0 \leq$ TENSJ(N) $\leq$ COJ(N)/TAN(PHJ(N))
41-50	IADJMT(N)	Material number of 2-D soil element next to the interface. Used only for build-up situations.

(b) SECOND LINE OF DATA --- FORMAT (5D10.5)

Column	Variable	Explanation
1-10	RKS(N)	Initial shear stiffness
11-20	STFSMN(N)	Failure shear stiffness
21-30	RKN(N)	Initial normal stiffness
31-40	STFNMN(N)	Failure normal stiffness
41-50	FRJ(N)	Correlation coefficient for shear displacement relationship, FRJ = 0.0 for bilinear; $1.0 \geq$ FRJ > 0.0 for hyperbolic

11. NODAL POINT DATA --- FORMAT (I10, 4D10.4)

One line of data is supplied for each node. The numbering of nodal points must be sequential and some of the nodes can be omitted. Those nodes omitted are automatically generated by the program at equal spacings between those specified. The first and last nodes must always be specified. Note that DP(N) and PP(N) are automatically generated in equal increments for those nodes omitted.

Column	Variable	Explanation
1-10	N	Nodal point number.
11-20	X(N)	X coordinate, positive to right.
21-30	Y(N)	Y coordinate, positive upward.
31-40	PP(N)	Pore pressure in head of water; zero or blank if not specified. Pore pressures are only used in the analysis of drained materials.
41-50	DP(N)	Change in pore pressure in head of water for

soil elements; change in temperature for linear elastic structural material; zero or blank otherwise.

12. BOUNDARY CONDITIONS

Four lines of data are supplied as required to specify restraints of boundary nodes. If there are no nodes restrained in the mode specified for a particular line of data, then that line of data is not required. For a given line of data, the nodes N = 1 to NOy, NOx or NOxy must be in sequential order.

(a) BOUNDARY TYPES USED --- FORMAT(3I5)

Column	Variable	Explanation
1-5	NOY	Number of nodal points fixed against Y-movement only.
6-10	NOX	Number of nodal points fixed against X-movement only
11-15	NOXY	Number of nodal points fixed against both X- and Y- movement.

(b) NOY NODES --- FORMAT (16I5)

Column	Variable	Explanation
1-5	IC(N)	Nodal point number of the first nodal point fixed against Y- movement. Additional nodal points fixed against Y - movement, N = 2 to NOY, are specified in the next 15 five-column fields and on additional lines of data as required.

(c) NOX NODES --- FORMAT (16I5)

Column	Variable	Explanation
1-5	IC(N)	Nodal point number of the first nodal point fixed against X- movement. Additional nodal points fixed against X-movement, N = 2 to NOX, are specified in the next 15 five-column fields and on additional lines of data as required.

(d) NOXY NODES — FORMAT (16I5)

Column	Variable	Explanation
1-5	IC(N)	Nodal point number of the first nodal point fixed against both X- and Y- movement. Additional nodal points fixed against both X- and Y- movement, N = 2 to NOXY, are specified in the next 15 five column fields and on additional lines of data as required.

13. ELEMENT DATA — FORMAT (6I5)

One line of data is supplied for each interface or two-dimensional element; bar elements are not included in this section. All interface elements are supplied in sequential order first, followed by two-dimensional elements, also in sequential order. Thus, interface elements must be numbered from N = 1 to NUMJT, and two-dimensional elements from N = (NUMJT + 1) to NUMEL. (If "Build" is used; place interface elements which will be built up at the end of the interface element list.)

Nodal point numbers must be specified consecutively, progressing counter-clockwise around the element (See Figure A1.1). The first and last nodal point numbers specified for interface elements must have the same coordinates. Triangular two-dimensional elements having four different nodal point numbers may not be used; the first and last point numbers of a triangular element must be identical.

Element numbers in a row may be omitted, in which case the omitted elements will be generated by incrementing the element number N and the nodal point numbers I, J, K, and L by one, and by assigning the same material type number as specified for the previous element. The first element in each row, and the last element in the problem, must be specified. If no elements are omitted, the element numbering may be done in any order, provided all interface elements are numbered first.

Column	Variable	Explanation
1-5	N	Element number.
6-10	IL(N,1)	Number of nodal point I.
11-15	IL(N,2)	Number of nodal point J.
16-20	IL(N,3)	Number of nodal point K.
21-25	IL(N,4)	Number of nodal point L.
26-30	IL(N,5)	Material type number.

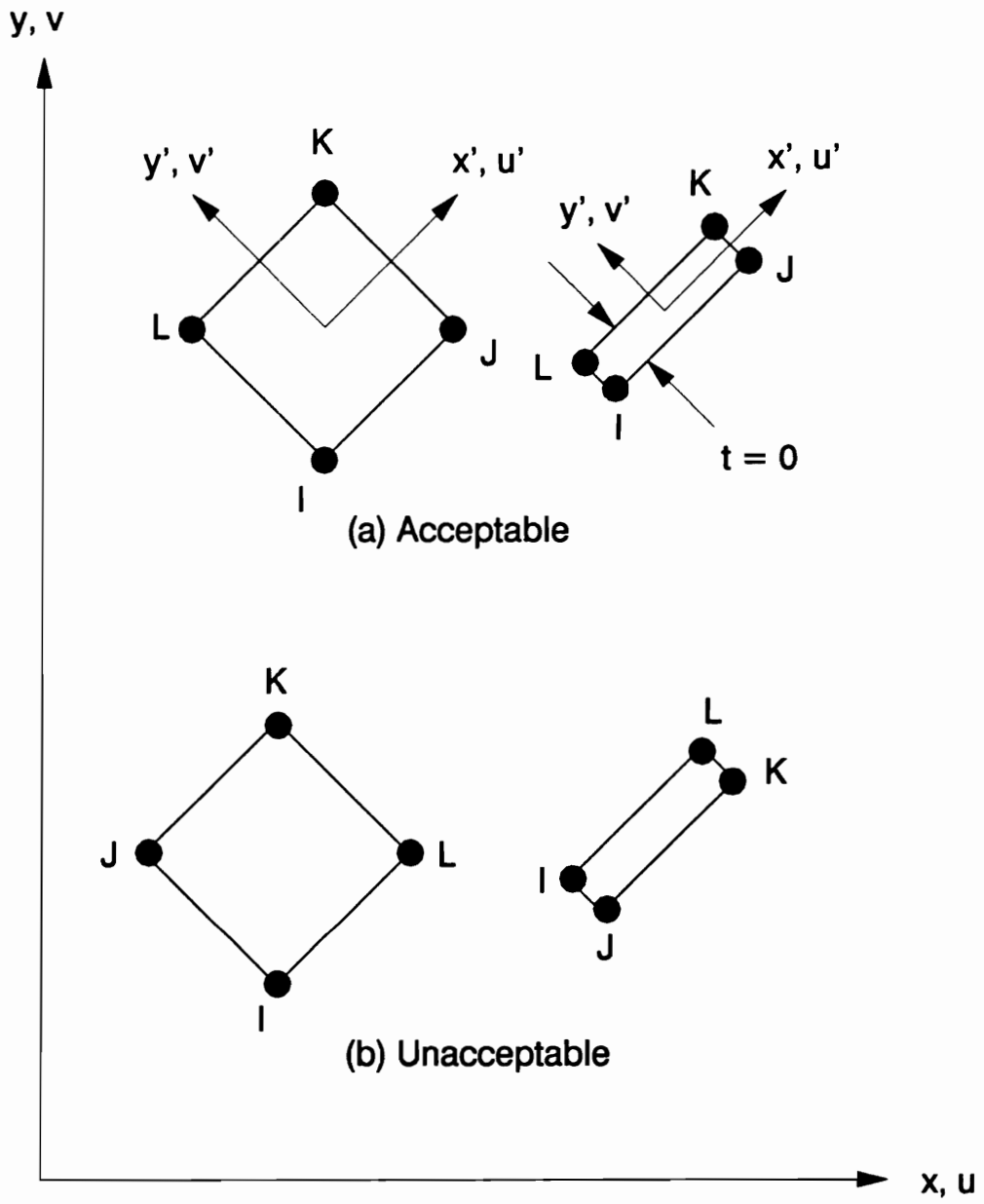

Figure A1.1 - Nodal Point Numbering of Isoparametric QM5 Element and One-dimensional Interface Element

14. BAR ELEMENT DATA — FORMAT (4I5, 2D10.7, 2D10.1, D10.5)

One line of data is supplied for each bar element initially in the mesh or, if a continuation analysis, added in an incremental loading step of the previous analysis. Note that for a continuation analysis these data lines are not automatically generated. Elements are numbered sequentially from N = 1 to NUMBAR.

Column	Variable	Explanation
1-5	N	Element number.
6-10	IB(N,1)	Number of nodal point I.
11-15	IB(N,2)	Number of nodal point J.
16-20	IB(N,3)	Spring response type code: = 1 if both compression and tension of bar allowed. = 2 if only compression allowed. = 3 if only tension allowed.
21-30	BAR(N,1)	cos α
31-40	BAR(N,2)	sin α

The sign of angle α is determined as shown in Figure A1.2. Angle α is measured counter-clockwise from a line drawn in the positive x-direction at the I node to the line of action connecting the I node to the J node. (See comments that follow).

41-50	BAR(N,3)	Prestress force in the bar element. This only inputs the normal force in the bar; a force is not applied to the mesh by BAR(N,3). the force must be applied as loads using loading/construction mode 9 in a loading step. For strut support, the load need only be applied at node I. For anchor support, the load should be applied at both nodes.
51-60	BAR(N,4)	Stiffness of bar element. This is usually computed as AE/L, but the mesh length (distance from node I to node J) need not, and usually does not, correspond to the actual length.
61-70	BAR(N,5)	Displacement of bar element at activation. This allows for a specified degree of slack at the strut connection; the bar will deform BAR(N,5) prior to its stiffness being activated.

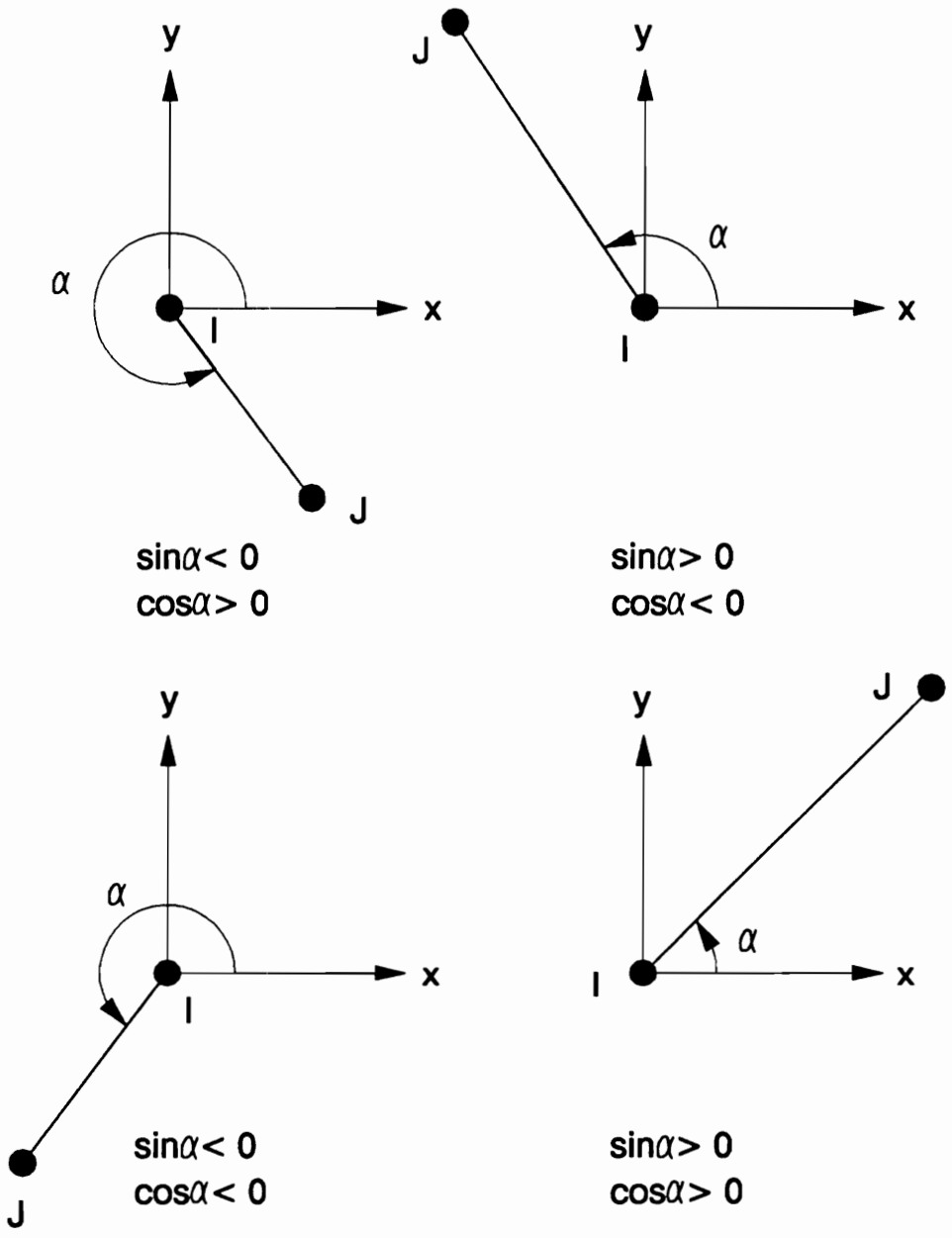

Figure A1.2 - Sign Convention and Definition of Local Axes for Bar Element

Bar elements can function as either anchors or strut (spring) supports. The required parameters are dependent on which type of bar element is desired.

To specify strut support, nodal point J is a node fixed against x- and y- movement. For program storage efficiency the number of node J should be as close as possible to the number of node I. Nodal point I represents the point of connection between the wall and the actual strut. Nodal points I and J are not necessarily physically connected, since the element stiffness is entered independently. Nodal point J allows the force at the J node to be carried into the system as a reaction at a fixed node. This is consistent with the typical mesh representation of one half of a symmetric excavation. The value of sin α and cos α are specified according to the sign convention shown in Figure A1.2. The values are entered to represent the line of action of the strut support, and do not need to correspond to the relative positions of the I and J nodes.

To specify anchor support, nodal points I and J physically represent two ends of the anchor, and must be restrained appropriately. The values of sin α and cos α must correspond to the relative positions of the I and J nodes representing the ends of the anchor. Stiffness is computed as AE/L, with L being the distance between nodes I and J, and either A or E altered to give the correct stiffness. Stiffness for an anchor or a strut is entered as force per length per length of wall.

For either type of support, specifying the prestress force does not apply the force. The concentrated force loading/construction mode must be used for this purpose.

15. SUPPLEMENTAL DATA FOR INIT = −1 — FORMAT (D10.4, I10)

This single line of data is required only if INIT = −1. In this option, ground stresses are established by direct gravity ($\sigma_x = K_o\sigma_y$). The stresses are computed for all elements whose centers (defined by the y-coordinate y_c) are below a horizontal ground surface (defined by the y-coordinate y_t). The vertical stress is computed as follows : σ_v=σ_y=$\gamma_s(y_t - y_c)$ for $y_c < y_t$. γ_s is the total unit weight of the material whose material number is given by MT.

Column	Variable	Explanation
1-10	YTOP	The y-coordinate of the horizontal ground surface.
11-20	MT	Material number of the material type (See Input Data Section 9) whose total unit weight will be used for calculating the ground stresses.

16. CONTINUATION OR INITIALIZATION DATA

These data are supplied only if INIT = 0; it can be obtained from external disk storage generated by a preceding analysis with IPUN = −1, −2, 1 or 2 (See Input Data Section 7). This option is provided so that a required sequence of loading steps can be stopped at an intermediate step, then restarted from that step without redoing the complete analysis. However, these data may also be used to specify values of particular variables in an initial

analysis without using the gravity turn-on procedure followed with INIT = 1 or the special procedures followed with INIT = −1 or 2. Similarly, particular parameter values can be changed, if the sequence of loading is stopped, prior to a restart analysis.

(a) ELEMENT INFORMATION — FORMAT (6I5)

Column	Variable	Explanation
1-5	NUMEL	Number of elements in the mesh, excluding bar and beam elements, but including interface elements.
6-10	NUMJT	Number of interface elements.
11-15	NUMBAR	Number of bar elements, including those initially in the mesh and those added in previous loading steps (if a restart analysis.)
16-20	NUMNP	Number of nodal points in the mesh.
21-25	NSTART	Element failure code = 0 if there are no shear or tension failures in interface or soil elements. IFLOLD and IFAIL keys are set equal to zero for all elements (indicating no failure) within the program. See card groups 16(h) and 16(i). = 1 if IFLOLD keys are to be read for all interface elements and IFAIL keys are to be read for all elements.

When NSTART = 1, the keys IFLOLD and IFAIL have usually been determined in a previous analysis and are included in the analysis continuation data when the disk storage option was activated.

26-30	NISTIF	Interface stiffness input code = 0 if the interface element stiffness values will be computed using the material properties specified in Input Data Section 10. = 1 if the interface element stiffness values are to be read (See Input Data Section 16(g)).

(b) INTERFACE ELEMENT STRESS INFORMATION

Three cards are supplied for each interface element, in numerical sequence from N = 1 to NUMJT. For each interface element, the pair of normal and shear stresses at node I (SIGI), the center (SIG) and node J (SIGJ) are suppled, as well as the maximum past stresses state (SSMPJT) of the element.

FIRST LINE OF DATA --- FORMAT (2(1P, 1D13.6, 2X))

Column	Variable	Explanation
1-13	SIGI(N,1)	Normal stress at node I of interface element
16-28	SIGI(N,2)	Shear stress at node I of interface element

SECOND LINE OF DATA --- FORMAT (3(1P, 1D13.6, 2X))

Column	Variable	Explanation
1-13	SIG(N,1)	Normal stress at center of interface element
16-28	SIG(N,2)	Shear stress at center of interface element
31-43	SSMPJT(N)	Maximum past stress state of interface element

THIRD LINE OF DATA --- FORMAT (2(1P, 1D13.6, 2X))

Column	Variable	Explanation
1-13	SIGJ(N,1)	Normal stress at node J of interface element
16-28	SIGJ(N,2)	Shear stress at node J of interface element

(c) 2-DIM ELEMENT STRESS INFORMATION --- FORMAT (5(1P, 1D13.6, 2X))

One line is supplied for each two-dimensional element, in numerical sequence from N = (NUMJT + 1) to NUMEL.

Column	Variable	Explanation
1-13	SIG(N,1)	Normal stress in the x-direction for a 2-d element, σ_x.
16-28	SIG(N,2)	Normal stress in the y-direction for a 2-d element, σ_y.
31-43	SIG(N,3)	x-y shear stress for a 2-d element, τ_{xy}
46-58	SIG(N,4)	Maximum past stress state for a 2-d element.
61-73	SIG(N,5)	Maximum previous major principal stress (σ_1) for a 2-d element.

(d) NODAL POINT INFORMATION --- FORMAT (3(1P, 1D14.6, 1X))

Information for two nodal points is supplied on each line of data. Nodal points are specified in numerical order, N = 1 to NUMNP.

Column	Variable	Explanation
1-14	DISPX(N)	Displacement in x-direction
16-29	DISPY(N)	Displacement in y-direction
31-44	PP(N)	Pore pressure in head of water.

Information for the next nodal point in sequence is supplied in the next three fields.

(e) MATERIAL TYPE DESIGNATION --- FORMAT (15I5)

Material type numbers for 15 two-dimensional or interface elements are specified on each line of data. Material type numbers for elements in numerical sequence, N = 1 to NUMEL, are specified.

Column	Variable	Explanation
1-5	IL(N,5)	Material type number. Material type numbers for the next 14 elements are supplied in the next 14 five-column fields.

Note that material type numbers supplied on these lines supersedes the material type numbers specified with the element data. Thus material type changes can be made as part of a restart analysis rather than including such changes in a loading step of an analysis.

(f) BAR ELEMENT INFORMATION ---FORMAT (3I5, 2D10.7, 2D10.1, D10.5)

These data are supplied only if bar elements are included (NUMBAR > 0). One line of data is necessary for each bar element.

Column	Variable	Explanation
1-5	IB(N,1)	Number of nodal point I
6-10	IB(N,2)	Number of nodal point J.
11-15	IB(N,3)	Spring response code.
16-25	BAR(N,1)	Cos α
26-35	BAR(N,2)	Sin α

36-45	BAR(N,3)	Force in the bar element.
46-55	BAR(N,4)	Bar element stiffness.
56-65	BAR(N,5)	Displacement of the bar element at activation.

Note that these parameters, if changed for a restart analysis, supersede those specified initially (Input Data section 15). Also, if bar elements are initially included in the mesh, and an initialization procedure is used, then this data must be included.

(g) INTERFACE INFORMATION --- FORMAT (8D10.4)

These data are supplied only if interface elements are included (NUMJT > 0) and the parameter NISTIF $\neq 0$ (See Data Input Section 16(a)). Information for four interface elements is specified on each line of data. Information is supplied for interface elements in numerical sequence, N = 1 to NUMJT.

Column	Variable	Explanation
1-20	STFS(N)	Shear stiffness of first interface element.
21-40	STFN(N)	Normal stiffness of first interface element.
		Information for the next three interface elements is supplied in the next six ten-column fields.

Note that if these stiffness values are read, they supersede the values specified on the Interface Property Data Line (Input Data Section 10(b)).

(h) MODULUS ASSIGNMENT KEY FOR INTERFACE ELEMENTS --- FORMAT (15I5)

This line is supplied if interface elements are included (NUMJT > 0) and NSTART $\neq 0$. Information for fifteen interface elements is specified on each line. Information is supplied for interface elements in numerical sequence, N = 1 TO NUMJT.

Column	Variable	Explanation
1-5	IFLOLD(N)	Modulus assignment key = 0 if interface element N is active. = 1 if tension failure occurred. = 2 if shear failure occurred.

(i) INTERFACE ELEMENT STRESS TRANSFER KEY / 2-D ELEMENT FAILURE KEY --- FORMAT (15I5)

This line is supplied if NSTART $\neq 0$. For interface elements, the key IFAIL is required only for

those elements along the horizontal base of the structure used to model the base separation, with element numbers NOELF1 to NOELF2 (See Input Data Section 3(b)). For other interface elements, the value of IFAIL is not used in this version of SOILSTRUCT. However IFAIL values need to be specified for these elements (may be left blank for convenience). For 2-D elements, IFAIL indicates whether the element is in a failure state prior to the restart analysis. Modulus values for these failed elements are supplied in the restart data input stream (See Input Data Section 13(j)).

Column	Variable	Explanation
1-5	IFAIL(N)	- Stress transfer key for interface elements with element numbers NOELF1 $\leq$ N $\leq$ NOELF2. = 0 if interface element number N is active. = 1 if transfer of normal and shear stress in failed interface element number N has been completed. - Idle for interface elements with element numbers either less than NOELF1 or greater than NOELF2. The entries for these elements may be left blank. - Failure key for 2-D elements = 0 if the 2-D element is not in a failure state. = 1 if the 2-D element is in a failure state.

(j) 2-D ELEMENT MODULUS VALUES — FORMAT (2X, I4, 3X, 3(1X, D10.4))

One line of data is required for each 2-D element number N for which IFAIL(N) $\neq$ 0.

Column	Variable	Explanation
3-6	M	Element number of 2-D element. The lines of data should be supplied in ascending order. If IFAIL(N) $\neq$ 0 and M $\neq$ N, an error message will be printed and program execution will stop.
11-20	ET(N)	Tangent modulus of 2-D element.
22-31	BMOD(N)	Bulk Modulus of 2-D element.

17. LOADING STEPS

These data are required only if NC > 0. Lines of data are assembled in the order specified on the Loading Information Data (Input Data Section 7) : data for the first loading/ construction mode specified for the first construction step are followed by the data for the second loading/construction mode specified for the first construction step, and so on to the data for the

last loading/construction mode specified for the last construction step.

For a given construction step, the lowest numbered loading/ construction mode is processed first, but the analysis of the construction step is made for the combined effect of all loading/construction modes included in the construction step. Care must therefore be exercised in specifying some loading/construction modes, such as material type changes or concentrated forces representing prestress forces, in the same construction step with other loading/construction modes.

** EXCAVATION**

These data are supplied only if KCS(N,1), KCS(n,2), or KCS(N,3) = 1. Input is handled by subroutine EXCAV. In this mode, 2-D soil or construction materials, and interface elements, can be excavated. Free excavated elements and common excavated elements are entered separately. A free excavated element is an element specified to be excavated that has no boundary in common with an element not specified to be excavated in the loading step. A common excavated element, on the other hand, has at least one boundary in common with an unexcavated element (See Figure A1.3).

Interface elements adjacent to excavated elements should be included as free excavated elements even if they have a boundary in common with an unexcavated element. Interface elements cannot be used as interpolation elements. Free, common, and/or unexcavated elements (other than interface elements) can be used as interpolation elements, though common excavated elements are more commonly used.

If possible, adjacent common excavated elements should be entered sequentially as this procedure avoids repetitive computation; nodal loads for a nodal point common to the two sequential elements will only be calculated once.

(a) CONTROL DATA --- FORMAT (215)

Column	Variable	Explanation
1-5	NFXEL	Number of free excavated elements.
6-10	NXELCB	Number of common excavated elements.

(b) FREE EXCAVATED ELEMENT DATA --- FORMAT (16I5)

Element numbers of 16 free excavated elements can be supplied by one line of data. A maximum of 50 can be specified in one loading step. Element numbers of all free excavated elements, N = 1 to NFXEL are to be specified.

Column	Variable	Explanation
1-5	LNXEL(N)	Element number of first free excavated element.Information for the next 15 free

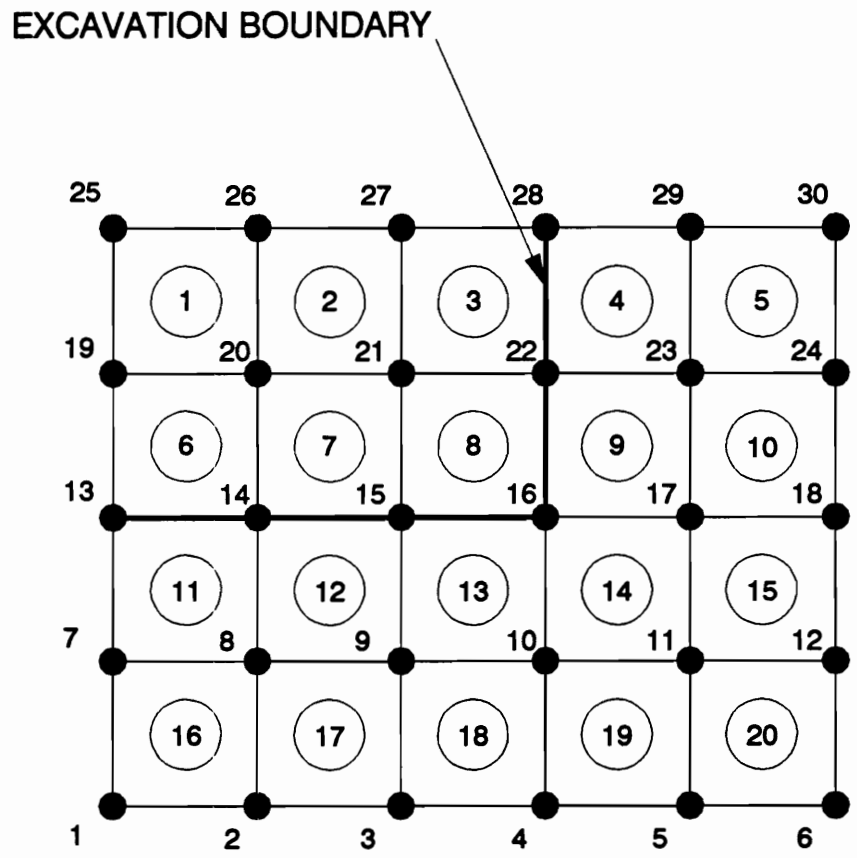

ELEMENTS 1 AND 2 ARE FREE EXCAVATED ELEMENTS
ELEMENTS 3, 6, 7 AND 8 ARE COMMON EXCAVATED ELEMENTS
NODES 13, 14, 15, 16, 22 AND 28 ARE LOADED BY EXCAVATION FORCES
ELEMENTS 6, 7 AND 8 SHOULD BE INPUT SEQUENTIALLY FOR OPTIMUM EFFICIENCY

Figure A1.3 - Example Excavation Load Step Defining Free and Common Excavated Elements in Relation to the Excavation Boundary

excavated elements is supplied in the next 15 five-column fields.

(c) COMMON EXCAVATED ELEMENT DATA --- FORMAT (8I5)

One line of data is supplied for each common excavated element, N = 1 to NSELCB. A maximum of 50 common excavated elements can be specified in one loading step. Loading codes are:

> 0 -the node is not loaded by excavation forces, and is not common to both an excavated and an unexcavated element.
>
> 1 -The node is loaded by excavation forces and is common to both an excavated and an unexcavated element.

Nodes I, J, K, and L refer to the same nodes I, J, K, and L specified on the Element data set (Input Data section 13).

Interpolation elements should be specified in a criss-cross fashion, as shown in Figure A1.4. Further, the x- or y- coordinates of diagonal elements must not be the same. If these rules are not adhered to, the interpolation routine will detect a singularity and processing will stop.

Column	Variable	Explanation
1-5	LUL(N,1)	Element number of the first common excavated element. This element is also the first interpolation element.
6-10	LUL(N,2)	Element number of second interpolation element.
11-15	LUL(N,3)	Element number of third interpolation element.
16-20	LUL(N,4)	Element number of fourth interpolation element.
21-25	LUL(N,5)	Loading code for node I.
26-30	LUL(N,6)	Loading code for node J.
31-35	LUL(N,7)	Loading code for node K.
36-40	LUL(N,8)	Loading code for node L.

Loading codes are specified for the nodes of the element to be excavated specified in columns 1-5.

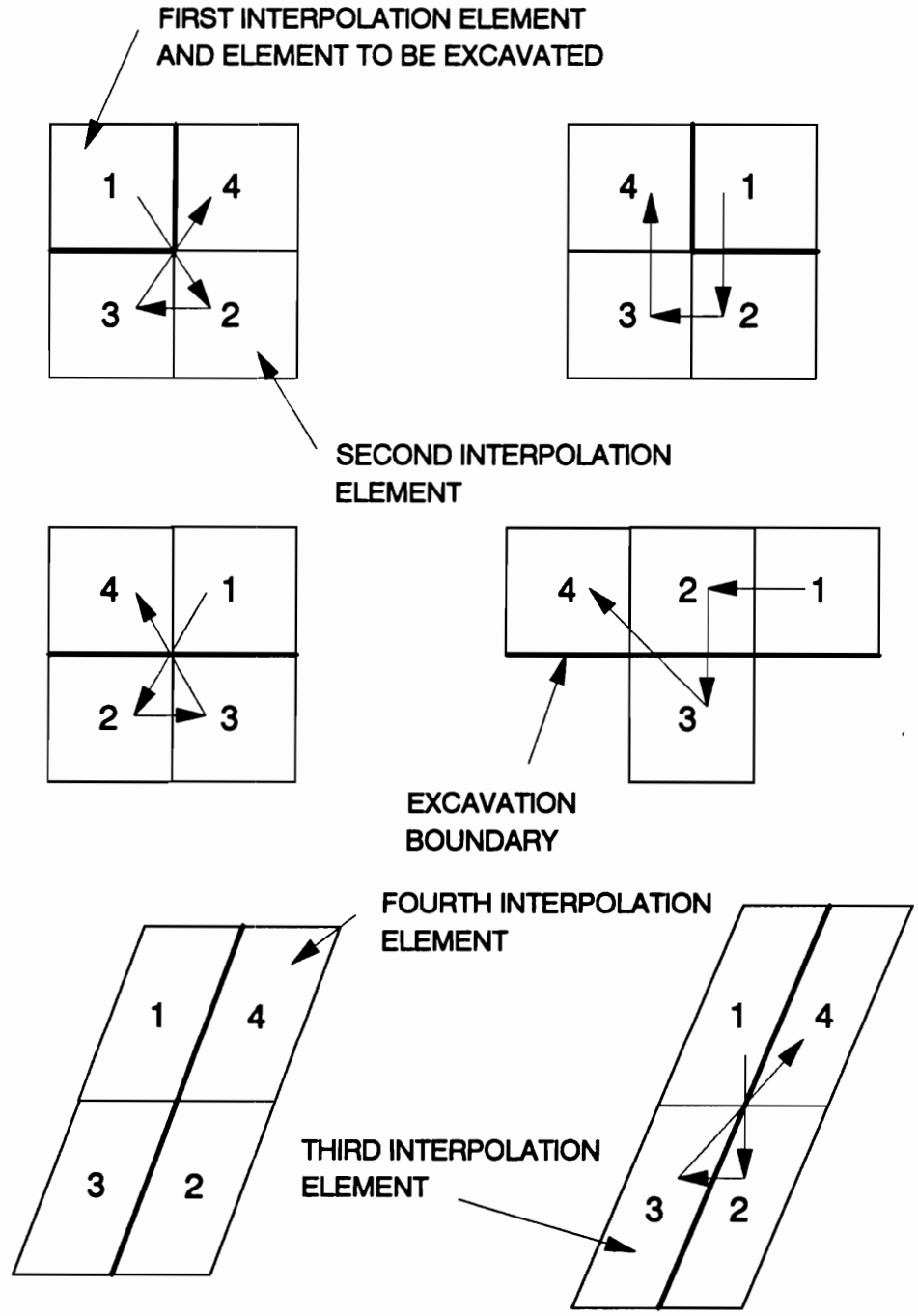

a) Above configutations are acceptable

b) Above configutations are not acceptable

Figure A1.4 - Illustration of numbering of Interpolation Elements for Calculation of Stresses at the Excavation Boundary

** FILL OR CONCRETE PLACEMENT **

These data are supplied only if KCS(N,1), KCS(N,2), or KCS(N,3) = 2. Input is handled by subroutine BUILD. The types of elements that can be placed include structural, soil, and interface elements.

(a) CONTROL DATA — FORMAT (5I5, D10.2)

Column	Variable	Explanation
1-5	NLEL	Total number of elements to be placed, including interface and structural elements.
6-10	NJ	Total number of elements to be placed less the number of inactive interface elements.
11-15	NONP	Number of nodal points within the placed layer(s) to be assigned zero displacements. This includes all nodal points of the elements to be placed except those nodal points in common with an already existing element.
16-20	NCE	Number of structural elements to be placed.
21-25	NB1E	Number of backfill type 1 elements to be placed.
26-35	HTB	New y-coordinate of the top of the placed backfill.

(b) ELEMENT NUMBERS — FORMAT (16I5)

Element numbers of 8 placed elements can be supplied on one line of data. A maximum of 100 can be specified in one construction step. Element numbers and element material types of all placed elements, N = 1 to NLEL, are to be supplied. The elements must be read in by material type according to the following sequence :

1. structural elements
2. backfill type 1 elements
3. backfill type 2 elements
4. interface elements to be activated
5. interface elements to be left inactive but to be placed between elements of like materials.

Column	Variable	Explanation
1-5	LEL(N,1)	Element number of first element to be placed.
5-10	LEL(N,2)	Element material type number of first element

		to be placed. Information for the next 7 placed elements is supplied in the next 14 five-column fields.

(c) NODE NUMBERS — FORMAT (16I5)

Nodal point numbers of 16 nodes to be assigned zero displacement can be supplied on one line of data. A maximum of 100 can be specified in one loading step. Nodal point numbers, N = 1 to NONP, may be specified in any order.

Column	Variable	Explanation
1-5	NP(N)	Nodal point number of first node assigned zero displacement. Information for the next 15 nodal points is supplied in the next 15 five-column fields.

** SEEPAGE **

These data are supplied only if KCS(N,1), KCS(N,2), or KCS(N,3) = 3. Input is handled by subroutine SEEP. Seepage loads are determined from change in pore pressure specified as DP(N) with the nodal point data, or from the specified phreatic level changes. SEEP does not compute negative pore water pressures. Nodal piezometric heads less than zero are set equal to zero. SEEP does not compute water pressures on impermeable boundaries. Water pressures on impermeable boundaries should be applied using KCS(N,I) = 6 or 9.

(a) CONTROL DATA — FORMAT (I5)

Column	Variable	Explanation
1-5	NCODE	Option code specifying how seepage loading data is entered: = 0 if specified as DP(N) with nodal point data. = 1 if to be calculated using the new phreatic surface entered on the following lines of data.

(b) NUMBER OF PHREATIC SEGMENTS — FORMAT (I5)

This line of data is required only if NCODE = 1.

Column	Variable	Explanation
1-5	NWAT	Number of phreatic surface segment end points used to specify the new phreatic surface.

NWAT must be greater than or equal to 2. The number of phreatic surface segments is equal to NWAT. The maximum value of NWAT is 30.

(c) PHREATIC LEVEL DATA --- FORMAT (6D10.2)

This data is required only if NCODE = 1.

The end points of the phreatic surface segments delineating the new and old phreatic surfaces are specified as x-coordinates that must be the same as the x-coordinate of a nodal point. (See Figure A1.5). Both the present and new phreatic surfaces are assumed to be linear between the bounding x- coordinates. The left hand side of the mesh is always the first x-coordinate specified. A bounding x-coordinate on the old phreatic surface will require, usually, specification of the same x-coordinate on the new phreatic surface.

Two end points (x- coordinates), each with associated new and old phreatic levels (y-coordinates), are supplied on each line of data. All end points, N = 1 to NWAT, must be specified.

Column	Variable	Explanation
1-10	XW(N)	x-coordinate for PREL(N) and FUEL(N). (must be the same as the x-coordinate of a nodal point.)
11-20	PREL(N)	Present level (y-coordinate) of the phreatic surface at XW(N)
21-30	FUEL(N)	New level (y-coordinate) of the phreatic surface at XW(N)
		Information for the next end point is supplied in the next three ten-column fields.

** DELETION OF BAR ELEMENTS **

These data are supplied only if KCS(N,1), KCS(N,2), or KCS(N,3) = 4. Input is handled by the main program.

The deleted bar elements remain in the mesh but with zero stiffness. The force the bar element carried is applied to the nodes at its ends.

This loading/construction mode cannot be specified in the same loading step as fill or concrete placement.

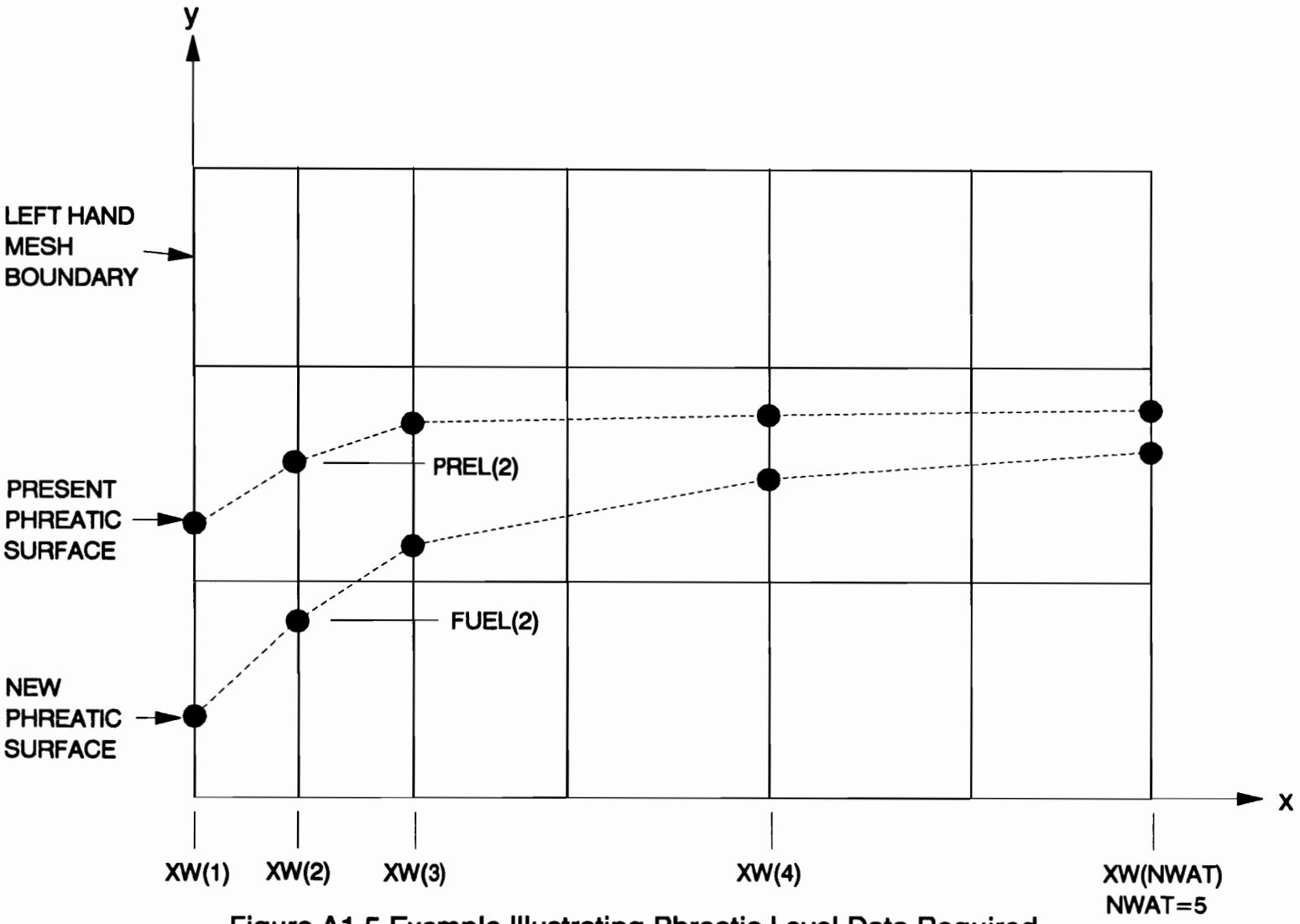

Figure A1.5 Example Illustrating Phreatic Level Data Required for the Seepage Loading/Construction Mode

(a) CONTROL DATA --- FORMAT (I5)

Column	Variable	Explanation
1-5	NCARDS	Number of deleted bar elements. There is no limit other than the number of bar elements presently in the mesh.

(b) ELEMENT NUMBERS --- FORMAT (16I5)

The element numbers of 16 deleted bar elements can be specified on one line of data.

Column	Variable	Explanation
1-5	N	Element number of bar element to be deleted. Element numbers for the next 15 elements are supplied in the next 15 five-column fields.

** ADDITION OF BAR ELEMENTS **

These data are supplied only if KCS(N,1), KCS(N,2), or KCS(N,3) = 5. Input is handled by the main program.

Information on the second line of data is the same as that explained for the Bar Element Data (Input Data Section 14). The added bar elements are numbered sequentially from NUMBAR + 1, where NUMBAR is the number of bar elements in the mesh before the present loading step.

As described in Input Data Section 14, BAR(N,3) only enters the nominal prestress force in the bar. The load must be applied to the mesh using construction mode 9. Ordinarily, the load is applied using mode 9 in a construction step prior to adding the bar with mode 5 in order to avoid "stretching" the bar during installation.

(a) CONTROL DATA --- FORMAT (I5)

Column	Variable	Explanation
1-5	NCARDS	Number of bar elements to be added. Any number can be added in a loading step, however, the maximum number of bar elements that can be in the mesh (including inactive or deleted elements) is 15.

(b) ADDED BAR ELEMENT DATA --- FORMAT (4I5,2D10.7,2D10.1,D10.5)

Column	Variable	Explanation

1-5	N	Element number of added bar element.
6-10	IB(N,1)	Number of nodal point I.
11-15	IB(N,2)	Number of nodal point J.
16-20	IB(N,3)	Spring response type code.
21-30	BAR(N,1)	cos α
31-40	BAR(N,2)	sin α
41-50	BAR(N,3)	Prestress force in the bar element.
51-60	Bar(N,4)	Stiffness of bar element.
61-70	BAR(N,5)	Displacement of bar element at activation.

** BOUNDARY PRESSURE LOADING **

These data are supplied only if KCS(N,1), KCS(N,2), or KCS(N,3) = 6. Input is handled by subroutine SURFLD. Linear pressure distributions are assumed, based on the pressures specified for the nodal points. Positive pressures are to the right (positive x-direction) and up (positive y-direction).

(a) CONTROL DATA --- FORMAT (I5)

Column	Variable	Explanation
1-5	NLDS	Number of loaded boundaries. There is no limit to the number of loaded boundaries that can be specified.
6-10	NPRTB	Print code = 1 if equivalent nodal point forces are to be printed.

(b) LOADED BOUNDARY DATA --- FORMAT (2I5,4D10.2)

Information for one loaded boundary is specified on each line of data. Nodes I and J are interchangeable; there is no convention regarding their assignment. A total of N = 1 to NLDS loaded boundaries must be specified.

Column	Variable	Explanation
1-5	I	Nodal point number of the first node of the loaded boundary.

6-10	J	Nodal point number of the second node of the loaded boundary.
11-20	WS1	Value of the pressure acting in the x-direction at node I.
21-30	WS2	Value of the pressure acting in the x-direction at node J.
31-40	WS3	Value of the pressure acting in the y-direction at node I.
41-50	WS4	Value of the pressure acting in the y-direction at node J.

** TEMPERATURE LOADING **

No data are required for this loading/construction mode. If KCS(N,1), KCS(N,2), or KCS(N,3) = 7, then the values of DP(N) are acknowledged by the main program and processed as temperature changes. Note that DP(N) can also be used to enter phreatic level changes for the seepage loading/ construction mode. Thus, if seepage is specified as being entered through values of DP(N), seepage and temperature loading cannot be included in the same loading step. If seepage loading is specified, temperature loading requires a restart analysis, with the DP(N) values being changed to reflect the temperature changes.

The temperature scale used (°C or °F) must correspond to the coefficient of thermal expansion designated with the Material Properties (Input Data section 9). Temperature changes are designated for structural materials (NCTYP) only.

** CONCENTRATED FORCE OR DISPLACEMENT LOADING **

These data are supplied only if KCS(N,1), KCS(N,2), or KCS(N,3) = 8 or 9. Input is handled by the main program. Refer to Loading Information (Input Data section 7) for instructions on using loading/construction modes 8 and 9.
(a) CONTROL DATA --- FORMAT (I5)

Column	Variable	Explanation
1-5	NUMNDE	Number of loaded or displaced nodes. There is no limit to the number of loaded or displaced nodes that can be specified.

(b) LOAD OR DISPLACEMENT DATA

DISPLACEMENT DATA --- FORMAT (2(I5, 2(1X, 1D14.7))
[LOAD DATA] --- FORMAT (2(I10,2D10.2)

Information for two loaded or displaced nodal points is supplied on each line of data. A total of

N = 1 to NUMNDE nodes must be specified. Sign convention is positive to the right (positive x-direction) and positive up (positive y-direction). Nodal points specified as being loaded or displaced do not have to be in numerical order.

Column	Variable	Explanation
1-5 [1-10]	I	Node number of the first loaded or displaced node.
7-20 [11-20]	X1	Component of force or displacement in the x-direction at node I.
22-35 [21-30]	Y1	Component of force or displacement in the y-direction at node I.
36-40 [31-40]	J	Node number of the second loaded or displaced node.
42-55 [41-50]	X2	Component of force or displacement in the x-direction at node J.
57-70 [51-60]	Y2	Component of force or displacement in the y-direction at node J.

If there is not a second, or J, node to be specified on the last line of data, then leave the second set of columns blank.

** ELEMENT MATERIAL TYPE CHANGE **

These data are supplied only if KCS(N,1), KCS(N,2), or KCS(N,3) = 10. Input is handled by the main program.

The material type of the specified element is changed before the analysis of the construction step which specifies the change. The material type change includes modifying the material property values and zeroing the stresses, SIG(N,I). Thus, if a material type change is specified in conjunction with boundary loading, in the same construction step, the elements whose material type is changed will respond to the loading with new material properties.

For example, this loading/construction mode may be used to represent the grouting of an anchor. At a given step in the analysis, the material types of soil elements can be changed to represent the assumed linear elastic grout zone.

(a) CONTROL DATA --- FORMAT (I5)

The maximum number of elements whose material type number can be changed in a load step is 150. The excavation and material type change loading/construction modes cannot be specified in the same construction step since the same variable, LUL(N,I), is used to enter data for both.

Column	Variable	Explanation
1-5	NELCH	Number of elements whose material type number is being changed.

(b) ELEMENT DATA — FORMAT (16I5)

The element numbers and new material type numbers of 8 elements can be supplied on one line of data. A total of N = 1 to NELCH elements must be specified.

Column	Variable	Explanation
1-5	LUL(N,1)	Element number of first element with a specified new material type number.
6-10	LUL(N,2)	New material type number of the specified element.

Information for the next seven elements is supplied in the next seven pairs of five-column fields.

VITA

Levi Regalado was born on October, 1961 in Manila, the Philippines. He received his Bachelor of Science degree in Civil Engineering in 1983 from the University of the Philippines, graduating with honors. He then joined the teaching staff of the Engineering Sciences Department of the same University as an instructor until 1987. He also worked as a computer applications programmer for Computer Information Systems, Inc. in Rizal, Metro-Manila, and as a lecturer on computer programing at the IMPACT Center, de la Salle University, Metro-Manila.

In September of 1987, he entered the graduate program in Civil Engineering at Virginia Tech, with emphasis in geotechnical engineering. He was employed by the Civil Engineering Department initially as a Graduate Teaching Assistant and later as a Graduate Research Assistant. He obtained an M. S. in Civil Engineering from Virginia Tech in the summer of 1989, and then proceeded to pursue a doctorate at the same institution. His Ph. D. research was supervised by Professors J. M. Duncan and G. W. Clough.

As of this writing he will be joining the engineering staff of GEI Consultants as a geotechnical engineer in their Winchester, Massachusetts office.